NAVAL POSTGRADUATE SCHOOL
Monterey, California

THESIS

TIME DELAY ESTIMATION FOR UNDERWATER SIGNALS AND APPLICATION TO LOCALIZATION

by

Stefanos D. Kouteas

June 2001

Thesis Advisor: Charles W. Therrien
Thesis Advisor: Kevin B. Smith

Approved for public release; distribution is unlimited.

REPORT DOCUMENTATION PAGE

Form Approved OMB No. 0704-0188

1. AGENCY USE ONLY (*Leave blank*)	2. REPORT DATE	3. REPORT TYPE AND DATES COVERED
	June 2001	Master's Thesis

4. TITLE AND SUBTITLE Time Delay Estimation for Underwater Signals and Application to Localization

5. FUNDING NUMBERS

6. AUTHORS Kouteas, Stefanos

7. PERFORMING ORGANIZATION NAME(S) AND ADDRESS(ES)
Naval Postgraduate School
Monterey CA 93943-5000

8. PERFORMING ORGANIZATION REPORT NUMBER

9. SPONSORING/MONITORING AGENCY NAME(S) AND ADDRESS(ES)

10. SPONSORING/MONITORING AGENCY REPORT NUMBER

11. SUPPLEMENTARY NOTES The views expressed in this thesis are those of the author and do not reflect the official policy or position of the Department of Defense or the U.S. Government.

12a. DISTRIBUTION/AVAILABILITY STATEMENT
Approved for public release; distribution is unlimited.

12b. DISTRIBUTION CODE

13. ABSTRACT(*maximum 200 words*)

The problem of time difference of arrival (TDOA) is important in underwater acoustics for both passive and active sonar. Classical approaches to this problem are based on generalized cross-correlation (GCC) methods implemented in the frequency domain. After appropriate weighting of the cross spectral data in the frequency domain, an inverse discrete Fourier transform (IDFT) is performed and the peak of the resulting GCC function is located in the time domain.

This thesis shows that the cross-spectrum of the data satisfies an appropriate signal subspace model; therefore the IDFT can be replaced with a signal subspace technique such as MUSIC. The result is an enhanced ability to locate the peak. Further, application of methods such as root-MUSIC or ESPRIT produce direct numerical estimates for TDOA without the need to search for a peak. Results are presented for an extensive set of simulations using both synthetic signal data and data from a ocean acoustic propagation model (MMPE). Results are further presented for an application of the new method to target localization and tracking. In all cases results are compared using both the new methods and the classical methods.

14. SUBJECT TERMS
Time Difference of Arrival, Subspace Methods, Generalized Cross-Correlation, Localization

15. NUMBER OF PAGES 232

16. PRICE CODE

17. SECURITY CLASSIFICATION OF REPORT	18. SECURITY CLASSIFICATION OF THIS PAGE	19. SECURITY CLASSIFICATION OF ABSTRACT	20. LIMITATION OF ABSTRACT
Unclassified	Unclassified	Unclassified	UL

NSN 7540-01-280-5500

Standard Form 298 (Rev. 2-89)
Prescribed by ANSI Std. 239-18 298-102

THIS PAGE INTENTIONALLY LEFT BLANK

Approved for public release; distribution is unlimited

TIME DELAY ESTIMATION FOR UNDERWATER SIGNALS AND APPLICATION TO LOCALIZATION

Stefanos D. Kouteas
Lieutenant J.G., Hellenic Navy
B.S., Hellenic Naval Academy, 1992

Submitted in partial fulfillment of the
requirements for the degrees of

MASTER OF SCIENCE IN ENGINEERING ACOUSTICS
AND
MASTER OF SCIENCE IN ELECTRICAL ENGINEERING

from the

NAVAL POSTGRADUATE SCHOOL
June 2001

Author: _____
Stefanos D. Kouteas

Approved by: _____
Charles W. Therrien, Thesis Advisor

_____
Kevin B. Smith, Thesis Advisor

_____
Kevin B. Smith, Chairman
Engineering Acoustics Academic Committee

_____
Jeffrey B. Knorr, Chairman
Department of Electrical and Computer Engineering

THIS PAGE INTENTIONALLY LEFT BLANK

ABSTRACT

The problem of time difference of arrival (TDOA) is important in underwater acoustics for both passive and active sonar. Classical approaches to this problem are based on generalized cross-correlation (GCC) methods implemented in the frequency domain. After appropriate weighting of the cross spectral data in the frequency domain, an inverse discrete Fourier transform (IDFT) is performed and the peak of the resulting GCC function is located in the time domain.

This thesis shows that the cross-spectrum of the data satisfies an appropriate signal subspace model; therefore the IDFT can be replaced with a signal subspace technique such as MUSIC. The result is an enhanced ability to locate the peak. Further, application of methods such as root-MUSIC or ESPRIT produce direct numerical estimates for TDOA without the need to search for a peak. Results are presented for an extensive set of simulations using both synthetic signal data and data from a ocean acoustic propagation model (MMPE). Results are further presented for an application of the new method to target localization and tracking. In all cases results are compared using both the new methods and the classical methods.

THIS PAGE INTENTIONALLY LEFT BLANK

TABLE OF CONTENTS

THIS PAGE INTENTIONALLY LEFT BLANK

LIST OF FIGURES

LIST OF TABLES

SYMBOLS, ACRONYMS AND ABBREVIATIONS

A_i	complex amplitude of the i_{th} signal
$\mathbf{A}^+$	pseudoinverse of matrix $\mathbf{A}$
$\hat{B}$	bearing angle
$\mathbf{b_k}$	basis vector
BW	bandwidth
c	speed of sound in the water
c_o	reference sound speed
D	time delay between two sensors
DFT	Discrete Fourier Transform
$\mathbf{E}$	matrix of eigenvectors of correlation matrix
$\mathbf{e_k}$	eigenvector or generalized eigenvector of correlation matrix
$\mathbf{E_{noise}}$	matrix of noise eigenvectors of correlation matrix
$\mathbf{E_{sig}}$	matrix of signal eigenvectors of correlation matrix
ESPRIT	Estimation of Signal Parameters via Rotational Invariance Techniques
f	frequency
f_c	center frequency
FFT	Fast Fourier Transform
f_r	received frequency
f_T	transmitted frequency
GCC	Generalized Cross-Correlation
$G_{y_1y_2}$	Cross Spectrum between two signals
H_{op}	Hamiltonian operator
IFFT	Inverse Fast Fourier Transform

k_c	vertical wavenumber corresponding to a steering of the source
k_o	reference wavenumber
k_z	vertical wavenumber
L	distance between two receivers
M	number of independent signals in noise
ML	Maximum Likelihood
MMPE	Monterey - Miami Parabolic Equation
MN	Minimum-Norm procedure
MUSIC	Multiple Signal Classification
n	acoustic index of refraction
N	number of samples of a random process
N	number of receivers
N_f	number of frequencies
$n_i(t)$	uncorrelated additive noise
p	acoustic pressure
$\hat{P}_{MN}$	Minimum-Norm pseudospectrum
$\hat{P}_{MU}$	MUSIC pseudospectrum
$\hat{P}_{PCLP}$	Principal Components Linear Prediction pseudospectrum
PCLP	Principal Components Linear Prediction
PE/SSF	Parabolic Equation / Split-Step Fourier algorithm
PHAT	Phase Transform
P_i	Power of a complex exponential process
$\mathbf{P_{noise}}$	projection matrix of noise subspace
$\mathbf{P_o}$	diagonal matrix of signal powers P_i
P_o	reference source level

$P_{op}, Q_{op}, T_{op}, U_{op}$	operators in Helmholtz equation
$\mathbf{P_{sig}}$	projection matrix of signal subspace
r	range
$\mathbf{r}$	position vector of the source (target)
$\hat{R}^{(g)}_{y_1y_2}$	Generalized Cross-Correlation between two signals
$\hat{R}^{(P)}_{y_1y_2}$	PHAT generalized cross-correlation between two signals
$\hat{R}^{(R)}_{y_1y_2}$	Roth generalized cross-correlation between two signals
$\hat{R}^{(S)}_{y_1y_2}$	SCOT generalized cross-correlation between two signals
$\hat{R}_{x_1x_2}$	Cross Correlation between two signals
$\mathbf{r_i}$	position vector of the receiver i
R_o	reference distance (1m)
$\mathbf{R_x}$	correlation matrix for x
$\mathbf{S}$	matrix whose columns are the signal vectors s_i
$s(t)$	transmitted transient
SCOT	Smoothed Coherence Transform
$\mathbf{s_i}$	signals vector
SNR	Signal to Noise ratio
SVD	Singular value decomposition
t	transmission time
TD	Time Delay
TDE	Time Delay Estimation
TDOA	Time Difference of Arrival
TL	Transmission Loss
TOA	Time of Arrival
TOAD	Time of Arrival Difference

v_S	source speed
$\mathbf{w}$	frequency vector
$\mathbf{x}$	observation vector
$x_i(t)$	received signal at buoy i
z_s	source depth
$\hat{\gamma}_{x_1x_2}$	coherence estimate
Δf	maximum frequency shift
δf	frequency sampling
$\boldsymbol{\eta}$	noise vector
θ	angle
$\boldsymbol{\Lambda}$	matrix of eigenvalues of correlation matrix
$\boldsymbol{\Lambda_{noise}}$	matrix of noise eigenvalues of correlation matrix
$\boldsymbol{\Lambda_{sig}}$	matrix of signal eigenvalues of correlation matrix
λ_κ	eigenvalue or generalized eigenvalue of correlation matrix
$\boldsymbol{\Sigma_\eta}$	normalized noise covariance matrix
σ_o^2	variance parameter
Φ	propagator function
ϕ, ϕ_S	direction of source motion
Ψ	envelope function or PE field function
ψ_E	Eckart filter
ψ_g	general frequency weighting
ψ_P	PHAT frequency weighting
ψ_R	Roth frequency weighting
ψ_S	SCOT frequency weighting

ACKNOWLEDGMENTS

This thesis would not be complete without the acknowledgment of several people, who have contributed in various ways to the success of the project.

First of all, I would like to dedicate this thesis to my parents, Dimosthenis and Loukia, for their continuous support, encouragement and guidance, even though they were thousands of miles away from me and for such a long time. I hope, that the completion of this work, will make them proud, since nothing would be possible without their love and understanding.

I want to express my gratitude and appreciation to my thesis advisors Dr. Charles W. Therrien and Dr. Kevin B. Smith for their guidance, their patience, their valuable teaching and their professional counsel. Their assistance was invaluable for the completion of this project.

Thanks is also due to the staff and faculty of the Naval Postgraduate School for making my education a fascinating experience and especially to Dr. J. Sanders for his guidance and help as my academic associate.

THIS PAGE INTENTIONALLY LEFT BLANK

EXECUTIVE SUMMARY

In the passive sonar problem, signals received at two or more sensors or hydrophones can be used to estimate the position and velocity of a detected acoustic source. Passive systems, unlike radar or active sonar systems, cannot control the amount of transmitted energy to be reflected from the source. However, the covertness of passive systems can be advantageous, both in military and biochemical applications. In practice, the number of receiving sensors, the observation time and the ratio of the background noise to the source signal strength after propagation loss, when balanced against total system cost, dictate the feasibility of passive systems.

In the ocean, sound usually arrives at each individual omnidirectional receiver through more than one path (e.g., direct and/or surface, bottom reflected paths). In order to deal with this problem from a signal processing point of view, it is useful to decouple two separate cases: the multipath and the planar problems. For multipath signals, a simple model of the received signal is that each receiver sees a signal plus an attenuated and delayed signal corrupted by additive uncorrelated noise, coming from different directions. For the planar problem (i.e., when all receivers and the source are in the same plane), it is usually assumed that the energy arrives at each receiver through only one propagation path in the same plane with all receivers and source. This means that the time delay to be estimated is the travel time of the acoustic wavefront between pairs of receivers, so that the source position and velocity can be estimated.

In this thesis we deal with the time difference of arrival (TDOA) problem. We begin by examining previous research for estimating time difference of arrival known as generalized cross-correlation (GCC) methods. We refer to these as "classical methods." With these methods, data from the two channels are transformed to the frequency domain to form the conjugate product XY^* (cross-spectrum). After appropriate weighting, an inverse discrete Fourier transform (IDFT) is performed and

the peak of the resulting generalized cross-correlation function is located in the time domain. Our main goal in this thesis was to prove that for this kind of problem it is possible to use so-called signal subspace methods. More specifically, we showed that the aforementioned cross-spectrum of the data satisfies an appropriate signal subspace model. In this way we were able to replace the IDFT with a signal subspace technique such as MUSIC, Minimum Norm, PCLP, or similar procedure. In our problem we apply the subspace methods in the frequency domain and observe their results in the time domain. This is in contrast to their more usual application for the estimation of signals in noise. We also applied the subspace methods of root-MUSIC and ESPRIT, which produce direct numerical estimates for TDOA, without the need to search for a peak in the "pseudo-correlation" function. Both types of methods performed efficiently.

We continued with a thorough series of simulations using synthetic data (MATLAB) and data created by an ocean acoustic propagation model (MMPE), each time testing the performance of all methods. The results showed that the subspace methods performed as well or better than the classical methods, especially with low SNR conditions and with more difficult environmental data. Finally we applied the various TDOA algorithms (classical and subspace methods) to the problem of target localization and tracking. All methods produced successful results.

I. INTRODUCTION

The problem of time-delay estimation (TDE) is important in the field of underwater acoustics for both passive and active sonar. In this problem a signal is emitted from a source (e.g., a submarine) and is received at two spatially separated sensors. If $s_1(t)$ represents the original undistorted source and $n_1(t)$ and $n_2(t)$ represent sequences of uncorrelated, additive noise, then the signals received at two spatially separated sensors may be modeled as

$$\begin{aligned} x_1(t) &= s_1(t) + n_1(t) \\ x_2(t) &= a s_1(t + D) + n_2(t) \end{aligned} \tag{I.1}$$

where D is the time delay between the two sensors. In a more complicated scenario, the received signals are attenuated and contain multipath reflections of the original source created by propagation through the ocean environment, in addition to the noise, as shown in Fig. 1. In the unknown source case (generally passive sonar), $x_1(t)$ and $x_2(t)$ and the ordinary cross correlation may be used to estimate the position and velocity of a moving source. For the known source case (generally active sonar) ordinary correlation involves using the original source and only one received signal to estimate the time it takes the signal to travel from the source to the receiver, i.e., $n_1(t) = 0$ in the model given above. In the absence of propagation distortion, this is matched filtering, which is the optimum linear method when the noise is white.

Once the signal has been detected and the time delay D has been estimated, the time delay can be used to estimate the bearing angle $\hat{B}$ shown in Fig. 2. The bearing estimate is given by the approximate rule

$$\hat{B} \cong \cos^{-1}(c\hat{D}/L) \tag{I.2}$$

where c is the speed of sound in water, $\hat{B}$ is the bearing estimate and $\hat{D}$ is the time delay estimate. It can be shown that $\hat{B}$ is the angle that the hyperbolic "line of

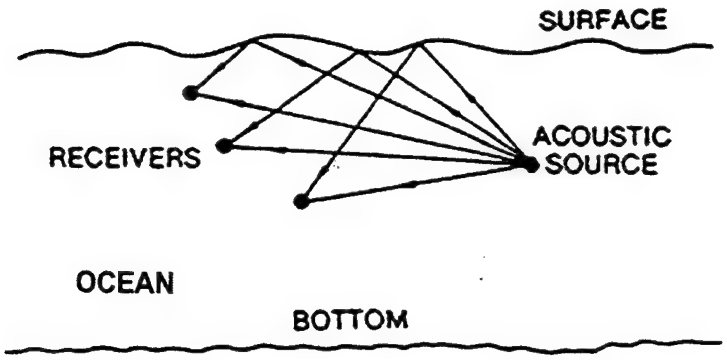

Figure 1. Model of direct and surface-reflected sound ray paths received at three sensors.

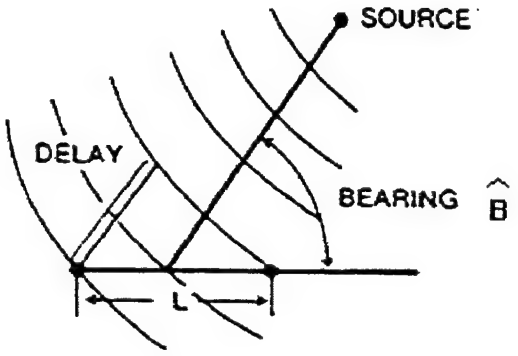

Figure 2. Planar model of two receivers separated by a distance L.

position" makes with the axis of the receivers; hence the approximation Eq. (I.2) is increasingly accurate as the range to the acoustic source increases.

The critical part for the passive bearing estimation problem, or in general for the localization, is the accurate estimation of time delay. In the literature, this problem is treated using terms like time delay estimation (TDE), time delay (TD), time difference of arrival (TDOA), group delay, time-of-arrival difference (TOAD), phase delay and others. For our purposes it is assumed that all these terms are "identical" and the terms TDE or TDOA will be used for the rest of our discussion.

A. PREVIOUS RELATED RESEARCH

Two conceptual procedures are basically known according to [Ref. 1].

- An intuitive approach and a familiarity with detection theory.
- A rigorous application of the *maximum likelihood* (ML) for white signals in white noise.

In both conceptual procedures it is attempted to "advance" the delayed received signal by a hypothesized amount in order to align it with the other received signal. In other words both received signals $x_1(t)$, $x_2(t)$ contain the same transient $s_1(t)$, coming from the same source, "buried" in different noise, $n_1(t)$, $n_2(t)$, and the only difference between them, is the time of arrival (TOA). After the above hypothesis either they are summed, squared and averaged as shown in Fig. 3 or multiplied and averaged as shown in Fig. 4. In both cases the hypothesized delays are adjusted in order to

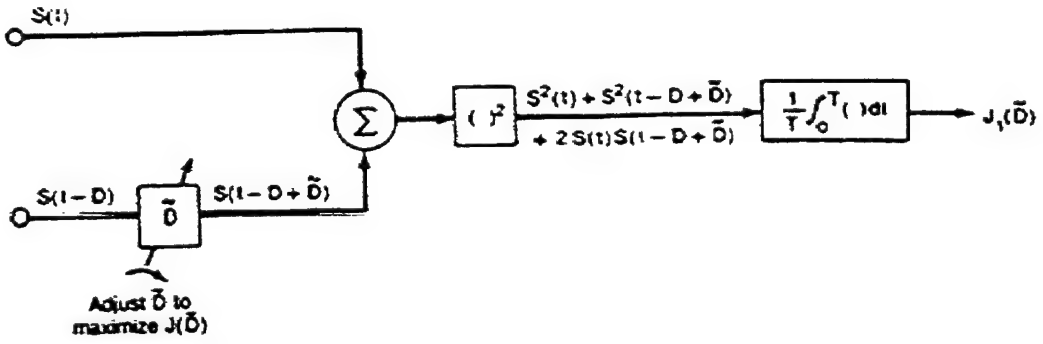

Figure 3. Conceptual delay, sum, square and integrate configuration.

maximize the configuration output. From the figures it is observed, that both configuration outputs consist of "signal-cross-signal" terms. Further, both configurations are ML estimators for time delay under the assumptions that the signal and noises are white and mutually uncorrelated [Ref. 1]. When the signal and noise spectral characteristics are nonwhite, the received waveforms must be prefiltered with particular equiphase filters (i.e., the prefilters must have the same phase characteristics) to

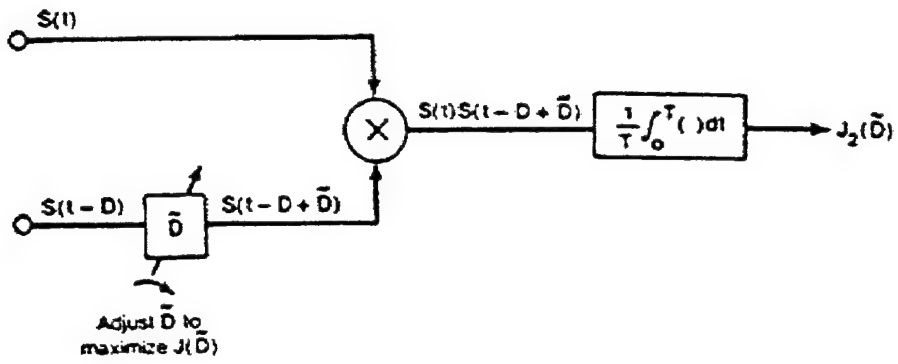

Figure 4. Conceptual cross correlator configuration.

accentuate the frequency bands with good *signal-to-noise ratio* (SNR). It is of interest to note that a signal detector can be realized by comparing either configuration output to a threshold. Moreover *in terms of detection* (but not estimation) in the presence of noise, the system in Fig. 3 outperforms the system in Fig. 4 [Ref. 1]; however, the system in Fig. 3 requires prior knowledge of power levels in order to set the proper threshold. The system in Fig. 4 has a zero mean output in the signal absent, noise present case.

A number of different approaches have been taken so that the conceptual systems in Figs. 3 and 4 can be achieved. The system in Fig. 3 can be implemented as shown in Fig. 5 which is called a time delay *beamformer*. It is presumed that $s(t)$ is a sampled version of the original broadband time signal and that the sampling rate is large in comparison with the required Nyquist rate. In particular, the sampling rate is much greater than twice the bandwidth. The system configuration shown in Fig. 4, including prefilters can be instrumented by a *generalized cross-correlation* (GCC) function, which in general is the inverse *fast Fourier transform* (FFT) of the product of a weighting function and the estimated complex cross-power spectrum. This means that data from the two sensors are transformed to the frequency domain to form the conjugate product XY^*. After appropriate weighting, an inverse DFT is performed and the peak of the resulting generalized cross-correlation function is located in the

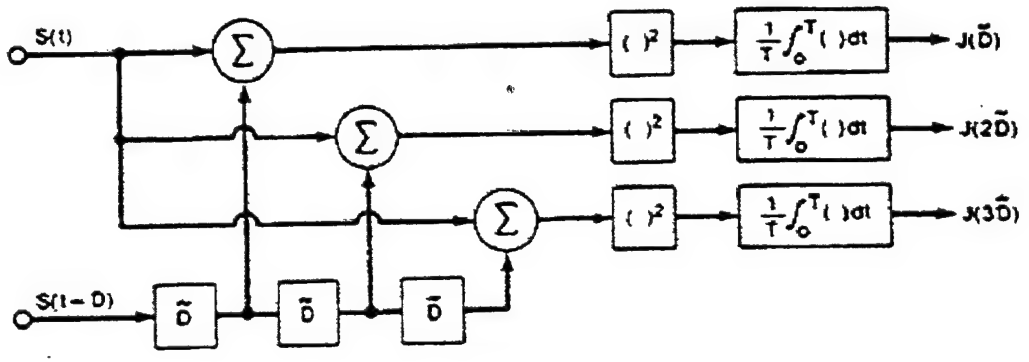

Figure 5. Time-domain beamformer implementation of one conceptual configuration for three hypothesized delays.

time domain. All the methods that follow this general approach will be referred to in this thesis as *classical methods* and quite extensive research has been conducted on these methods [Ref. 2, 3, 4, 1, 5].

More recently, techniques based on higher order statistics such as bicorrelation and bispectra have been introduced to the problem [Ref. 6, 7, 8, 9]. These methods are claimed to have some advantage when there is Gaussian noise present which is correlated between sensors. In particular, since higher order cumulants of Gaussian noise are theoretically zero, these methods are practically "blind" to Gaussian noise.

B. THESIS OBJECTIVES

This thesis has the following goals. The first objective is to research and develop an algorithm that can be used for Time-Difference-Of-Arrival (TDOA) estimation based on subspace methods. The next objective is to evaluate the performance of this algorithm by comparing it with the respective algortihm based on generalized cross-correlation (GCC) methods implemented in the frequency domain, through a thorough set of simulations using synthetic (MATLAB) and model-based acoustic (MMPE) data. Finally the last goal in this thesis is to develop localization and tracking algorithms implementing the above methods, and to evaluate their performance in target's extraction data (position-course-speed).

C. THESIS APPROACH

In this thesis we suggest an alternative to the classical methods based on some more modern approaches to spectral analysis. In particular, we focus on methods based on the signal subspace concept. We observe that the data product XY^* computed in the classical methods satisfies a signal subspace model and therefore a number of well-known techniques such as MUSIC [Ref. 10], ESPRIT [Ref. 11] and others can be used to estimate the time delay. Mathematically, the procedure can be viewed as replacing the inverse DFT in the classical methods with one of these other techniques. As we later see from experimental results the new methods retain the accuracy of the classical methods, but give a much "cleaner" indication of the peak. Further, the use of methods such as root MUSIC or ESPRIT for the estimation provides direct numerical estimates for the time delay without the need to search for a maximum. We also have to mention that we have obtained similar behavior with the "Maximum Likelihood" or "Minimum Variance" method proposed by J. Capon [Ref. 12, 13]. Our focus in this thesis however is on the subspace methods.

D. THESIS OUTLINE

The remainder of this thesis is organized as follows. Chapter II provides a short introduction of the concepts of the *classical methods* and also describes the special characteristics of each one method, that is going to be used later in the simulations from this family of methods. Chapter III discusses the general idea behind the *subspace methods*, gives a brief insight of all the methods from this group, and finally provides an argumentative presentation of the way that these methods are implemented into our problem (TDOA). Chapter IV presents the whole thesis approach to the TDOA problem, using various synthetic data (MATLAB software) and model based acoustic data using the Monterey-Miami Parabolic Equation (MMPE) model [Ref. 14, 15] for more realistic results, under different conditions/environments each time. Chapter V discusses the simulation results for both kinds of data (synthetic and

model-based acoustic) for the TDOA problem. Chapter VI develops a localization algorithm in two dimensions and discusses the implementation of the above methods in this localization problem in order to examine, how they ultimately function in the desired goal, namely the "Target Detection and Localization." Chapter VII further extends the research to "Target Tracking Problem." For this, one has to estimate not only target position, but also target course and speed, using Doppler measurements provided by MMPE. Chapter VIII presents conclusions and suggestions for future work.

THIS PAGE INTENTIONALLY LEFT BLANK

II. CLASSICAL METHODS

A. GENERAL APPROACH

We have seen that the transmission of a short transient signal from a remote source monitored in the presence of noise at two spatially separated sensors can be mathematically modeled as

$$x_1(t) = s_1(t) + n_1(t) \ ,$$
$$x_2(t) = as_1(t + D) + n_2(t) \ , \tag{II.1}$$

where $s_1(t)$, $n_1(t)$, and $n_2(t)$ are real, jointly stationary random processes. Signal $s_1(t)$ is assumed to be uncorrelated with noise $n_1(t)$ and $n_2(t)$.

One common method of determining the time delay D is to compute the cross correlation function

$$\hat{R}_{x_1x_2}(\tau) = \frac{1}{T-\tau}\int_{\tau}^{T} x_1(t)x_2(t-\tau)dt \ , \tag{II.2}$$

where T represents the observation interval. In order to improve the accuracy of the delay estimate $\hat{D}$, it is desirable to prefilter $x_1(t)$ and $x_2(t)$ prior to integration in Eq. (II.2). As shown in Fig. 6, x_i may be filtered through H_i to yield y_i for $i = 1, 2$. The resultant y_i are multiplied, integrated, and squared for a range of time shifts, τ, until the peak is obtained. The time shift causing the peak is an estimate of the true delay D. When the filters $H_1(f) = H_2(f) = 1, \forall f$, the estimate $\hat{D}$ is simply the value of τ at which the cross-correlation function peaks.

The cross-correlation between $x_1(t)$ and $x_2(t)$ is related to the cross-power spectral density function by the Fourier transform relationship

$$R_{x_1x_2}(\tau) = \int_{-\infty}^{\infty} G_{x_1x_2}(f)e^{j2\pi f\tau}df. \tag{II.3}$$

When $x_1(t)$ and $x_2(t)$ have been filtered as shown in Fig. 6, the cross-power spectrum between the filter outputs is given by

$$G_{y_1y_2}(f) = H_1(f)H_2^*(f)G_{x_1x_2}(f). \tag{II.4}$$

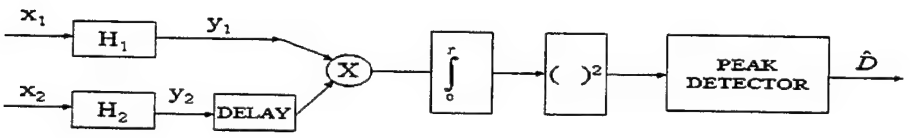

Figure 6. Received waveforms filtered, delayed, multiplied, and integrated for a variety of delays until peak output is obtained.

where $*$ denotes the complex conjugate. The generalized cross-correlation between $x_1(t)$ and $x_2(t)$ is defined by

$$R_{y_1y_2}^{(g)}(\tau) = \int_{-\infty}^{\infty} \psi_g(f) G_{x_1x_2}(f) e^{j2\pi f\tau} df, \tag{II.5}$$

where

$$\psi_g(f) = H_1(f) H_2^*(f) \tag{II.6}$$

and denotes the general frequency weighting.

In practice, $G_{x_1x_2}(f)$ is not known *a priori*, and only an estimate $\hat{G}_{x_1x_2}(f)$ of $G_{x_1x_2}(f)$ can be obtained from finite observations of $x_1(t)$ and $x_2(t)$. Consequently, the integral

$$\hat{R}_{y_1y_2}^{(g)}(\tau) = \int_{-\infty}^{\infty} \psi_g(f) \hat{G}_{x_1x_2}(f) e^{j2\pi f\tau} df \tag{II.7}$$

is evaluated and used for estimating delay. Indeed, depending on the particular form of $\psi_g(f)$ and the *a priori* information, it may also be necessary to estimate $\psi_g(f)$ in Eqs. (II.5) and (II.6). For example, when the role of the prefilters is to accentuate the signal passed to the correlator at those frequencies at which the signal-to-noise (S/N) ratio is highest, then $\psi_g(f)$ can be expected to be a function of signal and noise spectra which must either be known *a priori* or estimated.

B. PROCESSOR WEIGHTING EVALUATION

Before continuing to describe the weighting functions that are used in the generalized cross-correlation (GCC) in practice, it is informative to examine first the effect of processor weightings on the shape of $R_{y_1y_2}(\tau)$ under ideal conditions. For models of the form of (II.1), the cross correlation of $x_1(t)$ and $x_2(t)$ is

$$R_{x_1x_2}(\tau) = \alpha R_{s_1s_1}(\tau - D) + R_{n_1n_2}(\tau). \tag{II.8}$$

The Fourier transform of (II.8) gives the cross-power spectrum

$$G_{x_1x_2}(f) = \alpha G_{s_1s_1}(f)e^{-j2\pi fD} + G_{n_1n_2}(f). \tag{II.9}$$

If $n_1(t)$ and $n_2(t)$ are uncorrelated ($G_{n_1n_2}(f) = 0$), the cross-power spectrum between $x_1(t)$ and $x_2(t)$ is a scaled signal power spectrum times a complex exponential. Since multiplication in one domain is a convolution in the transformed domain, it follows for $G_{n_1n_2}(f) = 0$ that

$$R_{x_1x_2}(\tau) = \alpha R_{s_1s_1}(\tau) \circledast \delta(t - D). \tag{II.10}$$

where $\circledast$ denotes convolution.

One interpretation of (II.10) is that the delta function has been spread or "smeared" by the Fourier transform of the signal spectrum. If $s_1(t)$ is a white noise source, then its Fourier transform is a delta function and no spreading takes place. An important property of autocorrelation functions is that $|R_{ss}(\tau)| \leq R_{ss}(0)$. Equality will hold for certain τ for periodic functions. However, for most practical applications, equality does not hold for $\tau \neq 0$, and the true cross correlation (II.10) will peak at D regardless of whether or not it is spread out. The spreading simply acts to broaden the peak. For a single delay this may not be a serious problem. However, when the signal has multiple delays, the true cross correlation is given by

$$R_{x_1x_2}(\tau) = R_{s_1s_1}(\tau) \circledast \sum_i \alpha_i \delta(t - D_i). \tag{II.11}$$

In this case, the convolution with $R_{s_1 s_1}(\tau)$ can spread one delta function into another, thereby making it impossible to distinguish peaks or delay times. Under ideal conditions where $\forall f, \hat{G}_{x_1 x_2}(f) \cong G_{x_1 x_2}(f), \psi_g(f)$ should be chosen to ensure a large sharp peak in $R_{y_1 y_2}(\tau)$ rather than a broad one in order to ensure good time-delay resolution. However, sharp peaks are more sensitive to errors introduced by finite observation time, particularly in cases of low signal-to-noise S/N ratio. Thus, as with other spectral estimation problems, the choice of $\psi_g(f)$ is a compromise between good resolution and stability.

Having all the above in consideration, we are equipped with the appropriate background for the role that $\psi_g(f)$ is going to play. Thus, let us examine some generalizations of the cross-correlation function individually.

1. Roth Processor

The weighting proposed by Roth [Ref. 4], namely [1]

$$\psi_R(f) = \frac{1}{G_{x_1 x_1}(f)} \tag{II.12}$$

yields

$$\hat{R}^{(R)}_{y_1 y_2}(\tau) = \int_{-\infty}^{\infty} \frac{\hat{G}_{x_1 x_2}(f)}{G_{x_1 x_2}(f)} e^{j2\pi f \tau} df. \tag{II.13}$$

Equation (II.13) estimates the impulse response of the optimum linear (Wiener-Hopf) filter

$$H_m(f) = \frac{G_{x_1 x_2}(f)}{G_{x_1 x_1}(f)}, \tag{II.14}$$

which "best" approximates the mapping of $x_1(t)$ to $x_2(t)$. If $n_1(t) \neq 0$, as is generally the case for (II.1), then

$$G_{x_1 x_1}(f) = G_{s_1 s_1}(f) + G_{n_1 n_1}(f), \tag{II.15}$$

and

$$R^{(R)}_{y_1 y_2}(\tau) = \delta(\tau - D) \circledast \int_{-\infty}^{\infty} \frac{\alpha G_{s_1 s_1}(f)}{G_{s_1 s_1}(f) + G_{n_1 n_1}(f)} e^{j2\pi f \tau} df. \tag{II.16}$$

[1] the subscript R is used here to distinguish the choice of $\psi_g(f)$

Therefore, except when $G_{n_1n_1}(f)$ equals any constant (including zero) times $G_{s_1s_1}(f)$, the delta function will again be spread out. The Roth processor has the desirable effect of suppressing those frequency regions where $G_{n_1n_1}(f)$ is large and $\hat{G}_{x_1x_2}(f)$ is more likely to be in error.

2. Smoothed Coherence Transform (SCOT)

Errors in $\hat{G}_{x_1x_2}(f)$ may be due to frequency bands where $G_{n_2n_2}(f)$ is large, as well as bands where $G_{n_1n_1}(f)$ is large. One is therefore uncertain whether to form $\psi_R(f) = \dfrac{1}{G_{x_1x_1}(f)}$ or $\psi_R(f) = \dfrac{1}{G_{x_2x_2}(f)}$; hence, the SCOT [Ref. 3, 16] selects

$$\psi_S(f) = \frac{1}{\sqrt{G_{x_1x_1}(f)G_{x_2x_2}(f)}}. \tag{II.17}$$

This weighting gives the SCOT generalized cross-correlation

$$\hat{R}^{(S)}_{y_1y_2}(\tau) = \int_{-\infty}^{\infty} \hat{\gamma}_{x_1x_2}(f)e^{j2\pi f\tau}df, \tag{II.18}$$

where the coherence estimate is given by

$$\hat{\gamma}_{x_1x_2}(f) \equiv \frac{\hat{G}_{x_1x_2}(f)}{\sqrt{G_{x_1x_1}(f)G_{x_2x_2}(f)}}. \tag{II.19}$$

For $H_1(f) = \dfrac{1}{\sqrt{G_{x_1x_1}(f)}}$ and $H_2(f) = \dfrac{1}{\sqrt{G_{x_2x_2}(f)}}$, the SCOT can be interpreted (see Fig. 6) as prewhitening filters followed by a cross correlation. When $G_{x_1x_1}(f) = G_{x_2x_2}(f)$, the SCOT is equivalent to the Roth processor. If $n_1 \neq 0$ and $n_2 \neq 0$, the SCOT exhibits the same spreading as the Roth processor. This broadening persists because of an apparent inability to adequately prewhiten the cross power spectrum.

3. Phase Transform (PHAT)

To avoid the spreading evident above, the PHAT uses the weighting [Ref. 3]

$$\psi_P(f) = \frac{1}{|G_{x_1x_2}(f)|}, \tag{II.20}$$

which yields

$$\hat{R}^{(P)}_{y_1y_2}(\tau) = \int_{-\infty}^{\infty} \frac{\hat{G}_{x_1x_2}(f)}{|G_{x_1x_2}(f)|}e^{j2\pi f\tau}df. \tag{II.21}$$

For the model (II.1) with uncorrelated noise (i.e., $G_{n_1n_2}(f) = 0$),

$$|G_{x_1x_2}(f)| = \alpha G_{s_1s_1}(f). \tag{II.22}$$

Ideally, when $\hat{G}_{x_1x_2}(f) = G_{x_1x_2}(f)$,

$$\frac{\hat{G}_{x_1x_2}(f)}{|G_{x_1x_2}(f)|} = e^{j\theta(f)} = e^{j2\pi fD} \tag{II.23}$$

has unit magnitude and

$$R^{(P)}_{y_1y_2}(\tau) = \delta(\tau - D). \tag{II.24}$$

The PHAT was developed purely as an *ad hoc* technique. Notice that for models of the form of (II.1) with uncorrelated noises, the PHAT (II.21) ideally does not suffer from the spreading that other processors do. In practice, however, when $\hat{G}_{x_1x_2}(f) \neq G_{x_1x_2}(f)$, then $\theta(f) \neq 2\pi fD$ and the estimate of $R^{(P)}_{y_1y_2}(\tau)$ will not be a delta function. Another apparent defect of the PHAT is that it weights $\hat{G}_{x_1x_2}(f)$ as the inverse of $G_{s_1s_1}(f)$. Thus errors are accentuated where signal power is smallest. In particular, if $G_{x_1x_2}(f) = 0$ in some frequency band, then the phase $\theta(f)$ is undefined in that band and the estimate of the phase is erratic, being uniformly distributed in the interval $[-\pi, \pi]$ radians. For models of the form of (II.1), this behavior suggests that $\psi_P(f)$ should be additionally weighted to compensate for the presence or absence of signal power. The SCOT is one method of doing this.

4. The Eckart Filter

The Eckart filter derives its name from work in this area done in [Ref. 17]. Although it is not used in the experimental part of the thesis, derivations in [Ref. 18, 19, 20] and [Ref. 21] are outlined here briefly for completeness. The Eckart filter maximizes the deflection criterion, i.e., the ratio of the change in mean correlator output due to signal present to the standard deviation of correlator output due to noise alone. For long averaging time T, the deflection has been shown [Ref. 19] to be

$$d^2 = \frac{L[\int_{-\infty}^{\infty} H_1(f)H_2^*(f)G_{s_1s_2}(f)df]^2}{\int_{-\infty}^{\infty} |H_1(f)|^2|H_2(f)|^2 G_{n_1n_1}(f)G_{n_2n_2}(f)df}, \tag{II.25}$$

where L is a constant proportional to T, and $G_{s_1s_2}(f)$ is the cross-power spectrum between $s_1(t)$ and $s_2(t)$. For the model (II.1), $G_{s_1s_2}(f) = \alpha G_{s_1s_1}(f)\exp(j2\pi fD)$. Application of Schwartz's inequality to (II.25) indicates that

$$H_1(f)H_2^*(f) = \psi_E(f)e^{+2\pi fD}, \tag{II.26}$$

maximizes d^2 where

$$\psi_E(f) = \frac{\alpha G_{s_1s_1}}{G_{n_1n_1}(f)G_{n_2n_2}(f)}. \tag{II.27}$$

Notice that the weighting (II.27), referred to as the Eckart filter, possesses some of the qualities of the SCOT. In particular, both weightings act to suppress frequency bands of high noise. Also note that the Eckart filter, unlike the PHAT, provides us with zero weight when $G_{s_1s_1} = 0$. In practice, the Eckart filter requires knowledge or estimation of the signal and noise spectra. For (II.1), when $\alpha = 1$ this can be accomplished by letting

$$\psi_E(f) = |\hat{G}_{x_1x_2}(f)|[\hat{G}_{x_1x_1}(f) - |\hat{G}_{x_1x_2}(f)|] \cdot [\hat{G}_{x_2x_2}(f) - |\hat{G}_{x_1x_2}(f)|]. \tag{II.28}$$

Since in our problem it was not possible to have knowledge or estimation of the signal and noise spectra, it was not possible to use this weighting processor for the experimental part of the thesis. All the above processors are summarized in Table I and can be justified on the basis of reasonable performance criteria, whether heuristic or mathematical.

Processor Name	**Weight** $\psi(f) = H_1(f)H_2^*(f)$
Cross Correlation	1
Roth Impulse Response	$1/Gx_1x_1(f)$
SCOT	$1/\sqrt{Gx_1x_1(f)Gx_2x_2(f)}$
PHAT	$1/\lvert Gx_1x_2(f)\rvert$
Eckart	$G_{s_1s_1}/[G_{n_1n_1}(f)G_{n_2n_2}(f)]$

Table I. Candidate Processors

THIS PAGE INTENTIONALLY LEFT BLANK

III. SUBSPACE METHODS

A. CONCEPT AND PRINCIPLES

An entire class of spectral estimates is based on the concept of signal and noise subspaces associated with the correlation matrix for a random process. Subspace methods apply primarily to locating discrete components (lines) of the spectrum. Pisarenko's harmonic decomposition was the first of these methods and motivated other improved methods, such as MUSIC, that followed. These methods are all based on the fact that when the data consists of complex exponentials in noise, the frequency vector $\mathbf{w}$, defined by

$$\mathbf{w} = \begin{bmatrix} 1 \\ e^{j\omega} \\ \vdots \\ e^{j(N-1)\omega} \end{bmatrix} , \tag{III.1}$$

is an eigenvector of the correlation matrix. Its projection onto an orthogonal subspace complementary to the subspace defined by all of the signal vectors produces a null which can be exploited to estimate the frequency. The methods can be formulated either as a search for peaks in a function (called a pseudospectrum) or as a polynomial root-finding problem. In this section we give a short presentation of the general principles [Ref. 22] in these methods.

Consider M independent signals in noise, the observation vector $\mathbf{x}$, the noise vector $\boldsymbol{\eta}$, and the signals vectors $\mathbf{s_i}$, defined by N consecutive samples of the random process, and where it is assumed that $M < N$. Analytically, this means that the observation signals $x[n]$ (transient & noise) are equal with

$$x[n] = \sum_{i=1}^{M} s_i[n] + \eta[n] , \tag{III.2}$$

where the transients $s_i[n]$ are given by

$$s_i[n] = A_i e^{j\omega_i n} . \tag{III.3}$$

Specifically,

$$\mathbf{x} = \begin{bmatrix} x[0] \\ x[1] \\ \vdots \\ x[N-1] \end{bmatrix}, \tag{III.4}$$

$$\eta = \begin{bmatrix} \eta[0] \\ \eta[1] \\ \vdots \\ \eta[N-1] \end{bmatrix}, \tag{III.5}$$

$$\mathbf{s_i} = \begin{bmatrix} 1 \\ e^{j\omega_i} \\ \vdots \\ e^{j(N-1)\omega_i} \end{bmatrix}, \tag{III.6}$$

$$\mathbf{x} = \sum_{\mathbf{i=1}}^{\mathbf{M}} \mathbf{A_i s_i} + \eta \ , \tag{III.7}$$

where $\mathbf{s_i}$ is defined by (III.6), and A_i is the complex amplitude of the i^{th} signal,

$$A_i = |A_i| e^{j\phi i}. \tag{III.8}$$

This is the general signal model used in all of the subspace methods. If the noise is white, the correlation matrix is

$$\mathbf{R_x} = \sum_{\mathbf{i=1}}^{\mathbf{M}} \mathbf{P_i s_i s_i^{*T}} + \sigma_{\mathbf{o}}^{\mathbf{2}} \mathbf{I} \ , \tag{III.9}$$

where P_i is defined by

$$P_i \equiv E\{A_i A_i^*\} = E\left\{|A_i|^2\right\} \ . \tag{III.10}$$

The last two equations can also be written with more compact matrix notation as

$$\mathbf{x} = \mathbf{S} \begin{bmatrix} A_1 \\ A_2 \\ \vdots \\ A_M \end{bmatrix} + \boldsymbol{\eta} \tag{III.11}$$

and

$$\boldsymbol{R_x} = \mathbf{S}\mathbf{P_o}\mathbf{S}^{*\mathbf{T}} + \boldsymbol{\sigma_o^2}\mathbf{I}\,, \tag{III.12}$$

where

$$\mathbf{S} = \begin{bmatrix} | & | & & | \\ \mathbf{s_1} & \mathbf{s_2} & \cdots & \mathbf{s_M} \\ | & | & & | \end{bmatrix} \tag{III.13}$$

and

$$\mathbf{P_o} = \begin{bmatrix} P_1 & 0 & \cdots & 0 \\ 0 & P_2 & \cdots & 0 \\ \vdots & \vdots & \ddots & \vdots \\ 0 & 0 & \cdots & P_M \end{bmatrix}. \tag{III.14}$$

It can be shown that the correlation matrix $\mathbf{R_x}$ has M eigenvectors lying in the signal subspace, which is spanned by the $\mathbf{s_i}$, and $N-M$ eigenvectors lying in the orthogonal, complementary noise subspace. All $N-M$ noise subspace eigenvectors correspond to eigenvalues $\lambda_i = \sigma_o^2$ while all of the signal subspace eigenvectors correspond to eigenvalues $\lambda_i > \sigma_o^2$.

When the noise is not white, but is still uncorrelated with the signals, the foregoing development leads to the correlation matrix

$$\boldsymbol{R_x} = \mathbf{S}\mathbf{P_o}\mathbf{S}^{*\mathbf{T}} + \boldsymbol{\sigma_o^2}\boldsymbol{\Sigma_\eta} \tag{III.15}$$

instead of (III.12). Here $\boldsymbol{\Sigma_\eta}$ is a normalized covariance matrix that represents the covariance structure of the noise vector. In this case the whitening transformation

$$\mathbf{y} = \boldsymbol{\Sigma_\eta^{-1/2}}\mathbf{x} \tag{III.16}$$

leads to the correlation matrix

$$\mathbf{R_y} = \boldsymbol{\Sigma_\eta^{-1/2}}\mathbf{R_x}\boldsymbol{\Sigma_\eta^{-1/2}} = \mathbf{T}\mathbf{P_o}\mathbf{T}^{*\mathbf{T}} + \sigma_o^2\mathbf{I}\,, \tag{III.17}$$

where

$$\mathbf{T} = \boldsymbol{\Sigma_\eta^{-1/2}}\mathbf{S} \tag{III.18}$$

is the matrix with columns that are the transformed signal vectors

$$\mathbf{t_k} = \mathbf{\Sigma_\eta^{-1/2} s_k}; \qquad k = 1, 2, \cdots, M \ . \tag{III.19}$$

In the transformed vector space, the eigenvectors corresponding to the M largest eigenvalues span the signal subspace; those corresponding to the smallest eigenvalues (equal to σ_o^2) span the noise subspace. The eigenvectors and eigenvalues satisfy the equation

$$\mathbf{R_y e_k'} = \left(\mathbf{\Sigma_\eta^{-1/2} R_x \Sigma_\eta^{-1/2}}\right) \mathbf{e_k'} = \lambda_\mathbf{k} \mathbf{e_k'} \tag{III.20}$$

which can be written as the generalized eigenvalue problem

$$\mathbf{R_x e_k} = \lambda_\mathbf{k} \mathbf{\Sigma_\eta e_k} \ , \tag{III.21}$$

where

$$\mathbf{e_k} = \mathbf{\Sigma_\eta^{-1/2} e_k'} \ . \tag{III.22}$$

The basis vectors that span the signal and noise subspaces in the original coordinate system are

$$\mathbf{b_k} = \mathbf{\Sigma_\eta^{1/2} e_k'} = \mathbf{\Sigma_\eta^{1/2}} \left(\mathbf{\Sigma_\eta^{1/2} e_k}\right) \tag{III.23}$$

or

$$\mathbf{b_k} = \mathbf{\Sigma_\eta e_k} \ . \tag{III.24}$$

Neither the eigenvectors $\mathbf{e_k}$ nor the basis vectors $\mathbf{b_k}$ are orthonormal in the usual sense. The *eigenvalues* satisfy the same conditions, however. Those corresponding to the noise subspace are the $N - M$ smallest eigenvalues (equal to σ_o^2) and those corresponding to signal subspace are the M largest eigenvalues (all greater than σ_o^2).

Let us now return to the case of white noise and the correlation matrix (III.12). It is convenient for our later discussion to define the matrices of eigenvectors

$$\mathbf{E_{sig}} = \begin{bmatrix} | & | & & | \\ \mathbf{e_1} & \mathbf{e_2} & \cdots & \mathbf{e_M} \\ | & | & & | \end{bmatrix} \tag{III.25}$$

and

$$\mathbf{E_{noise}} = \begin{bmatrix} | & | & & | \\ \mathbf{e_{M+1}} & \mathbf{e_{M+2}} & \cdots & \mathbf{e_N} \\ | & | & & | \end{bmatrix}, \tag{III.26}$$

and also the two matrices of eigenvalues

$$\mathbf{\Lambda_{sig}} = \begin{bmatrix} \lambda_1 & 0 & \cdots & 0 \\ 0 & \lambda_2 & \cdots & 0 \\ \vdots & \vdots & \ddots & \vdots \\ 0 & 0 & \cdots & \lambda_M \end{bmatrix} \tag{III.27}$$

and

$$\mathbf{\Lambda_{noise}} = \begin{bmatrix} \lambda_{M+1} & 0 & \cdots & 0 \\ 0 & \lambda_{M+2} & \cdots & 0 \\ \vdots & \vdots & \ddots & \vdots \\ 0 & 0 & \cdots & \lambda_N \end{bmatrix} = \begin{bmatrix} \sigma_o^2 & 0 & \cdots & 0 \\ 0 & \sigma_o^2 & \cdots & 0 \\ \vdots & \vdots & \ddots & \vdots \\ 0 & 0 & \cdots & \sigma_o^2 \end{bmatrix}. \tag{III.28}$$

The complete matrices of eigenvectors and eigenvalues are thus given by

$$\mathbf{E} = [\mathbf{E_{sig}}\ \mathbf{E_{noise}}] \tag{III.29}$$

and

$$\mathbf{\Lambda} = \begin{bmatrix} \mathbf{\Lambda_{sig}} & \mathbf{0} \\ \mathbf{0} & \mathbf{\Lambda_{noise}} \end{bmatrix}. \tag{III.30}$$

Now observe that it is possible to write $\mathbf{R_x}$ as

$$\mathbf{R_x} = \mathbf{E\Lambda E^{*T}} = \mathbf{E_{sig}\Lambda_{sig}E_{sig}^{*T}} + \mathbf{E_{noise}\Lambda_{noise}E_{noise}^{*T}} \tag{III.31}$$

and to write $\mathbf{R_x^{-1}}$ as

$$\mathbf{R_x^{-1}} = \mathbf{E\Lambda^{-1}E^{*T}} = \mathbf{E_{sig}\Lambda_{sig}^{-1}E_{sig}^{*T}} + \mathbf{E_{noise}\Lambda_{noise}^{-1}E_{noise}^{*T}}. \tag{III.32}$$

Further, since the columns of $\mathbf{E_{sig}}$ are orthonormal and define the signal subspace, this matrix can be used to form a projection matrix for the signal subspace,

$$\mathbf{P_{sig}} = \mathbf{E_{sig}}\left(\mathbf{E_{sig}^{*T}E_{sig}}\right)^{-1}\mathbf{E_{sig}^{*T}} = \mathbf{E_{sig}E_{sig}^{*T}}, \tag{III.33}$$

where the last step follows because $\mathbf{E}_{\mathbf{sig}}^{*\mathbf{T}}\mathbf{E}_{\mathbf{sig}} = \mathbf{I}_{\mathbf{M}\times\mathbf{M}}$. Likewise, $\mathbf{E}_{\mathbf{noise}}$ can be used to form a projection matrix for the noise subspace

$$\mathbf{P}_{\mathbf{noise}} = \mathbf{E}_{\mathbf{noise}}\mathbf{E}_{\mathbf{noise}}^{*\mathbf{T}} = \mathbf{I} - \mathbf{P}_{\mathbf{sig}} \ , \tag{III.34}$$

where the last equality follows because the subspaces are orthogonal complements of each other.

B. TYPES OF SUBSPACE METHODS

1. MUSIC

The MUSIC (for MUltiple SIgnal Classification) method forms a correlation matrix of some size $N > M + 1$ from which we try to find the eigenvalues and eigenvectors. From the previous presentation, the eigenvalues and the corresponding eigenvectors are divided into two categories; the ones that "belong" to signal subspace and the others to noise subspace according to the estimated eigenvalues. If the number of signals is not known, it can be estimated by looking at the smallest eigenvalues and finding the set that are approximately equal. This number is equal to $N - M$. The MUSIC method involves projection of the signal onto the *entire noise subspace.* For the MUSIC method we have the following approaches:

1. Use the squared magnitude of the projection of $\mathbf{w}$ onto the noise subspace. Since each of the signals is orthogonal to the noise subspace, the quantity $\mathbf{w}^{*\mathbf{T}}\mathbf{P}_{\mathbf{noise}}\mathbf{w} = \mathbf{w}^{*\mathbf{T}}\mathbf{E}_{\mathbf{noise}}\mathbf{E}_{\mathbf{noise}}^{*\mathbf{T}}\mathbf{w}$ goes to zero for the values of the frequency where $\mathbf{w} = \mathbf{s_i}$. The MUSIC pseudospectrum is defined as

$$\hat{P}_{MU}(e^{j\omega}) = \frac{1}{\mathbf{w}^{*\mathbf{T}}\mathbf{P}_{\mathbf{noise}}\mathbf{w}} = \frac{1}{\mathbf{w}^{*\mathbf{T}}\mathbf{E}_{\mathbf{noise}}\mathbf{E}_{\mathbf{noise}}^{*\mathbf{T}}\mathbf{w}} \tag{III.35}$$

   and therefore exhibits sharp peaks at the signal frequencies where $\mathbf{w} = \mathbf{s_i}$.

2. Use an alternative root-finding variation of the method called "*root MUSIC*". In this approach an eigenfilter $E_i(z)$ is defined as

$$E_i(z) = e_i[0] + e_i[1]z^{-1} + \cdots + e_i[N-1]z^{-(N-1)} \ , \tag{III.36}$$

   where the $e_i[n]$ are components of the eigenvector $\mathbf{e_i}$. In this way the MUSIC pseudospectrum can be expressed as

$$\hat{P}_{MU}(e^{j\omega}) = \left.\frac{1}{\sum_{i=M+1}^{N} E_i(z)E_i^*(1/z^*)}\right|_{z=e^{j\omega}} . \tag{III.37}$$

Since the denominator goes to zero at $z = e^{j\omega_i}(i = 1, 2, \cdots, M)$, the denominator polynomial

$$\hat{P}_{MU}^{-1}(z) = \sum_{i=M+1}^{N} E_i(z) E_i^*(1/z^*) \qquad \text{(III.38)}$$

has M roots *lying on the unit circle.* These M roots (which are, in fact, double roots) correspond to the signal frequencies.

A modification to the MUSIC method was proposed by Johnson and DeGraff [Ref. 23]. From the previous discussion, the MUSIC pseudospectrum can be written as

$$\hat{P}_{MU}(e^{j\omega}) = \frac{1}{\mathbf{w^{*T}} \left(\sum_{\mathbf{i=M+1}}^{\mathbf{N}} \mathbf{e_i e_i^{*T}} \right) \mathbf{w}} \; . \qquad \text{(III.39)}$$

Since the eigenvalues for all the noise subspace eigenvectors are equal to σ_o^2, a pseudospectrum for MUSIC that differs from (III.35) only by a constant can be defined as

$$\hat{P}'_{MU}(e^{j\omega}) = \frac{\sigma_o^2}{\mathbf{w^{*T}} \left(\sum_{\mathbf{i=M+1}}^{\mathbf{N}} \mathbf{e_i e_i^{*T}} \right) \mathbf{w}} = \frac{1}{\mathbf{w^{*T}} \left(\sum_{\mathbf{i=M+1}}^{\mathbf{N}} \frac{\mathbf{1}}{\lambda_\mathbf{i}} \mathbf{e_i e_i^{*T}} \right) \mathbf{w}} \; , \qquad \text{(III.40)}$$

where the last equality follows because $\lambda_i = \sigma_o^2, i = M + 1, \cdots, N$. Equation (III.40) gives the pseudospectrum of the "*modified MUSIC method*" by Johnson and DeGraff which differs from the first approach in that, in practice, the estimated eigenvalues are not all exactly equal.

2. Minimum-Norm Procedure

In the Minimum-norm procedure [Ref. 24, 25] we find a single appropriately chosen vector $\mathbf{d}$ in the noise subspace and define the pseudospectrum in terms of this vector as

$$\hat{P}_{MN}(e^{j\omega}) \stackrel{\text{def}}{=} \frac{1}{|\mathbf{w^{*T}d}|^2} = \frac{1}{\mathbf{w^{*T}dd^{*T}w}} \; . \qquad \text{(III.41)}$$

The vector which lies in the subspace is chosen so that the squared magnitude $||\mathbf{d}||^2$ is minimized subject to the constraint that its first component is equal to 1. The resulting vector is given by

$$\mathbf{d} = \frac{\mathbf{1}}{\mathbf{c^{*T}c}} \mathbf{E_{noise} c} \; , \qquad \text{(III.42)}$$

where $\mathbf{E_{noise}}$ is the matrix of noise subspace eigenvectors and $\mathbf{c^{*T}}$ is the top row from the partition of $\mathbf{E_{noise}}$ such that

$$\mathbf{E_{noise}} = \begin{bmatrix} \mathbf{c^{*T}} \\ \mathbf{E'_{noise}} \end{bmatrix} . \tag{III.43}$$

If the components of $\mathbf{d}$ are denoted by $d[0], d[1], \cdots, d[N-1]$, with $d[0] = 1$, then the minimum-norm pseudospectrum can be equivalently expressed as

$$\hat{P}_{MN}(e^{j\omega}) = \frac{1}{|D(e^{j\omega})|^2} , \tag{III.44}$$

where $D(z)$ is the polynomial

$$D(z) = \sum_{k=0}^{N-1} d[k] z^{-k} . \tag{III.45}$$

Thus the frequencies can also be found as the roots of $D(z)$ on the unit circle.

3. Principal Components Linear Prediction

Another technique involving simple modifications to some of the previously presented methods suggests itself. Whenever there is added noise, let the estimated correlation matrix be represented in terms of only its eigenvectors and eigenvalues pertaining to the *signal* subspace.

$$\mathbf{R_x^{(M)}} \stackrel{\text{def}}{=} \sum_{\mathbf{i=1}}^{\mathbf{M}} \lambda_\mathbf{i} \mathbf{e_i} \mathbf{e_i^{*T}} . \tag{III.46}$$

This is sometimes referred to as the *principal components* approximation of the corelation matrix. This procedure, developed by Tufts and Kumaresan [Ref. 26, 27], amounts to eliminating some of the noise and increasing the overall signal-to-noise ratio. For model-based methods, a model derived from the reduced rank correlation matrix alone can then be generated and used to estimate the spectrum.

Tufts and Kumaresan tried to eliminate the terms in the noise subspace using the pseudoinverse. This task could have even more successful results if a high-order correlation matrix was implemented. If the value of the prediction order variable P

was approximately in the same range with the available data samples (N_s), then the rank of the estimated correlation matrix is automatically reduced. In order to have an exact equality between the rank of the estimated correlation matrix and the number of signals, then the following relationship should hold: $P = N_s - M/2$, where P and N_s are defined above and M is the rank of the pseudoinverse. This specific case is called *Kumaresan-Prony case*. It has the advantage of less computational demands since the SVD of the square matrix is the same as its eigenvalue decomposition, and there is no need for both estimations to be conducted. For minimizing the variance of the frequency estimates, however, a smaller value of $P \approx \frac{3}{4}N_s$ is suggested [Ref. 26, 27]. The filter coefficient vector is thus computed from

$$\mathbf{a}' = -\sum_{\mathbf{i=1}}^{\mathbf{M}} \left(\frac{\mathbf{e_i'^{*T}r}}{\lambda_i'} \right) \mathbf{e_i'} = -\mathbf{R_x'^{+(M)}r} \ , \tag{III.47}$$

where $\mathbf{R_x'}$ and $\mathbf{r}$ are the appropriate partitions of the correlation matrix $\mathbf{R_x}$, and the $\mathbf{e_i'}$, λ_i' are the eigenvectors and eigenvalues of $\mathbf{R_x'}$. The pseudospectrum is given by the final expression

$$\hat{P}_{PCLP}(e^{j\omega}) = \frac{1}{|\mathbf{w^{*T}a}|^2} = \frac{1}{|A(e^{j\omega})|^2}, \tag{III.48}$$

where

$$\mathbf{a} = \begin{bmatrix} 1 \\ \mathbf{a}' \end{bmatrix} . \tag{III.49}$$

If the number of signals M is not known, it has to be estimated from the eigenvalues. The signal frequencies are then determined by either finding the peaks of (III.48) or by finding the roots of $A(z)$.

4. ESPRIT

The ESPRIT (**E**stimation of **S**ignal **P**arameters via **R**otational **I**nvariance **T**echniques) [Ref. 28, 29] method takes a somewhat different approach to frequency spectrum estimation by exploiting a certain invariance principle that exists for the subspaces of two overlapping data sets. Let us consider a data set of $N + 1$ samples

$x[0], x[1], \cdots, x[N]$ and define the two vectors

$$\mathbf{x} = \begin{bmatrix} x[0] \\ x[1] \\ \vdots \\ x[N-1] \end{bmatrix} \quad \textit{and} \quad \mathbf{x}' = \begin{bmatrix} x[1] \\ x[2] \\ \vdots \\ x[N] \end{bmatrix} . \tag{III.50}$$

Let $\mathbf{B}$ and $\mathbf{B}'$ denote two matrices whose columns are basis vectors for the vector spaces associated with $\mathbf{x}$ and $\mathbf{x}'$. It can be shown [Ref. 22] that $\mathbf{B}$ and $\mathbf{B}'$ are related by a set of linear equations of the form

$$\boldsymbol{B\Psi = B'} \ , \tag{III.51}$$

where $\boldsymbol{\Psi}$ is an $M \times M$ square matrix and the eigenvalues of $\boldsymbol{\Psi}$ are of the form $\lambda_i = e^{j\omega_i}$, where ω_i are the desired frequencies.

In the next few lines there will be a short presentation of the steps in the ESPRIT algorithm (TLS version) in order to have an understanding of its functionality. We start by defining the $N+1$-dimensional random vector $\overline{x}$ pertaining to $N+1$ consecutive data samples $x[0], x[1], \cdots, x[N]$ and estimating the correlation matrix $\hat{\mathbf{R}}_{\overline{x}}$ from the data. Then we compute the eigenvectors and eigenvalues of $\hat{\mathbf{R}}_{\overline{x}}$: [1]

$$\hat{\mathbf{R}}_{\overline{x}} \overline{\mathbf{e}}_k = \overline{\lambda}_k \boldsymbol{\Sigma}_{\overline{\eta}} \overline{\mathbf{e}}_{\mathbf{k}} \qquad k = 1, 2, \cdots, N+1 \ . \tag{III.52}$$

If necessary, we estimate the number of signals M from the eigenvalues. Afterwards a basis spanning the signal subspace is generated and is partitioned as

$$\overline{\mathbf{B}} = \boldsymbol{\Sigma}_{\overline{\eta}} \begin{bmatrix} | & & | \\ \overline{\mathbf{e}}_1 & \cdots & \overline{\mathbf{e}}_M \\ | & & | \end{bmatrix} = \begin{bmatrix} & \mathbf{B} & \\ \times & \cdots & \times \end{bmatrix} = \begin{bmatrix} \times & \cdots & \times \\ & \mathbf{B}' & \end{bmatrix} . \tag{III.53}$$

Since $\mathbf{B}$ and $\mathbf{B}'$ will not satisfy III.51 exactly, a Total Least Squares (TLS) approach to computing $\boldsymbol{\Psi}$ is used. The details of TLS are beyond the scope of this presentation.

[1] If the noise is not white III.52 can be replaced by a generalized eigenvalue problem.

However, a general outline would be to first compute the matrix $\mathbf{V}$ of right singular vectors of

$$\begin{bmatrix} \mathbf{B} & \mathbf{B}' \end{bmatrix} \tag{III.54}$$

and then partition $\mathbf{V}$ into four $M \times M$ submatrices

$$\mathbf{V} = \begin{bmatrix} \mathbf{V_{11}} & \mathbf{V_{12}} \\ \mathbf{V_{21}} & \mathbf{V_{22}} \end{bmatrix} . \tag{III.55}$$

The desired estimate for $\mathbf{\Psi}$ is then given by

$$\mathbf{\Psi_{TLS}} = -\mathbf{V_{12}}\mathbf{V_{22}^{-1}} . \tag{III.56}$$

Finally, the desired frequencies are computed as the angle of the complex eigenvalues of $\mathbf{\Psi_{TLS}}$ as shown below

$$\omega_k = \angle\lambda_k; \qquad k = 1, 2, \cdots, M . \tag{III.57}$$

C. APPLICATION TO THE TDOA PROBLEM

A model for the TDOA problem as we have already seen is as follows. We assume that a short transient signal $d[n]$ is emitted from the source. We further assume the signal received at each sensor is subject to amplitude attenuation and additive noise so that the signals x and y can be written in discrete time as

$$\begin{aligned} x[n] &= d[n] + w[n] \\ y[n] &= Ad[n - L] + u[n], \end{aligned} \tag{III.58}$$

where A is the relative amplitude, L is the time delay to be estimated, and u and w are the additive noise terms. Note that we assume the transient signals, d, received at each location are identical but arrive at different times. This assumption will be relaxed in the simulations presented later [Ref. 30]. Let us define $R[k]$ as the product

$$R[k] = X[k]Y^*[k], \tag{III.59}$$

where $X[k]$ and $Y[k]$ are the DFT's of the sequences $x[n]$ and $y[n]$ computed at a size equal to at least twice the length of the data. Thus the inverse transform of $R[k]$ represents an estimate of cross-correlation in the time domain. Now let ω_o represent the frequency resolution of the DFT. The DFT sequences $X[k]$ and $Y[k]$ are then given by

$$\begin{aligned} X[k] &= D[k] + W[k] \\ Y[k] &= AD[k]e^{-\jmath\omega_o kL} + U[k] \end{aligned} \tag{III.60}$$

and from (III.59) and (III.60)

$$R[k] = A|D[k]|^2 e^{\jmath\omega_o kL} + \{D[k]U^*[k] + AD^*[k]W[k]e^{\jmath\omega_o kL} + W[k]U^*[k]\}. \tag{III.61}$$

Let us also assume that the signal $d[n]$ is broadband, and that the source spectrum is flat and therefore the magnitude $|D[k]|$ is approximately constant. Further, if the observed time sequences (x and y) are sufficiently long, the points in the DFT sequence for the term enclosed in brackets will be approximately uncorrelated. Thus the sequence $R[k]$ satisfies the basic model for signal subspace analysis [Ref. 22], but with time and frequency interchanged.

For the following discussion, we shall consider both related approaches to estimating TDOA. In the first approach a steering vector of the form

$$\begin{bmatrix} 1 & e^{\jmath\omega_o l} & e^{\jmath 2\omega_o l} & \cdots & e^{\jmath(N-1)\omega_o l} \end{bmatrix}$$

is projected onto the noise subspace and the reciprocal of the result is plotted as the lag parameter l is varied. (Here N is the dimension of the observation used in the chosen subspace method.) The resulting function, which we refer to as a delay indicator function (DIF), peaks at the desired estimate $l = L$. Although the DIF resembles a generalized cross-correlation function, it is strictly speaking *not* a GCC. It is analogous to the pseudospectrum used in the spectral estimation problem. In the second approach, direct numerical estimates are computed and no DIF is formed. Root MUSIC and ESPRIT follow this approach.

IV. THESIS APPROACH TO THE PROBLEM

In order to verify all the theoretical results described in Chapters 2 and 3, various simulations were conducted. All the simulations are divided into two categories depending on the kind of the data that were used. The first category used synthetic data generated from equations in MATLAB while the second category used data generated by the Monterey-Miami Parabolic Equation (MMPE) acoustic propagation model [Ref. 14, 15].

All the simulations using the synthetic data assumed the same shape and form and length of transient at each receiver but for each one we added different noise with variations according to kind (white-colored), characteristics (variance), and amount of noise (SNR). White or colored Gaussian noise was generated in MATLAB and added to the signals to achieve a specified signal-to-noise ratio (SNR). The SNR specifically was defined by the formula

$$SNR = \frac{\frac{1}{N}\sum_{n=0}^{N-1} s^2[n]}{\sigma_N^2}\ , \tag{IV.1}$$

where N is the number of the samples of the signal, $s[n]$, and σ_N^2 is the variance of the additive noise (white or colored). For the MMPE data, the received transients were different, in general, and noise was added with variations as before. In this way we kept all the basic assumptions that we made in Chapter 1 for the TDOA problem.

A. SYNTHETIC DATA

For the synthetic data five different kinds of transients were used:

1. exponential transient of the form

$$s(t) = \begin{cases} \exp(-dt), & 0 \le t \le T \\ 0, & otherwise \end{cases}\ , \tag{IV.2}$$

where d is the decay factor and T is the time duration (length) of the exponential transient;

2. sinusoidal transient of the form

$$s(t) = \begin{cases} \sin(2\pi f t), & 0 \le t \le T \\ 0, & otherwise \end{cases}, \tag{IV.3}$$

where f is the frequency and T is the time duration (length) of the sinusoidal transient;

3. damped sinusoidal transient which is a combination of the first two transients,

$$s(t) = \begin{cases} \exp(-dt) \cdot \sin(2\pi f t), & 0 \le t \le T \\ 0, & otherwise \end{cases}, \tag{IV.4}$$

4. linear swept-frequency cosine generator ($chirp(T, f_0, T_1, f_1)$) transient,

$$s(t) = \begin{cases} e^{\left(j2\pi\left[f_0 t + \frac{1}{2}\beta t^2\right]\right)}, & 0 \le t \le T \\ 0, & otherwise \end{cases}, \tag{IV.5}$$

This function creates samples of a linear swept-frequency cosine signal at the time instances defined in array T, f_0 is the instantaneous frequency at time 0, and f_1 is the instantaneous frequency at time T_1. Both f_0 and f_1 are in Hertz. In our case the instantaneous frequency sweep $f_i(t)$ given by

$$f_i(t) = \begin{cases} f_0 + \beta t, & 0 \le t \le T \\ 0, & otherwise \end{cases}, \tag{IV.6}$$

where

$$\beta = \frac{f_1 - f_0}{T_1}; \tag{IV.7}$$

5. damped chirp transient which is the combination of the first and fourth transients,

$$s(t) = \begin{cases} \exp(-dt) \cdot e^{\left(j2\pi\left[f_0 t + \frac{1}{2}\beta t^2\right]\right)}, & 0 \le t \le T \\ 0, & otherwise \end{cases}, \tag{IV.8}$$

In this way we were able to compare the performance of the classical and subspace methods not only by varying the characteristics of the noise but also by changing the characteristics of the original transients. This was done in order to have a more complete evaluation of the above methods.

B. MODEL BASED ACOUSTIC DATA

Although they provide a way to test algorithms under ideal conditions, we understand the simulated data in MATLAB does not approach the real conditions that occur in the ocean. For this reason we used data from the MMPE model to test the TDOA methods under more realistic conditions. This allowed us to test them in more complex environments, where additional factors like area geography, water column and bottom characteristics, sound speed profile, etc., can change and influence the result of the sound wave propagation.

1. Monterey-Miami Parabolic Equation (MMPE) Model and Split-Step Fourier (PE/SSF) Algorithm

Before presenting data generated by the MMPE model, it is informative to describe what the model is what the model is and what it is capable of. We begin by defining the time-harmonic acoustic field in cylindrical coordinates (r, z, ϕ)

$$P(r, z, \phi, \omega t) = p(r, z, \phi)e^{-i\omega t}. \tag{IV.9}$$

The result of the combination of Eq. (IV.9) with the wave equation, also in cylindrical coordinates, produces the Helmholtz equation,

$$\frac{1}{r}\frac{\partial}{\partial r}\left(r\frac{\partial p}{\partial r}\right) + \frac{1}{r^2}\frac{\partial^2 p}{\partial \phi^2} + \frac{\partial^2 p}{\partial z^2} + k_o^2 n^2(r, z, \phi)p = -4\pi P_o \delta(\vec{x} - \vec{x_S}) \ , \tag{IV.10}$$

where $k_o = \frac{\omega}{c_o}$ is the reference wavenumber, $n(r, z, \phi) = \frac{c_o}{c(r,z,\phi)}$ is the acoustic index of refraction, c_o is the reference sound speed, and $c(r, z, \phi)$ is the acoustic sound speed. Most of the properties of the environment are provided by $c(r, z, \phi)$. Regarding the source function, it is assumed to be a point source located at a distance of $r = 0$m and depth $z = z_S$ and with reference source level P_o. This reference source level is the pressure amplitude at a reference distance of $R_o = 1m$, and

$$\delta(\vec{(x)}) = \frac{1}{2\pi r}\delta(\vec{z} - \vec{z_S})\delta(r) \tag{IV.11}$$

is the Dirac-delta function defining the point source contribution.

For simplification of the Helmholtz equation, we assume that the cylindrical spreading dominates the propagation, and the magnitude of the pressure vector will be given by

$$p(r,z) = \frac{1}{\sqrt{r}} u(r,z). \tag{IV.12}$$

Substituting Eq. (IV.12) into the Helmholtz equation and neglecting the source term, we end up with the following equation

$$\frac{\partial^2 u}{\partial r^2} + \frac{1}{r^2}\frac{\partial^2 u}{\partial \phi^2} + \frac{\partial^2 u}{\partial z^2} + k_o^2\left(n^2 + \frac{1}{4k_o^2 r^2}\right)u = 0. \tag{IV.13}$$

In Eq. (IV.13), we observe that both the final term and the second term , which introduces azimuthal coupling between different radials, are proportional to $\frac{1}{r^2}$. Therefore, invoking the uncoupled azimuth approximation, these terms will be neglected in this analysis.

Defining the operator notation

$$P_{op} = \frac{\partial}{\partial r} \tag{IV.14}$$

and

$$Q_{op} = (\mu + \varepsilon + 1)^{1/2}\ , \tag{IV.15}$$

where

$$\varepsilon = n^2 - 1, \quad \mu = \frac{1}{k_o^2}\frac{\partial^2}{\partial z^2}\ , \tag{IV.16}$$

the homogeneous form of Eq. (IV.10) then becomes

$$(P_{op}^2 + k_o^2 Q_{op}^2)u = 0\ . \tag{IV.17}$$

Proper factorization of the outward propagation field is obtained by defining

$$u = Q_{op}^{-1/2}\Psi. \tag{IV.18}$$

Because of the small range dependence of the environment it is also assumed that the commutator $[P_{op}, Q_{op}]$ is negligible. The outgoing wave then satisfies [Ref. 14, 15].

$$-ik_o^{-1}\frac{\partial \Psi}{\partial r} = Q_{op}\Psi. \tag{IV.19}$$

The physical meaning of the Eq. (IV.19) is the representation acoustic energy in the waveguide, particularly the forward propagating acoustic energy when the backscattered energy is not significant. In other words Eq. (IV.19) is considered to be the basic equation upon which all one-way PE models are "built". The next step is to create a method for generating solutions to this equation by developing approximations to the pseudo-differential operator Q_{op}.

For the creation of the numerical algorithm which will solve the PE, we observe that the acoustic field can be divided into a slowly modulating envelope function and a phase term which oscillates at the acoustic frequency. The PE field function, $\psi(r, z, \phi)$, is defined as

$$\Psi = \psi e^{ik_o r} \tag{IV.20}$$

or, in terms of the acoustic pressure,

$$p(r, z, \phi) = P_o \sqrt{\frac{R_o}{r}} Q_{op}^{-1/2} \psi(r, z, \phi) e^{ikor}. \tag{IV.21}$$

The last equation is scaled in such a way that at $r = R_o$, $|\psi| = 1$ and $|p| = P_o$. Combining Eq. (IV.21) with the Helmholtz equation will provide us with wave equation for the PE field function,

$$\frac{\partial \psi}{\partial r} = -ik_o \psi + ik_o Q_{op} \psi = -ik_o H_{op} \psi, \tag{IV.22}$$

where

$$H_{op} = 1 - Q_{op} \tag{IV.23}$$

is a Hamiltonian-like operator which defines the evolution of the PE field function in range.

In Eq. (IV.22), the function ψ is a vector (in z) in Hilbert space. The relationship between the values of ψ at different ranges can now be expressed as

$$\psi(r + \Delta r) = \Phi(r)\psi(r). \tag{IV.24}$$

To propagate the solution out in range requires a representation of the propagator $\Phi(r)$. The MMPE model uses the split-step Fourier (PE/SSF) method to compute PE solutions.

In the SSF algorithm the operators H_{op} and Q_{op} are a combination of scalar and differential operators. For the appropriate functionality of the SSF algorithm the different terms within H_{op} should be separated, requring an approximation to the square-root operator. In the MMPE model, the wide-angle PE (WAPE) approximation of Thompson and Chapman is employed [Ref. 14, 15], such that

$$H_{op} \approx T_{op} + U_{op} \tag{IV.25}$$

where

$$T_{op} = 1 - \left[1 + \frac{1}{k_o^2}\frac{\partial^2}{\partial z_2}\right]^{1/2}, \tag{IV.26}$$

and

$$U_{op} = -(n-1). \tag{IV.27}$$

In this form, the differential operator has been separated from the index of refraction term as required for implementation with the SSF technique. In z-space, the operator U_{op} is a simple scalar multiplication operator, in other words a diagonal matrix, but the operator T_{op} is not a diagonal matrix, so different depth eigenfunctions are coupled. However, in vertical wavenumber space, the corresponding operator $\hat{T}_{op}$ is diagonal.

The MMPE propagator function is then based on the "centered step" scheme,

$$\Phi(r) = e^{-ik_o\frac{\Delta r}{2}U_{op}(r+\Delta r)}e^{-ik_o\Delta r T_{op}}e^{-ik_o\frac{\Delta r}{2}U_{op}(r)}, \tag{IV.28}$$

where error analysis shows that this scheme provides third order accuracy in Δr, and is the method used in the MMPE implementation. The general algorithm behind the PE/SSF implementation is then as follows. The PE field function ψ is specified at some range r in the z-domain. A multiplication of the z-space operator $e^{-ik_o\frac{\Delta r}{2}U_{op}(r)}$ defined at the beginning of the range-step is applied. A transformation is then made

to the k_z-domain followed by a multiplication of the k_z-space operator $e^{-ik_o\Delta r\hat{T}_{op}}$. The result is then transformed again to the z-domain followed by a multiplication of the z-space operator $e^{-ik_o\frac{\Delta r}{2}U_{op}(r+\Delta r)}$ defined at the end of the range-step. The final result is the field function at $r+\Delta r$. The discrete fast Fourier transform (FFT) subroutine employed in the numerical code assumes the convention

$$\psi(z) = FFT(\psi(k_z)) \tag{IV.29}$$

and

$$\psi(k_z) = IFFT(\psi(z)). \tag{IV.30}$$

Therefore, the PE/SSF implementation can be represented by

$$\psi(r+\Delta r, z) = e^{-ik_o\frac{\Delta r}{2}U_{op}(r+\Delta r,z)} \times FFT\left\{e^{-ik_o\Delta r T_{op}(k_z)} \times IFFT\left[e^{-ik_o\frac{\Delta r}{2}U_{op}(r,z)} \times \psi(r,z)\right]\right\}, \tag{IV.31}$$

where, in k_z-space,

$$\hat{T}_{op}(k_z) = 1 - \left[1 - \left(\frac{k_z}{k_o}\right)^2\right]^{1/2}. \tag{IV.32}$$

2. Data Modulation-Demodulation

The MMPE model is a broadband, full-wave acoustic propagation model based on the parabolic approximation to the Helmholtz equation. After defining all the necessary parameters for the entire environment (such as sound speed profile, bathymetry of the water/bottom interface, the acoustic parameters of the bottom, the source information), this model computes the complex pressure, transmission loss, and arrival time structure for any point on a computational grid in range and depth.

Broadband results are obtained by running the MMPE model for all discrete frequencies in the chosen bandwidth. The travel time results are then realized by performing a Fourier synthesis and a necessary multiplication by some window function, $S(f)$. The complex arrival structure of the pressure field can then be written

$$P(r,z,t) = \int_{-\infty}^{\infty} S(f)p(r,z,f)e^{-i2\pi ft}df = \frac{P_oR_o}{\sqrt{r}}\int_{-\infty}^{\infty} S(f)e^{-ik_or}\Psi(r,z,f)e^{-i2\pi ft}df. \tag{IV.33}$$

By defining the reduced time $T = t - \left(\frac{r}{c_o}\right)$, the phase factor $e^{-ik_o r} = e^{-i2\pi f \frac{r}{c_o}}$ can be absorbed, such that

$$P(r, z, T) = \frac{P_o R_o}{\sqrt{r}} \int_{-\infty}^{\infty} S(f)\Psi(r, z, \phi)e^{-i2\pi fT} df. \qquad \text{(IV.34)}$$

Note that the use of reduced time does not influence the autocorrelation function.

For all the environments tested the same window function was used. The modeled transmitted pulse had a center frequency of 400 Hz with a bandwidth of 128 Hz and with 256 frequency bins computed in the DFT. This creates a signal of duration 2 sec in the time-domain. In order to obtain the real pressure for each sonobuoy (receiver) while maintaining the initial assumption that all the receivers were receiving the signals of the same duration, we developed the following procedure.

- First the frequency-domain complex pressure vector, corresponding to each receiver, was multiplied by a "Hanwin" factor. This "Hanwin" factor is a Hanning window with length equal of the number of the frequency bins.
- In order to add the carrier in the baseband signal, we had to append to both sides of the frequency-domain vector a number of zeros, creating a total length of 1024 bins. This will assist us with the frequency resolution that we are going to work with in order not to lose any information from the original transient. In this way, that part of spectrum corresponding to positive frequencies is formed.
- The part of the spectrum corresponding to negative frequencies was formed by taking the conjugate reverse of the original vector and appending it to the original vector. This produced a complete frequency-domain representation of the measured signal over 2048 frequency bins. The corresponding sampling frequency on the receiver was then 512 Hz.
- Performing an FFT on this complex frequency-domain signal produced a real time-domain signal that represented the measurement on the receiver. Due to a small imaginary component due to the numerical processing, the real part of this signal was extracted for use in the TDOA algorithms.
- Before adding noise to the transients, all transients must be in absolute time and not in reduced time, as in the previous step. For this procedure, a number of zeros are pre-appended, which for each pair of receivers is equal to the fraction of the difference of the two distances (of the 2 receivers) divided by the factor $dt = 1/1024$.

3. MMPE Environments

Before proceeding with the simulation results, let us describe the four test cases that were used with the MMPE model. This will provide a common reference not only for the TDOA simulation results but also for the localization and tracking problems presented in the next chapters. The four environments are:

1. **Flat Bottom**
2. **Sound Channel**
3. **Shelf Break**
4. **Internal Waves**

The first two of these are *range-independent (RI)* while the last two are *range-dependent (RD)*. The main difference between these two categories is that in the range-independent case the received signal at each sonobuoy depends only on the distance between the source and the receiver. In other words, the sound speed profile and bottom are the same at every point in the area of interest. In the range-dependent case the sound speed profile and/or bottom changes according to range and direction from the source. This makes it more difficult to simulate since one has to be aware in more detail about the environmental conditions. Range-dependent simulations provide more realistic data consistent with the complicated conditions that occur in the ocean.

a. Flat Bottom

This environment is defined by a flat ocean bottom and isospeed water column. In our case we have regularly spaced values of bottom parameters. At each range location, the bottom is assumed to be a homogeneous half-space below that position. The specific values of the properties for the case are listed in Table II:

b. Sound Channel

This range-independent case is similar to the previous one with the following major differences. First, the bottom bathymetry is varying and the sound

Bathymetry	flat (300 m depth)
Sound Speed Profiles	isospeed (1500 m/s)
Water Density	1 g/cm^3
Water Attenuation	0.0 dB/λ
Bottom Sound-Speed	1700 m/s
Bottom Density	1.6 g/cm^3
Compressional Bottom Attenuation	0.1 dB/km/Hz
Shear	None

Table II. Environmental Properties for RI Test case: "Flat Bottom".

speed profile, which is the same for the entire computational grid, is defined by the following equations:

$$c = \begin{cases} 1515 + 0.016z & \text{when } z \in [z_{surf}, z_{duct}] \\ 1490\left[1 + 0.25\left(e^{\left(-\frac{z-z_{axis}}{500}\right)} + \left(\frac{z-z_{axis}}{500}\right) - 1\right)\right] & \text{when } z \in [z_{duct}, z_{max}] \end{cases}, \quad \text{(IV.35)}$$

where $z_{surf} = 0$m is the surface depth, $z_{duct} = 75$m is the depth of the surface duct, $z_{max} = 500$m is the maximum depth and $z_{axis} = 200$m is the depth of the axis of the sound channel. The sound speed profile is shown in Fig. 7. The specific values of the properties for the case are listed below in Table III.

Bathymetry	varying
Sound Speed Profiles	varying
Water Density	1 g/cm^3
Water Attenuation	0.0 dB/λ
Bottom Sound-Speed	1700 m/s
Bottom Density	1.6 g/cm^3
Compressional Bottom Attenuation	0.1 dB/km/Hz
Shear	None

Table III. Environmental Properties for RI Test case: "Sound Channel".

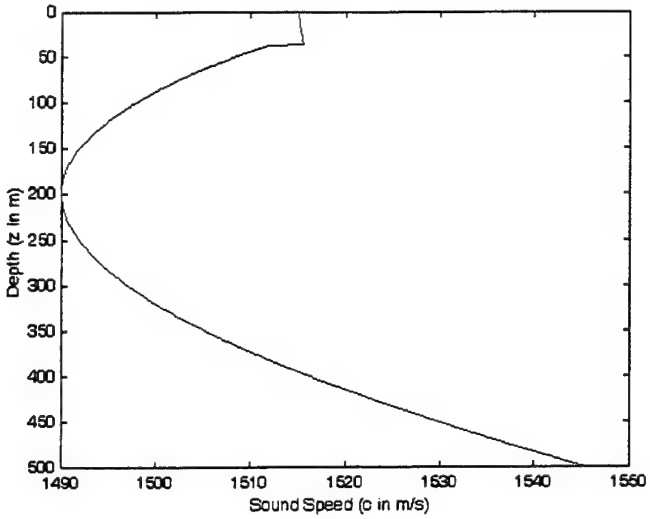

Figure 7. Sound Speed Profile for RI Test case: Sound Channel.

c. Shelf Break

The next case has to do with a range-dependent environment similar to that found in the regions of continental shelf breaks. This environment is defined by both a varying water column sound speed and bottom bathymetry with homogeneous bottom acoustical properties. This environment is loosely based on shelf break front structures observed during the ONR Primer experiment [Ref. 31]. The general properties of this test case are defined in Table IV.

Bathymetry	varying
Sound Speed Profiles	varying
Water Density	1 g/cm^3
Water Attenuation	0.0 dB/λ
Bottom Sound-Speed	1700 m/s
Bottom Density	1.5 g/cm^3
Compressional Bottom Attenuation	0.1 dB/km/Hz
Shear	None

Table IV. Environmental Properties for RD Test case: "Shelf Break".

The vertical sound speed profile and bathymetry for this case are displayed in Fig. 8(a). This characteristic is extended infinitely in the direction perpendicular to the page providing a 3-D shelf break environment. The locations of the source and two of the receivers are shown in Fig. 8(b), which is the same environment as Fig. 8(a) but viewed from the top. Isobaths are also drawn to provide a better perspective on the relative positions of the source and receivers.

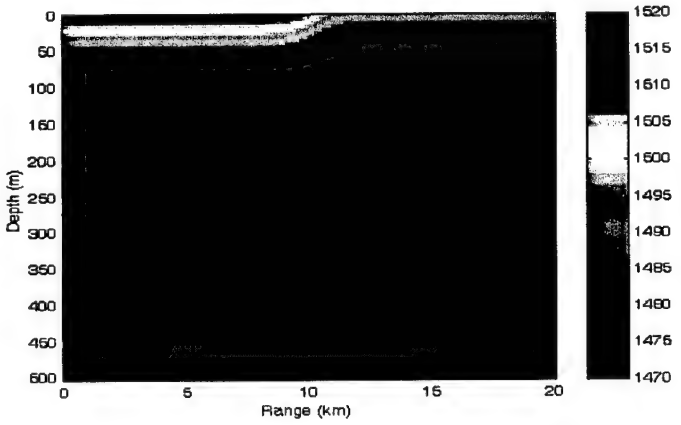

(a)

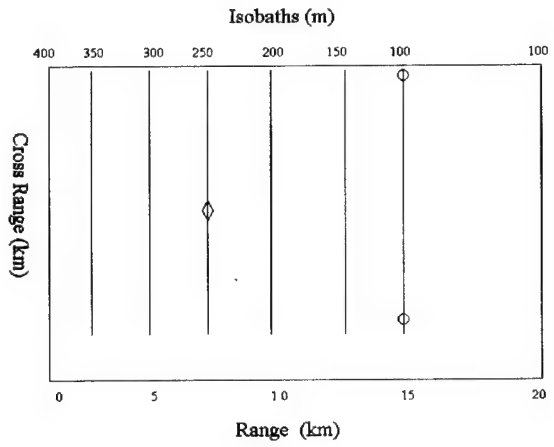

(b)

Figure 8. Sound speed profile: (a) Shelf break environment vertical view. (b) Shelf break environment horizontal view with sample locations of source and receivers.

d. Internal Waves

This environment is defined by varying water column sound speed features and a flat, homogeneous bottom. More specifically this test case is the combination of a simple, sinusoidally varying perturbation with a soliton wavefield, and is loosely based on the work of Tielburger, Finette, and Wolf [Ref. 32]. The aforementioned environment is characterized by the following properties as shown in Table V.

Bathymetry	Flat bottom (zb = 200 m depth)
Sound Speed Profiles	varying
Water Density	1 g/cm^3
Water Attenuation	0.0 dB/λ
Bottom Sound-Speed	1700 m/s
Bottom Density	1.5 g/cm^3
Compressional Bottom Attenuation	0.1 dB/km/Hz
Shear	None

Table V. Environmental Properties for RD Test case: "Internal Waves".

The background (range-independent) sound speed profile used is the same as defined in Eq. (IV.35). The perturbations to this background are a combination of a sum of simple sinusoids and a train of soliton waves. The sinusoidal perturbations are defined by

$$dcsin(z,r) = C\left(\frac{z}{B}\right)e^{\left(-\frac{z}{B}\right)}\sum_{i=1}^{5}\{\cos\left(K(i)r\right)\} \tag{IV.36}$$

where $K(i) = \frac{2\pi}{[(2000m)-(i-1)(300m)]}$, $B = 25m$, and C is defined such that the maximum value for $dcsin$ is $7.5m/s$.

The soliton perturbation is defined by

$$dcsol(z,r) = C\left(\frac{z}{B}\right)e^{\left(-\frac{z}{B}\right)}\sum_{i=1}^{6}\left\{A(i)\left[sech\left(\frac{(R(i)-r)}{D(i)}\right)\right]^2\right\} \tag{IV.37}$$

where $B = 25m$, $A(i) = 10e^{(-0.3(i-1))}$, $D(i) = \sqrt{\left(\frac{34300}{A_i}\right)}$, $R(i) = R(i-1) - (7-i)500$ for $i = 2, \cdots, 6$, $R(1) = 14000m$, and C is defined such that the maximum value for dc is $12.5m/s$.

The combination of the above perturbations is then simply defined by

$$dc(z,r) = dcsol(z,r) + dcsin(z,r) \tag{IV.38}$$

and the result for the total sound speed structure is depicted in Fig. 9. Note that the solitons are modeled as propagating only in the plane of the page while the internal wave sinusoids are considered randomly oriented in all directions. For the

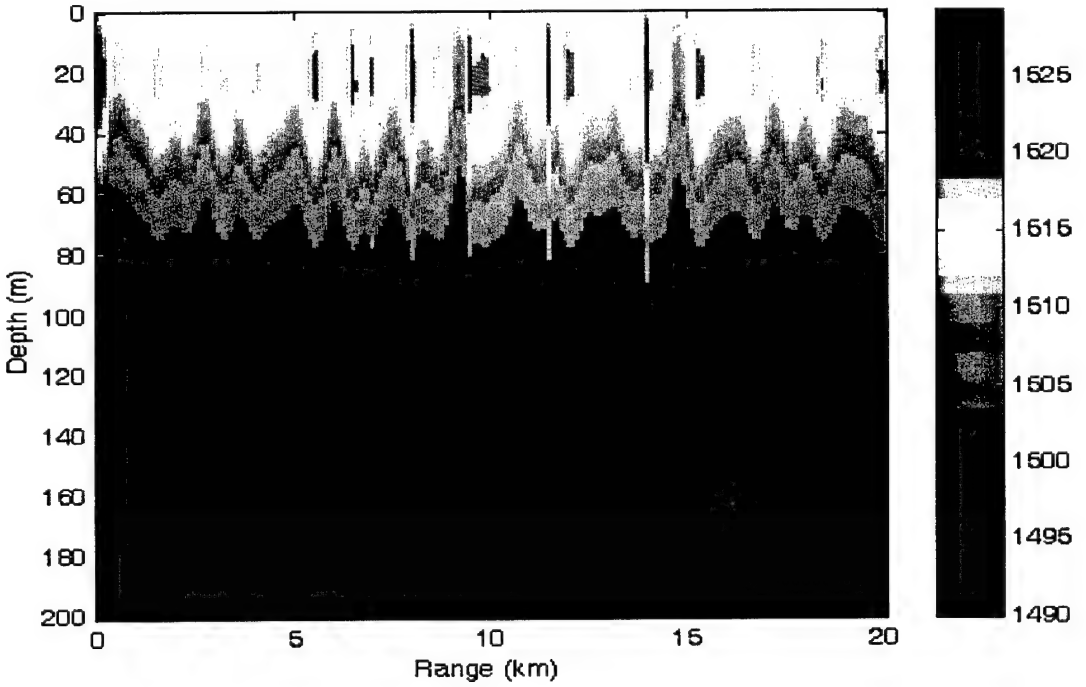

Figure 9. Sound speed profile: Combination of Sinusoidal and Soliton Perturbations.

range-independent environments the source depth was between 140m and 160m and the locations of the receivers were at ranges between 2km and 8km and at depths between 40m and 60m. For the Shelf Break environment the source depth was at 250m and the receivers were at a depth of 100m at ranges between 2km and 5km,

while for the Internal Waves environment the source depth was at 150m and the receivers were at a depth of 50m and at the same ranges as in the Shelf Break. Better insight to the scenarios is given in the next chapter, where the simulation results for the TDOA are presented.

THIS PAGE INTENTIONALLY LEFT BLANK

V. TDOA SIMULATION RESULTS

A. SYNTHETIC DATA

In this section we present simulation results using synthetic data in the TDOA estimation problem. Our purpose is to distinguish how the two families of methods (classical - subspace) perform, what their basic differences are, and finally which method(s) produce the best overall results. Since the number of combinations using different signals, kind and amount of noise, and different characteristics of the signals and of the methods is huge, we have tried to provide some typical cases in order to provide insight into the behavior of the methods. We will try to explain how the different factors attribute to the final result, which is the estimation of TDOA.

In the first subsection of the synthetic data we present cases from "Exponential", "Sinusoidal", "Damped Sinusoidal", "Chirp" and finally "Damped Chirp" signals at different noise levels (SNR 15, 10, 5 dB). Our intent is to show the behavior of the methods when the transient duration changes (short to long) and how successful they are when the desired TDOA to be predicted is large or small. In all cases there are different realizations of white noise with different variance added to each transient. For the subspace methods, the size of the covariance matrix (see Chapter 3) taken was 10 and 20 samples, and for the classical methods the number of segments (see Chapter 2) was either 1 or 2. In addition to the figures, corresponding tables summarize the results in order to provide a quick appreciation of each method's behavior.

In the second subsection of the synthetic data, we merge both kinds of methods (classical-subspace) to examine how the category of methods influences the other and, of course, if there is any substantial improvement in the results.

1. Implementation Using Individual Methods

The cases, whose results are presented in this subsection and in Appendix A, using synthetic data are the following:

- exponential transient with length of 100s and actual TDOA 50s;
- exponential transient with length of 20s and actual TDOA 100s;
- exponential transient with length of 50s and actual TDOA -10s;
- sinusoidal transient with length of 100s and actual TDOA 50s;
- damped sinusoidal transient with length of 100s and actual TDOA 50s;
- chirp transient with length of 100s and actual TDOA 50s; and
- damped chirp transient with length of 100s and actual TDOA 50s .

Each case was tested with different realizations of additive noise and under three different levels of SNR. The figures and the comparative table for the first case is presented in this subsection. The remaining case results are submitted in Appendix A. Even though we have tested each kind of transient thoroughly changing various parameters, apart from the ones already defined, we have observed that the major influence to the desired result of TDOA is provoked by the noise (SNR), length of transient, amount of predicted TDOA, size of covariance matrix (for subspace methods), number of segments (for classical methods), and kind of transient. Having all the above in mind, we picked three typical cases from one kind of transient in order to see how the methods perform under different values of the aforementioned factors, and the same case from the rest of the transients for checking possible difficulties in estimating the TDOA for a particular type of signal.

Figures 10 through 15 show TDOA results for the exponential transient for all methods using SNR values of 15dB, 10dB, and 5dB. The estimated values of time delay are listed in Table VI.

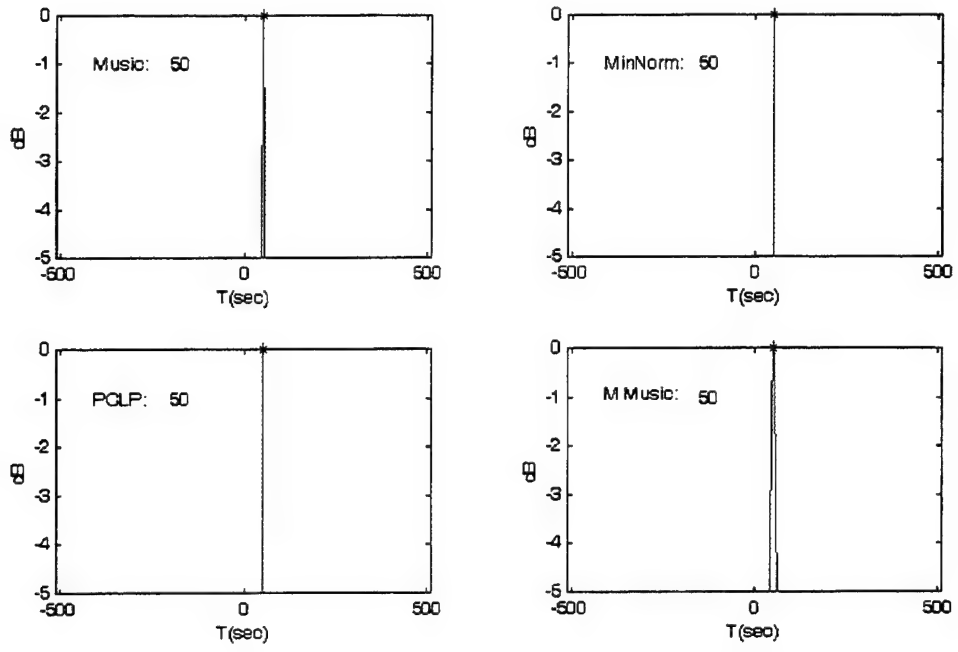

(a)

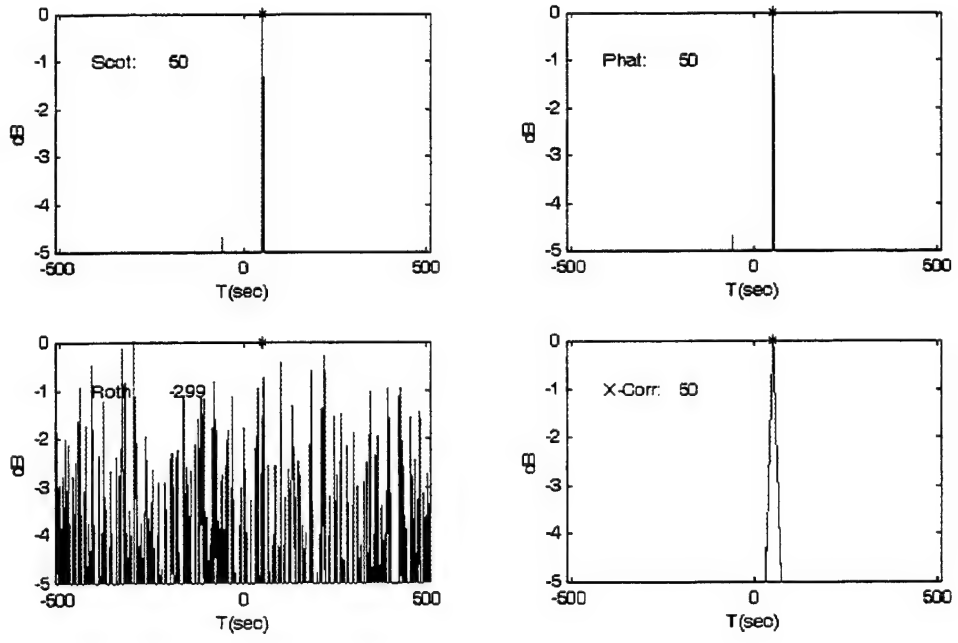

(b)

Figure 10. Exponential transient: length L=100s; Actual TDOA=50s; SNR=15dB; White-Noise (σ_o^2). (a) Subspace methods, Covariance Size=10. (b) Classical methods, number of segments=1.

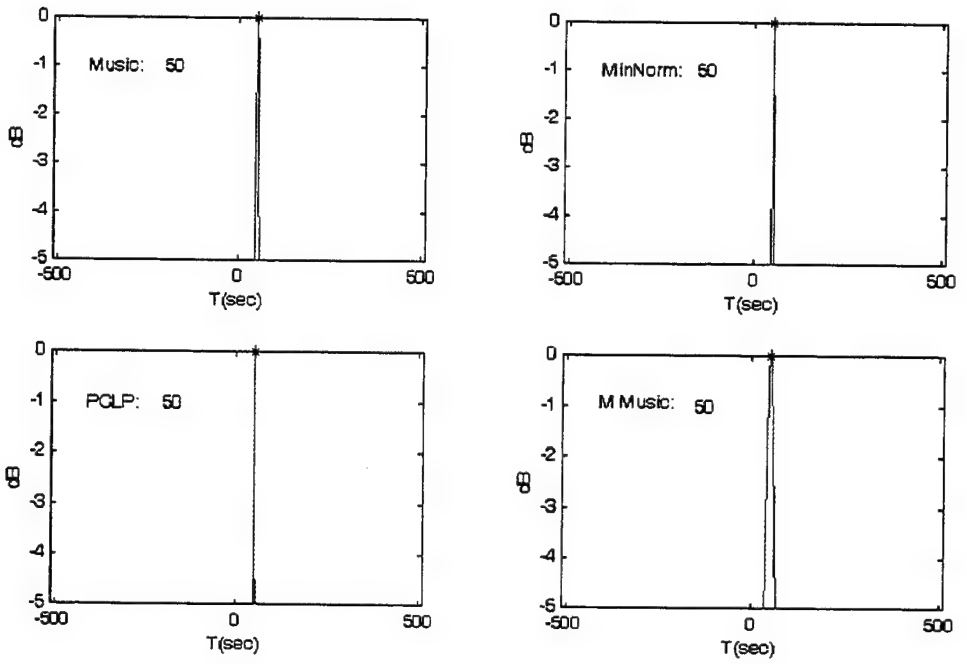

(a)

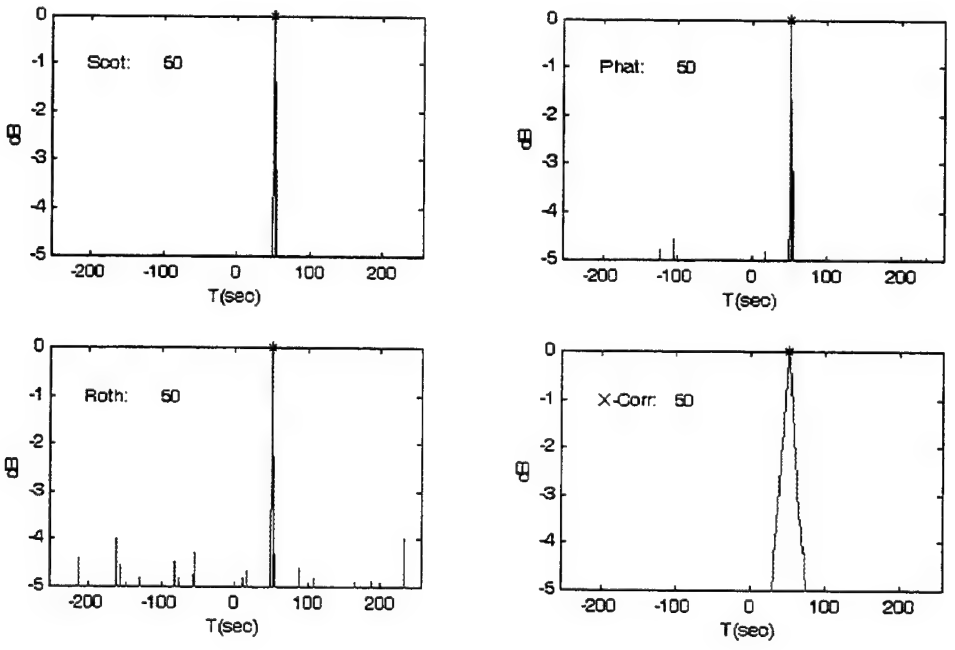

(b)

Figure 11. Exponential transient: length L=100s; Actual TDOA=50s; SNR=15dB; White-Noise (σ_o^2). (a) Subspace methods, Covariance Size=20. (b) Classical methods, number of segments=2.

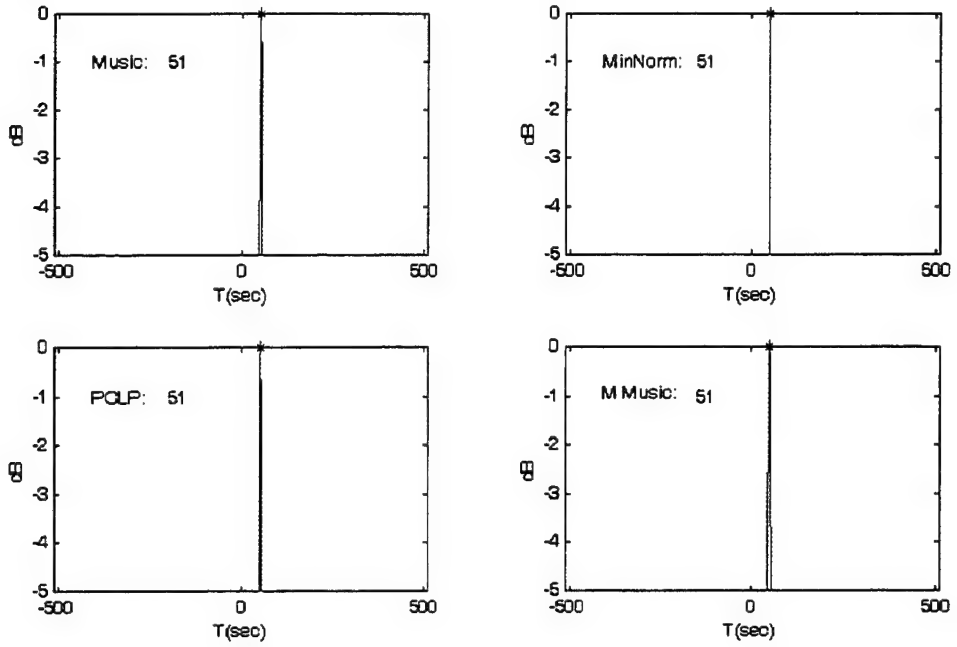

(a)

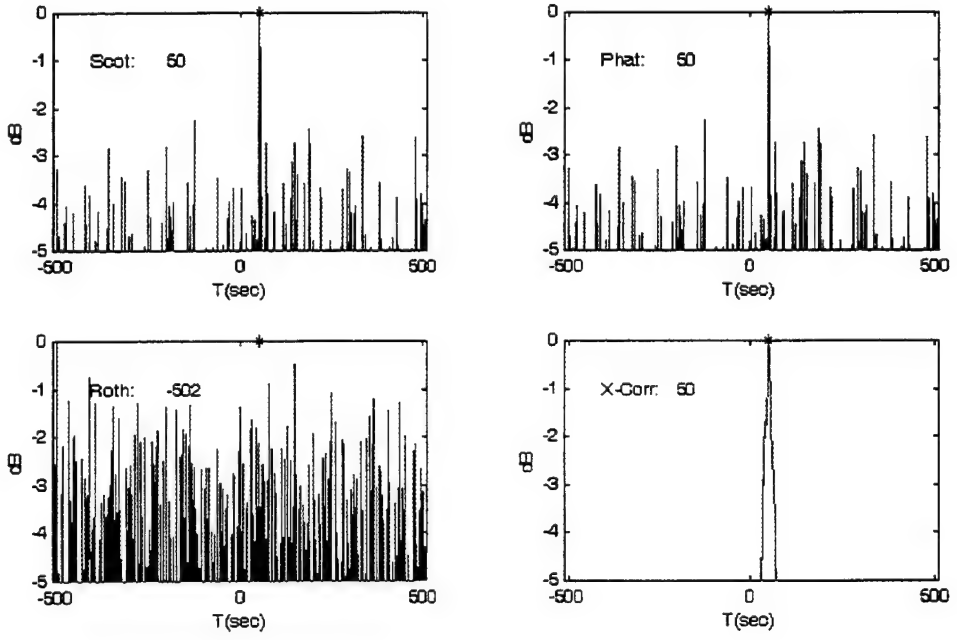

(b)

Figure 12. Exponential transient: length L=100s; Actual TDOA=50s; SNR=10dB; White-Noise (σ_o^2). (a) Subspace methods, Covariance Size=10 (b) Classical methods, number of segments=1

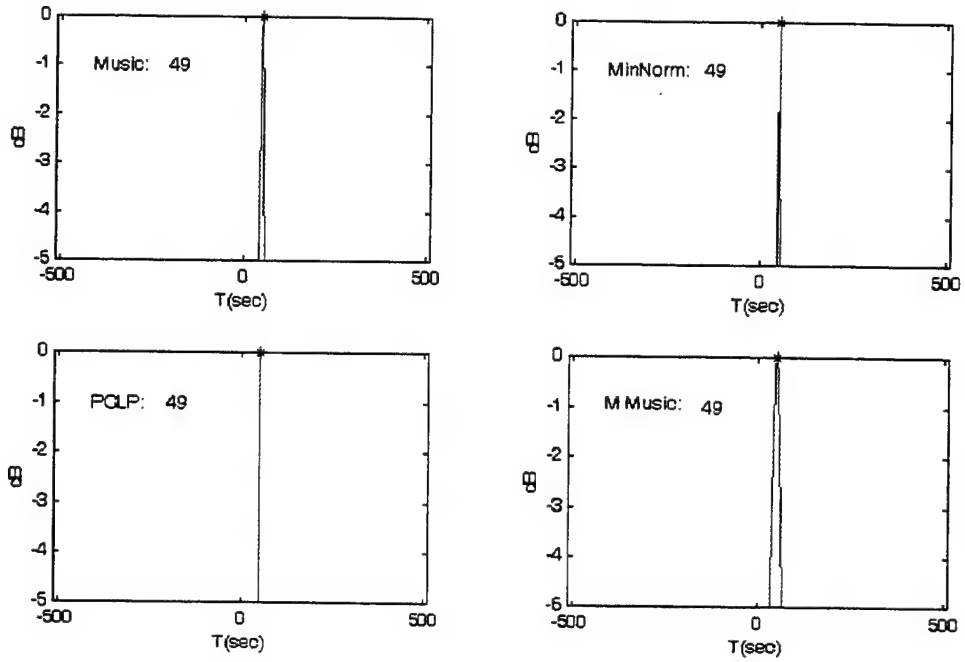

(a)

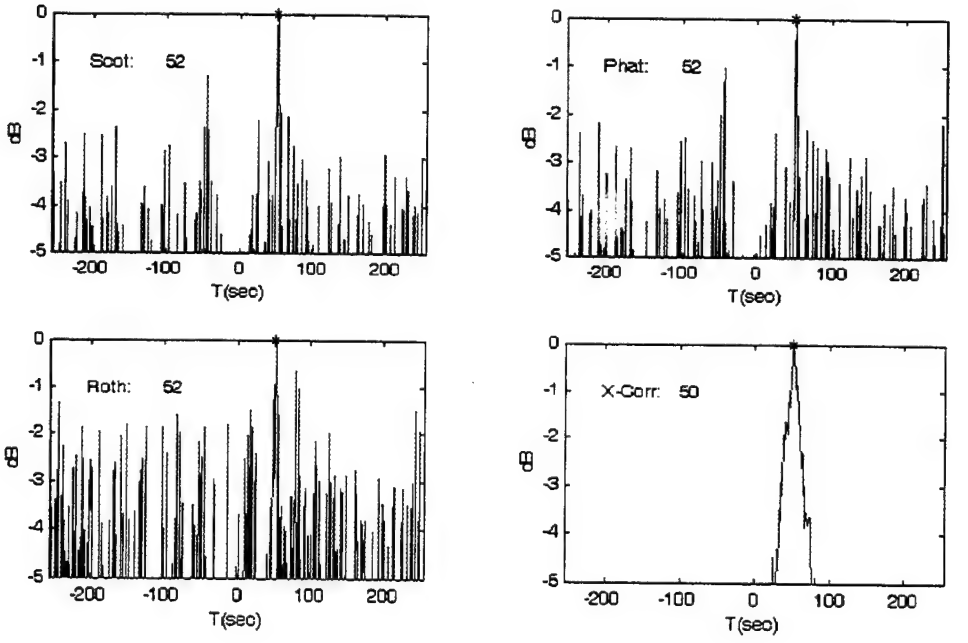

(b)

Figure 13. Exponential transient: length L=100s; Actual TDOA=50s; SNR=10dB; White-Noise (σ_o^2). (a) Subspace methods, Covariance Size=20. (b) Classical methods, number of segments=2.

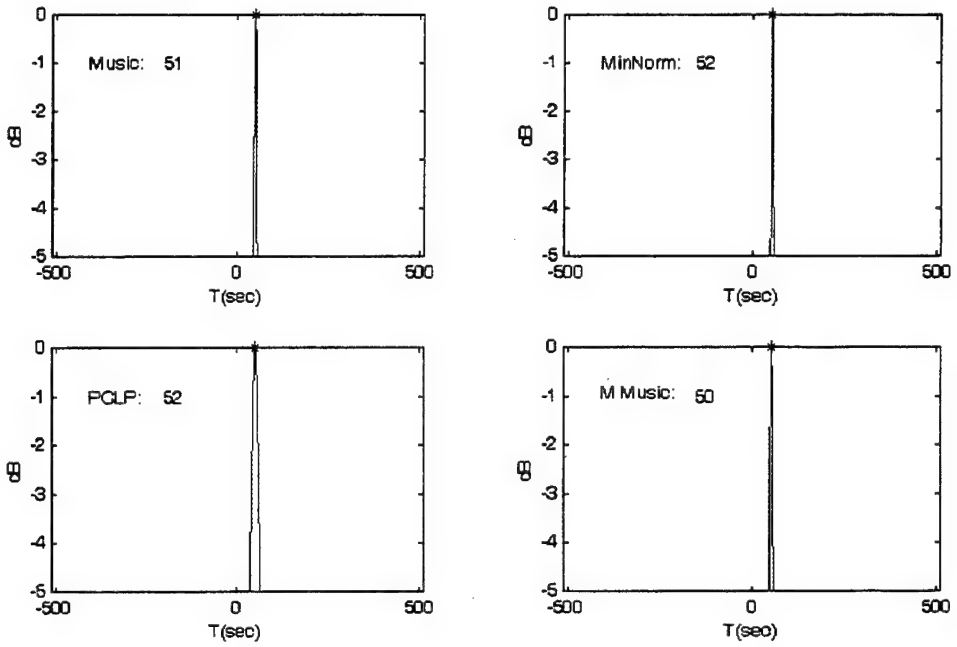

(a)

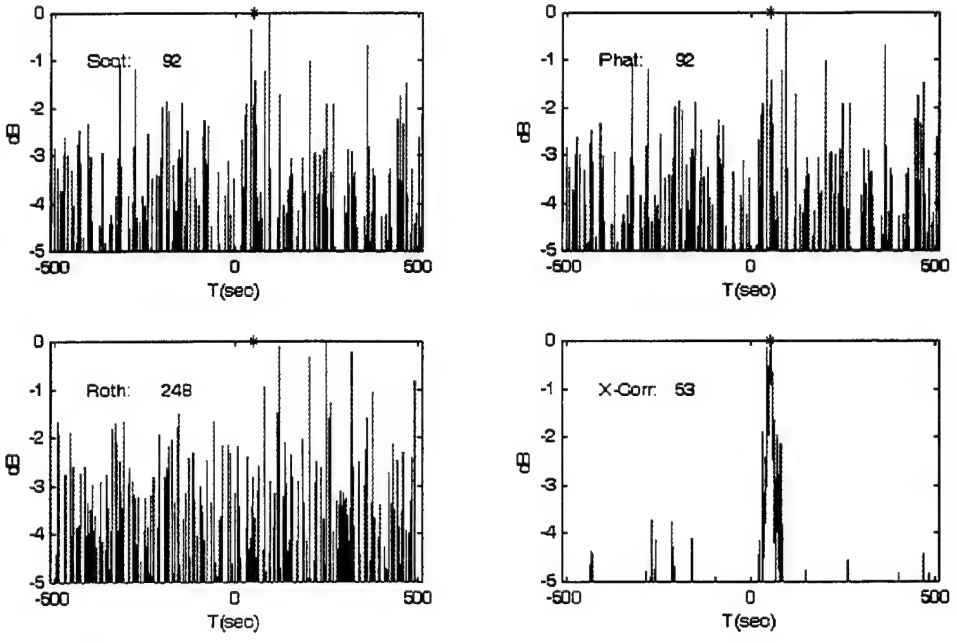

(b)

Figure 14. Exponential transient: length L=100s; Actual TDOA=50s; SNR=05dB; White-Noise (σ_o^2). (a) Subspace methods, Covariance Size=10 (b) Classical methods, number of segments=1

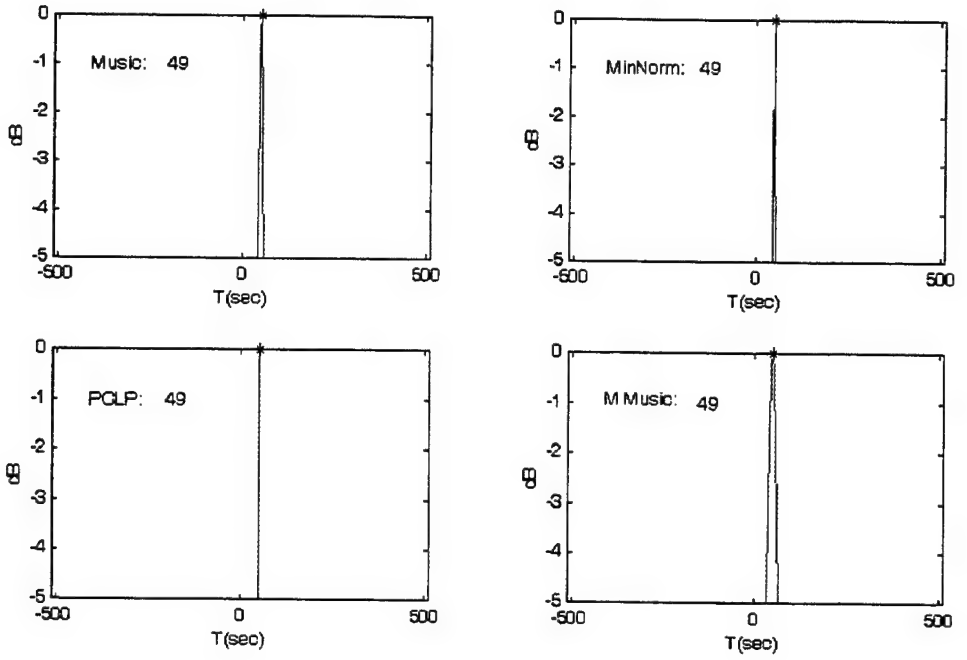

(a)

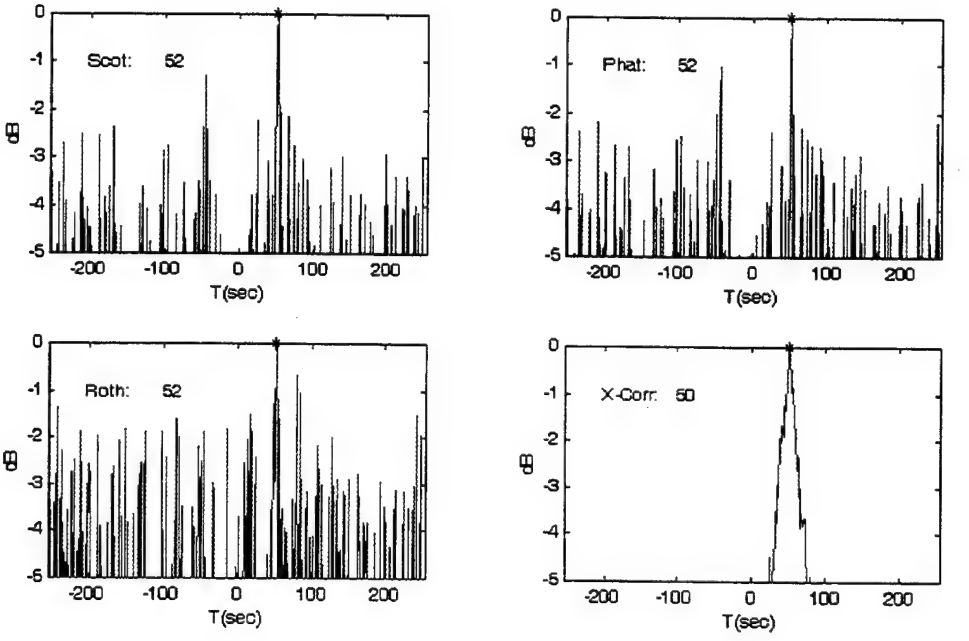

(b)

Figure 15. Exponential transient: length L=100s; Actual TDOA=50s; SNR=05dB; White-Noise (σ_o^2). (a) Subspace methods, Covariance Size=20 (b) Classical methods, number of segments=2

Method	Parameters	SNR 15 dB	SNR 10 dB	SNR 5 dB
MUSIC	Cov-Mat: 10	50	51	51
	Cov-Mat: 20	50	49	49
Modified MUSIC	Cov-Mat: 10	50	51	52
	Cov-Mat: 20	50	49	50
MIN-NORM	Cov-Mat: 10	50	51	50
	Cov-Mat: 20	50	49	49
PCLP	Cov-Mat: 10	50	51	52
	Cov-Mat: 20	50	49	49
ESPRIT	Cov-Mat: 10	49	51	50
	Cov-Mat: 20	50	50	50
Root-MUSIC	Cov-Mat: 10	50	50	49
	Cov-Mat: 20	50	49	49
SCOT	#-Segs: 1	50	50	92
	#-Segs: 2	50	52	47
PHAT	#-Segs: 1	50	50	92
	#-Segs: 2	50	52	47
Roth	#-Segs: 1	-299	-502	248
	#-Segs: 2	50	52	-204
X-Corr	#-Segs: 1	50	50	53
	#-Segs: 2	50	50	47

Table VI. Exponential transient: length L=100s; white noise ($\sigma_o^2 = 2$); actual TDOA=50s.

After examining the corresponding Figs. 10 - 15 and Table VI for the first case of the synthetic data we can say that almost all the methods performed satisfactorily. The figures for the subspace methods in all cases, Figs. 10(a) - 15(a), were clear without any subsidiary peaks, compared with the respective figures of the classical methods, Figs. 10(b) - 15(b). For medium noise level (SNR=10dB), Figs. 12 - 13, and even more for high noise level (SNR=5dB), Figs. 14 - 15, the subspace methods gave more accurate results. The increase of the size of the covariance matrix had a slight improvement in the performance for the subspace methods. On the contrary the increase of the number of segments for the classical methods had more positive influence on their performance, especially when the SNR became very low (5dB). Of

the classical methods, Roth had the worst performance and cross-correlation had the best performance, on average. Subspace methods with both approaches had similar behavior in all conditions.

In summary, after reviewing all cases of the synthetic data (see Figs. 51 - 86 and Tables XX - XXIV in Appendix A) for the performance of all methods, the following observations can be made.

- The subspace methods uniformly had very efficient performance compared with the classical methods
- The subspace methods were more consistent in the quality of the results as a group. The classical methods, on the other hand, in some cases had great diversity among them in the quality of their performance. Among the classical methods, Roth had the poorest performance; and in general the cross correlation was more consistent in accuracy than the other methods.
- The plots of the subspace methods were more distinct and it was easier to identify the peak corresponding to the correct Time Difference of Arrival (TDOA).
- In cases where both methods provided the expected results the classical methods had more accurate peaks than the subspace methods. However both methods provided results in which accuracy was completely acceptable.
- In order to perform with multiple segments the classical methods needed to have appropriate length of input data (signal plus noise). Otherwise phenomena of aliasing appeared especially in cases with a large "value" of TDOA between the two data sets. This drawback did not affect the subspace methods at all since they do not deal with segmentation.
- Methods like root MUSIC or ESPRIT can produce direct numerical estimates for the time delay without the need to search for a peak.
- Subspace methods were more "resistant" to noise compared to the classical methods.
- For short duration of transients the performance of the methods decreased in accuracy, especially when it was combined with low SNR. In this case classical methods gave totally wrong results compared with the subspace methods, whose performance was inside the permissible limits of error (Table XX).
- For the case of a small value of predicted TDOA (Table XXI) the subspace methods performed more than satisfactorily even under high "noise conditions". The performance of the classical methods was similar with that of

the subspace methods for high SNR, but they became quite inferior when the noise was increased.

- In general the increase in the size of the covariance matrix in subspace methods improved their performance, especially when the SNR was small. Better results were achieved when the size of the covariance matrix was greater than 20, but increased the total number of computations something that made the subspace methods to delay enough in order to provide us with the desired result.

For the cases where all the remaining factors are the same (except for the type of transient), Tables XXII, XXIII, XXIV, and Figs. 10 - 15 and 63 - 86, we can say that all the methods have almost the same behavior with different transients as with the exponential transient. Only the sinusoidal transient had noticeably worse performance than the others and was influenced more with high noise level than the rest of the transients.

2. Implementation Using Combination of Methods

Before we continue with the MMPE data, it is worth examining if the "combination" of the two families of methods, subspace and classical, perform better than each one separately. In our case the word "combination" means that before we apply the subspace methods in the frequency domain (cross-spectrum), the desired weighting factor will be implemented according to the processor we would like to use. The main idea was to examine if the subspace methods, with the assistance of the weighting factor, could provide us with more accurate results (peaks). Several test cases were conducted and it was determined that the peaks were more accurate but the results were not better than without implementing the combination. As a general remark, each weighting factor influenced the performance of the subspace methods differently in such a way that the subspace methods lost their good consistency in results. Figures 16 - 17 and the corresponding Table VII give a sample of the "combination" performance.

Method	SCOT	PHAT	ROTH	CROSS CORRELATION	NONE
MUSIC	95	95	-879	103	103
Modified-MUSIC	96	96	-600	103	103
MIN-NORM	90	90	-620	103	103
PCLP	91	91	-871	103	103
ESPRIT	95	95	-728	103	103
Root-MUSIC	96	96	-864	103	103

Table VII. Damped Sinusoidal transient: length L=400s; white noise ($\sigma_o^2 = 2$); SNR=10dB; actual TDOA=100s.

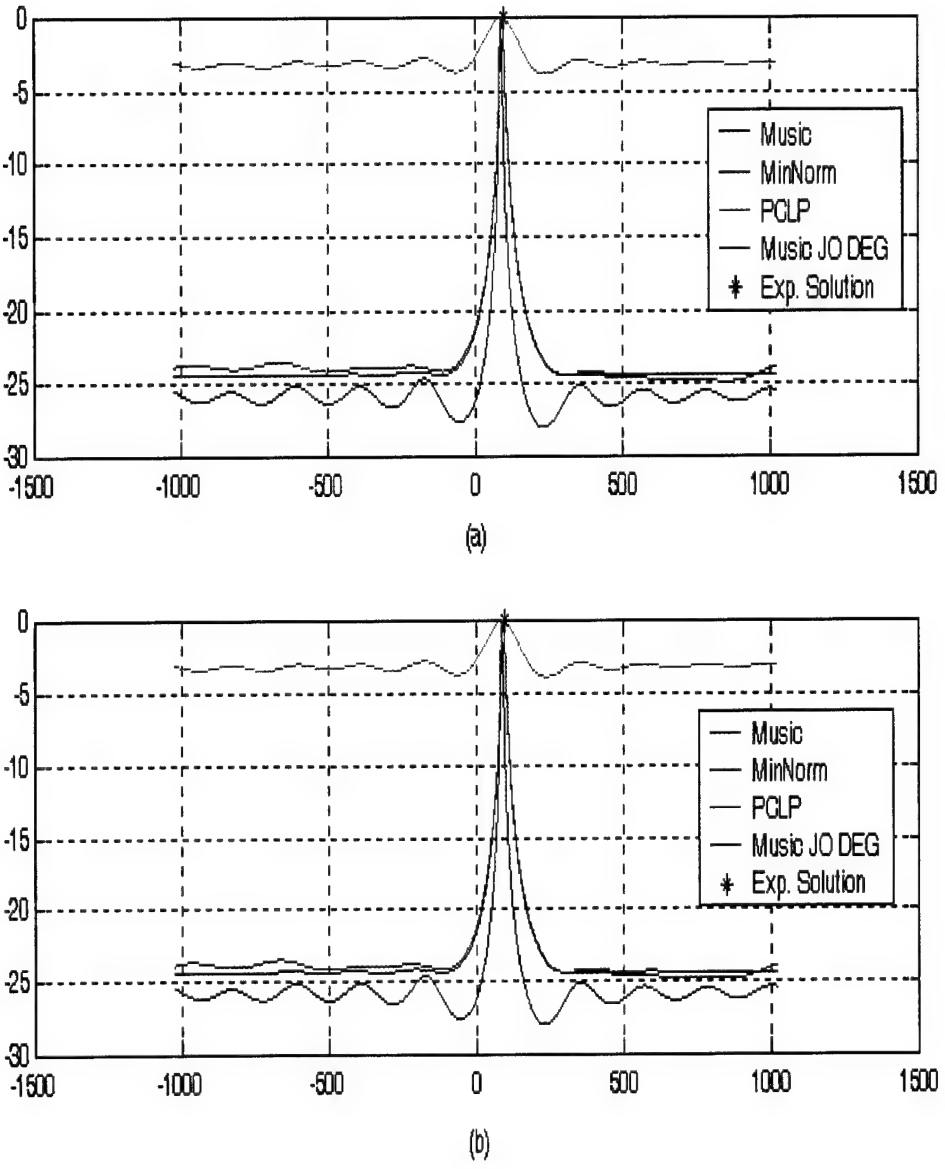

Figure 16. Damped Sinusoidal transient: Actual TDOA=100s; SNR=10dB; White-Noise (σ_o^2) Covariance Size=10, number of segments=1. (a) Subspace methods with SCOT. (b) Subspace methods with PHAT.

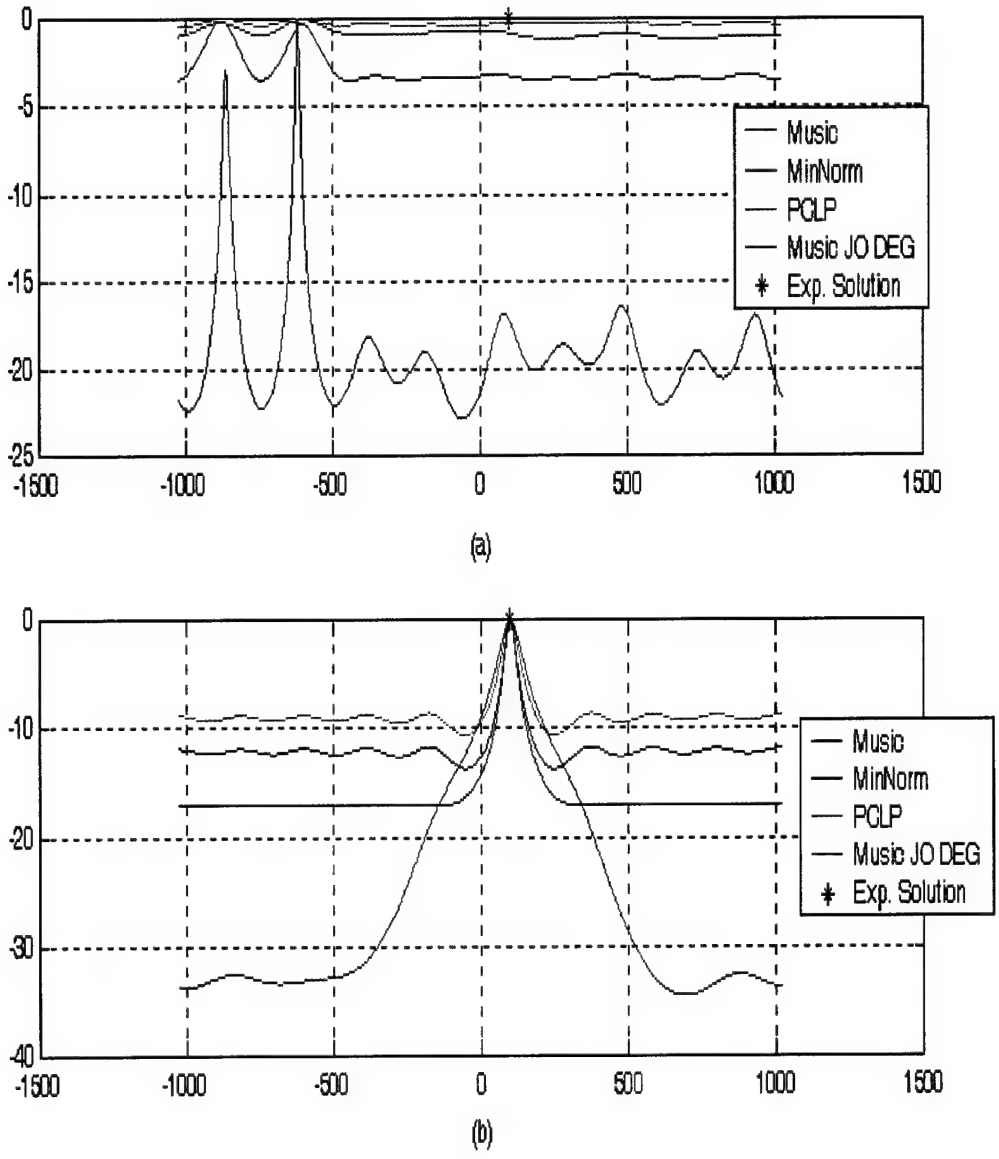

Figure 17. Damped Sinusoidal transient: Actual TDOA=100s; SNR=10dB; White-Noise (σ_o^2) Covariance Size=10, number of segments=1. (a) Subspace methods with ROTH. (b) Subspace methods with Cross Correlation.

B. MMPE DATA

In this section results from data generated by the MMPE propagation model are presented. The particular environments that were used to generate these data are the ones presented in Chapter 4. These simulations were conducted to verify the observations from the synthetic data and to test the methods with broadband transients under more complicated environmental conditions. For each environment, we provide a Transmission Loss (TL) plot relative to the depth and the frequency bandwidth, the waveforms of the source and of the two receivers in the time domain, and the results of all TDOA methods. It will be seen that in all cases the signals in each location have totally different shape and magnitude due to the multipath structure of the waveguide. As mentioned before, the environments are divided into two categories: *range-independent* (the received signal depends only on the distance between the source and the receiver [Flat - Sound Channel cases], and *range-dependent* (the sound speed profile changes according to range and direction from the source [Shelf Break - Internal Waves cases]. Two cases are considered for each environment. For the range-independent environments the receivers are chosen to be at different ranges from the source. For the range-dependent environments the receivers are selected to be at the same ranges but in different relative directions from the source. In this way the difference between the two categories will be more evident. For more detailed description of the MMPE environments see Chapter 4.

1. Flat Bottom

Two cases are considered for this environment. The receivers are at distances of 2km and 3km, and 2km and 5km for each case, respectively. In all cases different realizations of white noise were added to each transient with SNR=10dB. In Figs. 18 and 19 are shown the Transmission Loss (TL) plot of depth versus frequency and the waveforms at the source and at the two receivers in the time domain for one of the two cases. The results for both cases are shown in Figs. 20 and 21 and summarized in Table VIII. From these results, it appears that all methods perform in a similar

manner to that in the section with the synthetic data. All of them gave results very close to the actual value for both cases with slightly better accuracy by the subspace methods. The difference in the figures between the two group of methods is still the same. Subspace methods have more clear plots and it is easier to pick up the correct peak from their graphs than the corresponding ones from classical methods (subsidiary peaks.) In this environment the root-finding subspace methods (ESPRIT - rootMUSIC) had the best performance of all the methods and Roth gave the worst results compared with the rest.

Method	Estimated TDOA Case 1	Estimated TDOA Case 2
ACTUAL	***0.6936***	***2.1209***
MUSIC	0.6953	2.1250
Modified-MUSIC	0.6641	2.0879
MIN-NORM	0.6943	2.1240
PCLP	0.6943	2.1240
ESPRIT	0.6934	2.1221
Root-MUSIC	0.6943	2.1230
SCOT	0.7324	2.1182
PHAT	0.7324	2.1182
Roth	0.5713	2.1328
X-Corr	0.7285	2.1133

Table VIII. TDOA results for Flat Bottom isospeed case.

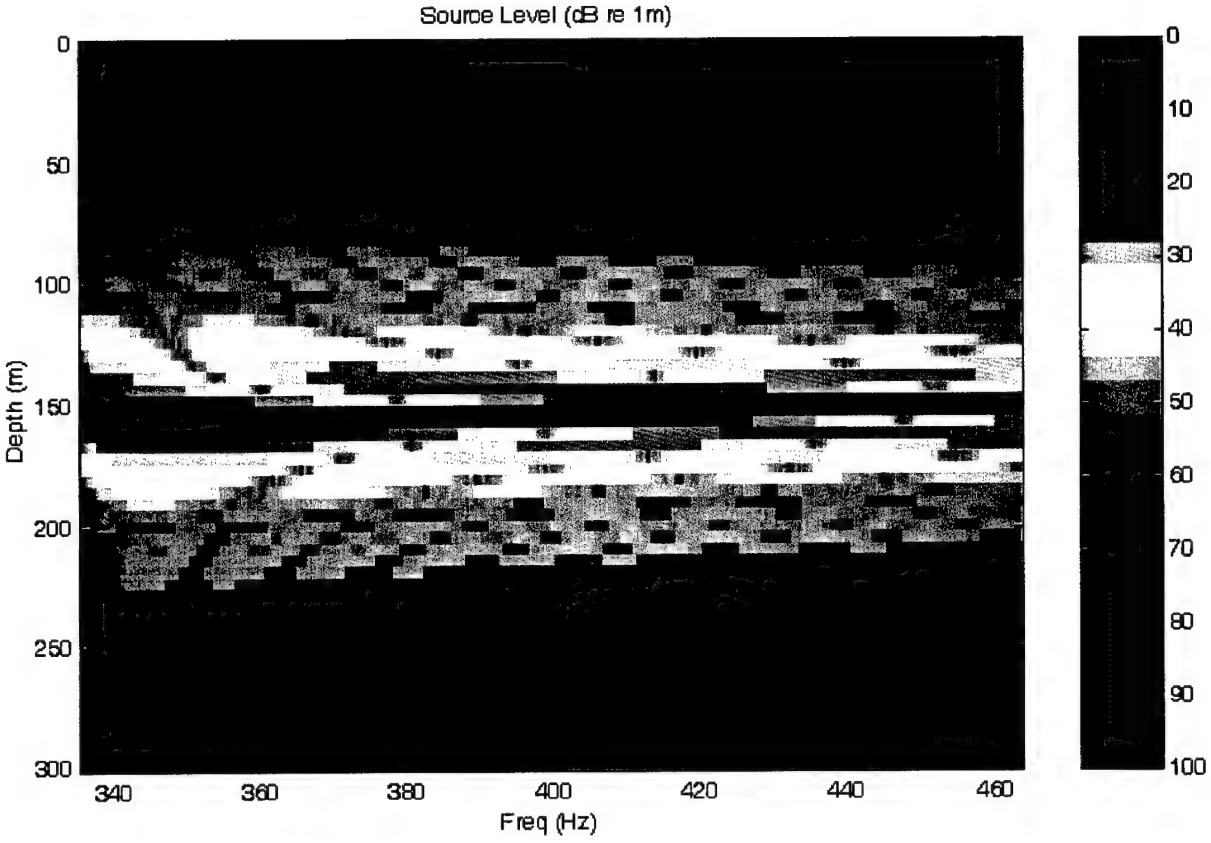

Figure 18. Transmission Loss for FLAT Bottom environment.

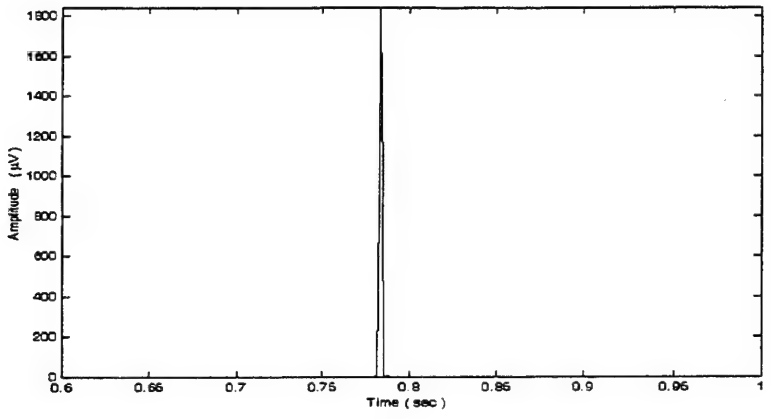

(a)

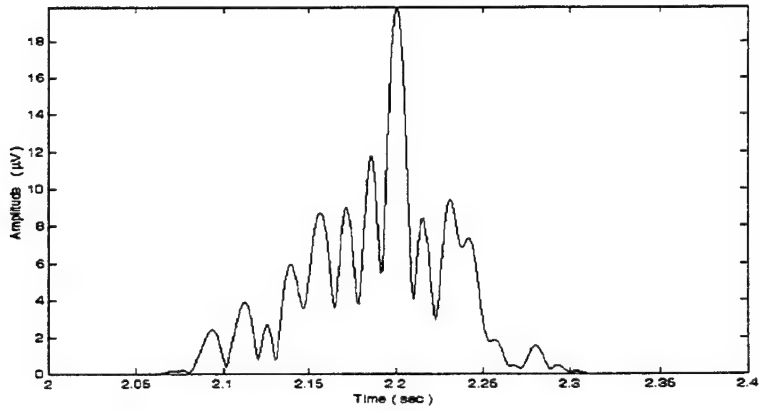

(b)

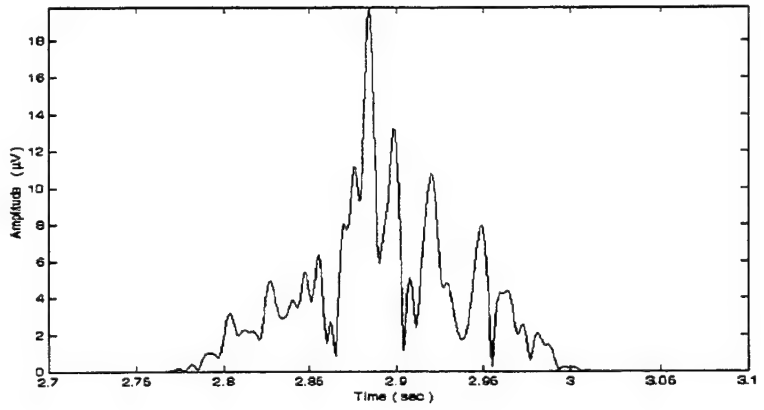

(c)

Figure 19. Time domain waveforms for FLAT Bottom environment. (a) Source. (b) Receiver 1. (c) Receiver 2.

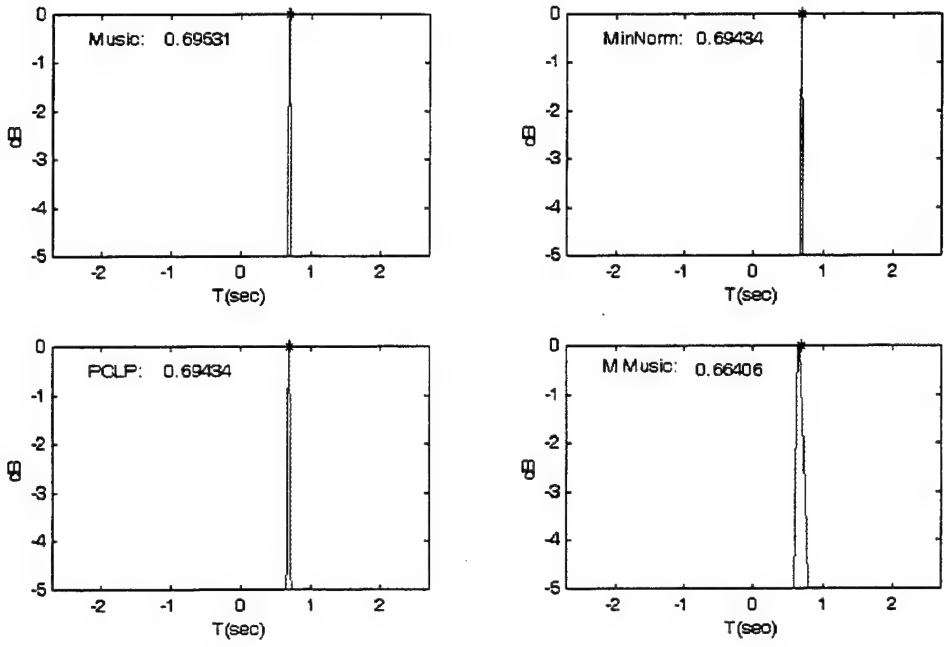

(a)

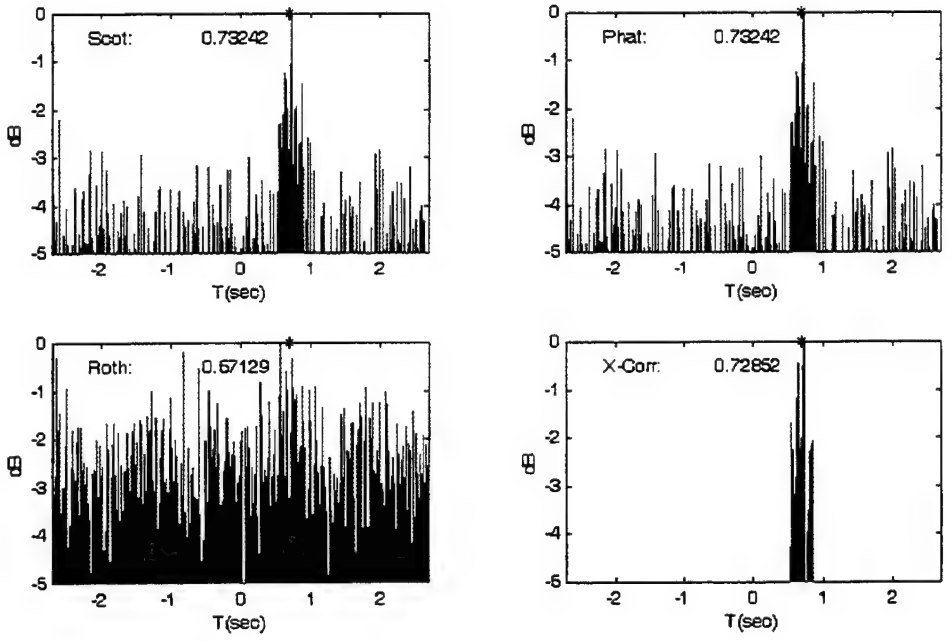

(b)

Figure 20. FLAT Bottom environment Subcase 1: Actual TDOA=0.6939s; SNR=10dB; White-Noise (σ_o^2). (a) Subspace methods, Covariance Size=10. (b) Classical methods, number of segments=1.

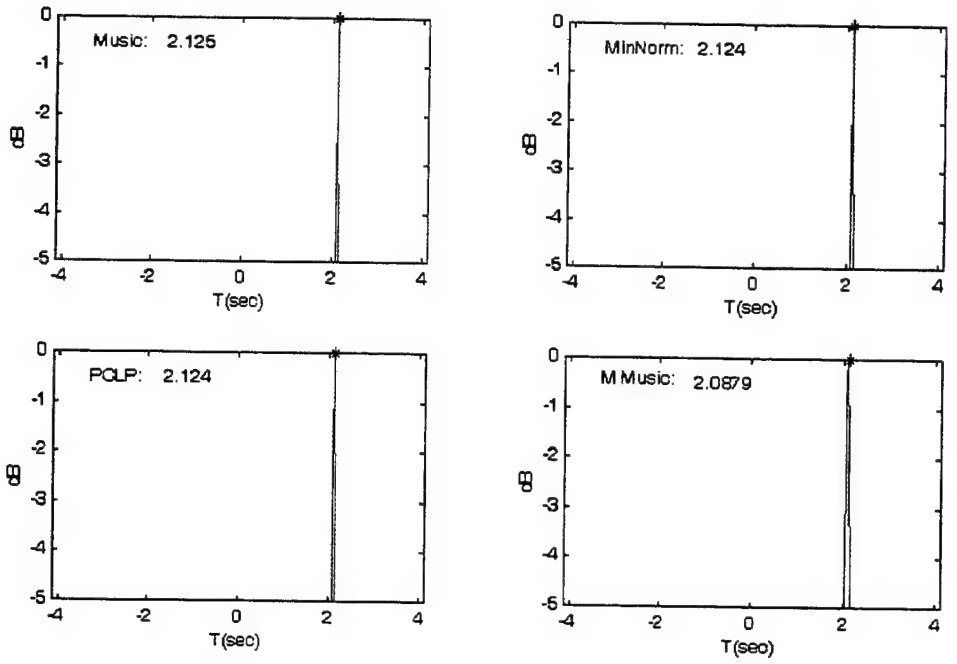

(a)

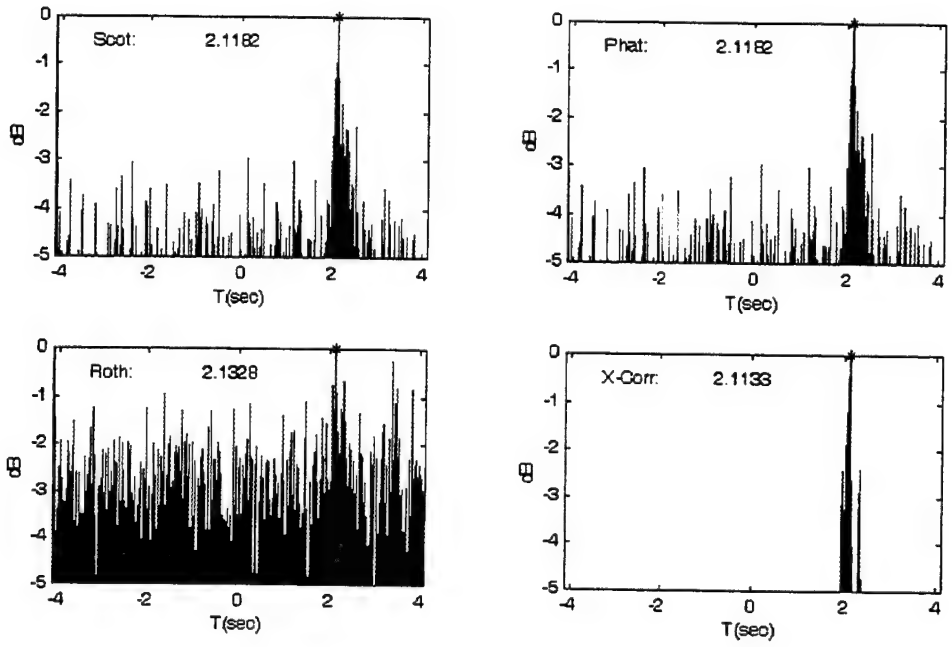

(b)

Figure 21. FLAT Bottom environment Subcase 2: Actual TDOA=2.1209s; SNR=10dB; White-Noise (σ_o^2). (a) Subspace methods, Covariance Size=10. (b) Classical methods, number of segments=1.

2. Sound Channel

Two cases are considered for this environment. In the first case the receivers are at distances 2km and 4km, while in the second case they are at 2km and 8km. In all cases a different realization of white noise was added to each transient to obtain a SNR of 10dB. Figures 22 and 23 show the Transmission Loss (TL) plot of depth versus frequency and the waveforms of the source and of the two receivers in the time domain for one of the two cases. The results for both cases are shown in Figs. 24 and 25 and summarized in Table IX. The results show us a similar picture for the performance of the methods. The only difference is that in this environment the "gap" between the estimated values of TDOA from the classical methods and the actual predicted value becomes larger.

Method	Estimated TDOA Case 1	Estimated TDOA Case 2
ACTUAL	***1.5830***	***4.5929***
MUSIC	1.5830	4.5967
Modified-MUSIC	1.5781	4.5967
MIN-NORM	1.5830	4.5967
PCLP	1.5830	4.5967
ESPRIT	1.5820	4.5967
Root-MUSIC	1.5820	4.5967
SCOT	1.5771	4.5527
PHAT	1.5571	4.5527
Roth	1.5596	4.5527
X-Corr	1.5732	4.5527

Table IX. TDOA results for SOUND CHANNEL case.

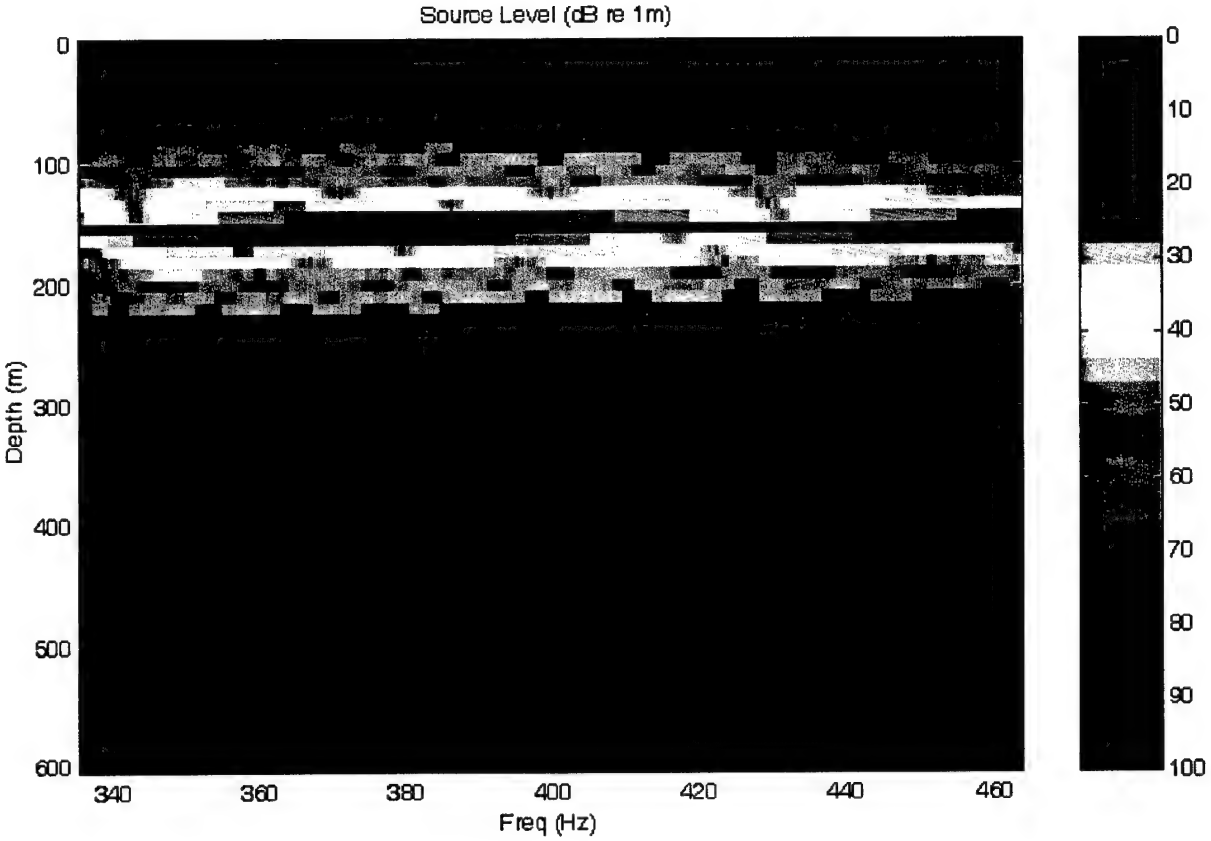

Figure 22. Transmission Loss for SOUND CHANNEL environment.

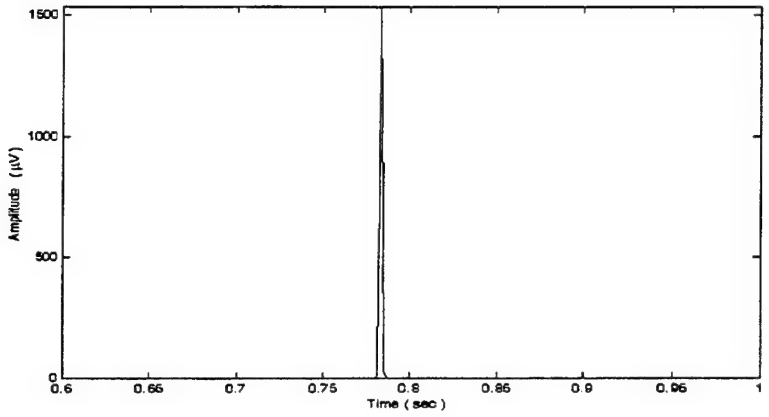

(a)

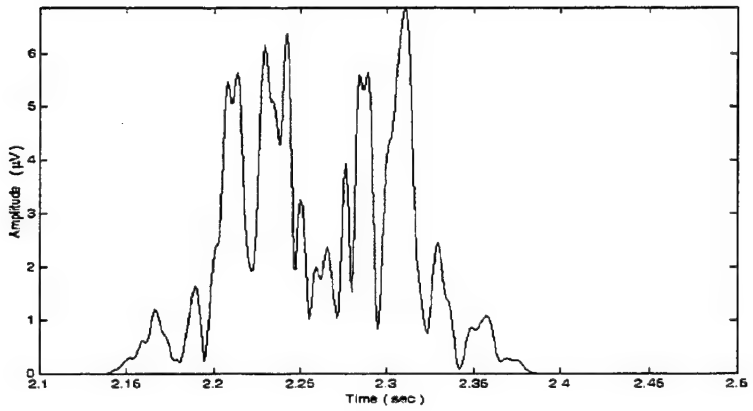

(b)

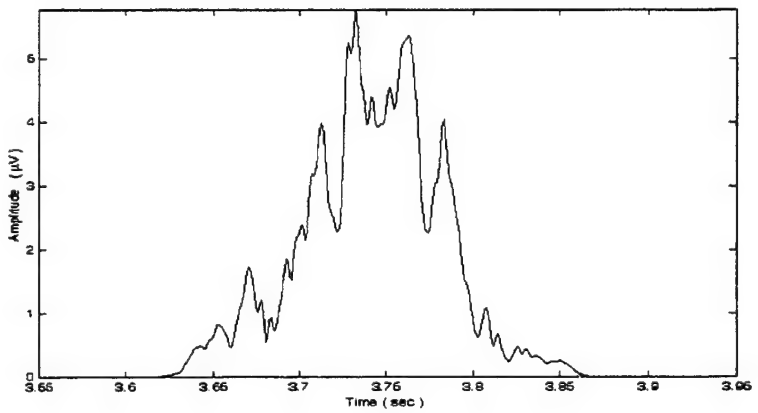

(c)

Figure 23. Time domain waveforms for SOUND CHANNEL environment. (a) Source. (b) Receiver 1. (c) Receiver 2.

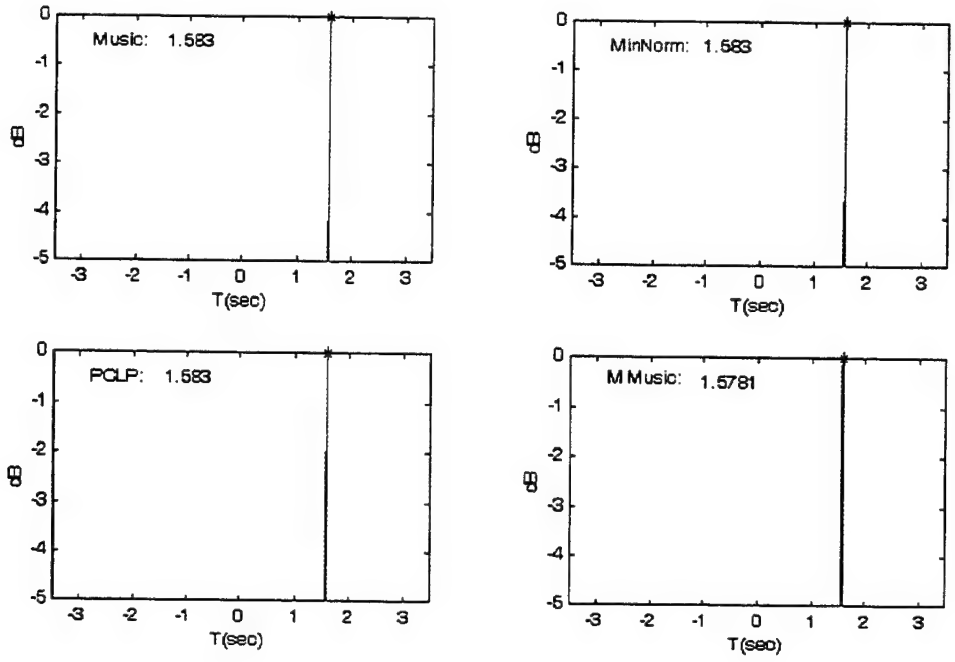

(a)

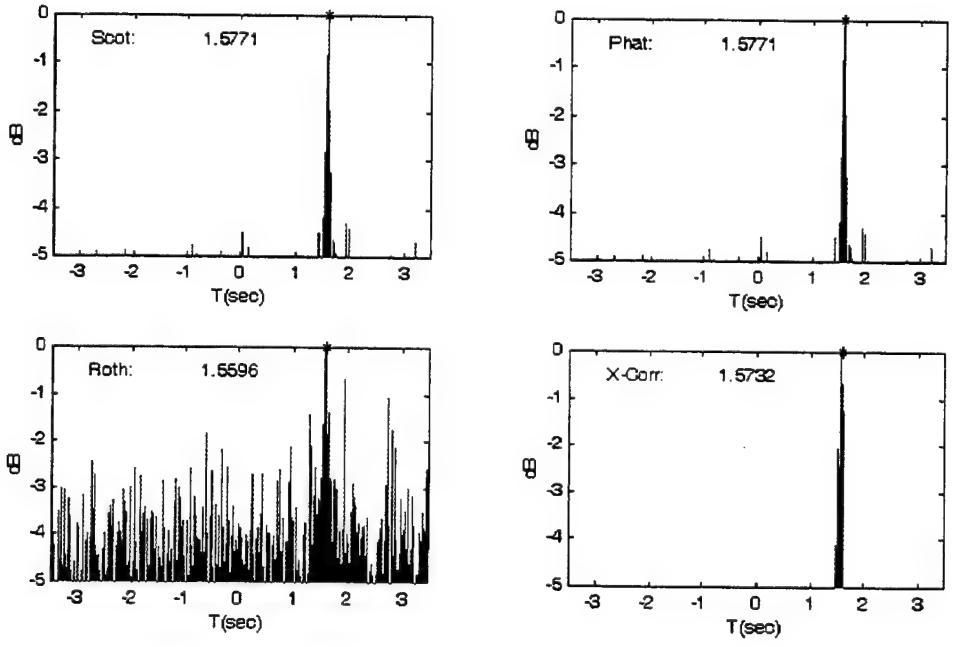

(b)

Figure 24. SOUND CHANNEL environment Subcase 1: Actual TDOA=1.5830s; SNR=10dB; White-Noise (σ_o^2). (a) Subspace methods, Covariance Size=10. (b) Classical methods, number of segments=1.

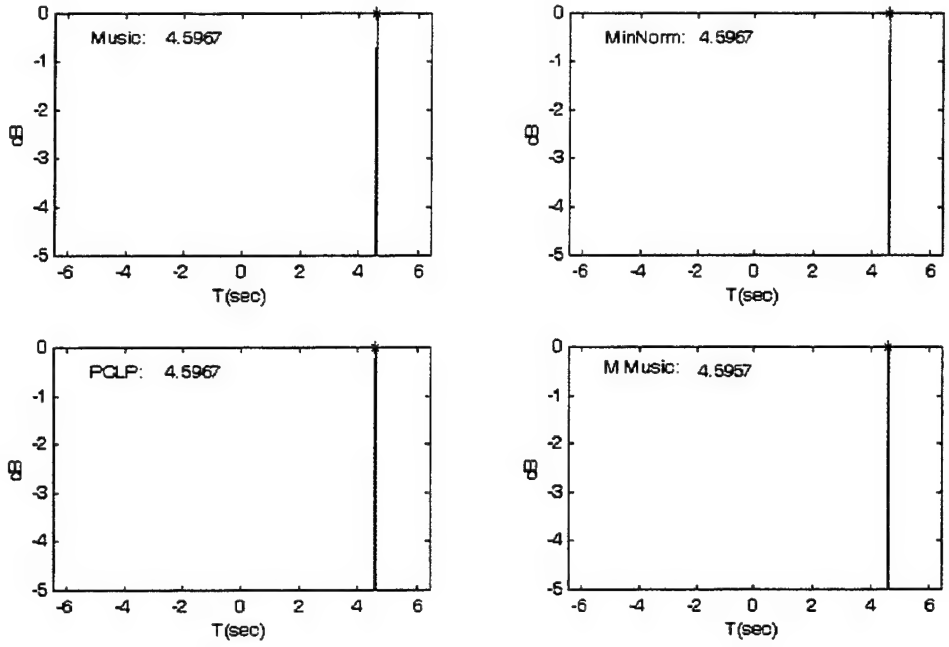

(a)

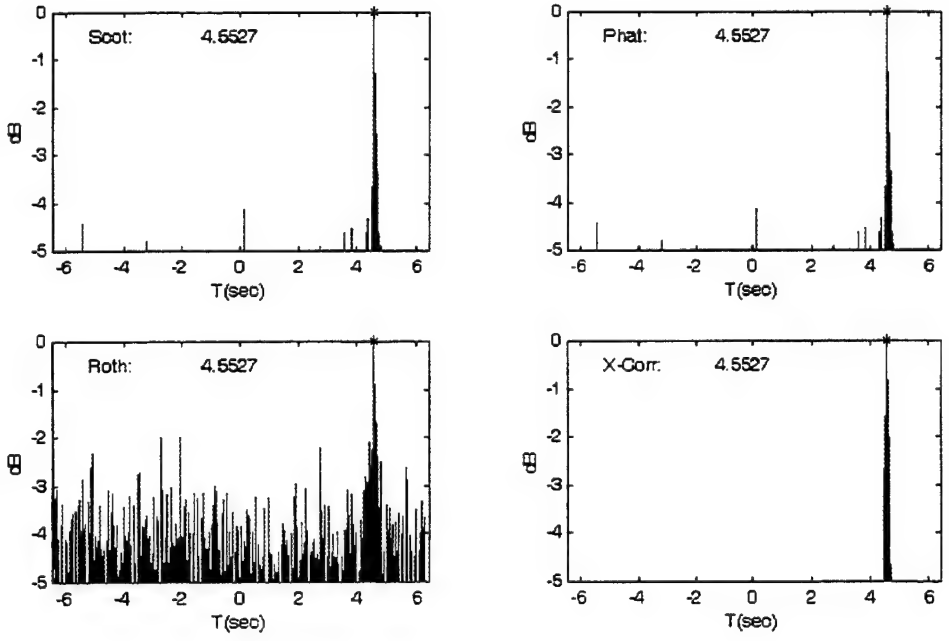

(b)

Figure 25. SOUND CHANNEL environment Subcase 2: Actual TDOA=4.5967s; SNR=10dB; White-Noise (σ_o^2). (a) Subspace methods, Covariance Size=10. (b) Classical methods, number of segments=1.

3. Shelf Break

For this environment the receivers are at distances 2km and 3km but in positions relative to the source as shown in Fig. 26 for each of the two cases considered. In particular Fig. 26 provides us with a top view of the geometry for the two cases, indicating the positions of the source and of the receivers relative to the source, noting also the corresponding depths and the respective ranges for each case. Once again, different realizations of white noise were added to each transient to obtain a SNR of 10dB. Figures 27 and 28 show the Transmission Loss (TL) plot of depth versus frequency and the waveforms of the source and of the two receivers in the time domain for one of the two cases. The results for both cases are shown in Figs. 29 and 30 and summarized in Table X. As we now get into more complex environments (range-dependent), it is obvious that the graphs of the classical methods become more "noisy" than the ones in the range-independent environments, and also that they had an abrupt decrease in their performance except for the Cross-correlation method. Subspace methods still gave us accurate results and all of them were very consistent about the small diversity of their estimated values of TDOA.

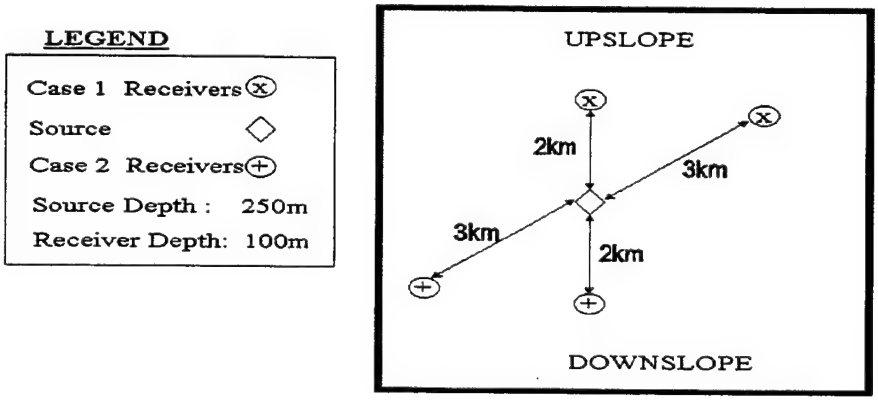

Figure 26. Top view of positions of source and receivers for both cases of SHELF BREAK environment.

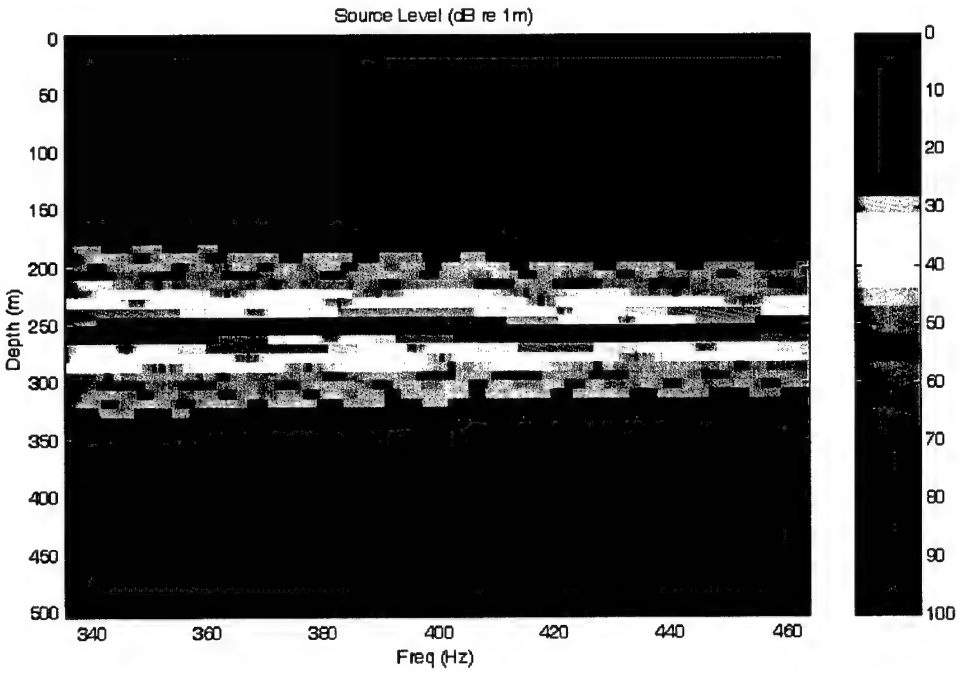

Figure 27. Transmission Loss for SHELF BREAK environment.

Method	Estimated TDOA Case 1	Estimated TDOA Case 2
ACTUAL	***0.7173***	***0.7407***
MUSIC	0.7139	0.7402
Modified-MUSIC	0.7139	0.7490
MIN-NORM	0.7139	0.7432
PCLP	0.7139	0.7422
ESPRIT	0.7139	0.7471
Root-MUSIC	0.7139	0.7471
SCOT	-0.8613	-0.2793
PHAT	-0.8613	-0.2793
Roth	1.2998	1.6211
X-Corr	0.8154	0.7803

Table X. TDOA results for SHELF BREAK case.

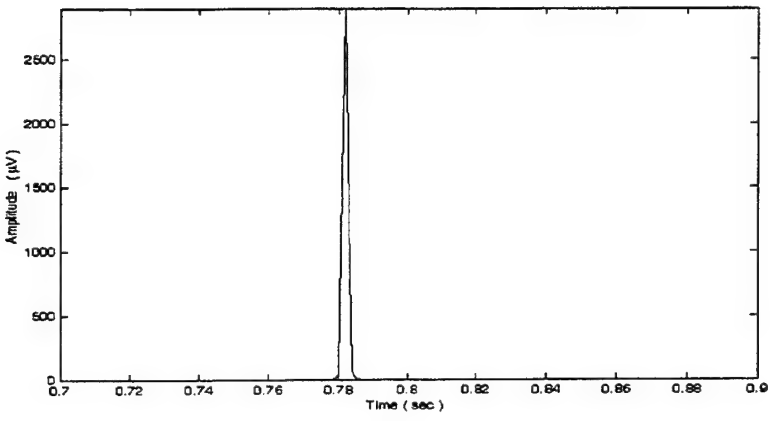

(a)

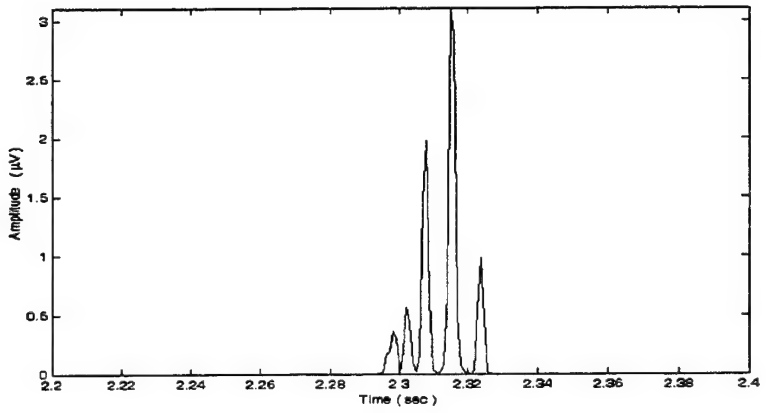

(b)

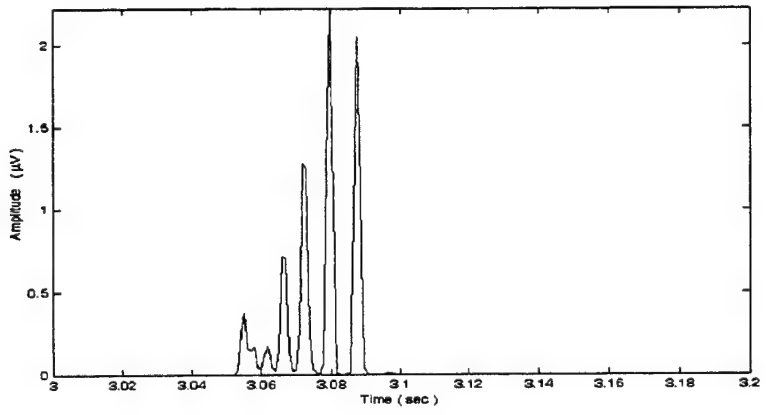

(c)

Figure 28. Time domain waveforms for SHELF BREAK environment. (a) Source. (b) Receiver 1. (c) Receiver 2.

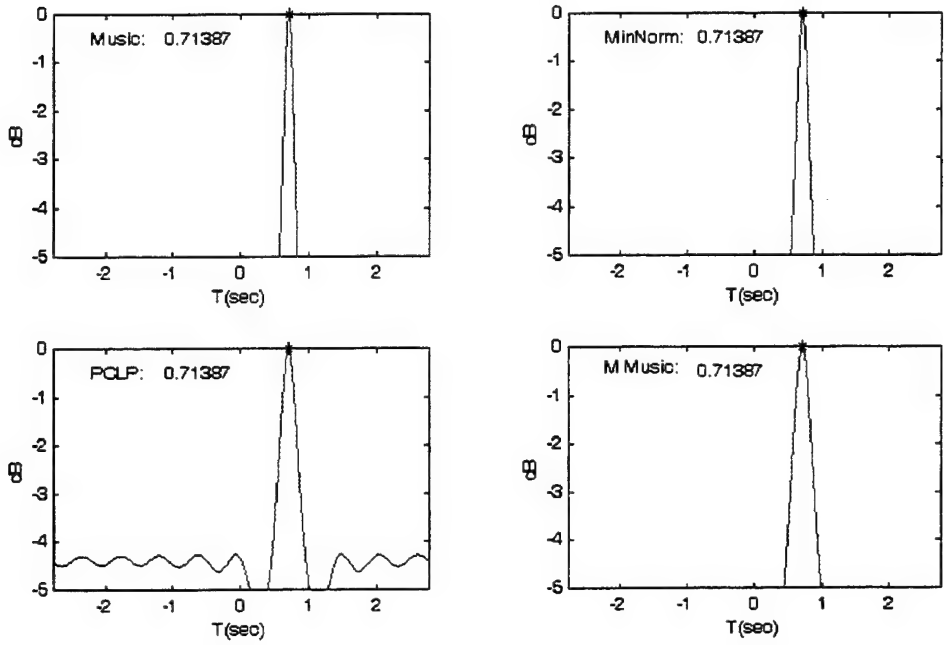

(a)

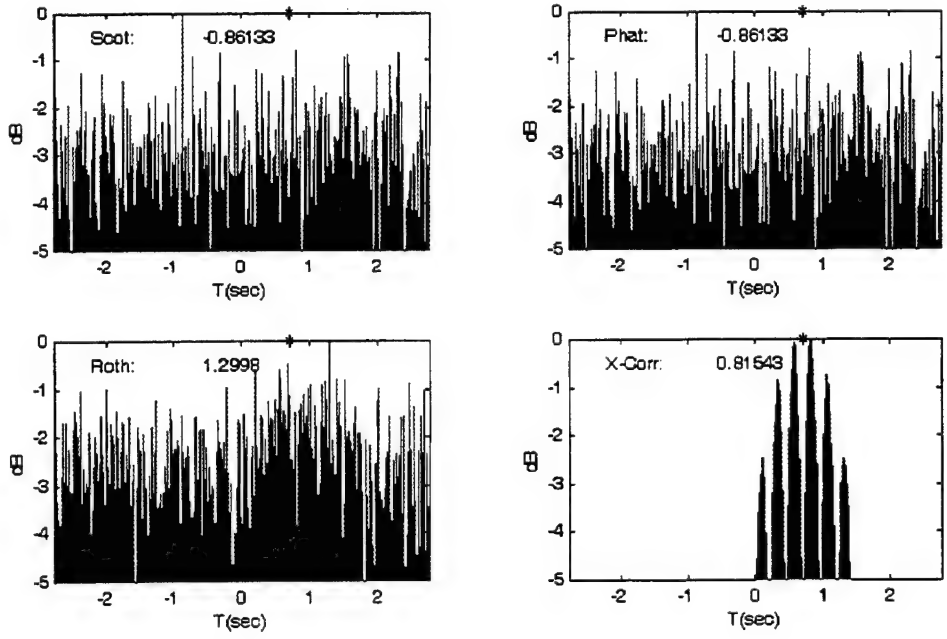

(b)

Figure 29. SHELF BREAK environment Subcase 1: Actual TDOA=0.7173s; SNR=10dB; White-Noise (σ_o^2). (a) Subspace methods, Covariance Size=10. (b) Classical methods, number of segments=1.

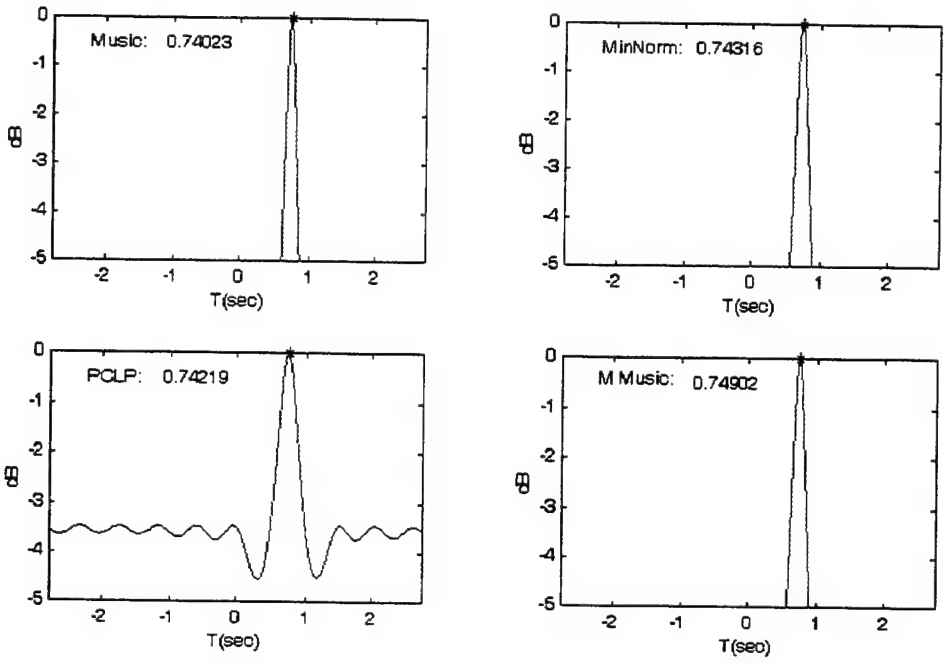

(a)

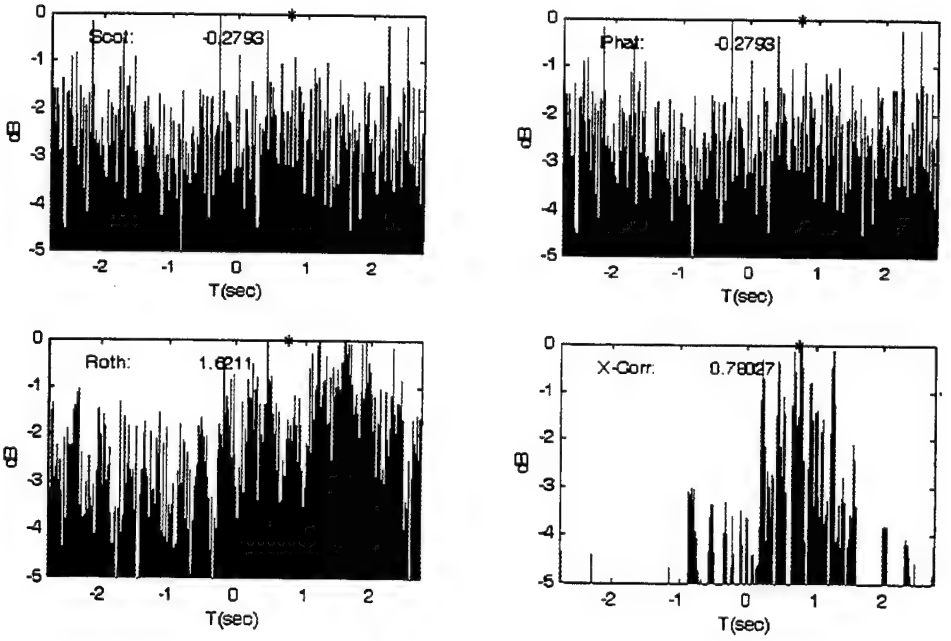

(b)

Figure 30. SHELF BREAK environment Subcase 2: Actual TDOA=0.7407s; SNR=10dB; White-Noise (σ_o^2). (a) Subspace methods, Covariance Size=10. (b) Classical methods, number of segments=1.

4. Internal Waves

For this environment both receivers are at a distance of 3km but at different positions relative to the source as shown in Fig 31 for each of the two cases considered. Figure 31 provides a top view of the geometry for the two cases, indicating the positions of the source and of the receivers relative to the source, noting also the corresponding depths and the respective ranges for each case. As with the previous environments, different realizations of white noise were added to each transient to obtain a SNR of 10dB. Figures 32 and 33 show the Transmission Loss (TL) plot of depth versus frequency and the waveforms at the source and at the two receivers in the time domain for one of the two cases. The results for both cases are shown in Figs. 34 and 35 and summarized in Table XI. Our observations for this environment are almost the same as with the Shelf Break. The only difference is that even the subspace methods give slightly worse results compared with the actual value of TDOA. This was expected since the Internal Waves was the most complex environment used in this thesis. These results are still within the permissible limits of error.

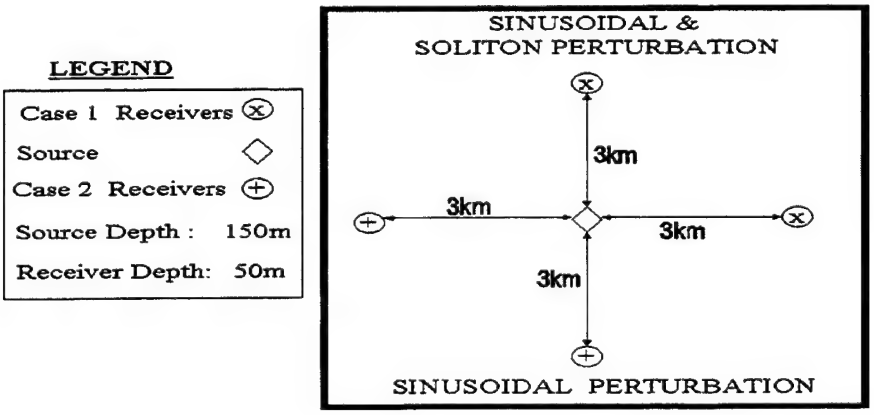

Figure 31. Top view of positions of source and receivers for both cases of INTERNAL WAVES environment.

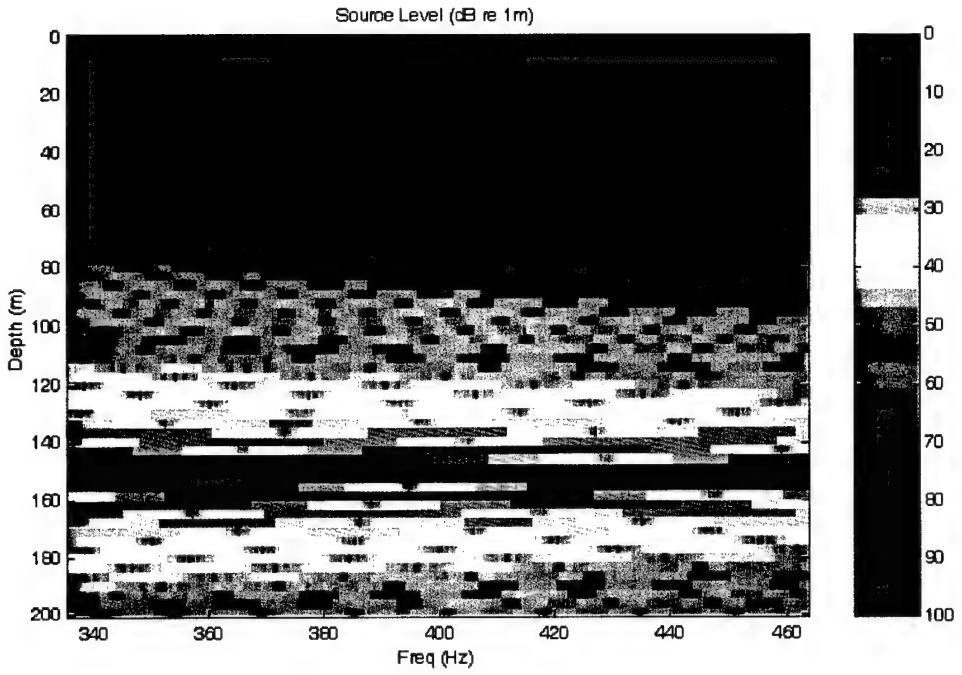

Figure 32. Transmission Loss for INTERNAL WAVES environment.

Method	Estimated TDOA Case 1	Estimated TDOA Case 2
ACTUAL	***0.7770***	***0.2109***
MUSIC	0.7734	0.2090
Modified-MUSIC	0.8311	0.1885
MIN-NORM	0.7822	0.2061
PCLP	0.7793	0.2061
ESPRIT	0.7959	0.2012
Root-MUSIC	0.7930	0.2041
SCOT	0.6299	0.1289
PHAT	0.6299	0.1289
Roth	2.5938	0.0361
X-Corr	0.8574	0.1357

Table XI. TDOA results for INTERNAL WAVES case.

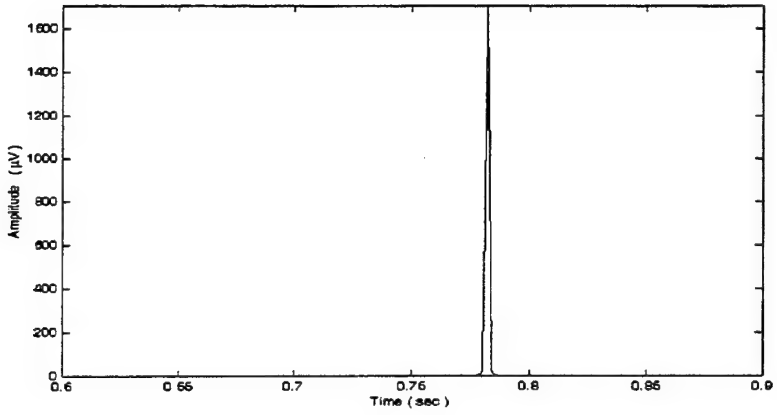

(a)

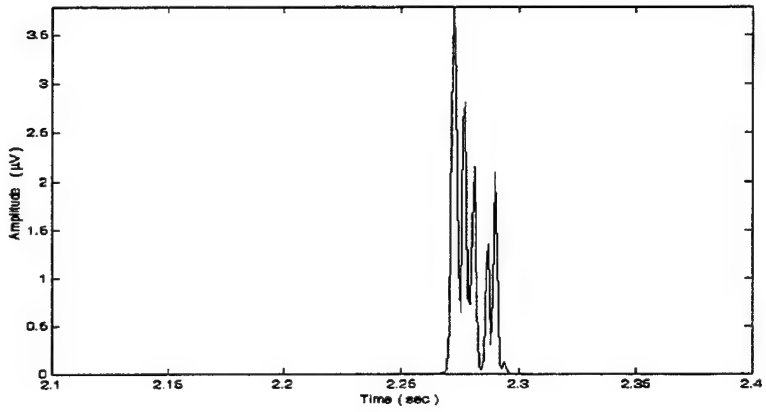

(b)

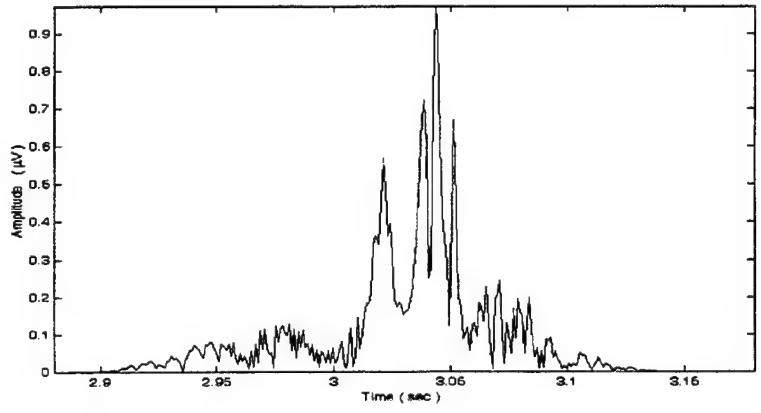

(c)

Figure 33. Time domain waveforms for INTERNAL WAVES environment. (a) Source. (b) Receiver 1. (c) Receiver 2.

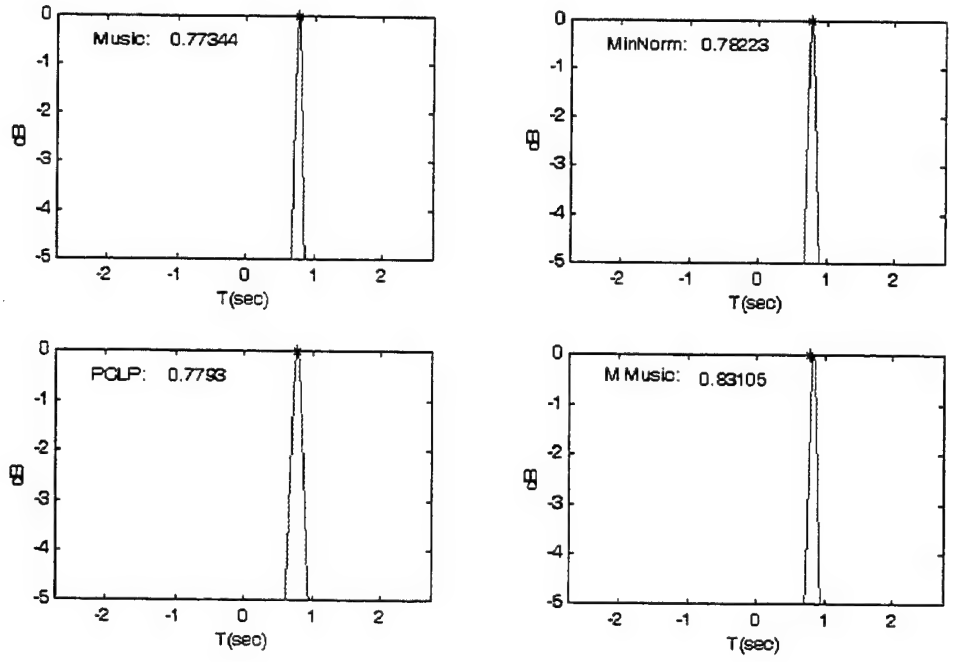

(a)

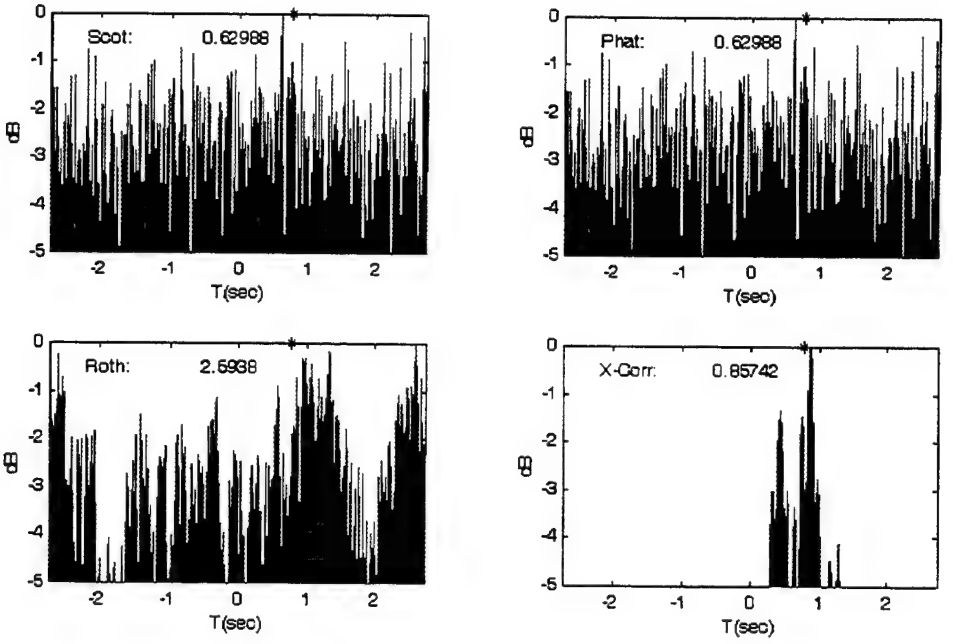

(b)

Figure 34. INTERNAL WAVES environment Subcase 1: Actual TDOA=0.7770s; SNR=10dB; White-Noise (σ_o^2). (a) Subspace methods, Covariance Size=10. (b) Classical methods, number of segments=1.

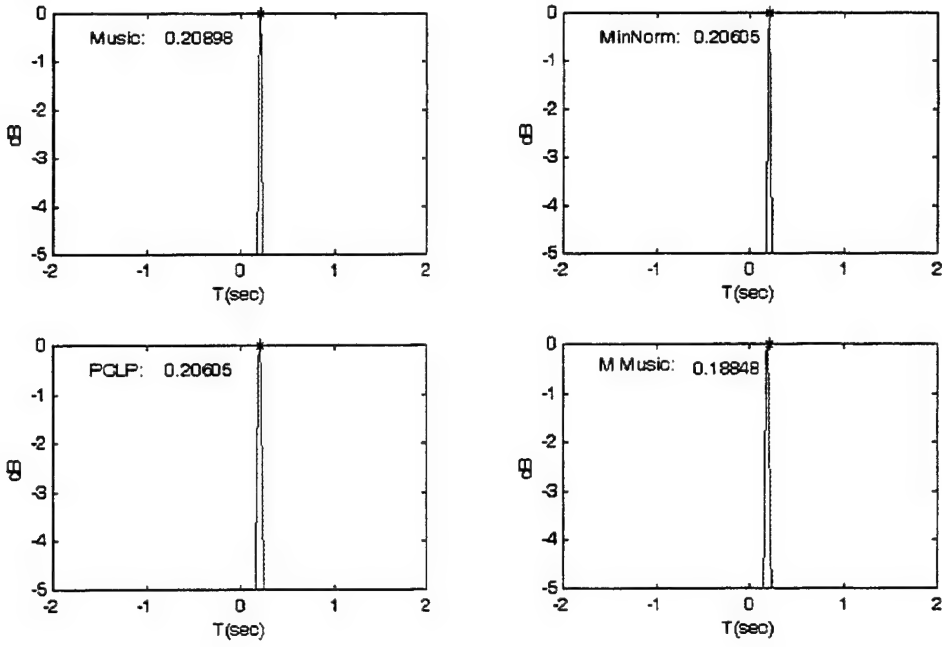

(a)

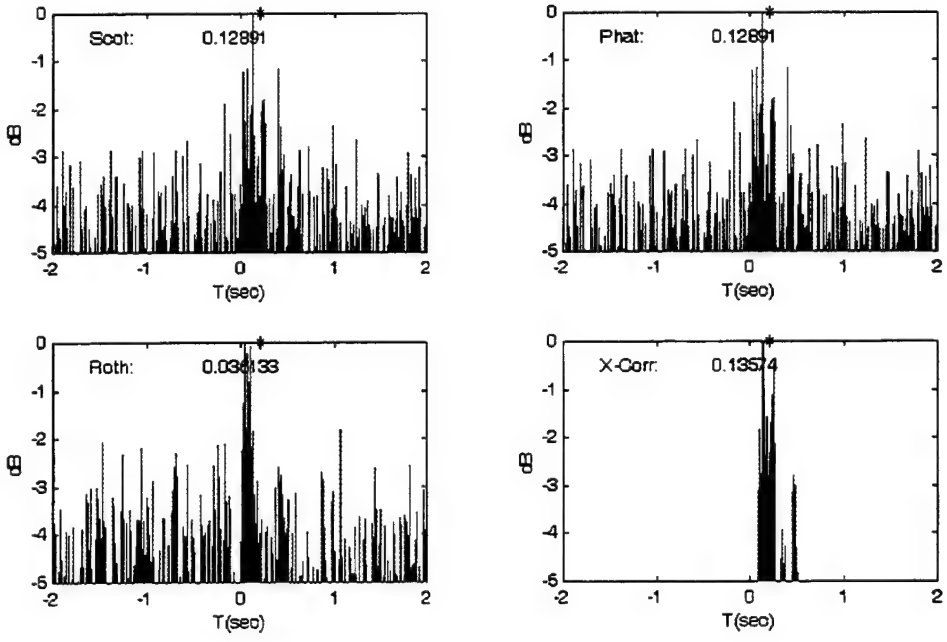

(b)

Figure 35. INTERNAL WAVES environment Subcase 2: Actual TDOA=0.2109s; SNR=10dB; White-Noise (σ_o^2). (a) Subspace methods, Covariance Size=10. (b) Classical methods, number of segments=1.

Taking into consideration the figures and the tables with the TDOA results from all the environments, we observe that all the methods performed quite accurately. It should be noted that the subspace methods were more consistent than the classical ones. This can be verified from the range-dependent environments, where all the subspace methods gave results more close to the actual value and they had only a small dispersion among them. On the contrary, the classical methods had slightly inferior performance in the range-independent environments and much worse in the range-dependent ones, with a wider dispersion of values. This difference in the performance among all the methods between the two categories of the environments also appears in the results of the localization problem in the next chapter.

VI. THE LOCALIZATION PROBLEM

In this chapter, we use the TDOAs between the receivers, estimated by the various methods, in order to estimate the location of the target. For this purpose a homonymous algorithm will be implemented whose main characteristic is to provide us the passive assessment of target position by using a corresponding set of equations, called Time of Arrival (TOA) equations. The TOA equations try to correlate the positions of the receivers with the position of the target using the time that a transient needs to travel from one location to the other. In other words, these equations try to find a correspondence between the signal arrival times and the target range. By solving the TOA equations for only two receivers, we are not going to get one specific location of the target, but an infinite number of possible locations since this solution corresponds to a bearing from this particular pair of receivers. Under these conditions, in order to eliminate this ambiguity we need to solve the TOA equations for all the receivers at the same time, so the desired target position will be the result of the crossing of all the bearings. This expectation is quite natural since, as far as we know, only one solution (target position) can account simultaneously for the travel time of the transient to each receiver. The algorithm that is implemented is simpler than most since it transforms the original nonlinear TOA equations into a set of linear equations. The inputs (receiver position and signal's arrival time for each receiver) correspond to a specific set of outputs (target position and transmission time of the transient). The rest of this chapter is based on a former thesis [Ref. 33] related to this subject.

A. PRESENTATION OF TDOA ALGORITHM

In this section, a brief description of the TDOA algorithm will be provided to the reader since a detailed derivation of this algorithm is not within the scope of this thesis. Before we continue with the rest of our discussion, it would be advisable to

make clear that the solution to the localization problem, which is attempted to be given here, is conducted in two dimensions in the $x-y$ plane. Let us assume that we have one source (target) and N receivers (buoys). The location for each receiver is given by the vector

$$\mathbf{r_i} = \begin{bmatrix} x_i \\ y_i \end{bmatrix}, \qquad i = 1, \cdots, N \tag{VI.1}$$

where x_i and y_i are the $x-y$ coordinates of buoy i. Let the arrival time of the transient at buoy i, defined as the time it takes the leading edge of the transient to travel from the source to the receiver, be denoted as t_i. In a similar manner, the transmission time of the transient from the target will be denoted as t, and the desired position of the target is defined by

$$\mathbf{r} = \begin{bmatrix} x \\ y \end{bmatrix}, \tag{VI.2}$$

where x equals the target's x coordinate position, y equals the target's y coordinate position.

In order to estimate the desired variables, t and $\mathbf{r}$, we have to solve the following equation in matrix form

$$\mathbf{Ar} = \mathbf{q}t + \mathbf{s}, \tag{VI.3}$$

where

$$\mathbf{A} = \begin{bmatrix} x_1 - x_2 & y_1 - y_2 \\ x_2 - x_3 & y_2 - y_2 \\ \vdots & \vdots \\ x_{N-1} - x_N & y_{N-1} - y_N \end{bmatrix}, \tag{VI.4}$$

$$\mathbf{q} = c^2 \begin{bmatrix} t_1 - t_2 \\ t_2 - t_3 \\ \vdots \\ t_{N-1} - t_N \end{bmatrix}, \tag{VI.5}$$

and

$$\mathbf{s} = \frac{1}{2}\begin{bmatrix} ||r_1||^2 - ||r_2||^2 - c^2t_1^2 + c^2t_2^2 \\ ||r_2||^2 - ||r_3||^2 - c^2t_2^2 + c^2t_3^2 \\ \vdots \\ ||r_{N-1}||^2 - ||r_N||^2 - c^2t_{N-1}^2 + c^2t_N^2 \end{bmatrix}. \tag{VI.6}$$

The variable c represents the sound speed, which in our case will be assumed constant throughout the whole computational grid. Equation (VI.3) is simply the transformation of the nonlinear TOA equation

$$(x_i - x)^2 + (y_i - y)^2 - c^2(t_i - t)^2 = 0 \tag{VI.7}$$

into a linear TDOA equation which relates target position to transmission time

$$x(x_n - x_{n+1}) + y(y_n - y_{n+1}) = c^2t(t_n - t_{n+1}) + \frac{1}{2}(x_n^2 - x_{n+1}^2 + y_n^2 - y_{n+1}^2 - c^2t_n^2 + c^2t_{n+1}^2). \tag{VI.8}$$

This equation is formed by subtracting two equations like (VI.7) for successive pairs of the N receivers.

The solution of Eq. (VI.3) is computed in a least squares sense in order to find the target range $\mathbf{r}$ in terms of the transmission time t. Equation (VI.3) becomes

$$\mathbf{r} = \mathbf{g}t + \mathbf{h}, \tag{VI.9}$$

where

$$\mathbf{g} = (\mathbf{A})^+\mathbf{q}, \tag{VI.10}$$

$$\mathbf{h} = (\mathbf{A})^+\mathbf{s}, \tag{VI.11}$$

and $+$ denotes the pseudoinverse. Here we make the distinction that when $N = 3$ the expected solution is exact for the corresponding set of equations, but for the case $N > 3$ the result is the least squares solution, which minimizes the equation error for the same set of Eqs. (VI.7).

After some calculations, we come up with the following formula for the k^{th} range equation:

$$||\mathbf{r_k} - \mathbf{g}\mathbf{t} - \mathbf{h}||^2 = c^2(t_k - t)^2, \tag{VI.12}$$

which after expanding and simplification produces

$$\alpha t^2 + 2bt + d = 0, \tag{VI.13}$$

where

$$\alpha = ||\mathbf{g}||^2 - c^2, \tag{VI.14}$$

$$b = \mathbf{g^T} \cdot \mathbf{h} - \mathbf{g^T} \cdot \mathbf{r_k} + c^2 t_k, \tag{VI.15}$$

$$d = ||\mathbf{h} - \mathbf{r_k}||^2 - c^2 t_k^2. \tag{VI.16}$$

By solving the quadratic formula (VI.13), we find two possible solutions for transmission time t, but only one of them is correct. We must use the correct solution in Eq. (VI.9) in order to find the location of the target.

In theory, the solution for t is independent of which particular range equation (k) was used to develop the quadratic equation. In practice, because of measurement errors, the solutions will be different. Therefore, it is advisable to develop $N-1$ estimates for t using $k = 1, 2, \cdots, N-1$, discarding any erroneous values and average the remaining solutions. This multiple solution technique also resolves which root is correct. The result can then be used in (VI.9) to find target position.

B. MATLAB IMPLEMENTATION

This section explains how the localization testing was implemented in MATLAB using data produced by the MMPE propagation model. The problem was represented by a "target", which is the sound source, and two or more sonobuoys, which are the receivers. More specifically, we specified a cartesian coordinate system and set the true position of the target. The buoy positions were given to the MATLAB program relative to the target's position. This was done by having as inputs the quadrant number, the distance (range) to the buoy, and the distance in x-coordinate to the buoy. In this way, it was possible to create any geometric scenario in two dimensions.

After specifying the geometry of the scenario, we had to find the value of the sound speed that would be used for each environment. To be as realistic as possible with each case, we evaluated the group speed of a specific mode that would dominate during propagation of the signal. This was executed for each water column corresponding to each buoy location in the range-dependent cases and only once in range-independent cases, since the sound speed profile remains the same throughout the computational grid. For the range-dependent environments, we averaged those values of the group speed for each buoy in order to end up with one value to use for the rest of the algorithm.

After these steps, the data from MMPE (after being modulated/demodulated as described in Chapter 4) was read into the localization program. Then using all the previously described methods (subspace - classical) we evaluated the TDOAs for all combinations of pairs of buoys. Since we don't know absolute TOA for any of the buoys, we set TOA for the 1st buoy equal to zero, $TOA(1) = 0$, and measured the relative TOA for the other buoys with respect to the first buoy as a reference.

The rest of the algorithm continues as it was presented in the last section to evaluate the "Estimated Target Position." The entire procedure is repeated for all the TDOA methods for each environment and for each case and using the same signals. In this way, it is possible to evaluate the performance of all the methods under the same circumstances and compare results among them. Figure 36 summarizes all the steps of the localization procedure.

C. SIMULATION RESULTS

In this section, simulation results for the localization problem using the four MMPE environments are presented. For each environment, there are two cases considered. In the first, the minimum number of three sonobuoys is used. (Recall that three is the minimum, since we require at least two separate TDOA measurements to locate the target.) In the second case, more than three sonobuoys are used.

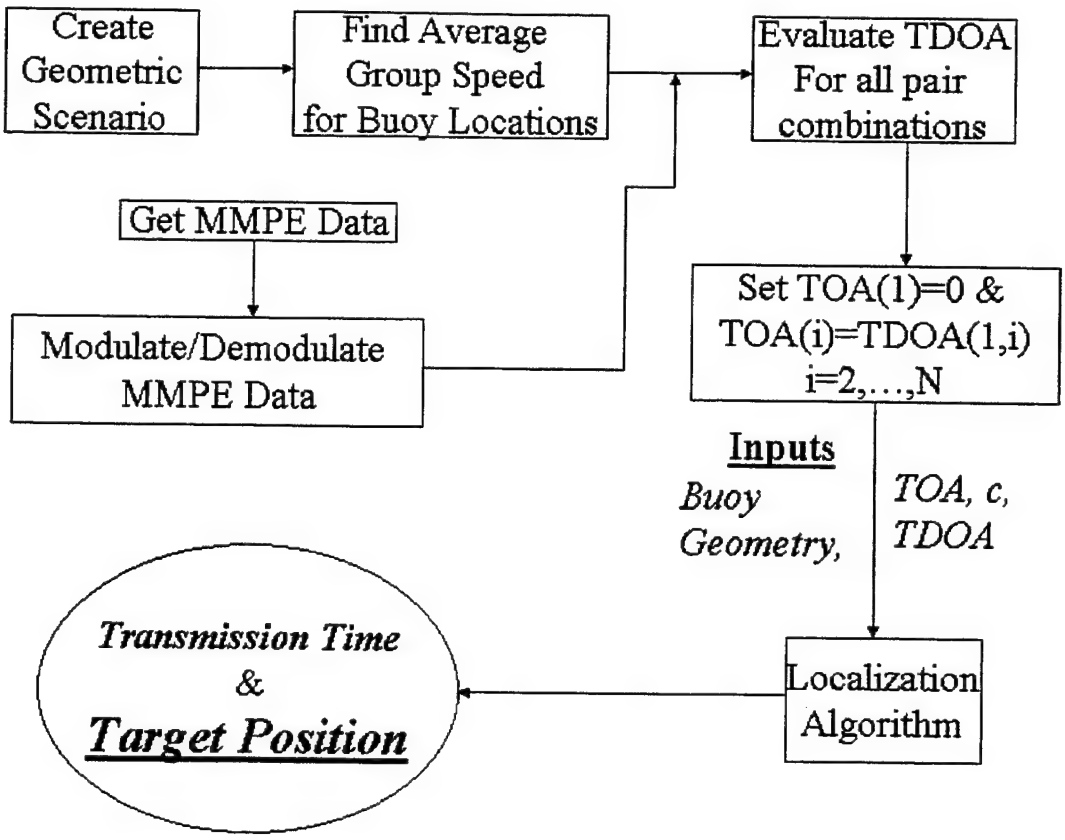

Figure 36. Flowchart of Localization Algorithm implemented in MATLAB environment using data from MMPE.

For each environment and each TDOA method we show a pair of figures with the locations of the buoys, the real target location and the estimated location from each method. Each figure in the pair corresponds to the two cases mentioned above (3 buoys and more than 3 buoys), and contains two subfigures with the results from the subspace and from the classical methods respectively. Each environment is accompanied by a table. The tables contain the error in target's position, i.e., the difference between the actual location and the estimated one for each method. In this way there is a fair evaluation for all the methods, since for this kind of problem the difference of the two positions (real-estimated) is of most concern.

1. Flat Bottom

The characteristics of this environment are described in Chapter 4. The true geometric positions for two scenarios with 3 and 5 receivers (buoys) are presented in Figs. 37 and 38 respectively. The source was at a depth of 150m while the receivers were at a depth of 50m and ranges of 2, 3 and 5 km from the source. Table XII has the target position error for all methods for both cases in this environment.

Observing Table XII, we conclude that all methods performed efficiently, but the position accuracy was better for the subspace methods than the classical methods. In both groups of methods there was an improvement with the increase of the number of sonobuoys, except from the Roth method. The variance of the results from the subspace methods was much smaller than the respective one from the classical methods. Further, the cross-correlation (X-Corr) had the best performance from the classical methods and was the only one from this family whose results were closer to those of the subspace methods.

Method	**Target Position Error in (m)**	
	3 buoys	5 buoys
MUSIC	29.68	23.74
Modified-MUSIC	47.46	24.67
MIN-NORM	30.16	22.45
PCLP	30.16	22.42
ESPRIT	30.76	21.86
Root-MUSIC	30.06	21.81
SCOT	100.87	67.52
PHAT	100.87	67.52
Roth	87.17	183.81
X-Corr	37.04	31.42

Table XII. Target position Error for Flat bottom isospeed case.

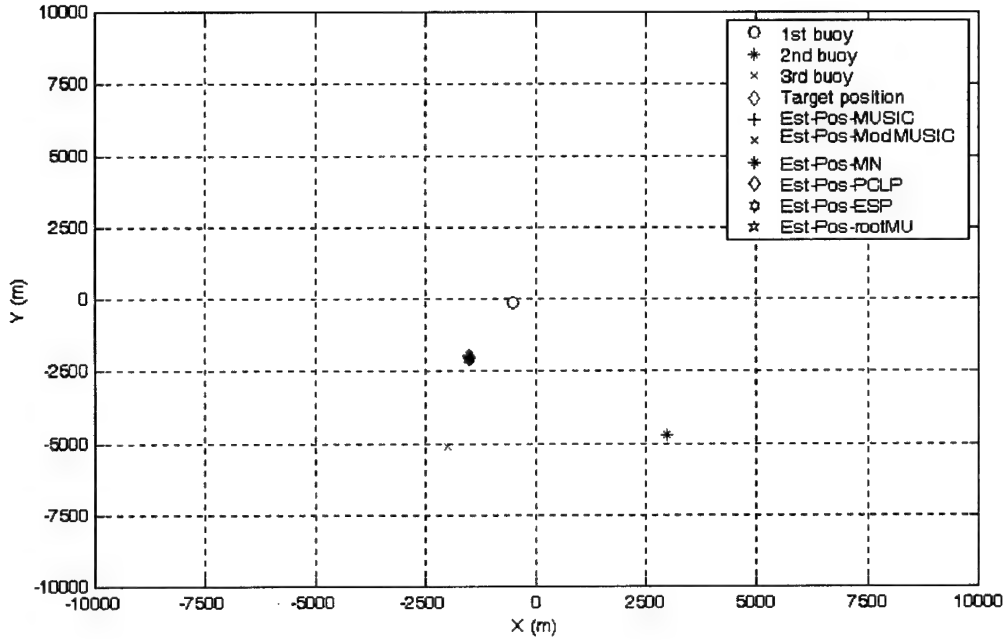

(a)

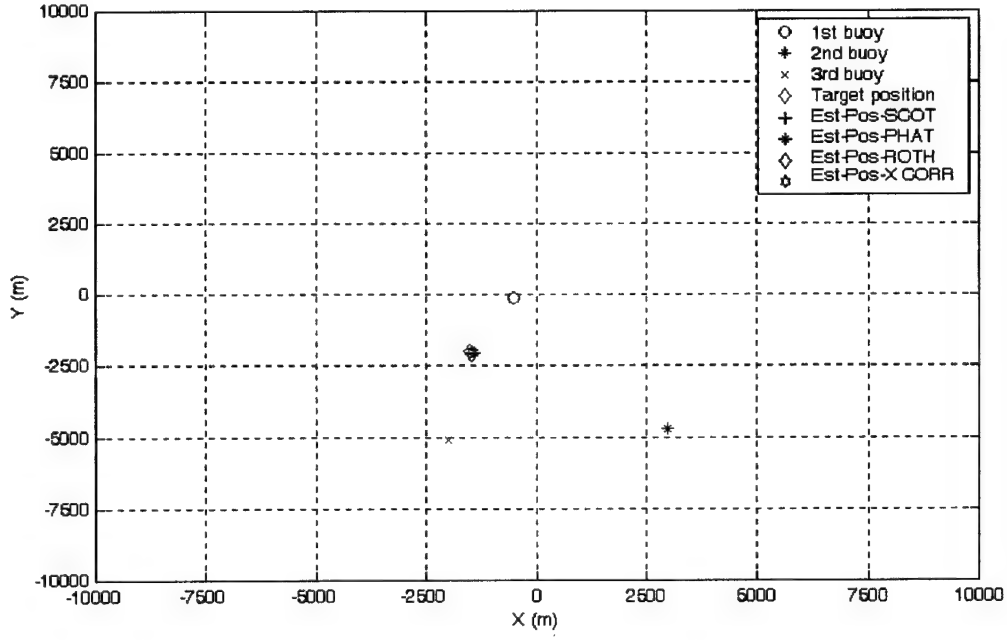

(b)

Figure 37. Localization problem for Flat bottom isospeed case with 3 sonobuoys. (a) Subspace methods. (b) Classical methods.

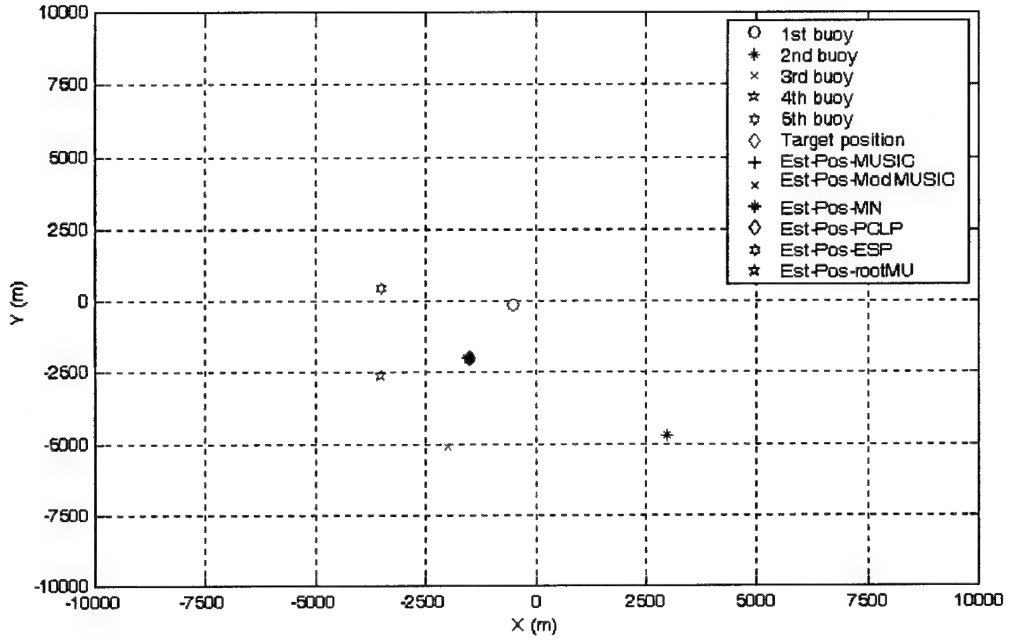

(a)

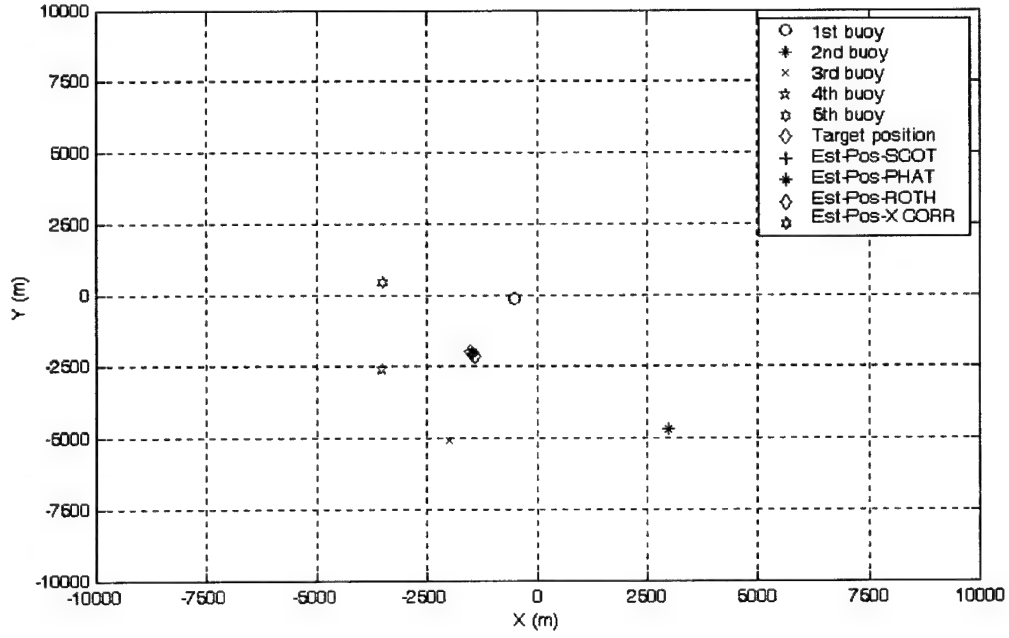

(b)

Figure 38. Localization problem for Flat bottom isospeed case with 5 sonobuoys. (a) Subspace methods. (b) Classical methods.

2. Sound Channel

The characteristics of this environment are described again in Chapter 4. The true geometric positions of the two scenarios with 3 and 5 receivers (buoys) are shown in Figs. 39 and 40, respectively. The source was at a depth of 150m and the receivers were at a depth of 50m and at ranges of 2 and 4 km from the source. The results are also accompanied by Table XIII presenting the Target Position Error for all methods. Once again the subspace methods had better accuracy than the classical methods as a group. In both families of methods, we observe that increasing the number of the buoys does not, by itself, assist the algorithm to more accurately predict the target position. The main consideration that has to be made is the disposition of the receivers and then the number of them. If the disposition is suitable, then an increase of the number of the sonobuoys may improve the result since, as we have seen in section A of this chapter, Eq. VI.3 will be solved either uniquely if $N = 3$ or in a least squares sense if $N > 3$. The performance was similar to the Flat bottom case, with Roth being more unstable in the results, and SCOT, PHAT performing better than X-Corr.

Method	**Target Position Error in (m)**	
	3 buoys	5 buoys
MUSIC	19.65	25.72
Modified-MUSIC	21.35	28.42
MIN-NORM	19.65	26.65
PCLP	19.65	26.65
ESPRIT	20.50	26.20
Root-MUSIC	19.65	26.65
SCOT	47.04	53.02
PHAT	47.04	53.02
Roth	24.70	487.13
X-Corr	45.92	65.09

Table XIII. Target position Error for Sound Channel case .

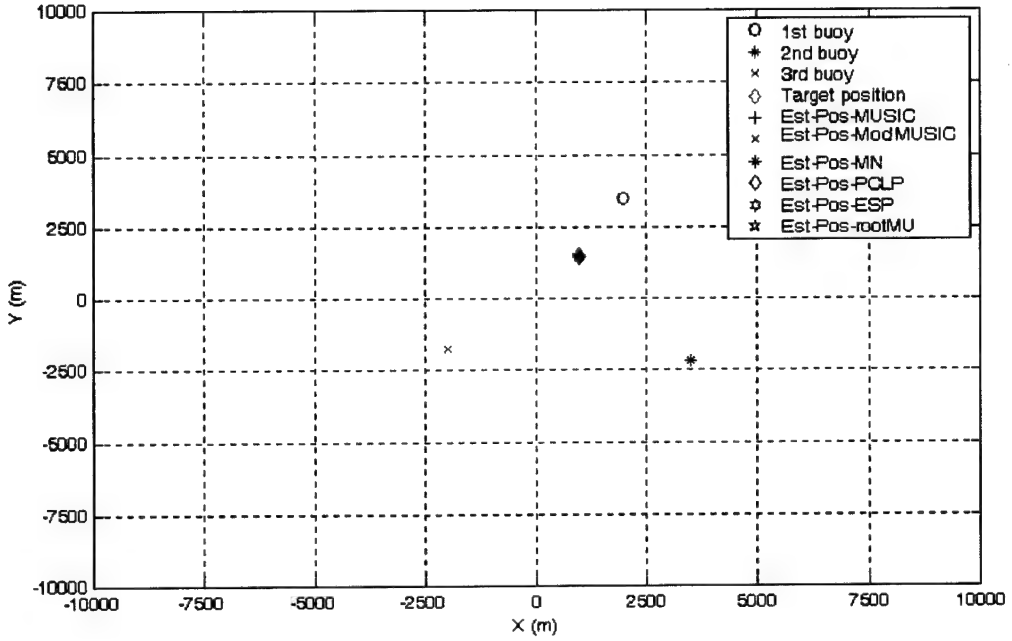

(a)

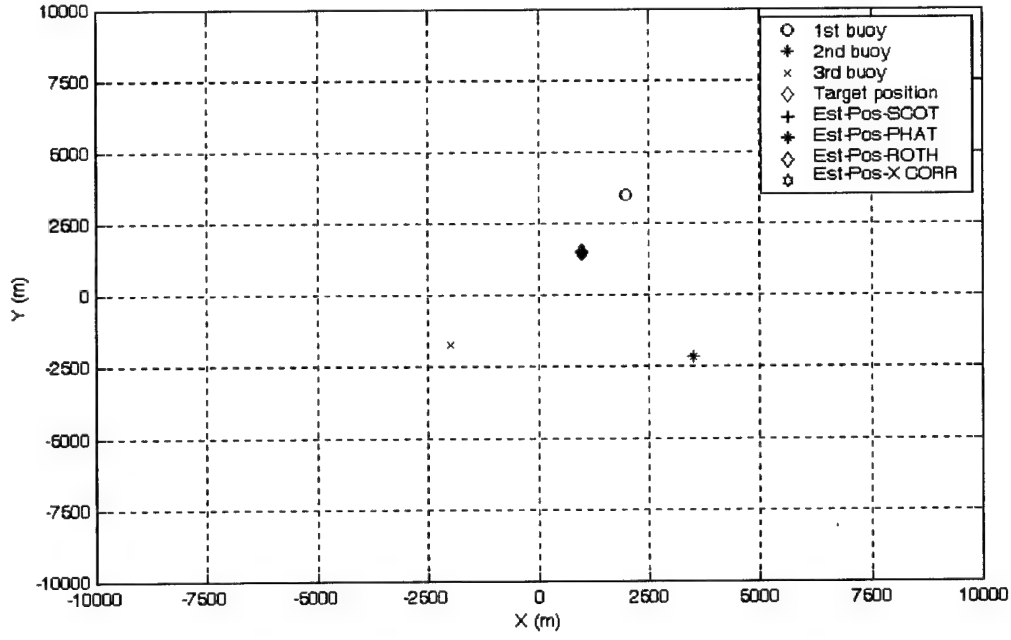

(b)

Figure 39. Localization problem for Sound Channel case with 3 sonobuoys. (a) Subspace methods. (b) Classical methods.

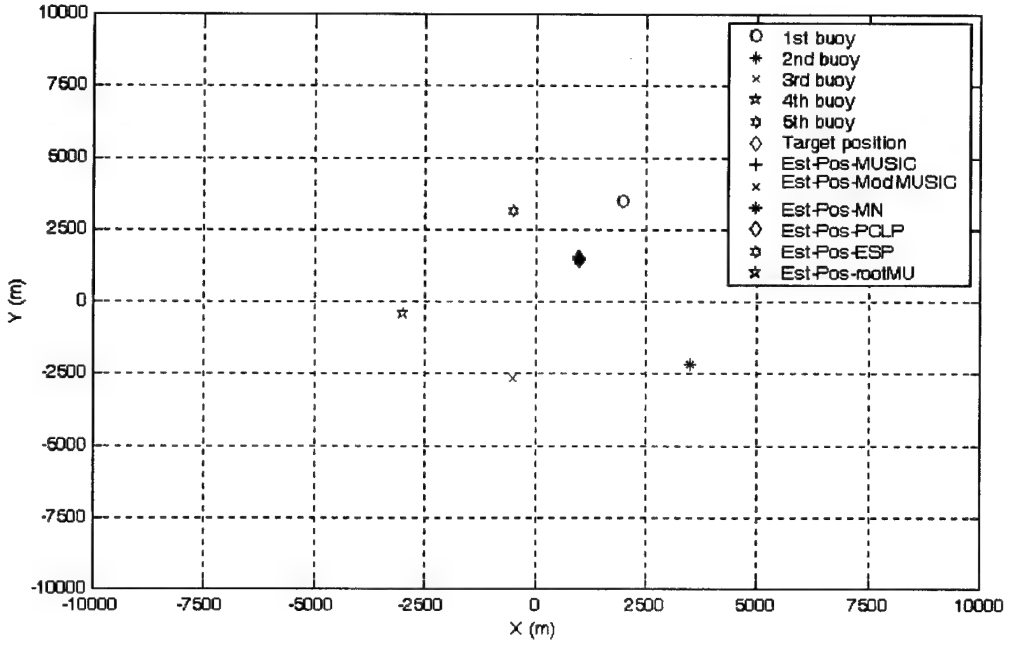

(a)

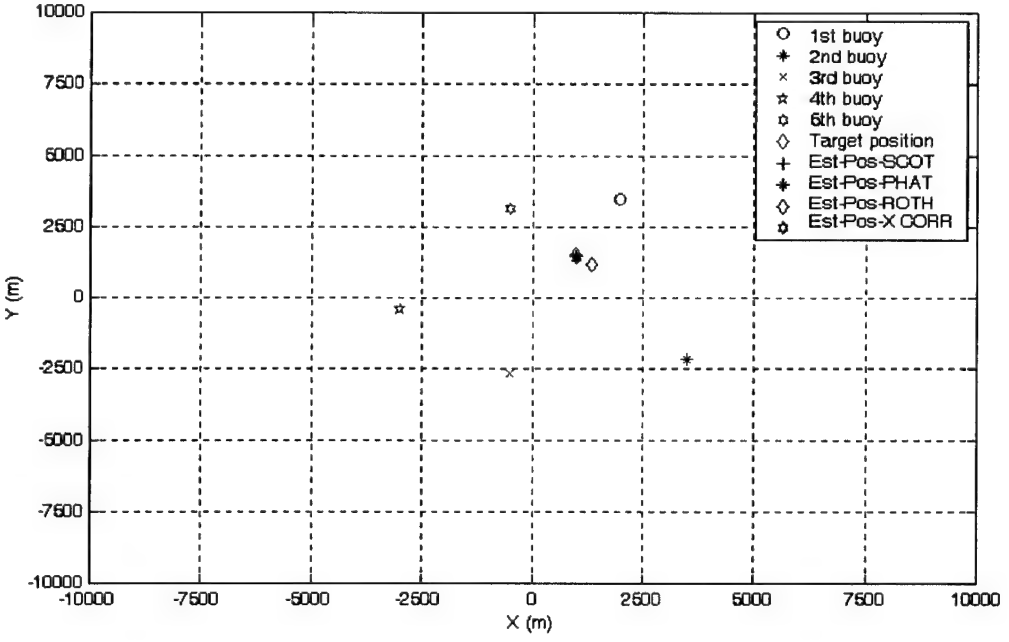

(b)

Figure 40. Localization problem for Sound Channel case with 5 sonobuoys. (a) Subspace methods. (b) Classical methods.

3. Shelf Break

Using the characteristics for this environment discussed in Chapter 4, the true geometric positions of two scenarios with 3 and 6 receivers (buoys) are presented in Figs. 41 and 42 respectively. The source was at a depth of 250m and the receivers were at a depth of 50m and at range of 3 km from the source, located upslope and downslope concurrently (see similar Fig. 26). Table XIV summarizes the results of the performance for all methods. In this range-dependent environment, we see that subspace methods have similar accuracy in their results compared with the one in the range-independent environments. In comparison with the subspace methods, the classical methods performed much poorer. This could be expected if we recall their quality of results in the estimation of TDOA (see Table X.) In general, there was an improvement of the results for all methods (except X-Corr) with an increase in the number of the sonobuoys. This improvement was more drastic for Roth, something that also was expected considering the diversity of the results from this method. Another remark is that because of the complexity of the range-dependent environments the buoys disposition is very critical. An inappropriate disposition can create larger errors in target position than the range-independent environments.

Method	**Target Position Error in (m)**	
	3 buoys	6 buoys
MUSIC	24.65	22.48
Modified-MUSIC	31.04	22.64
MIN-NORM	25.32	20.45
PCLP	25.32	20.48
ESPRIT	27.29	21.96
Root-MUSIC	27.29	21.89
SCOT	434.35	432.77
PHAT	434.35	432.77
Roth	787.43	418.26
X-Corr	93.53	215.67

Table XIV. Target position Error for Shelf Break case .

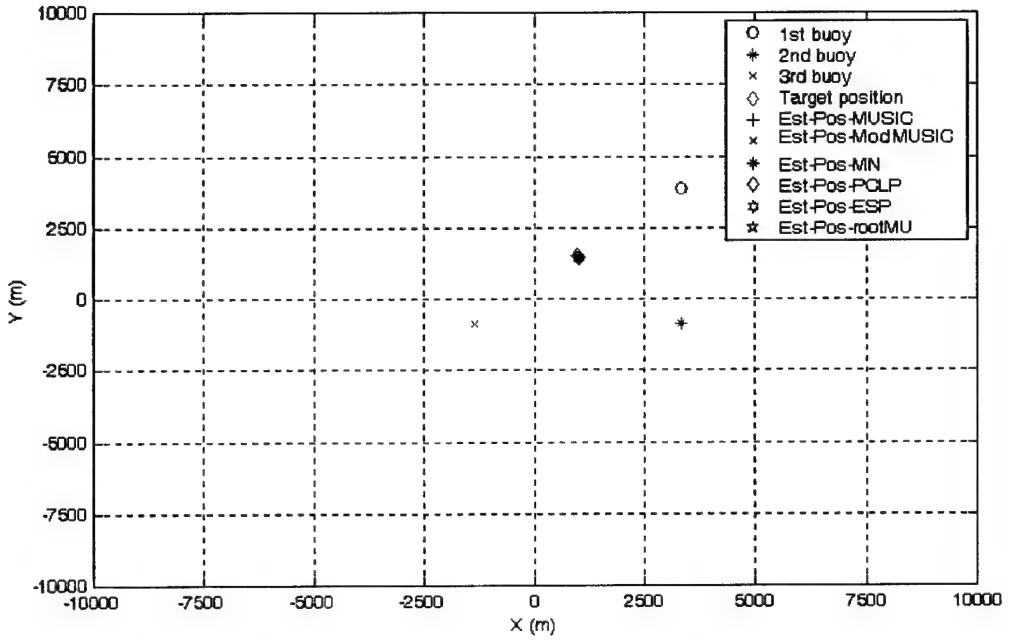

(a)

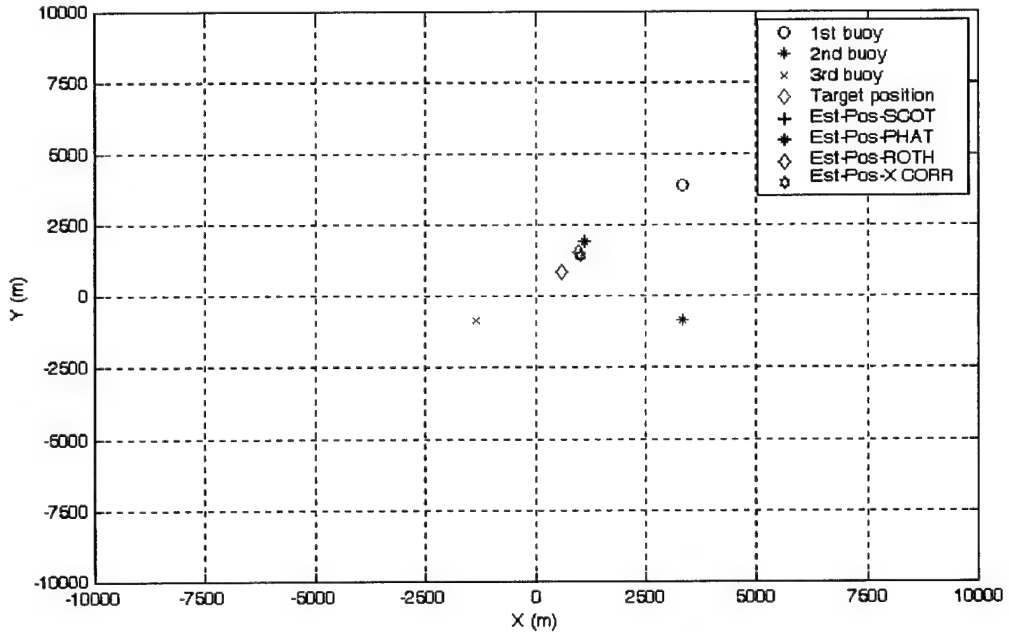

(b)

Figure 41. Localization problem for Shelf Break case with 3 sonobuoys. (a) Subspace methods. (b) Classical methods.

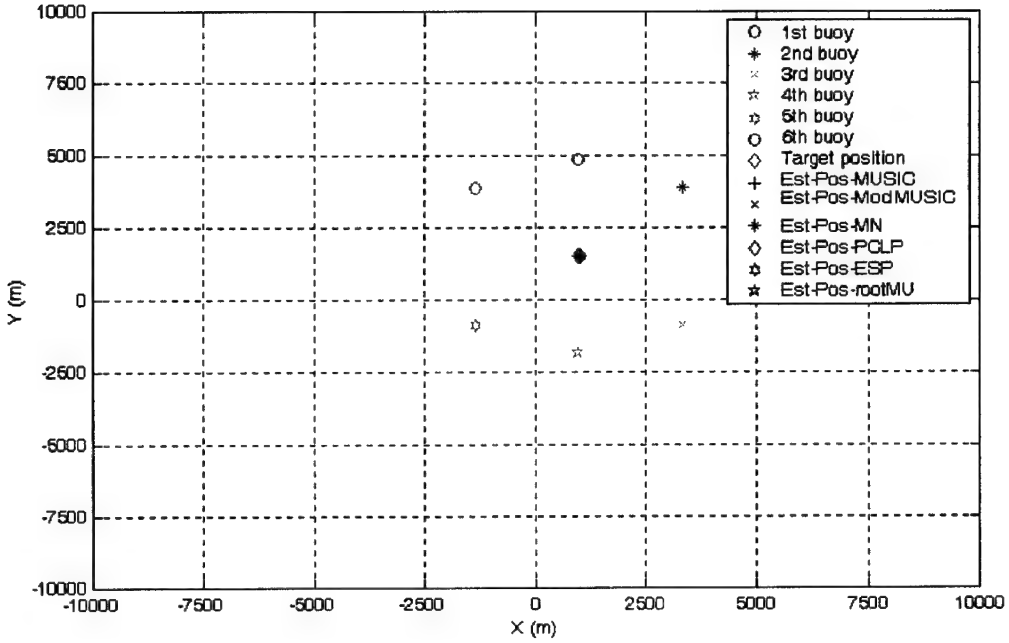

(a)

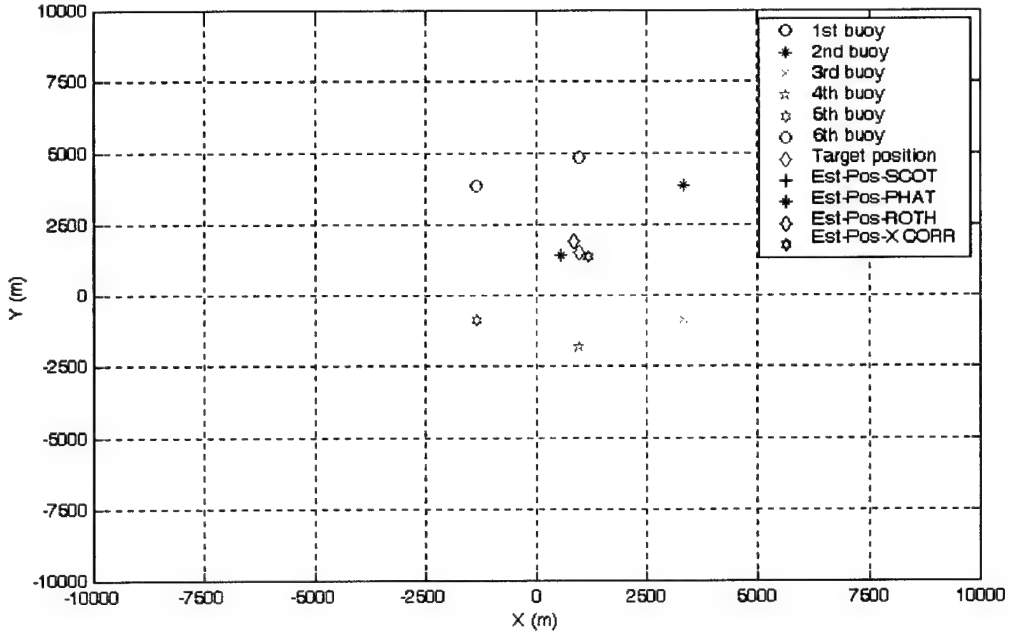

(b)

Figure 42. Localization problem for Shelf Break case with 6 sonobuoys. (a) Subspace methods. (b) Classical methods.

4. Internal Waves

Using the characteristics for this environment described in Chapter 4, the true geometric positions of two scenarios are shown with 3 and 6 receivers (buoys) in Figs. 43 and 44, respectively. The source was at a depth of 150m and the receivers were at a depth of 50m and at range of 2 km from the source located on both the sides. We have to mention that some of the receivers were located in the section of the computational grid with sinusoidal and soliton perturbations and the rest of them were in the other section with sinusoidal perturbations only (see similar Fig. 31). Table XV contains the results of the performance for all methods. This environment is the most complex that we used so far and it deviates considerably from the basic concept of the localization algorithm, which assumes a constant value for the sound speed. For this environment all the methods have decreased performance. The difference between subspace and classical was the same as before, shown in Table XI. The only difference is that the increase in the number of the sonobuoys with different disposition had worse results than in the Shelf Break environment and that X-Corr gave similar results to the subspace methods.

Method	**Target Position Error in (m)**	
	3 buoys	6 buoys
MUSIC	65.90	160.52
Modified-MUSIC	64.64	153.58
MIN-NORM	63.02	164.64
PCLP	62.29	165.85
ESPRIT	63.81	164.78
Root-MUSIC	66.11	155.57
SCOT	423.57	849.08
PHAT	423.57	849.08
Roth	226.81	515.59
X-Corr	49.22	160.37

Table XV. Target position Error for Internal Waves case .

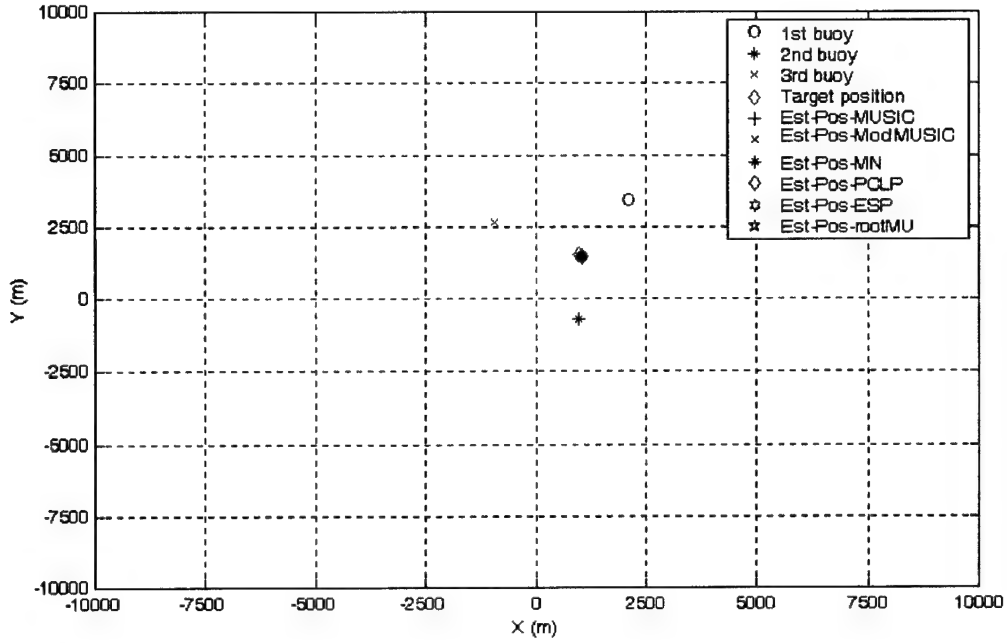

(a)

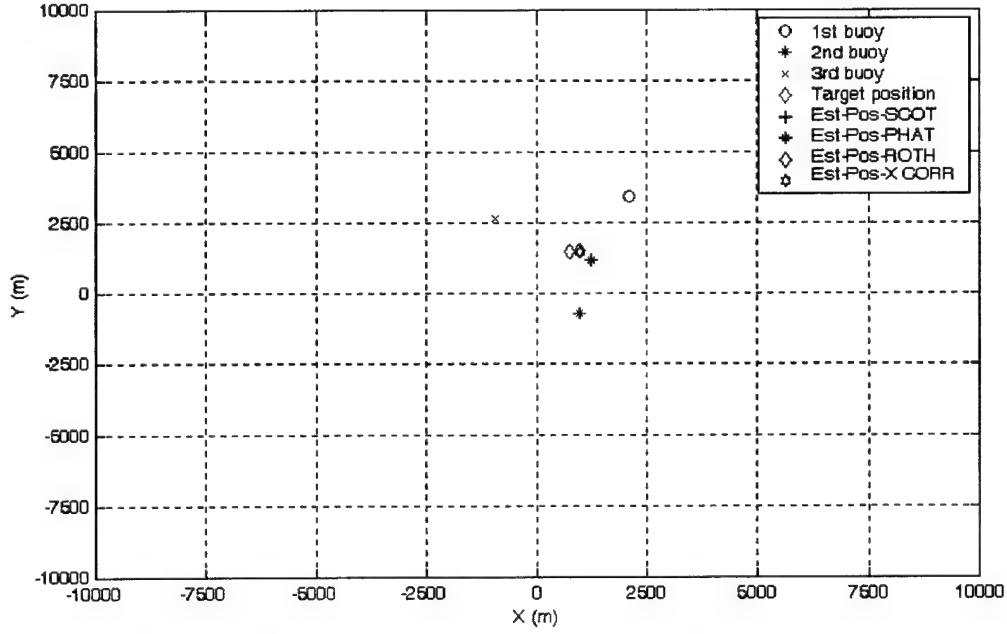

(b)

Figure 43. Localization problem for Internal Waves case with 3 sonobuoys. (a) Subspace methods. (b) Classical methods.

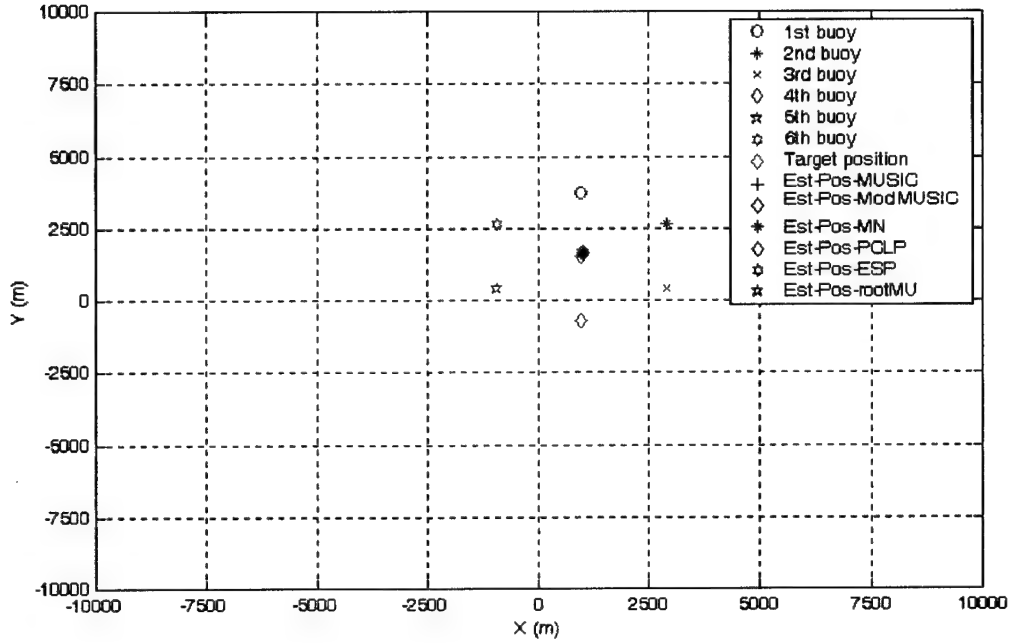

(a)

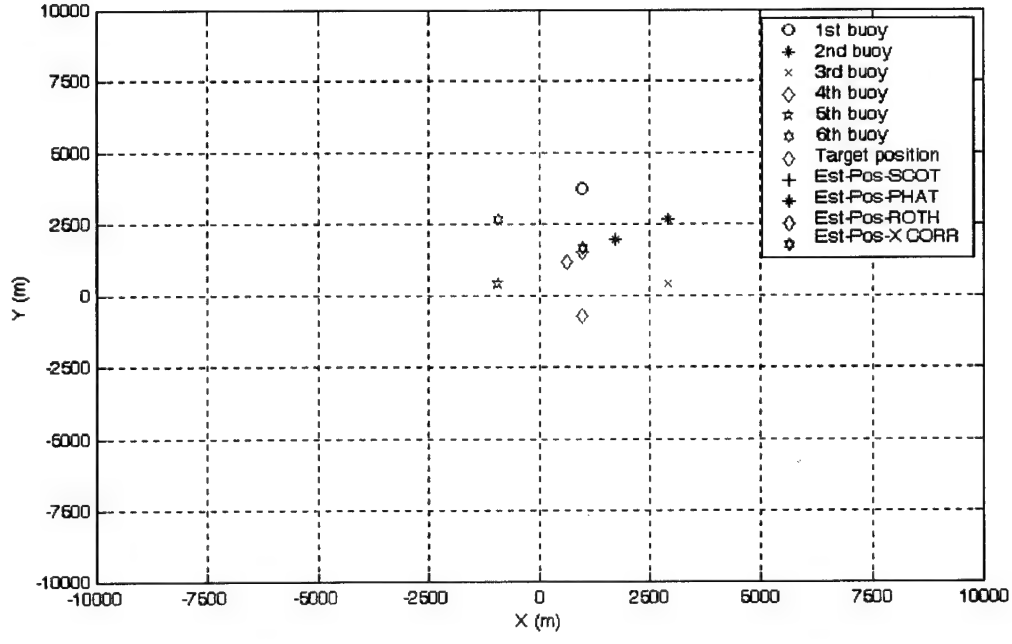

(b)

Figure 44. Localization problem for Internal Waves case with 6 sonobuoys. (a) Subspace methods. (b) Classical methods.

From the corresponding figures and tables for each environment, one can conclude that in most cases all the methods performed quite successfully. The subspace methods were more consistent in their results as a group; this is something that didn't happen with the classical methods. Further, with different realizations of the noise, the variance of the results of the subspace methods was much smaller than for the classical methods. The location accuracy in the range-dependent environments was less than in the range-independent environments and was reduced even more when the distance between receivers and source became greater (4 to 8km). Another major factor for the successful localization of the target was the geometrical disposition of the receivers relative to the source position. In other words, if the receivers were located in such a way that the bearing from each pair formed an angle of between 60^o and 120^o, then the estimate of their crossing will have less error than otherwise.

A larger number of receivers does not always contribute to more accurate detection. This can be justified from the fact that when N is equal to 3, the solution from Eq. (VI.9) is unique, while a value of $N > 3$ requires a least squares solution to minimize the equation error in the over specified set of equations. As discussed in Section A of this chapter, the solution for t is independent of which particular range equation (k) is used to develop the quadratic equation, and in order to overcome the obstacle of measurement errors, we have to develop $N-1$ estimates for t using $k = 1, 2, \cdots, N-1$, discarding any erroneous values and averaging the remaining solutions. A larger value of N does not always lead to a better result. In other words for more accurate results, the placement of the buoys is more important than the number of the buoys.

THIS PAGE INTENTIONALLY LEFT BLANK

VII. TRACKING PROBLEM

A. DOPPLER IMPLEMENTATION IN MMPE

In actual underwater acoustics problems, the source and/or the receiver are not stationary, but they are in motion. This motion causes temporal fluctuations, something we have to take into consideration if we want to find out how the underwater acoustic channel influences various applications such as communications [Ref. 34]. In our case we will consider motion only due to the source (target), and the receivers (buoys) will be stationary. Figure 45 gives a characteristic example of the effect. The result of the source motion is to provoke a change in the value of the actual source frequency observed, $f_S(\theta)$, in other words in the received frequency at buoy i compared with the original transmitted frequency, f_T. The received frequency, $f_S(\theta)$, will depend on the transmitted frequency, f_T, the observation angle, θ, the source speed, v_S, and the direction of motion, ϕ_S [Ref. 35],

$$f_S(\theta) = \frac{f_T}{1 - \left(\frac{v_S}{c}\right)\cos(\theta - \phi_S)}. \tag{VII.1}$$

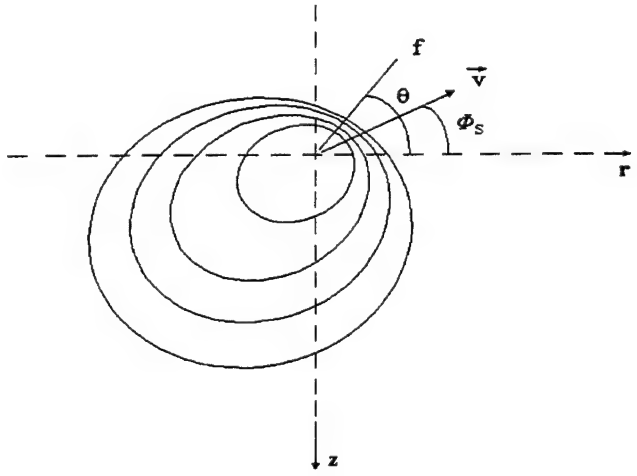

Figure 45. Effect of Doppler due to linear motion of the source.

According to [Ref. 35] when $|\phi_S| < 90°$ then the observed frequency bandwidth downrange, BW_S^{r+}, will be equal to

$$BW_S^{r+} = BW_T + \frac{v_S}{c}\left(f_{T,max} + f_{T,min}|\sin\phi_S|\right), \tag{VII.2}$$

where BW_T is the actual transmitted bandwidth, and $f_{T,max}$ and $f_{T,min}$ are the actual transmitted maximum and minimum frequencies, respectively, of the transmitted band. The observed center frequency downrange is defined as [Ref. 35]

$$f_{S,c}^{r+} = f_{T,c} + \frac{v_S}{2c}\left(f_{T,max} - f_{T,min}|\sin\phi_S|\right), \tag{VII.3}$$

where $f_{T,c}$ is the actual transmitted center frequency. When $|\phi_S| > 90°$, then the observed bandwidth downrange will be [Ref. 35]

$$BW_S^{r-} = BW_T + \frac{v_S}{c}\left(f_{T,max}|\sin\phi_S| + f_{T,min}\right), \tag{VII.4}$$

and the observed center frequency is equal to

$$f_{S,c}^{r-} = f_{T,c} + \frac{v_S}{c}\left(f_{T,max}|\sin\phi_S| + f_{T,min}\right). \tag{VII.5}$$

The equation for the PE starting field in the vertical wavenumber domain has the general form [Ref. 35]

$$\hat{\psi}\left(r = 0, k_z, f\right) = e^{-ik_z z_s}\hat{\psi}_o(k_z, f) - e^{ik_z z_s}\hat{\psi}_o(k_z, f), \tag{VII.6}$$

where the functions $\hat{\psi}_o(k_z, f)$ represent the starting field in free space. The role of the exponentials in Eq. (VII.6) is the creation of the appropriate interference structure between the source (target), which lies at depth z_S and its image about the plane of the free surface ($z = 0$). The vertical wavenumber is defined by

$$k_z = k_o \sin\theta = \frac{2\pi f}{c_o}\sin\theta, \tag{VII.7}$$

where θ is the angle of propagation relative to horizontal and k_o is the reference wavenumber.

For the rest of this chapter, we assume that we have a point source, which is modeled in such way that [Ref. 35]

$$\hat{\psi}(k_z, f) = \alpha(k_o)S(f), \tag{VII.8}$$

where

$$\alpha(k_o) = \sqrt{\frac{iR_o}{2\pi k_o}}, \tag{VII.9}$$

and $S(f)$ is the amplitude spectrum of the pulse in the frequency domain. The MMPE uses a Hanning window in order to create the aforementioned spectrum, defined by

$$S(f) = \begin{cases} \cos^2\left(\frac{f-f_c}{BW}\pi\right), & |f - f_c| < \frac{BW}{2} \\ 0, & |f - f_c| > \frac{BW}{2} \end{cases}, \tag{VII.10}$$

where f_c is the center frequency of the transmitted band and BW is the transmission bandwidth.

Now that there is motion of the source, Eq. (VII.6) should be stated in accordance with the transmission parameters (see [Ref. 35]) as

$$\hat{\psi}\left(r = 0, k_z, f\right) = e^{-ik_z z_s}\hat{\psi}_o(k_{z,T}, f_T) - e^{ik_z z_s}\hat{\psi}_o(k_{z,T}, f_T), \tag{VII.11}$$

where

$$k_{z,T} = \frac{k_o \sin\theta}{\left[1 + \frac{v_S}{c_o}\cos\left(\theta - \phi_S\right)\right]}. \tag{VII.12}$$

The frequency in the enviromental frame is defined by the transmitted frequency, f_T, with the assistance of Eq. (VII.1), which determines the relationship between f_T and $f_S(\theta)$. Finally the source spectrum $S(f)$ will take the form [Ref. 35]

$$S(f_T) = S\left(\frac{f}{\left[1 + \frac{v_S}{c_o}\cos\left(\theta - \phi_S\right)\right]}\right). \tag{VII.13}$$

Finally the factor α has to be replaced by the corresponding transmitted value α_T.

One of the differences between the two cases, with and without Doppler, is the different size of the observed frequency bandwidth. In order to be able to compare results, the computational bandwidth of the non-Doppler case has to be set to the same size as the Doppler case. This is achieved by applying a weighting of zero to those frequency bins that are outside of the actual non-Doppler bandwidth.

B. MATLAB IMPLEMENTATION AND SIMULATION RESULTS

For the tracking problem, the MATLAB implementation is almost the same as the implementation for the localization problem. However, there are two main differences. The first is the different manipulation of the MMPE data, since the code has now been changed in order to give us the effect of the Doppler. The second is an addition to the previous code, which has as inputs the coordinates of the buoys, the estimated coordinates of the source, the received signals corresponding to each buoy, and the evaluated group speed (see Chapter 6, section 2). The computed outputs will then be the ***course*** and the ***speed*** of the target. Regarding the new manipulation of the MMPE data, most of the procedure was shown in the previous section. So after re-mapping the original "MMPE" signal with the desired frequency resolution to account for the shift of the center frequency, we take the product of the real part of the re-mapped signal with the phasor $\exp^{(-j2\pi f_c \mathbf{Time})}$, where f_c is the center frequency of the received signal, and **Time** is the re-mapped time vector with the desired resolution. Finally there is an interpolation of the pressure vector from its original time spanning vector **Time** to a fixed time spanning vector $\mathbf{Time_{fix}}$ which is the same for all received signals.

For the computation of the course and the speed of the target, the procedure that we implemented was the following. First, we find the spectrum of each received signal and from the spectrum we extract the center frequency. Afterwards, with the coordinates of the buoy locations and the estimated target location, we extract the angles between the relative position vectors for each pair of the buoys. Then we find the relative Doppler frequency that corresponds to each pair of center frequencies of the received signals. Finally we estimate the course of the target for each buoy by the following equations. Note that for the simplicity of the problem we used only three receivers (N=3), otherwise the system of equations becomes very complex.

$$Course(1) \;=\; acos(A(1)) + B(1) \qquad \text{(VII.14)}$$

$$Course(2) = acos(A(2)) + B(2) \quad \text{(VII.15)}$$

$$Course(3) = acos(A(3)) + B(3) \quad \text{(VII.16)}$$

where

$$A(1) = \frac{(K_2^2 + K_3^2) - K_1^2}{2K_2K_3} \quad \text{(VII.17)}$$

$$A(2) = \frac{(K_3^2 + K_1^2) - K_2^2}{2K_3K_1} \quad \text{(VII.18)}$$

$$A(3) = \frac{(K_1^2 + K_2^2) - K_3^2}{2K_1K_2} \quad \text{(VII.19)}$$

and

$$B(1) = \frac{1}{2}(\phi(1) + \phi(2)) \quad \text{(VII.20)}$$

$$B(2) = \frac{1}{2}(\phi(2) + \phi(3)) \quad \text{(VII.21)}$$

$$B(3) = \frac{1}{2}(\phi(3) + \phi(1)) \quad \text{(VII.22)}$$

and

$$K_1 = \frac{\Delta f_{12} c \frac{1}{2}}{\sin\left(\frac{1}{2}(\phi(1) - \phi(2))\right)} \quad \text{(VII.23)}$$

$$K_2 = \frac{\Delta f_{23} c \frac{1}{2}}{\sin\left(\frac{1}{2}(\phi(2) - \phi(3))\right)} \quad \text{(VII.24)}$$

$$K_3 = \frac{\Delta f_{31} c \frac{1}{2}}{\sin\left(\frac{1}{2}(\phi(3) - \phi(1))\right)} \quad \text{(VII.25)}$$

In Eqs. (VII.20) - (VII.22) and (VII.23) - (VII.25), the quantities $\phi(1), \phi(2), \phi(3)$ represent the angles in the horizontal plane of the position vectors of the buoys and in Eqs. (VII.23) - (VII.25) the variables $\Delta f_{12}, \Delta f_{23}, \Delta f_{31}$ stand for the relative Doppler frequencies between the center frequencies of the received signals. In the end, the course of the target will be the average of the outcomes of Eqs. (VII.14) - (VII.16).

Regarding the speed, it will be the average of the following calculations

$$Speed(1) = \frac{\Delta f_{12} c}{2 f_c \sin\left(\frac{\phi(1)-\phi(2)}{2}\right) \sin\left(Course(1) - \frac{\phi(1)+\phi(2)}{2}\right)} \quad \text{(VII.26)}$$

$$Speed(2) = \frac{\Delta f_{23} c}{2 f_c \sin\left(\frac{\phi(2)-\phi(3)}{2}\right) \sin\left(Course(2) - \frac{\phi(2)+\phi(3)}{2}\right)} \quad \text{(VII.27)}$$

$$Speed(3) = \frac{\Delta f_{31} c}{2 f_c \sin\left(\frac{\phi(3)-\phi(1)}{2}\right) \sin\left(Course(3) - \frac{\phi(3)+\phi(1)}{2}\right)}, \quad \text{(VII.28)}$$

where f_c is the theoretical center frequency of the transmitted signal. Since this quantity is unknown in our case, we substitute it with the average of the center frequencies of the received signals. This substitution will not significantly distort the result, since the shift of the center frequency due to Doppler is not large enough (low speeds) and the difference between the f_c (transmitted) and the average of f_c (received) is small. Figure 46 gives a geometrical overview of the problem.

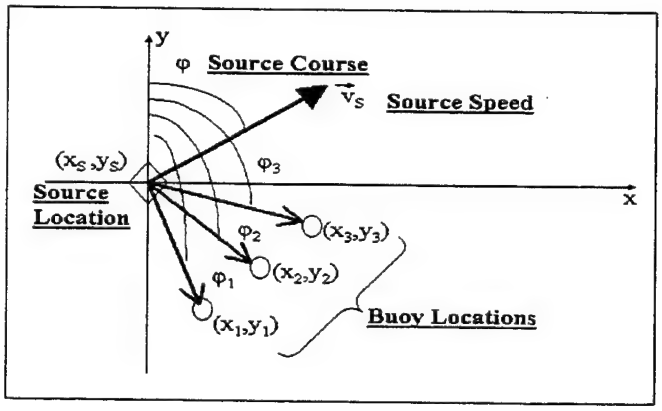

Figure 46. Top view of the Tracking problem.

Some simulation results will follow, one from each environment. For each case there will be figures indicating the geometric scenario and the solution that each method gives for the localization problem and also tables with *Target's Position Error in (m)* and the *Target's motion Data*, $Course(0 - 359^o)$ and $Speed(m/s)$.

1. Flat Bottom

The characteristics of this range-independent environment remain the same as were presented in Chapters 4, 5 and 6. In this case, the source is at depth 100m and the 3 buoys are located at ranges 2, 3 and 5km and at depth 30m as shown in Fig.

47. The source course and speed are 40° and 15m/s, respectively. Table XVI presents the results for the localization and tracking accuracy.

Method	**Target's Position Error in (m)**	
MUSIC	130.8	
Modified-MUSIC	120.2	
MIN-NORM	132.0	
PCLP	131.1	
ESPRIT	137.4	
Root-MUSIC	137.1	
SCOT	1010.0	
PHAT	1010.0	
Roth	1293.0	
X-Corr	53.6	
Target's Motion	**Estimated**	**Actual**
Course $(0 - 359^{o})$	37.73	40.00
Speed (m/s)	13.95	15.00

Table XVI. Target's Motion & position Error for Flat bottom isospeed case (Number of receivers = 3).

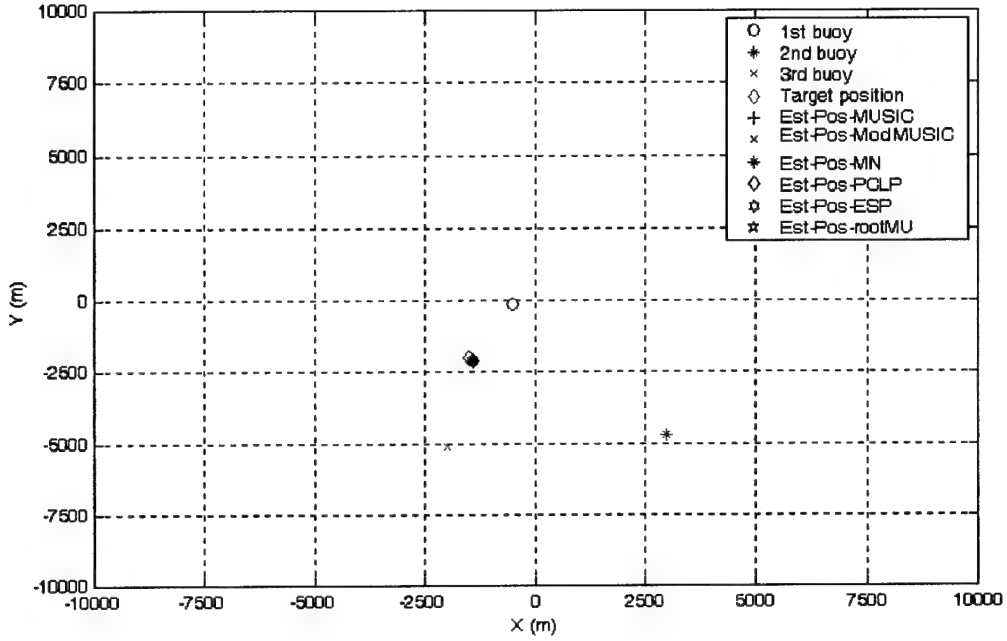

(a)

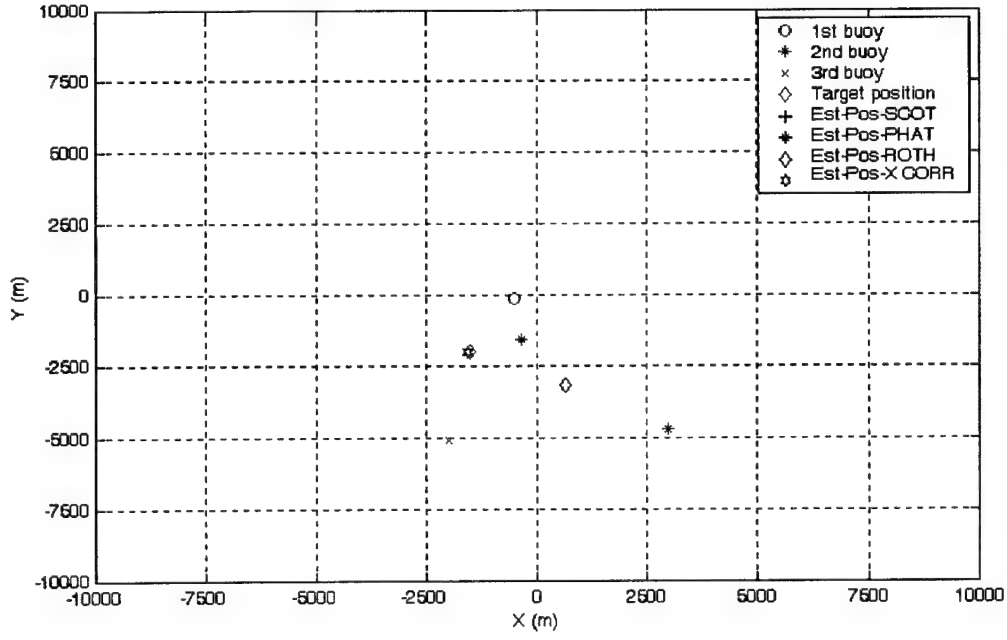

(b)

Figure 47. Tracking problem for Flat bottom isospeed case with N=3 sonobuoys. (a) Subspace methods. (b) Classical methods.

2. Sound Channel

As before, this range-independent environment retains the same properties as shown in Chapters 4, 5 and 6. For this case, the source is at depth 150m and the 3 buoys are located at ranges 2 and 4km and at depth 40m as shown in Fig. 48. The source course and speed are 75^o and 10m/s, respectively. Table XVII presents the results for the localization and tracking accuracy.

Method	**Target's Position Error in (m)**	
MUSIC	126.0	
Modified-MUSIC	131.7	
MIN-NORM	127.6	
PCLP	126.3	
ESPRIT	130.6	
Root-MUSIC	129.4	
SCOT	2234.5	
PHAT	2234.5	
Roth	4413.0	
X-Corr	229.3	
Target's Motion	**Estimated**	**Actual**
Course $(0 - 359^o)$	75.17	75.00
Speed (m/s)	11.41	10.00

Table XVII. Target's Motion & position Error for Sound Channel case (Number of receivers = 3).

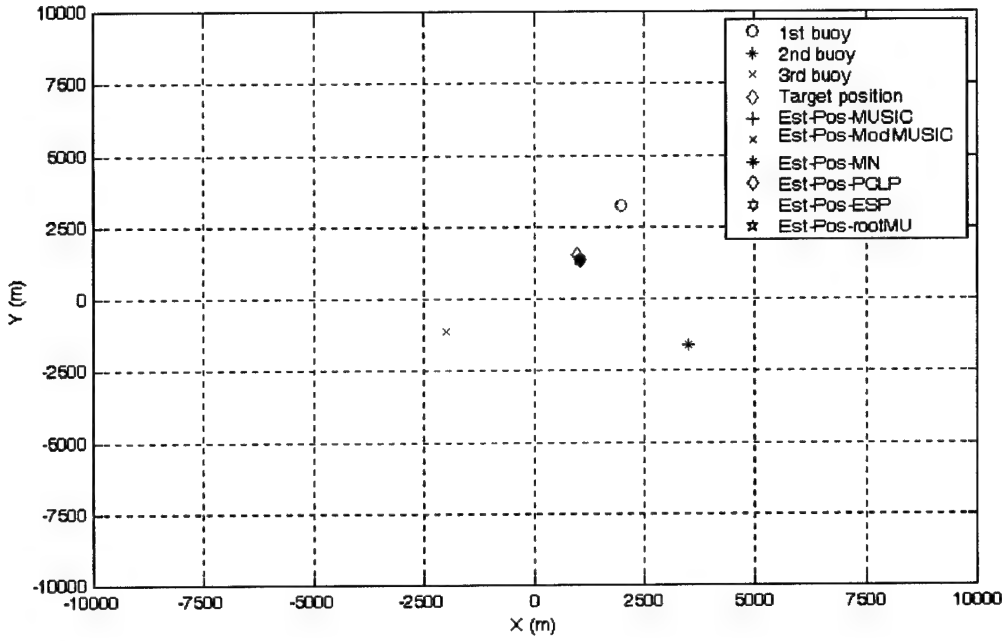

(a)

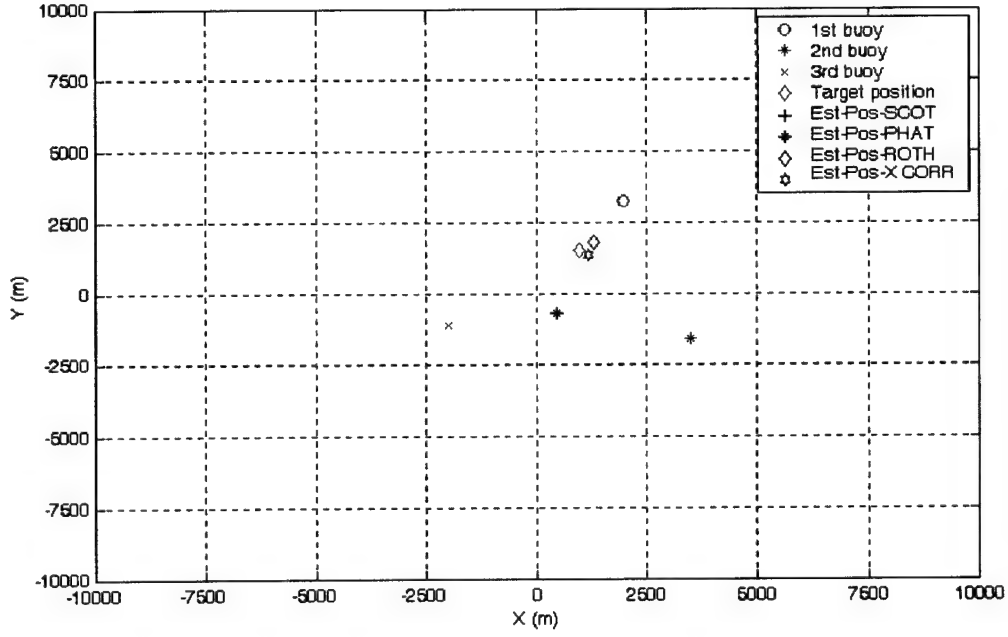

(b)

Figure 48. Tracking problem for Sound Channel case with N=3 sonobuoys. (a) Subspace methods. (b) Classical methods.

3. Shelf Break

The properties of the current range-dependent environment are the same as described in previous Chapters. In this case, the source is at depth 250m and the 3 buoys are located at ranges 3 and 4km and at depth 100m as shown in Fig. 49. The source course and speed are 100^o and 8m/s, respectively. Table XVIII presents the results for the localization and tracking accuracy.

Method	**Target's Position Error in (m)**	
MUSIC	259.2	
Modified-MUSIC	289.3	
MIN-NORM	282.8	
PCLP	275.6	
ESPRIT	335.7	
Root-MUSIC	303.5	
SCOT	671.4	
PHAT	671.4	
Roth	1947.6	
X-Corr	185.2	
Target's Motion	**Estimated**	**Actual**
Course $(0 - 359^o)$	105.64	100.00
Speed (m/s)	8.43	8.00

Table XVIII. Target's Motion & position Error for Shelf Break case (Number of receivers = 3).

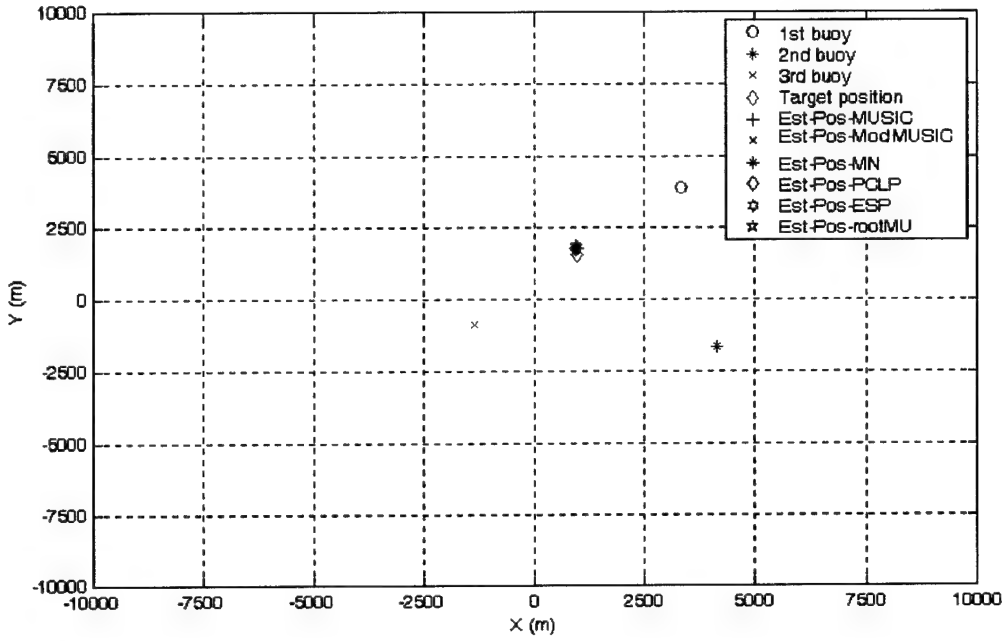

(a)

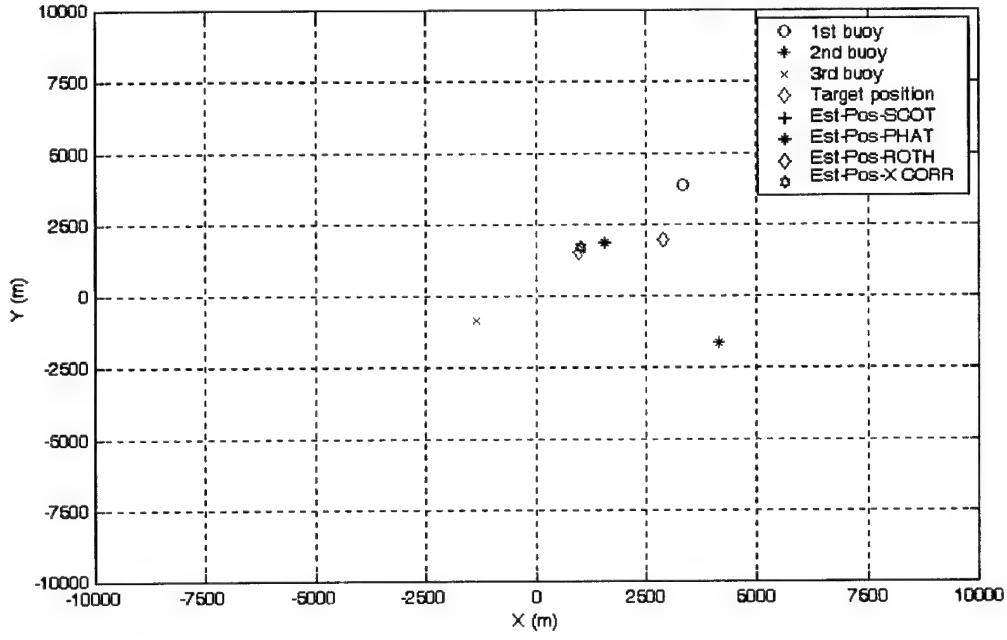

(b)

Figure 49. Tracking problem for Shelf Break case with N=3 sonobuoys. (a) Subspace methods. (b) Classical methods.

4. Internal Waves

Finally this range-dependent environment retains the properties that we have already seen in our previous discussion. During the present simulation, the source is at depth 150m and the positions for the 3 buoys are at range 2km and at depth 50m as shown in Fig. 50. The source course and speed are 230° and 5m/s, respectively. Table XIX presents the results for the localization and tracking accuracy.

Method	**Target's Position Error in (m)**	
MUSIC	176.5	
Modified-MUSIC	186.3	
MIN-NORM	176.7	
PCLP	176.2	
ESPRIT	181.4	
Root-MUSIC	181.3	
SCOT	938.5	
PHAT	938.5	
Roth	1504.8	
X-Corr	103.2	
Target's Motion	**Estimated**	**Actual**
Course $(0 - 359°)$	228.77	230.00
Speed (m/s)	4.21	5.00

Table XIX. Target's Motion & position Error for Internal Waves case (Number of receivers = 3).

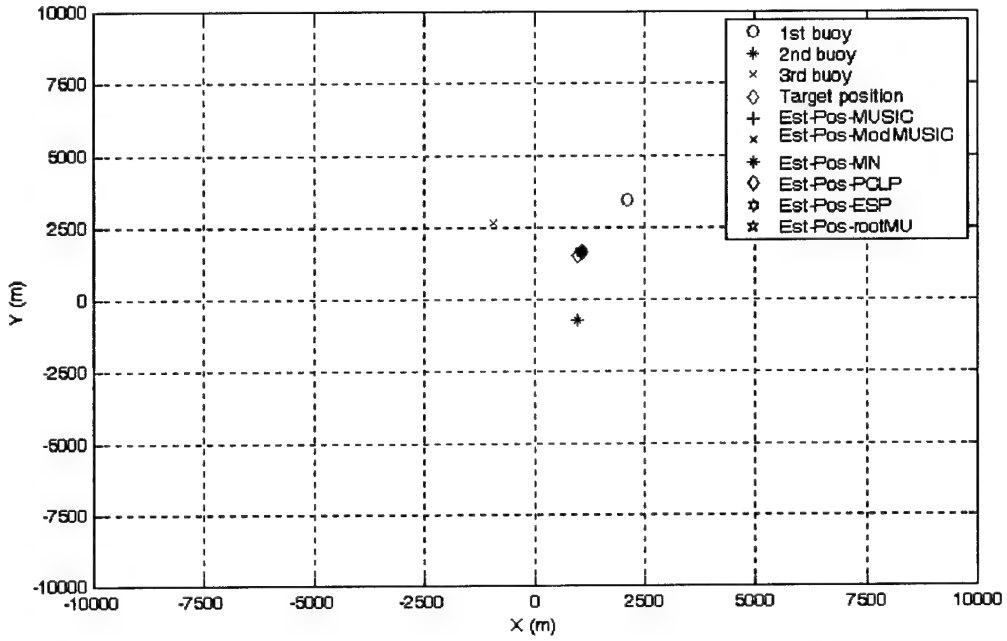

(a)

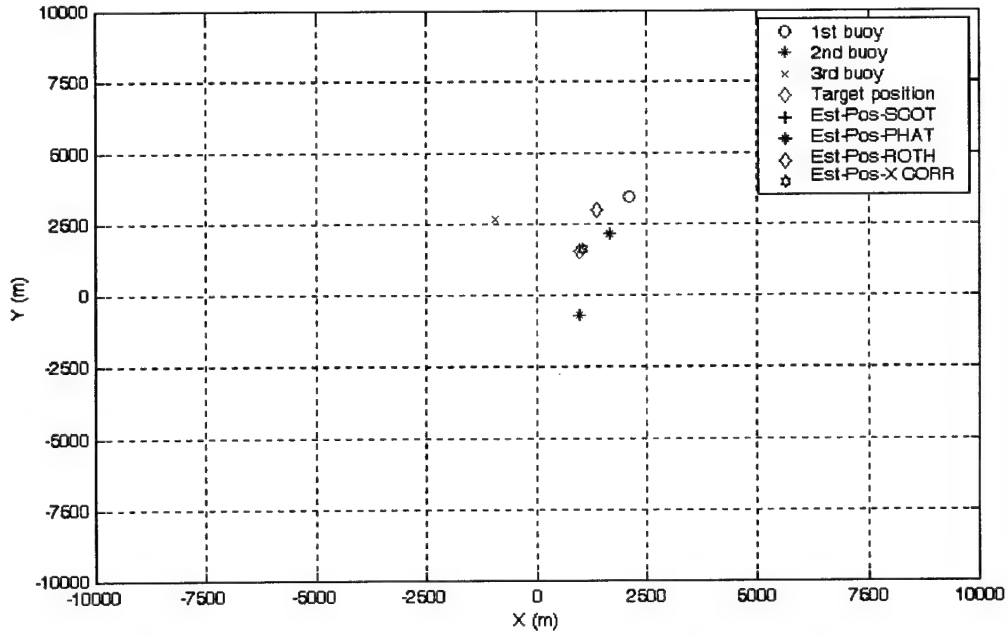

(b)

Figure 50. Tracking problem for Internal Waves case with N=3 sonobuoys. (a) Subspace methods. (b) Classical methods.

From the presented results, we observe that the accuracy of the localization of the target has been decreased, compared with the cases where there was no movement of the source (zero Doppler). Especially for the classical methods, the error in position's target was large enough to say that they failed to estimate the location of the source. One possible reason for the poor performance of the methods on the target localization is the approximation that we made during the manipulation of the data from MMPE when we were trying to set all signals in a fixed time spanning vector. On the other hand, the estimation of the target course and speed was quite accurate, or at least inside the acceptable limits of error, $\pm 5^o$ for the course and $\pm 2m/s$ for the speed.

THIS PAGE INTENTIONALLY LEFT BLANK

VIII. CONCLUSIONS AND FUTURE WORK

A. CONCLUSIONS

In this thesis, new techniques were developed to estimate the Time Difference of Arrival (TDOA) between two received signals at two seperate locations which contain the same transient but different noise. These techniques are based on subspace methods, a class of techniques based on the concept of signal and noise subspaces associated with the correlation matrix for a random process, and whose principal application is to locate narrowband lines in a spectrum or to estimate bearing of narrowband sources using array processing. As far as we know, the use of subspace methods to estimate TDOA for broadband transient sources is new. Our objectives were to implement the subspace methods in our problem, and to test them thoroughly comparing their performance with traditional methods of TDOA based on generalized cross-correlation ("classical methods"). The testing was conducted using synthetic data generated in MATLAB and data from an acoustic propagation model (MMPE). Tests were conducted under different scenarios using various transients, noise, or environmental conditions.

The thesis went further to apply these methods in the localization of a target using the TDOA ranging algorithm and data from MMPE generated for various ocean environments. In this way, we tried to simulate realistic conditions in the ocean as much as possible. This second step was further expanded by the use of Doppler data from the MMPE algorithm to estimate not only the position but also course and speed; in other words, to track the source.

From the various types of testing, we can conclude that the subspace methods provide good results in almost all cases. As a group, the subspace methods were more consistent in the accuracy of the results than the classical methods. This was observed not only in the TDOA testing but also in the localization and tracking experiments, where the subspace methods were more consistently accurate than the

classical methods.

The plots produced by the subspace methods provide a clear and more easily identified correct peak than those corresponding to the classical methods and were not influenced as much by the noise. In addition some of these subspace methods can also be used to produce direct numerical estimates for the time delay without the need to search for a peak (ESPRIT - root MUSIC).

Almost all methods (classical and subspace) performed satisfactorily in the localization problem. However accuracy tended to be more degraded for the range-dependent problems. This is not too surprising since the basic localization algorithm makes the assumption of a constant speed of sound. In the tracking experiments, the subspace methods had limited performance for estimation of target position but much better performance for estimation of course and speed.

B. SUGGESTIONS FOR FUTURE DEVELOPMENT

The results of this thesis show promising results for the subspace methods, and their application to target localization and tracking via TDOA estimation. The testing should be continued with more complex environments using acoustic models and also with real data from ocean experiments. A comparison of the subspace methods with other families of methods for TDOA (e.g., bicorrelation and bispectra [Ref. 6, 7, 8, 9]), or even a combination of these, would give a wider view of the possible solutions to the problem. Finally, implementation of a three-dimensional localization algorithm may give more realistic results and could assist in the tracking problem, provided that it can overcome obstacles such as multipath propagation.

APPENDIX A. SYNTHETIC DATA

This appendix presents sample figures and tables with summary results of the time delay estimation obtained from various forms of synthetic data. The transients that were used are the following:

- Exponential
- Sinusoidal
- Modified-Exponential
- Chirp
- Modified-Chirp

The definitions of the transients are given in Chapter 4 Eqs. (IV.2) - (IV.8).

Method	Parameters	SNR 15 dB	SNR 10 dB	SNR 5 dB
MUSIC	Cov-Mat: 10	101	100	106
	Cov-Mat: 20	99	99	104
Modified MUSIC	Cov-Mat: 10	101	100	107
	Cov-Mat: 20	99	99	104
MIN-NORM	Cov-Mat: 10	100	100	110
	Cov-Mat: 20	99	98	102
PCLP	Cov-Mat: 10	100	100	109
	Cov-Mat: 20	99	98	103
ESPRIT	Cov-Mat: 10	100	101	107
	Cov-Mat: 20	99	98	103
Root-MUSIC	Cov-Mat: 10	101	100	106
	Cov-Mat: 20	99	99	104
SCOT	#-Segs: 1	102	385	5
	#-Segs: 2	101	102	9
PHAT	#-Segs: 1	102	385	5
	#-Segs: 2	101	202	98
Roth	#-Segs: 1	-228	315	233
	#-Segs: 2	101	201	9
X-Corr	#-Segs: 1	98	107	93
	#-Segs: 2	101	102	109

Table XX. Exponential transient: length L=20s; white noise ($\sigma_o^2 = 2$); actual TDOA=100s.

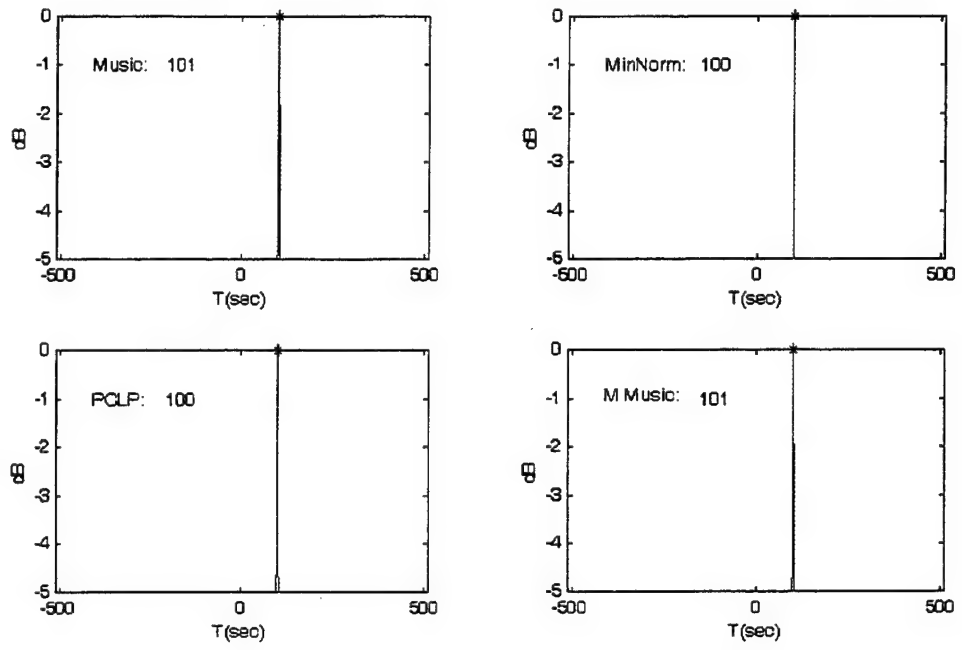

(a)

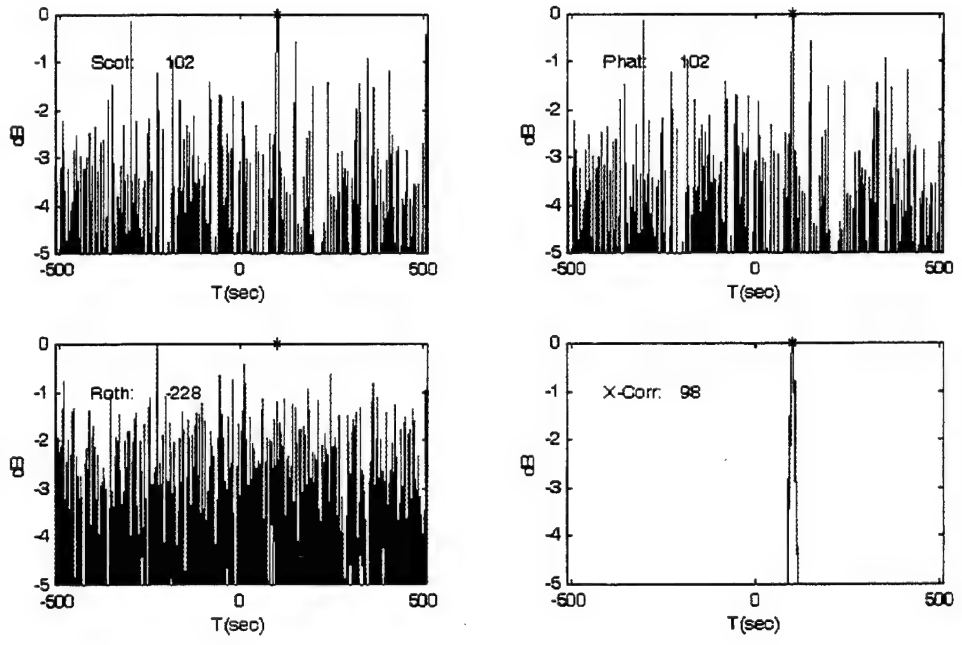

(b)

Figure 51. Exponential transient: Actual Tdoa=100s; SNR=15dB; White-Noise (σ_o^2). (a) Subspace methods, Covariance Size=10. (b) Classical methods, number of segments=1.

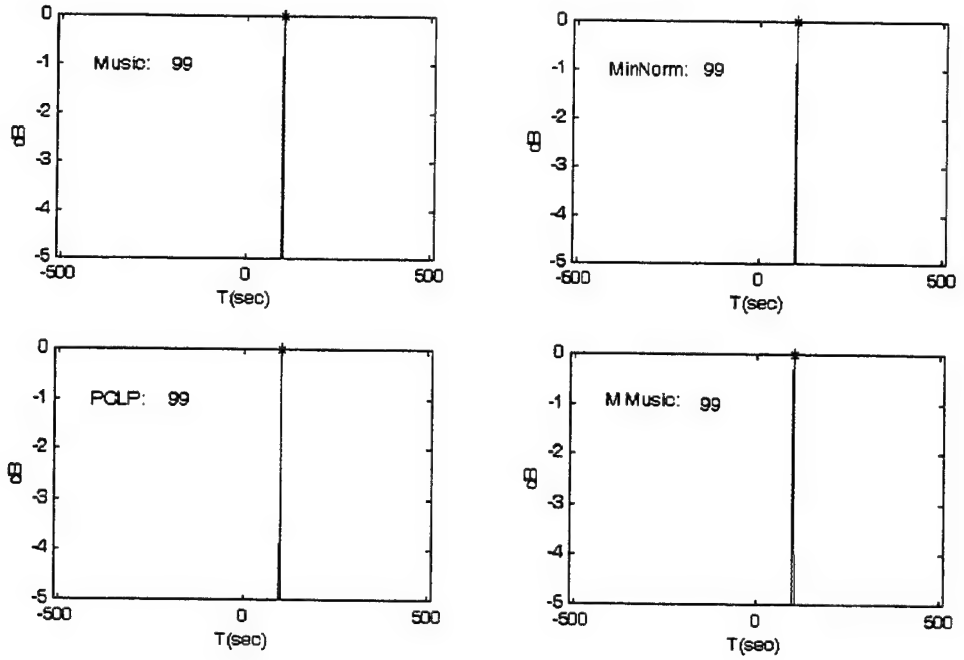

(a)

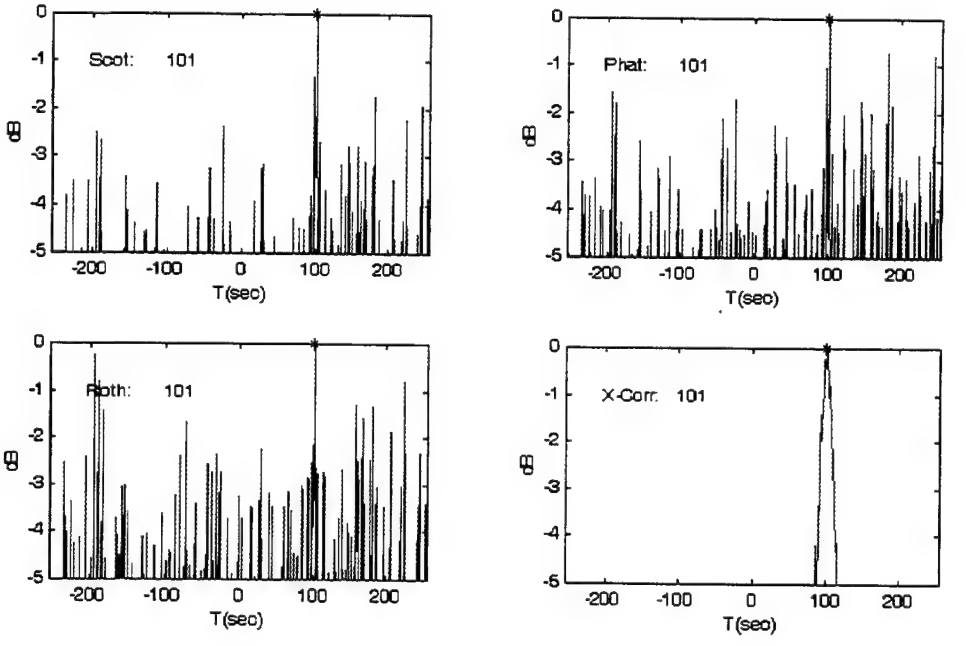

(b)

Figure 52. Exponential transient: Actual Tdoa=100s; SNR=15dB; White-Noise (σ_o^2). (a) Subspace methods, Covariance Size=20. (b) Classical methods, number of segments=2.

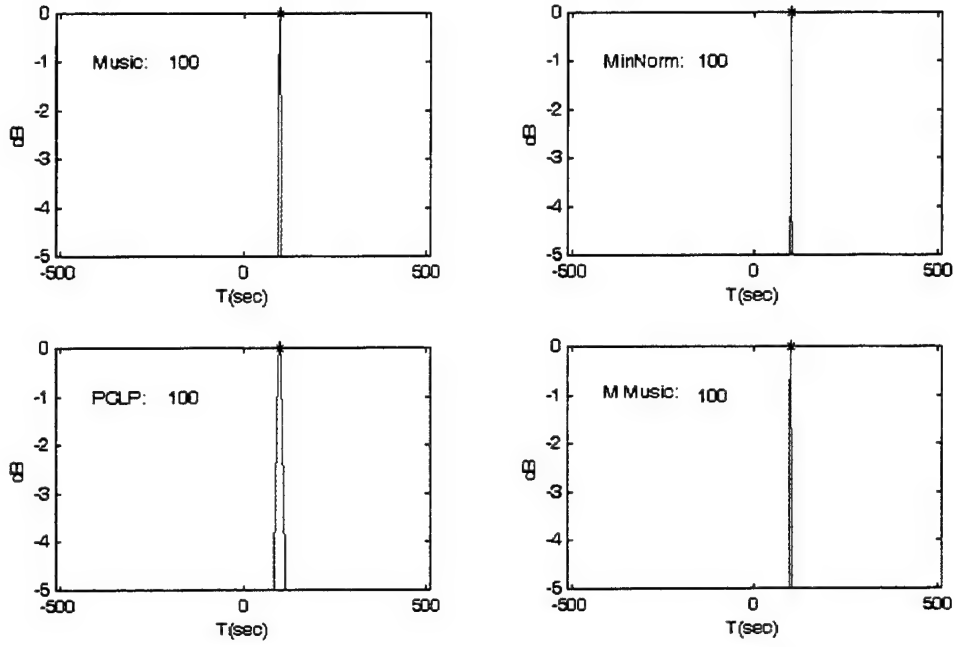

(a)

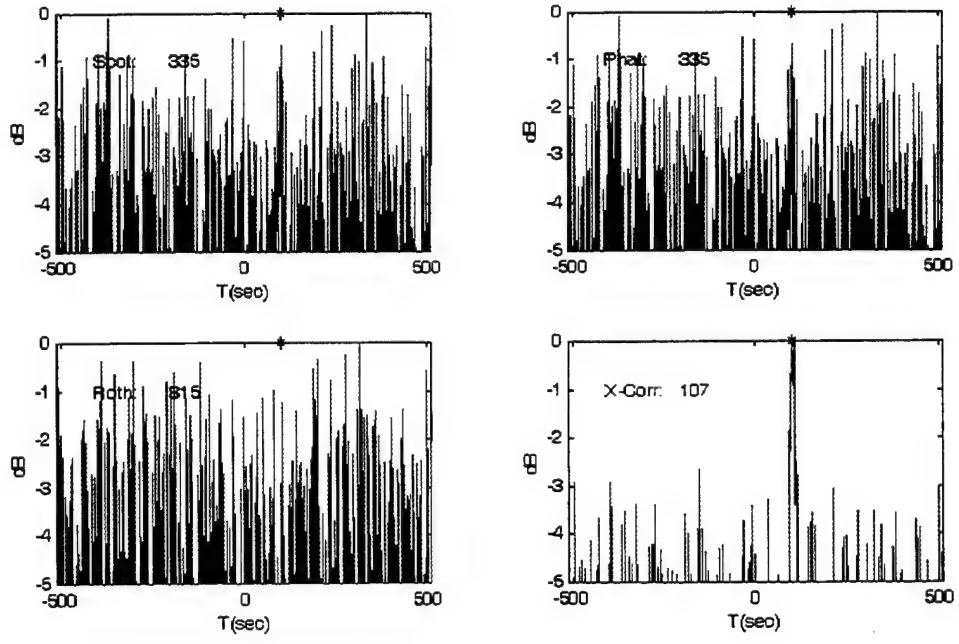

(b)

Figure 53. Exponential transient: Actual Tdoa=100s; SNR=10dB; White-Noise (σ_o^2). (a) Subspace methods, Covariance Size=10. (b) Classical methods, number of segments=1.

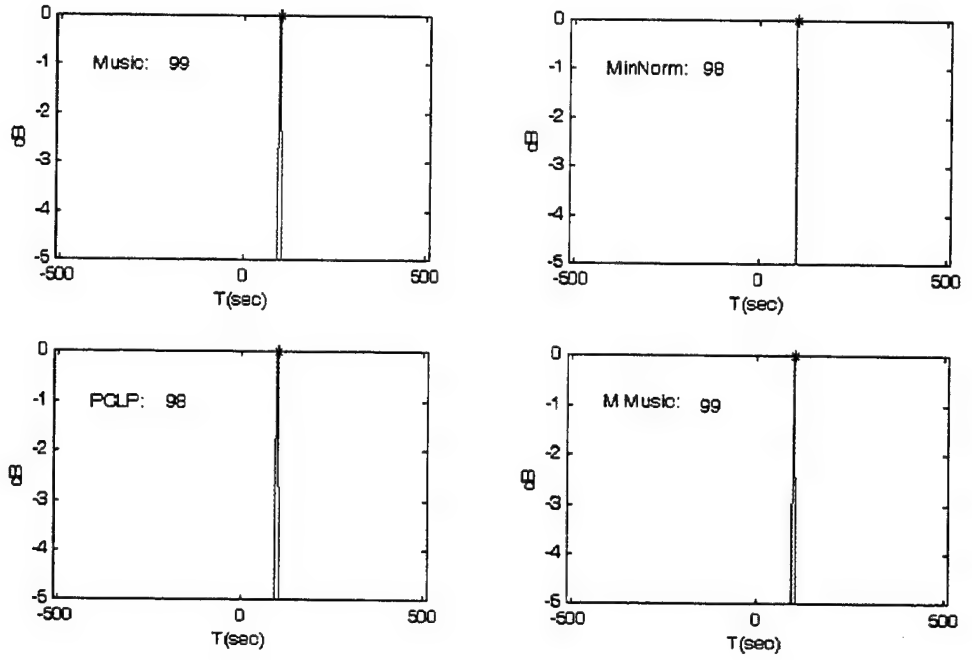

(a)

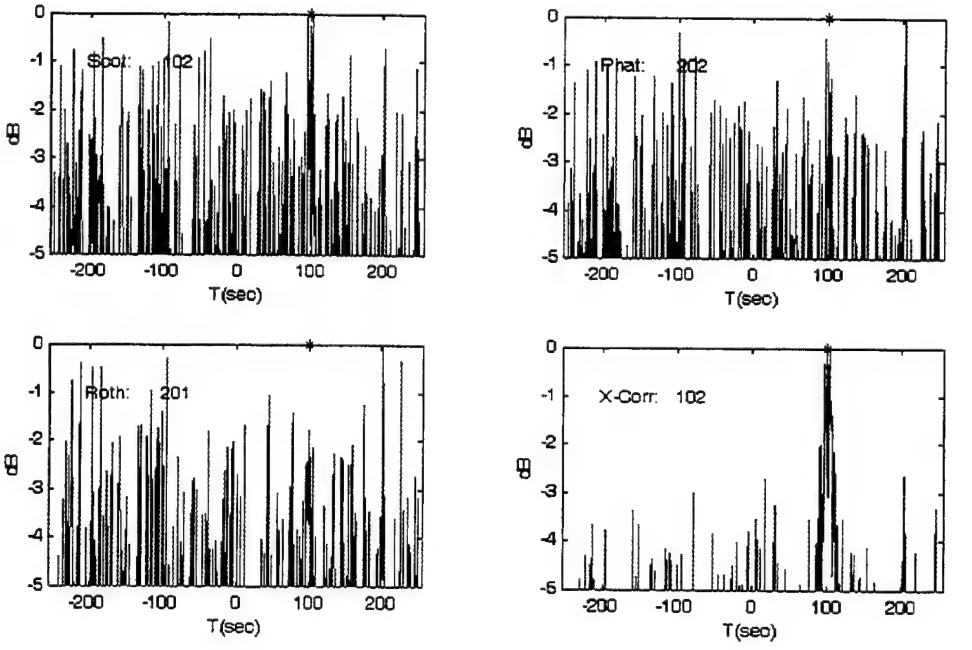

(b)

Figure 54. Exponential transient: Actual Tdoa=100s; SNR=10dB; White-Noise (σ_o^2). (a) Subspace methods, Covariance Size=20. (b) Classical methods, number of segments=2.

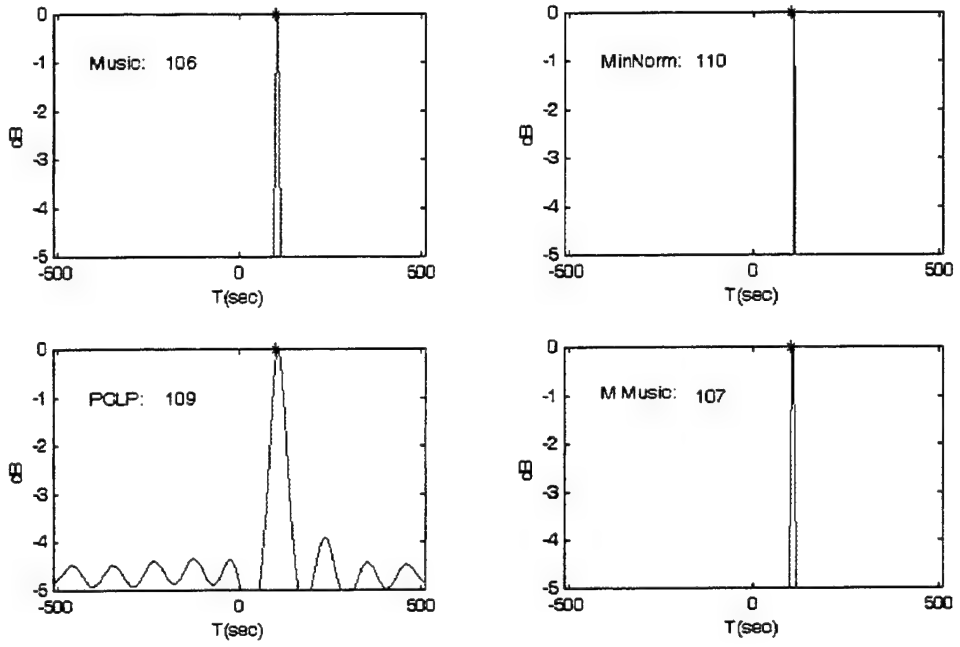

(a)

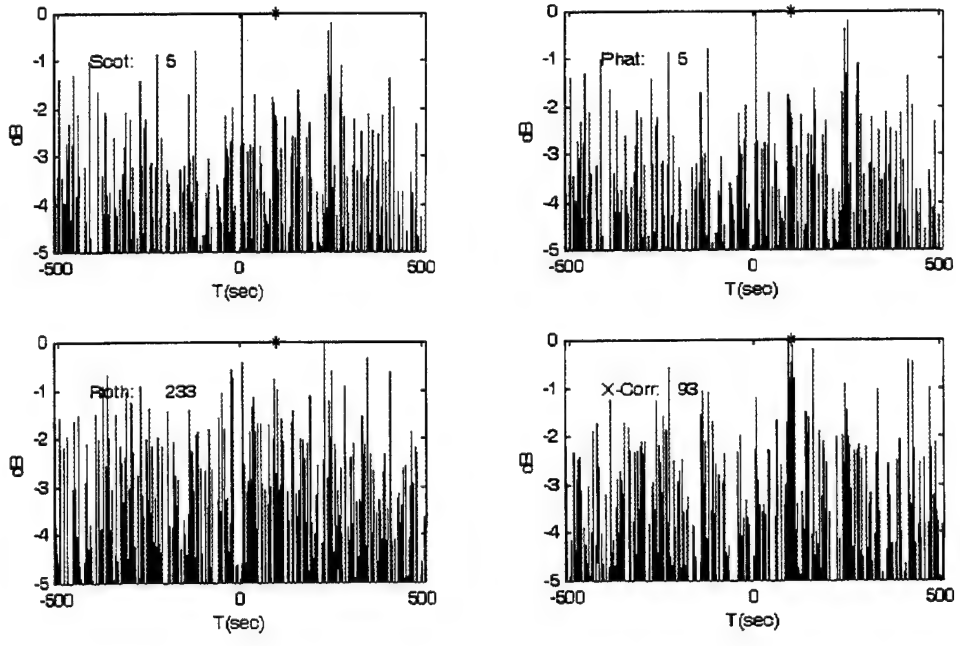

(b)

Figure 55. Exponential transient: Actual Tdoa=100s; SNR=05dB; White-Noise (σ_o^2). (a) Subspace methods, Covariance Size=10. (b) Classical methods, number of segments=1.

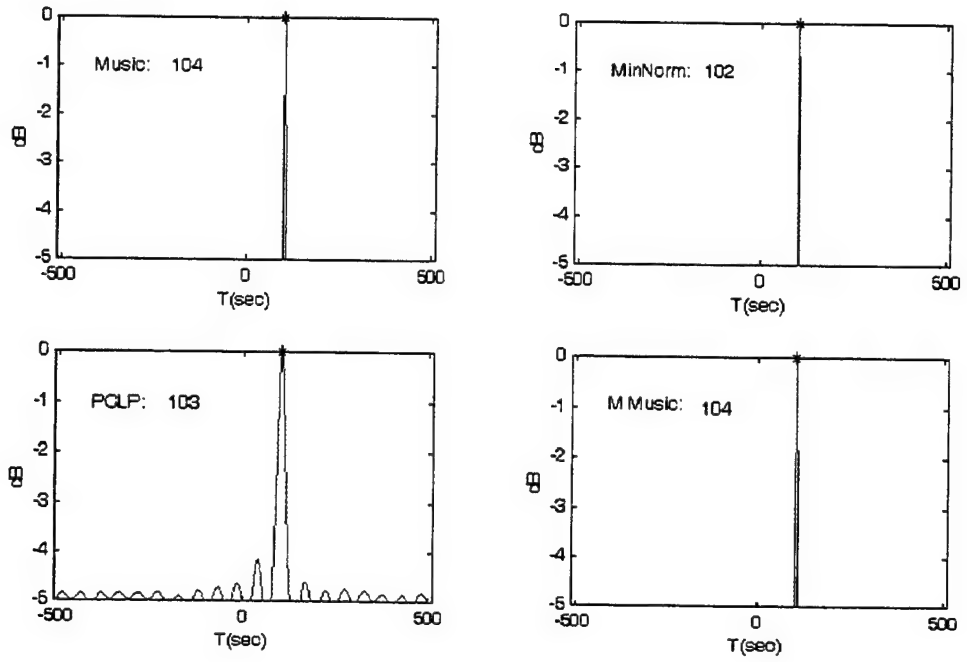

(a)

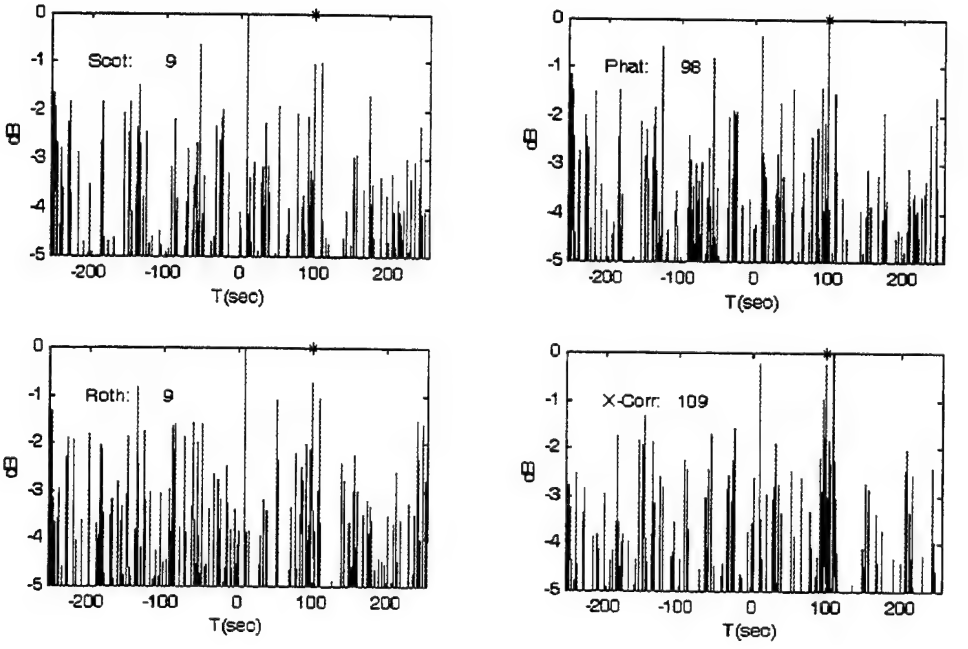

(b)

Figure 56. Exponential transient: Actual Tdoa=100s; SNR=05dB; White-Noise (σ_o^2). (a) Subspace methods, Covariance Size=20. (b) Classical methods, number of segments=2.

Method	Parameters	SNR 15 dB	SNR 10 dB	SNR 5 dB
MUSIC	Cov-Mat: 10	-10	-10	-10
	Cov-Mat: 20	-10	-8	-10
Modified MUSIC	Cov-Mat: 10	-10	-10	-10
	Cov-Mat: 20	-11	-8	-10
MIN-NORM	Cov-Mat: 10	-10	-10	-9
	Cov-Mat: 20	-10	-9	-10
PCLP	Cov-Mat: 10	-10	-10	-9
	Cov-Mat: 20	-10	-9	-10
ESPRIT	Cov-Mat: 10	-10	-10	-9
	Cov-Mat: 20	-10	-9	-14
Root-MUSIC	Cov-Mat: 10	-10	-10	-9
	Cov-Mat: 20	-10	-8	-10
SCOT	#-Segs: 1	-10	-10	-76
	#-Segs: 2	-10	-11	-5
PHAT	#-Segs: 1	-10	-10	-76
	#-Segs: 2	-10	-15	-91
Roth	#-Segs: 1	-371	-42	-131
	#-Segs: 2	-10	-209	169
X-Corr	#-Segs: 1	-10	-9	-9
	#-Segs: 2	-10	-11	-5

Table XXI. Exponential transient: length L=50s; white noise ($\sigma_o^2 = 2$); actual TDOA=-10s.

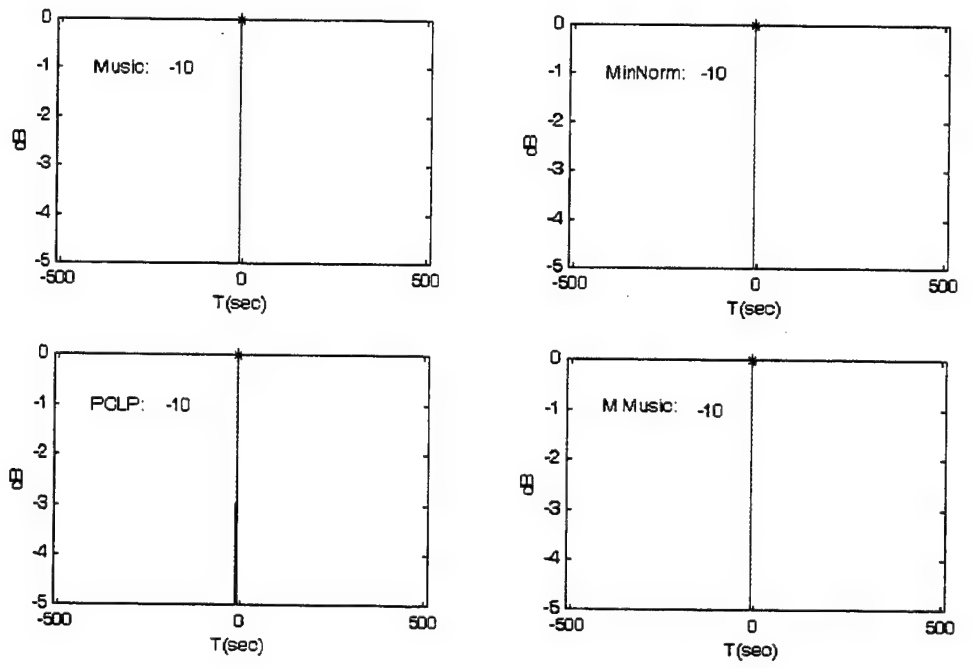

(a)

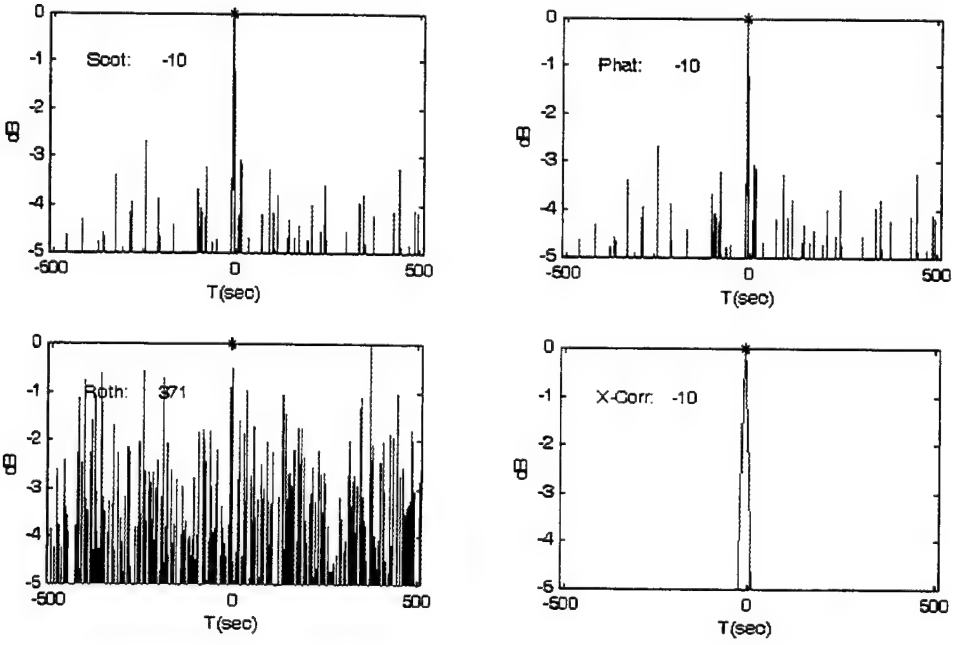

(b)

Figure 57. Exponential transient: Actual Tdoa=-10s; SNR=15dB; White-Noise (σ_o^2). (a) Subspace methods, Covariance Size=10. (b) Classical methods, number of segments=1.

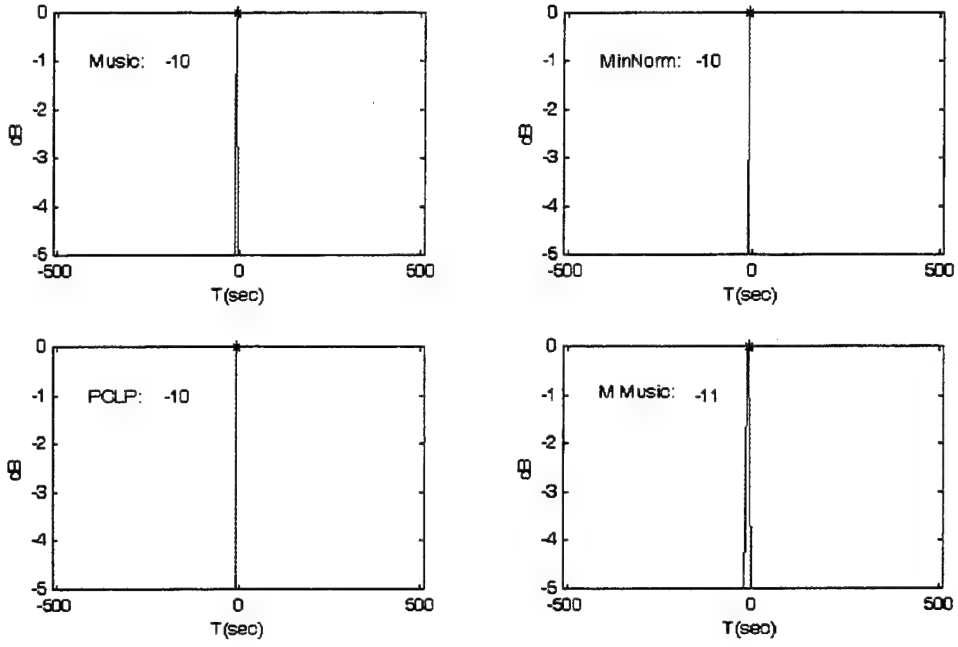

(a)

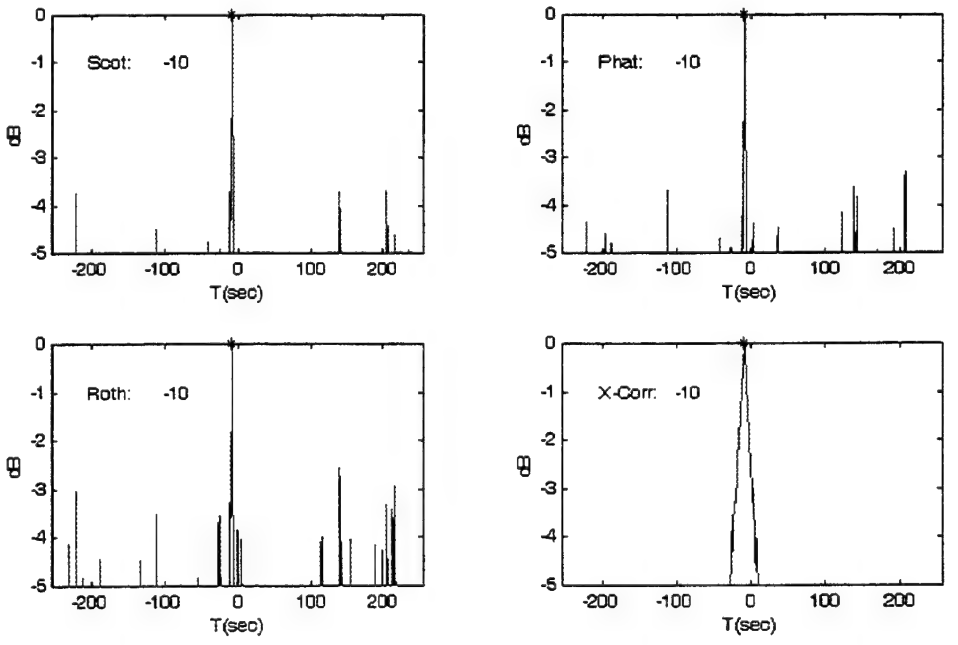

(b)

Figure 58. Exponential transient: Actual Tdoa=-10s; SNR=15dB; White-Noise (σ_o^2). (a) Subspace methods, Covariance Size=20. (b) Classical methods, number of segments=2.

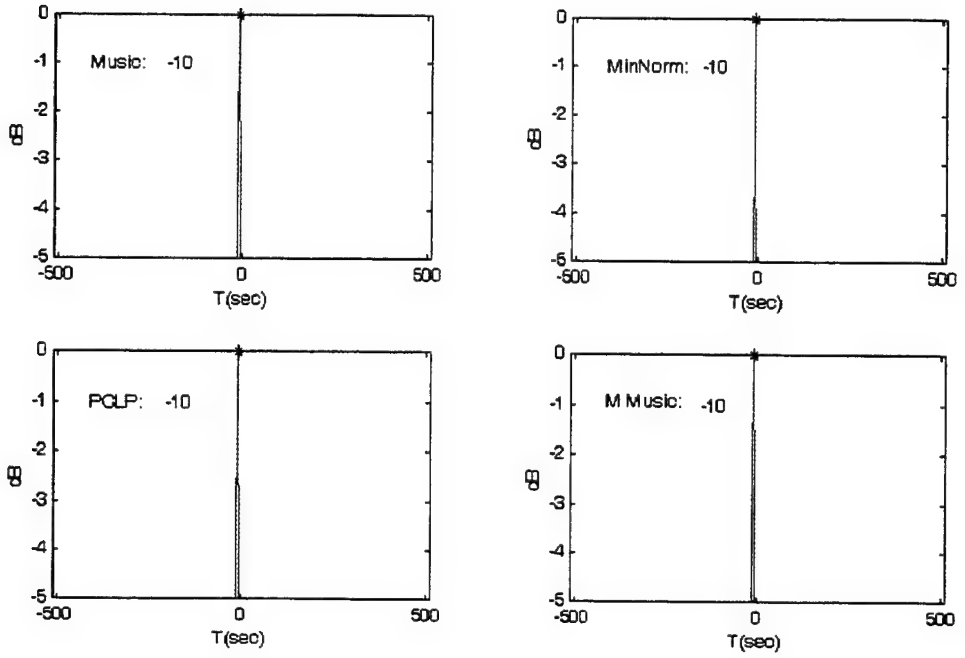

(a)

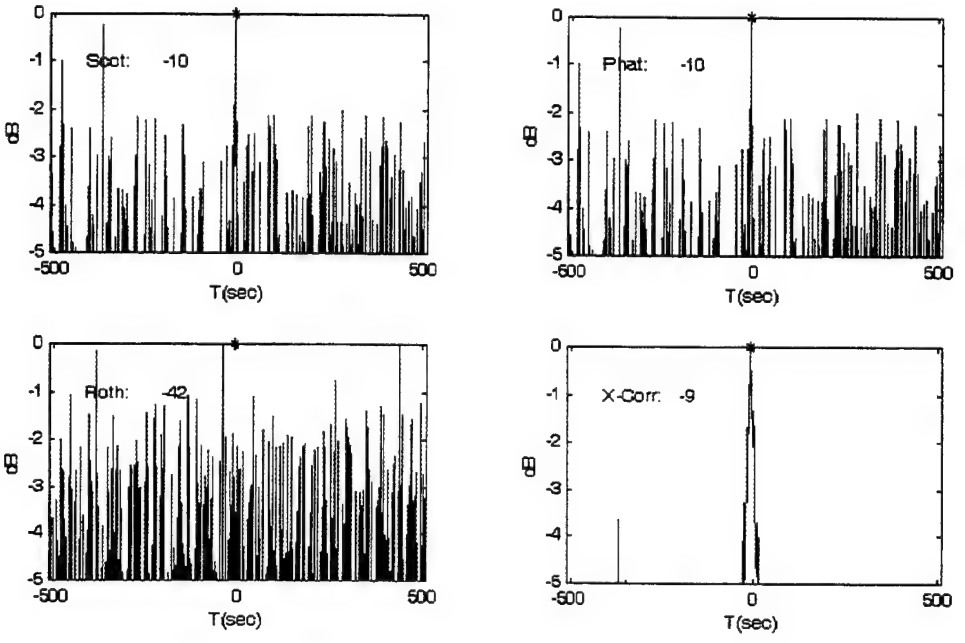

(b)

Figure 59. Exponential transient: Actual Tdoa=-10s; SNR=10dB; White-Noise (σ_o^2). (a) Subspace methods, Covariance Size=10. (b) Classical methods, number of segments=1.

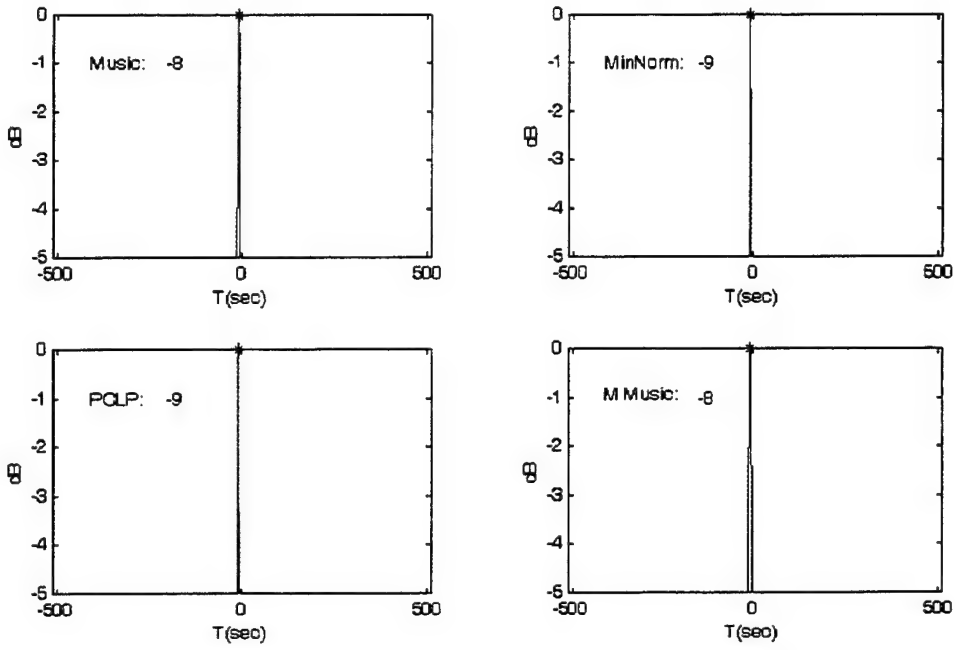

(a)

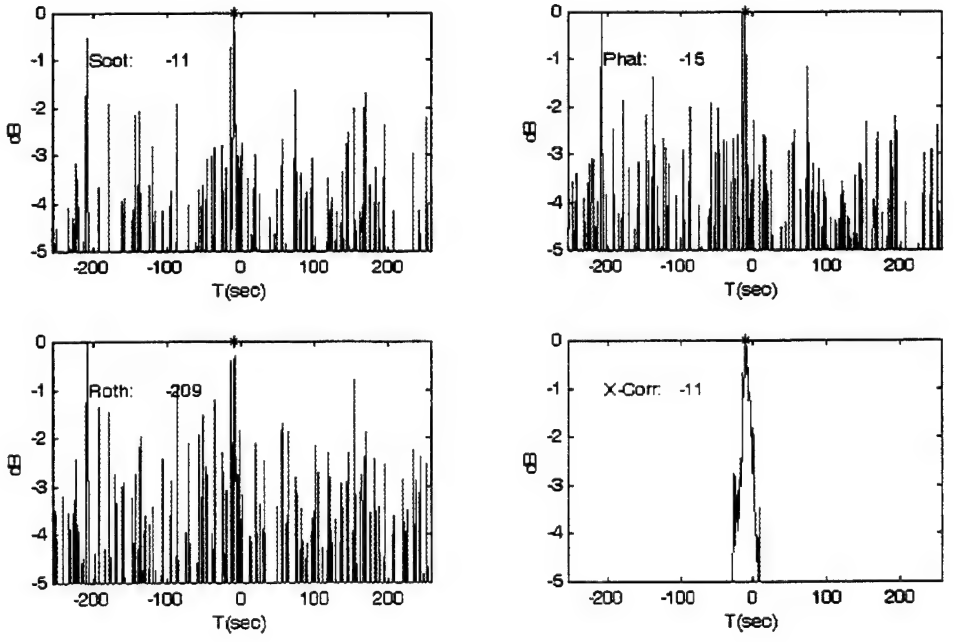

(b)

Figure 60. Exponential transient: Actual Tdoa=-10s; SNR=10dB; White-Noise (σ_o^2). (a) Subspace methods, Covariance Size=20. (b) Classical methods, number of segments=2.

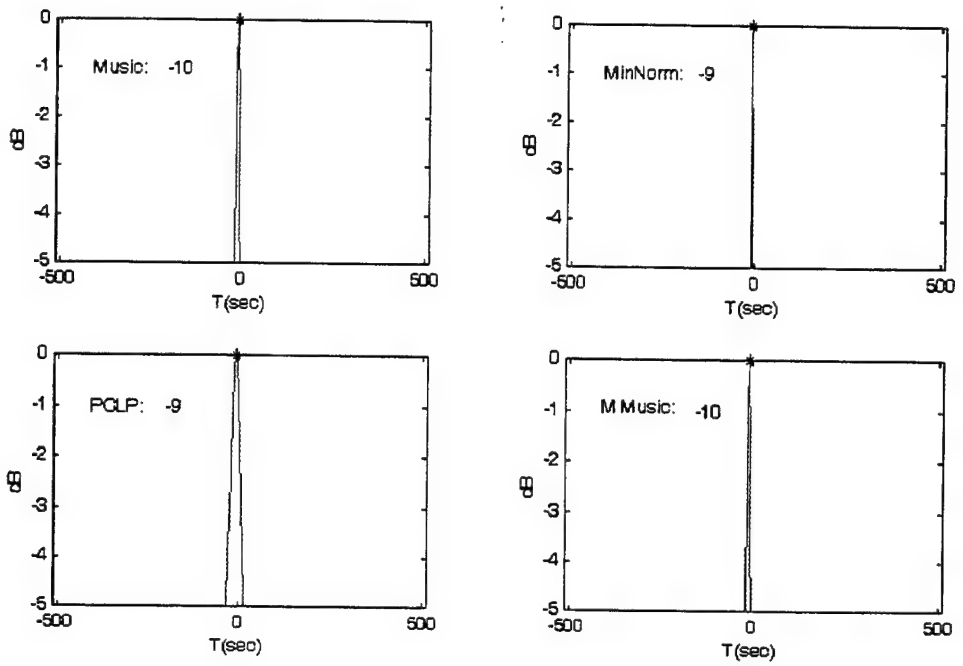

(a)

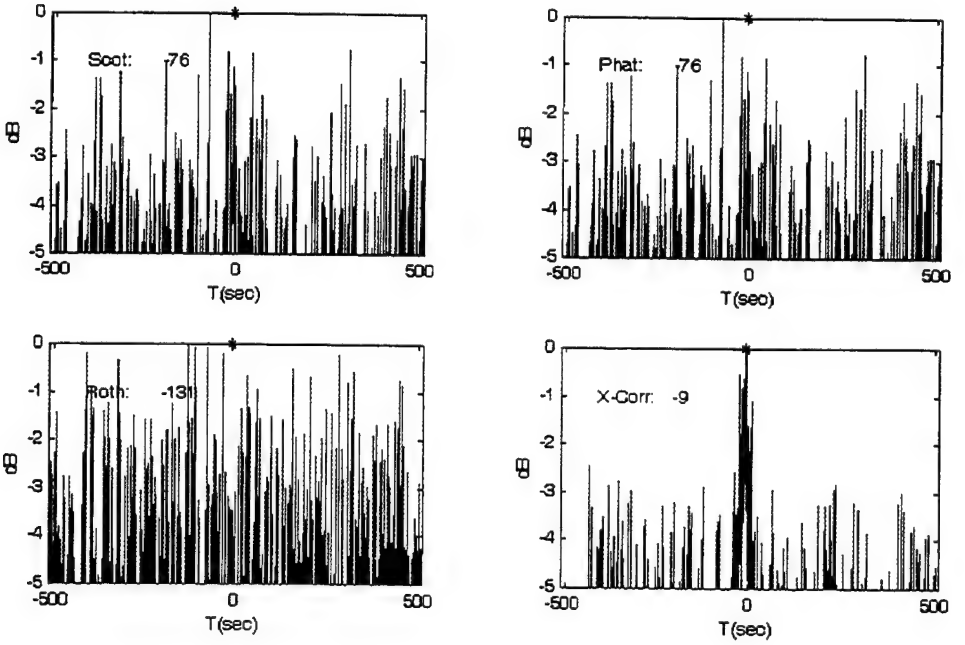

(b)

Figure 61. Exponential transient: Actual Tdoa=-10s; SNR=05dB; White-Noise (σ_o^2). (a) Subspace methods, Covariance Size=10. (b) Classical methods, number of segments=1.

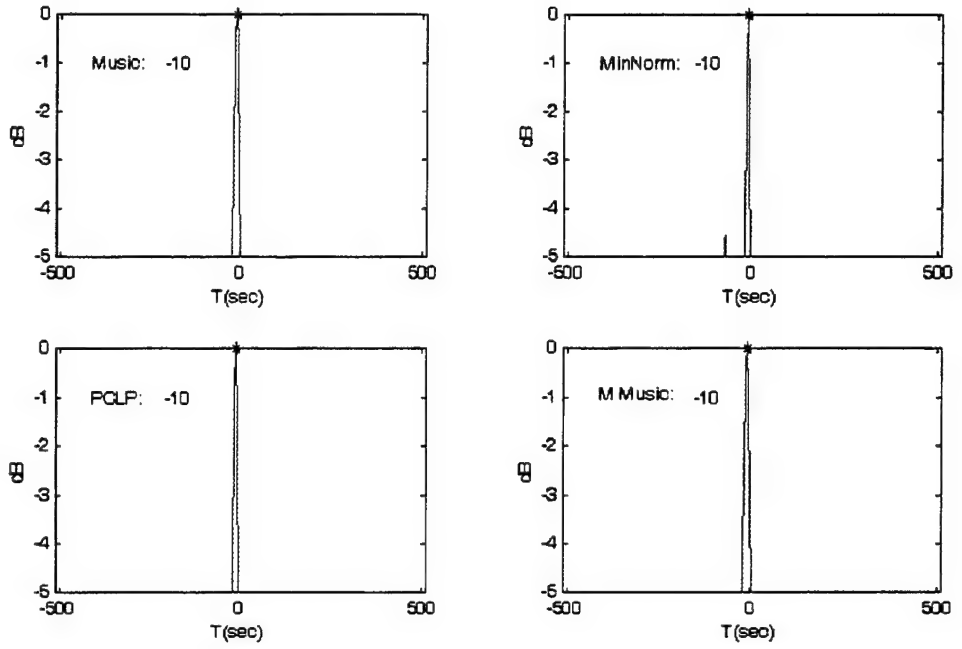

(a)

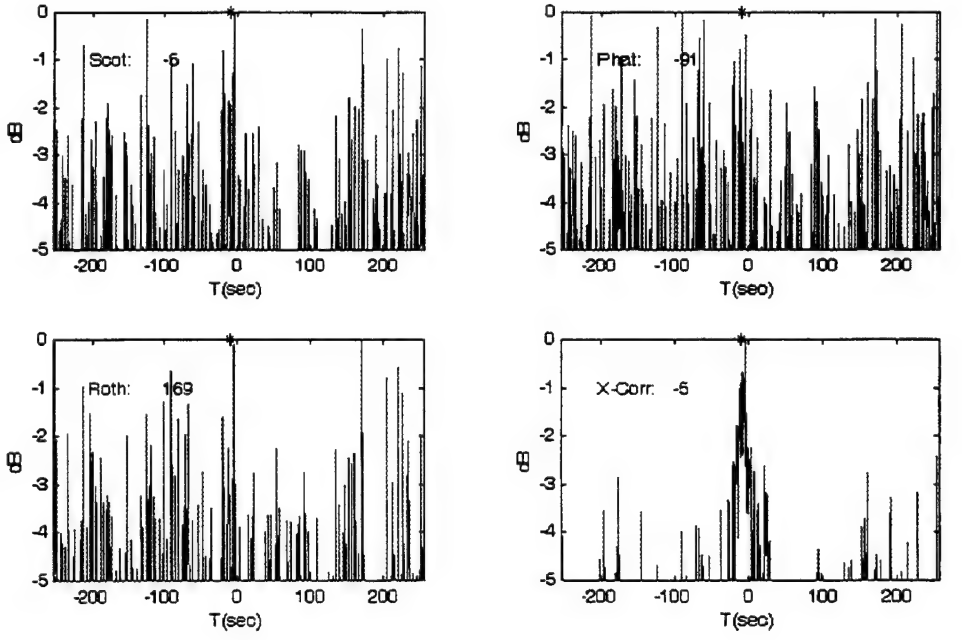

(b)

Figure 62. Exponential transient: Actual Tdoa=-10s; SNR=05dB; White-Noise (σ_o^2). (a) Subspace methods, Covariance Size=20. (b) Classical methods, number of segments=2.

Method	Parameters	Exp	Sin	Damped Sin	Chirp	Damped Chirp
MUSIC	Cov-Mat: 10	50	49	50	50	50
	Cov-Mat: 20	50	51	50	50	50
Modified-MUSIC	Cov-Mat: 10	50	50	50	50	50
	Cov-Mat: 20	50	50	50	50	50
MIN-NORM	Cov-Mat: 10	50	49	50	50	50
	Cov-Mat: 20	50	51	50	50	50
PCLP	Cov-Mat: 10	50	49	50	50	50
	Cov-Mat: 20	50	51	50	50	50
ESPRIT	Cov-Mat: 10	49	49	50	50	50
	Cov-Mat: 20	50	51	50	50	50
Root-MUSIC	Cov-Mat: 10	50	49	50	50	50
	Cov-Mat: 20	50	51	50	50	50
SCOT	#-Segs: 1	50	50	50	50	50
	#-Segs: 2	50	-74	50	50	50
PHAT	#-Segs: 1	50	50	50	50	50
	#-Segs: 2	50	-74	50	50	50
Roth	#-Segs: 1	-299	-61	50	50	50
	#-Segs: 2	50	48	50	50	50
X-Corr	#-Segs: 1	50	50	50	50	50
	#-Segs: 2	50	48	50	50	50

Table XXII. Transients: same length; white noise ($\sigma_o^2 = 2$); SNR=15dB; actual TDOA=50s.

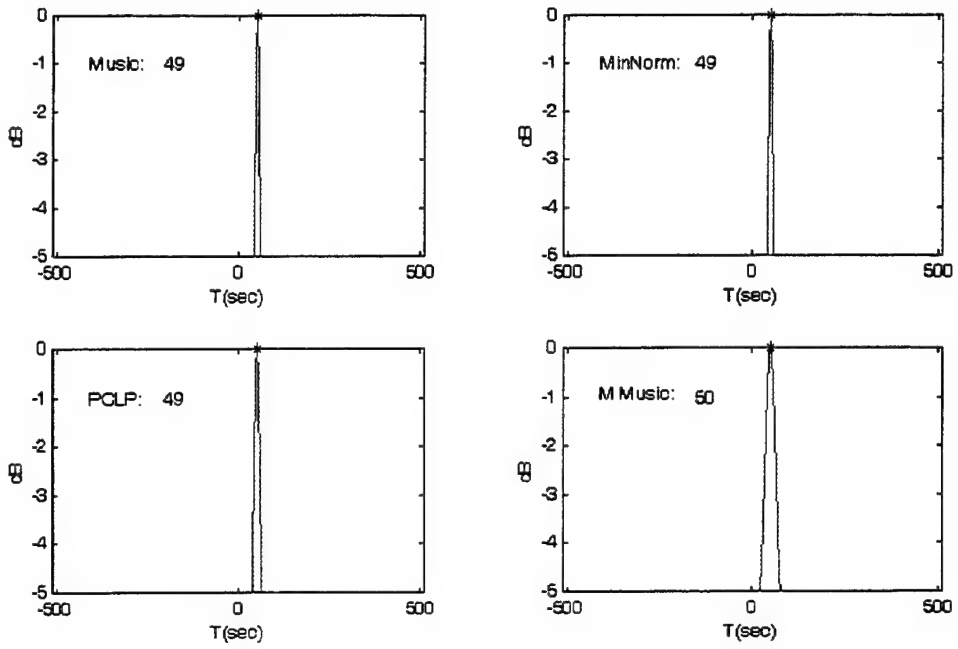

(a)

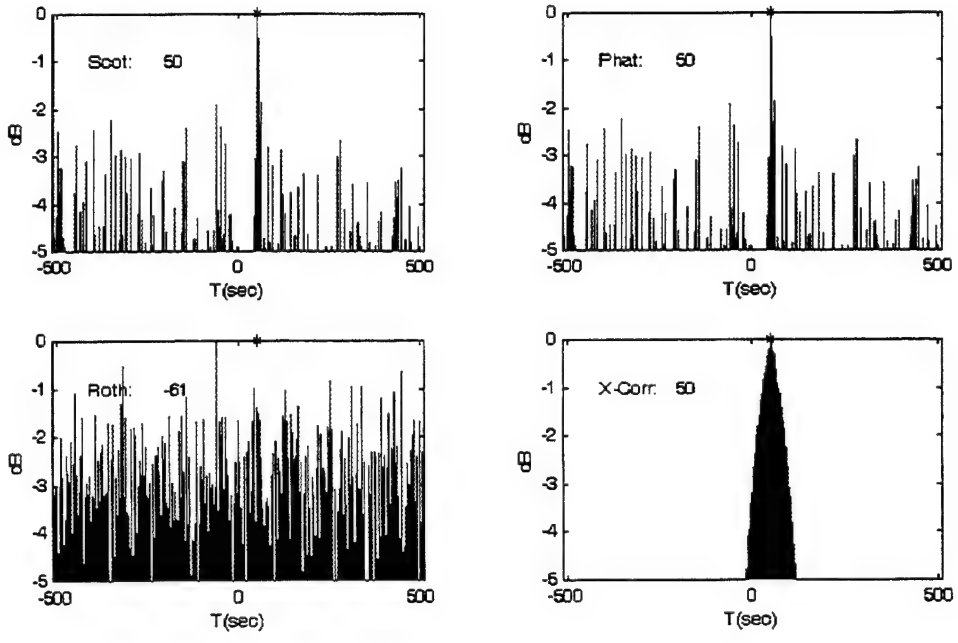

(b)

Figure 63. Sinusoidal transient: Actual Tdoa=50s; SNR=15dB; White-Noise (σ_o^2). (a) Subspace methods, Covariance Size=10. (b) Classical methods, number of segments=1.

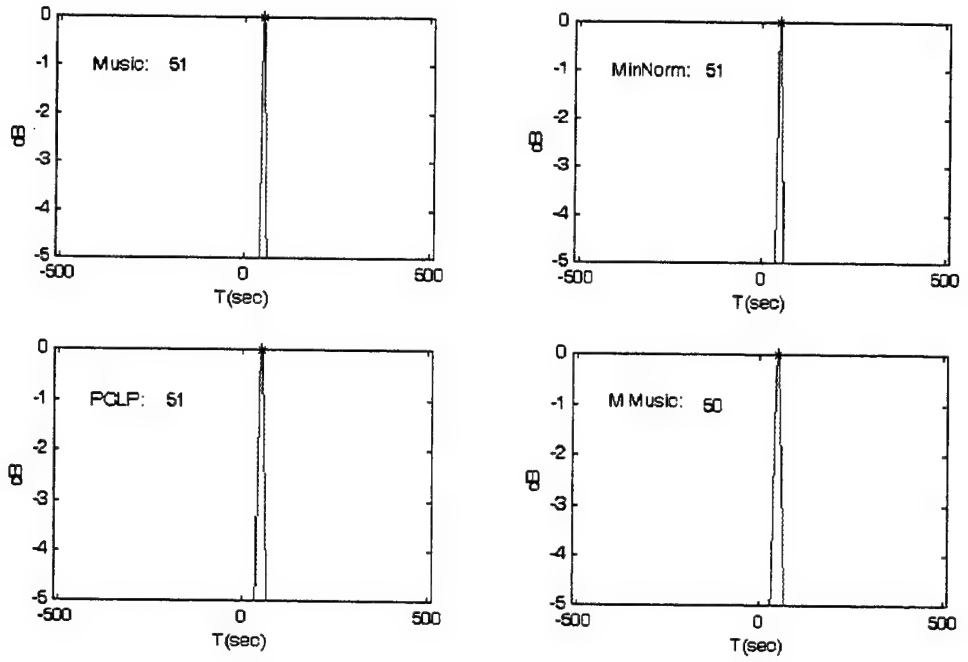

(a)

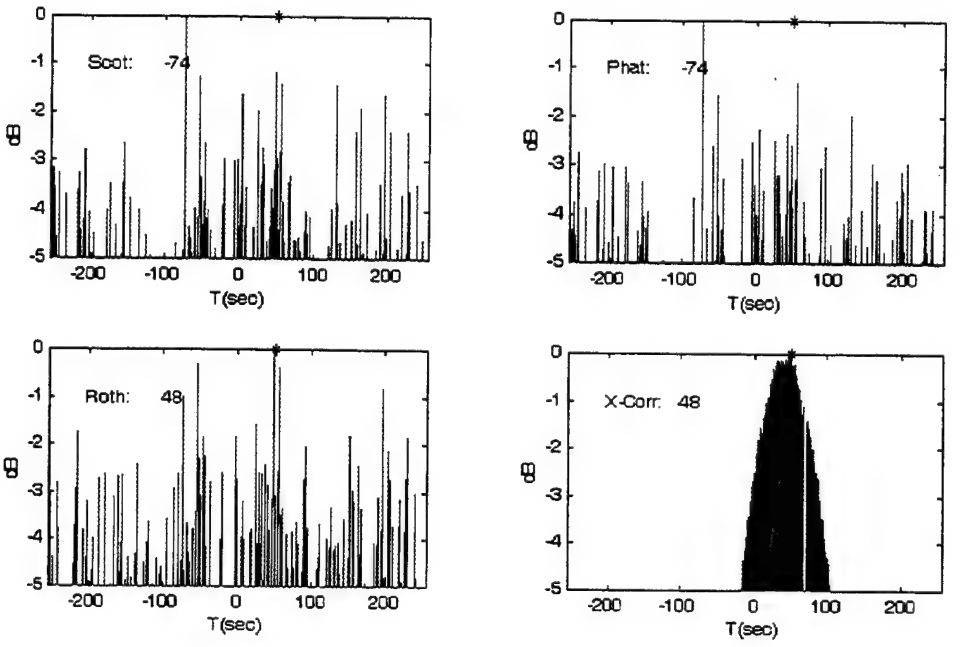

(b)

Figure 64. Sinusoidal transient: Actual Tdoa=50s; SNR=15dB; White-Noise (σ_o^2). (a) Subspace methods, Covariance Size=20. (b) Classical methods, number of segments=2.

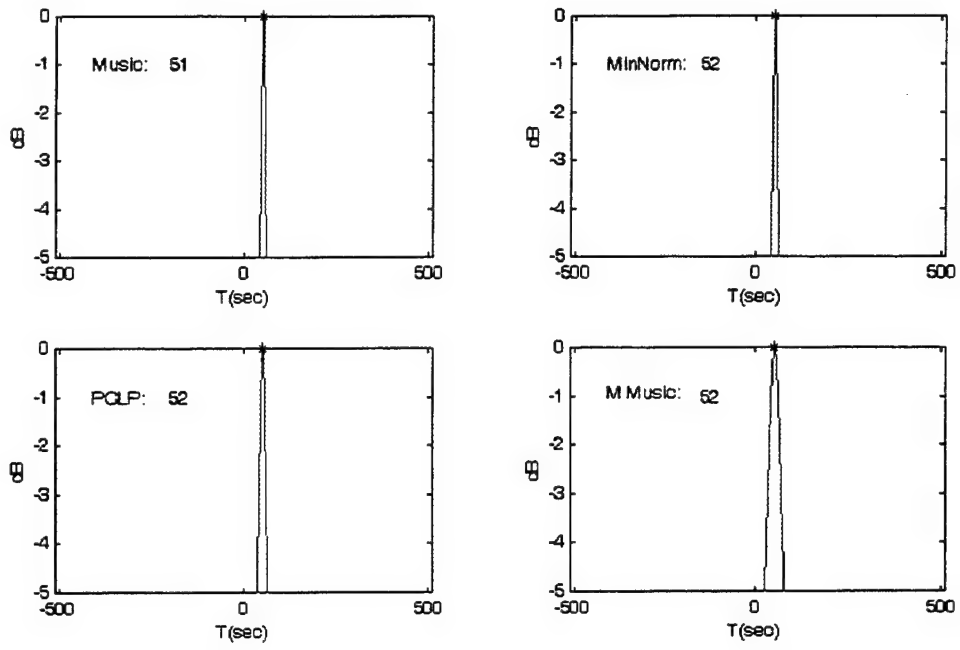

(a)

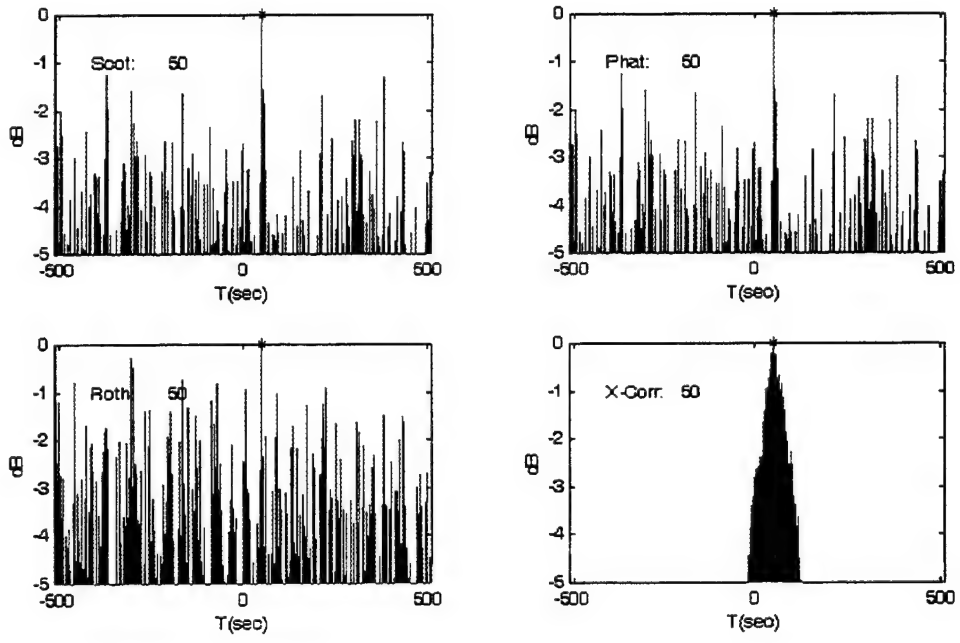

(b)

Figure 65. Sinusoidal transient: Actual Tdoa=50s; SNR=10dB; White-Noise (σ_o^2). (a) Subspace methods, Covariance Size=10. (b) Classical methods, number of segments=1.

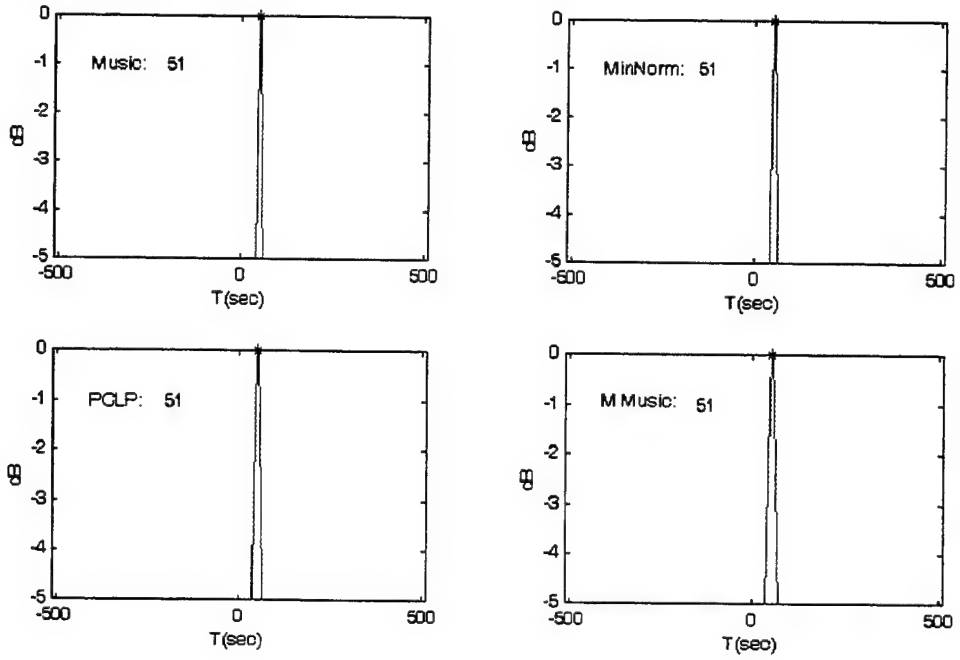

(a)

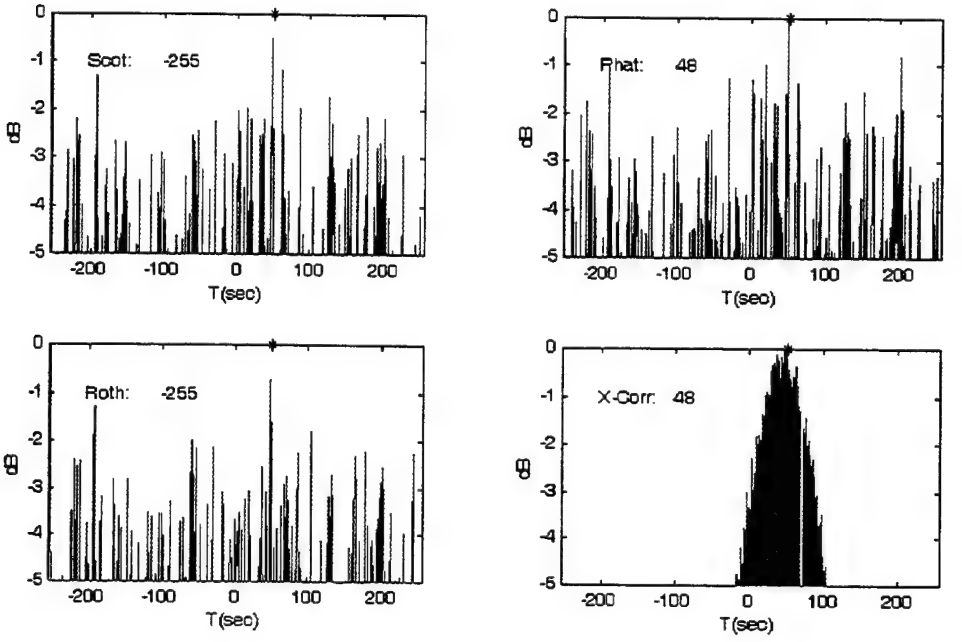

(b)

Figure 66. Sinusoidal transient: Actual Tdoa=50s; SNR=10dB; White-Noise (σ_o^2). (a) Subspace methods, Covariance Size=20. (b) Classical methods, number of segments=2.

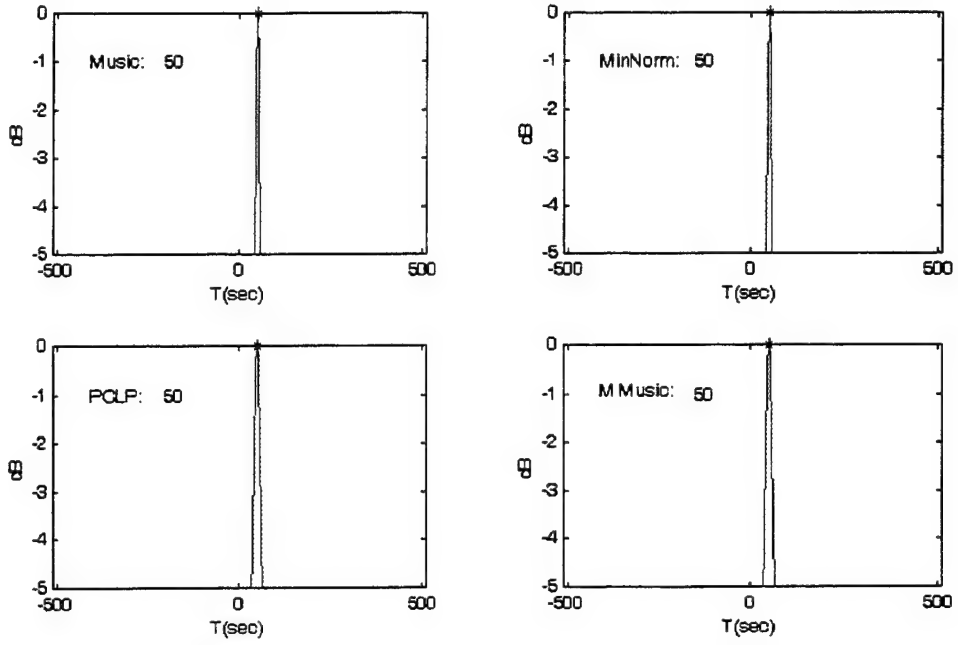

(a)

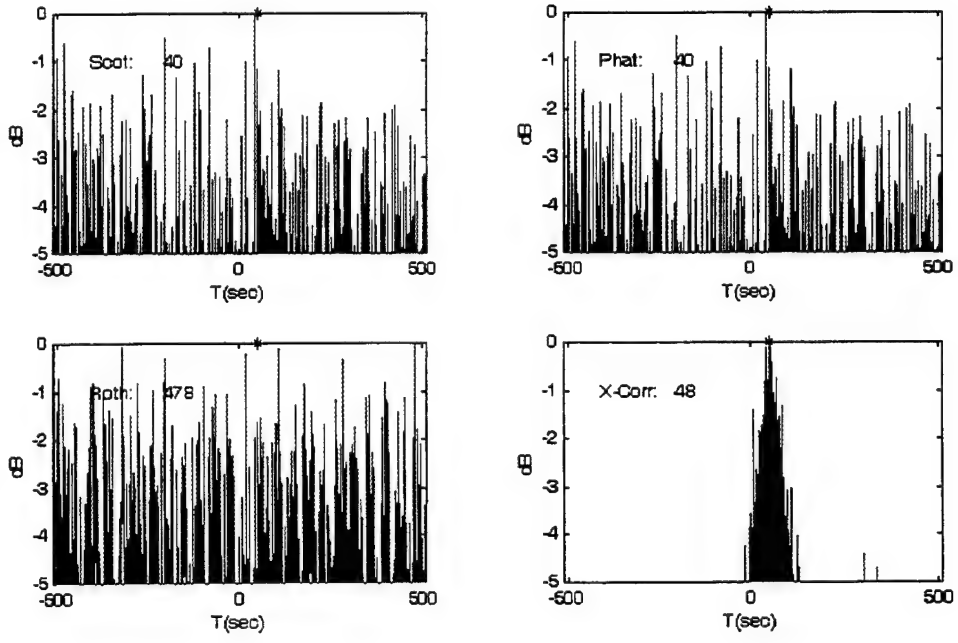

(b)

Figure 67. Sinusoidal transient: Actual Tdoa=50s; SNR=05dB; White-Noise (σ_o^2). (a) Subspace methods, Covariance Size=10. (b) Classical methods, number of segments=1.

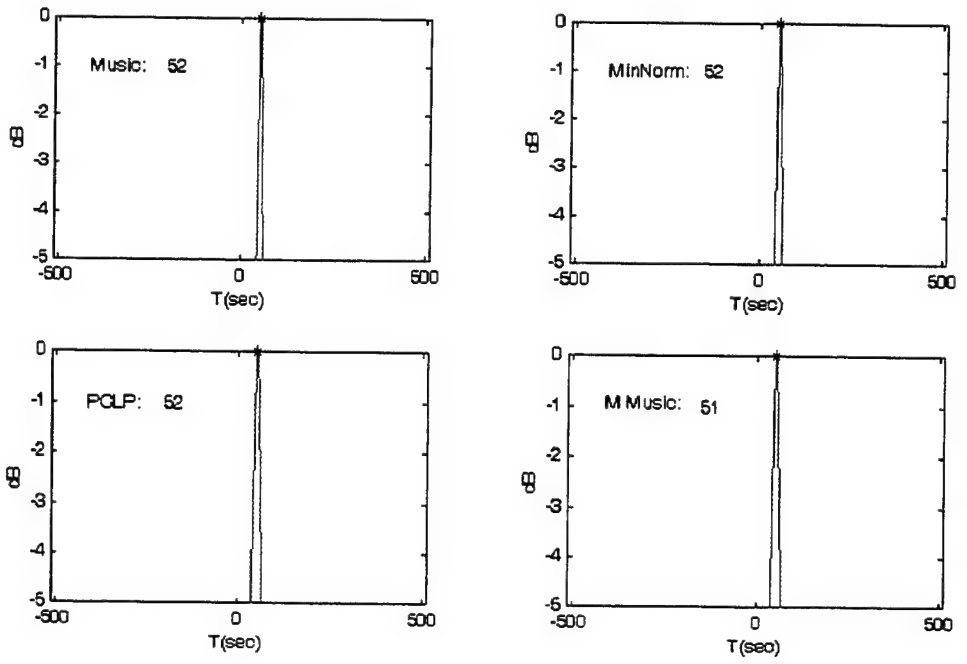

(a)

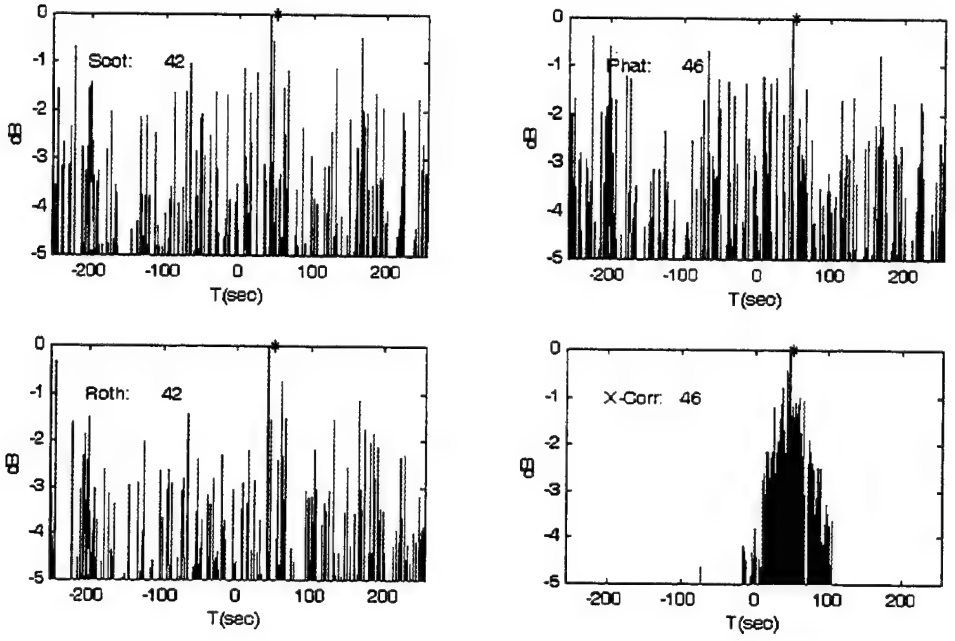

(b)

Figure 68. Sinusoidal transient: Actual Tdoa=50s; SNR=05dB; White-Noise (σ_o^2). (a) Subspace methods, Covariance Size=20. (b) Classical methods, number of segments=2.

Method	Parameters	Exp	Sin	Damped Sin	Chirp	Damped Chirp
MUSIC	Cov-Mat: 10	51	51	50	53	49
	Cov-Mat: 20	49	51	50	50	50
Modified-MUSIC	Cov-Mat: 10	51	52	50	53	49
	Cov-Mat: 20	49	51	50	50	50
MIN-NORM	Cov-Mat: 10	51	52	50	54	49
	Cov-Mat: 20	49	51	50	50	50
PCLP	Cov-Mat: 10	51	52	50	54	49
	Cov-Mat: 20	49	51	50	50	50
ESPRIT	Cov-Mat: 10	51	52	50	54	49
	Cov-Mat: 20	50	51	50	50	50
Root-MUSIC	Cov-Mat: 10	50	52	50	54	49
	Cov-Mat: 20	49	51	50	50	50
SCOT	#-Segs: 1	50	50	50	50	50
	#-Segs: 2	52	-255	50	50	50
PHAT	#-Segs: 1	50	50	50	50	50
	#-Segs: 2	52	48	50	50	50
Roth	#-Segs: 1	-502	50	108	50	50
	#-Segs: 2	52	-255	50	50	50
X-Corr	#-Segs: 1	50	50	50	50	50
	#-Segs: 2	50	48	50	50	50

Table XXIII. Transients: same length; white noise ($\sigma_o^2 = 2$); SNR=10dB; actual TDOA=50s.

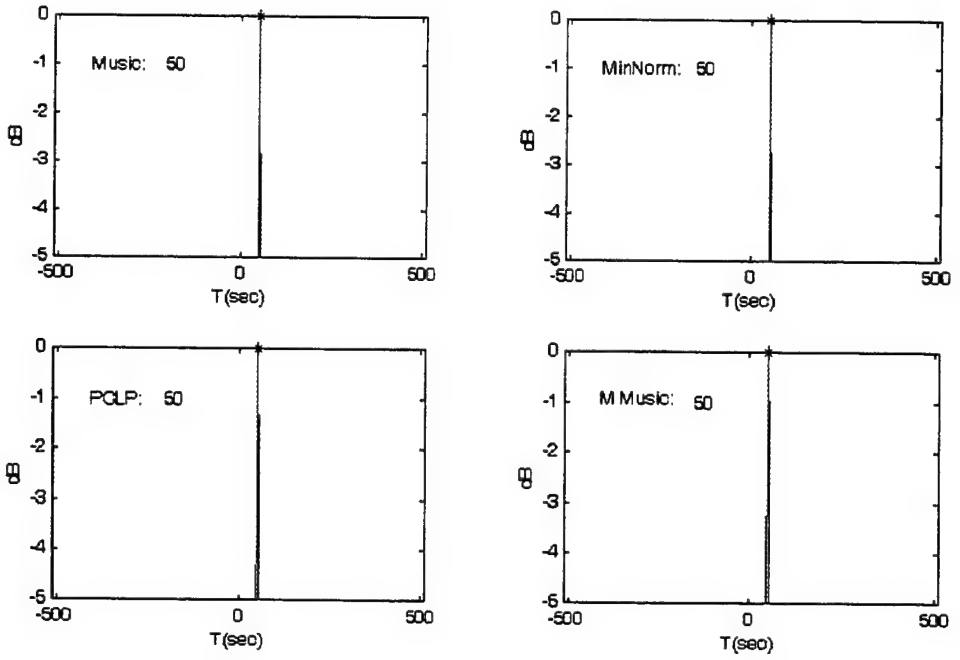

(a)

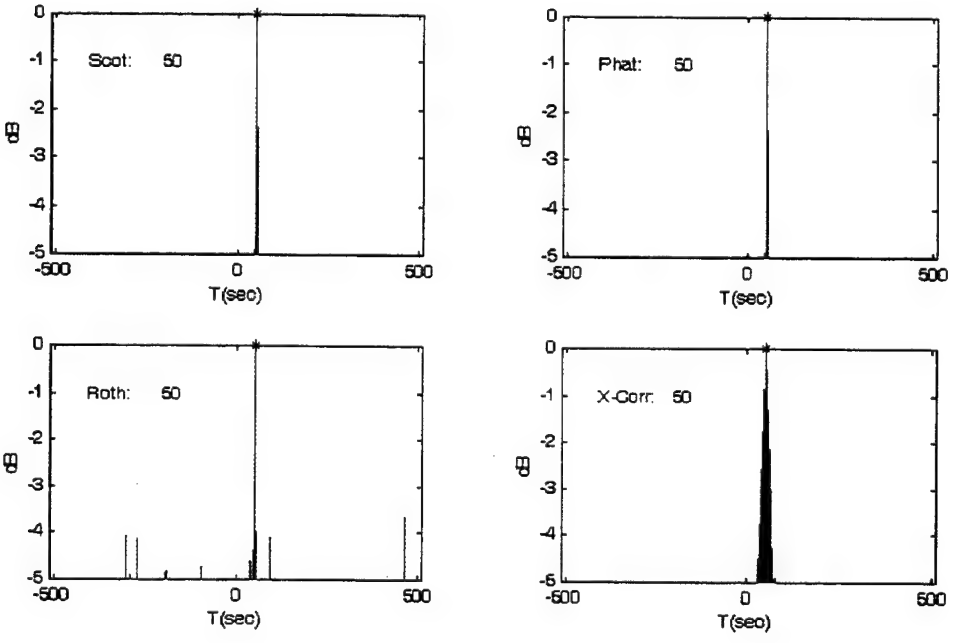

(b)

Figure 69. Damped Sinusoidal transient: Actual Tdoa=50s; SNR=15dB; White-Noise (σ_o^2). (a) Subspace methods, Covariance Size=10. (b) Classical methods, number of segments=1.

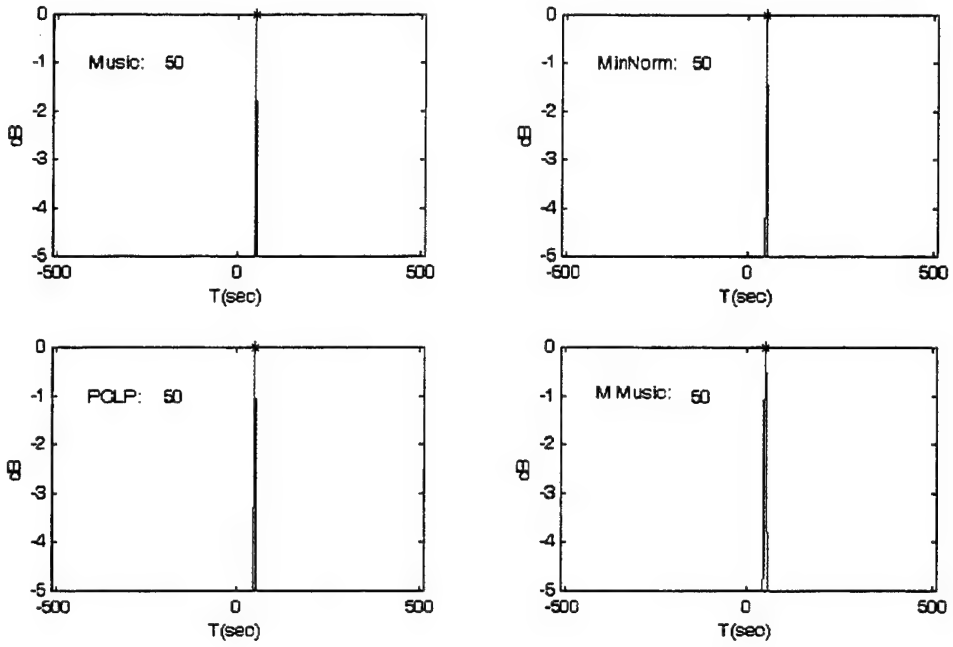

(a)

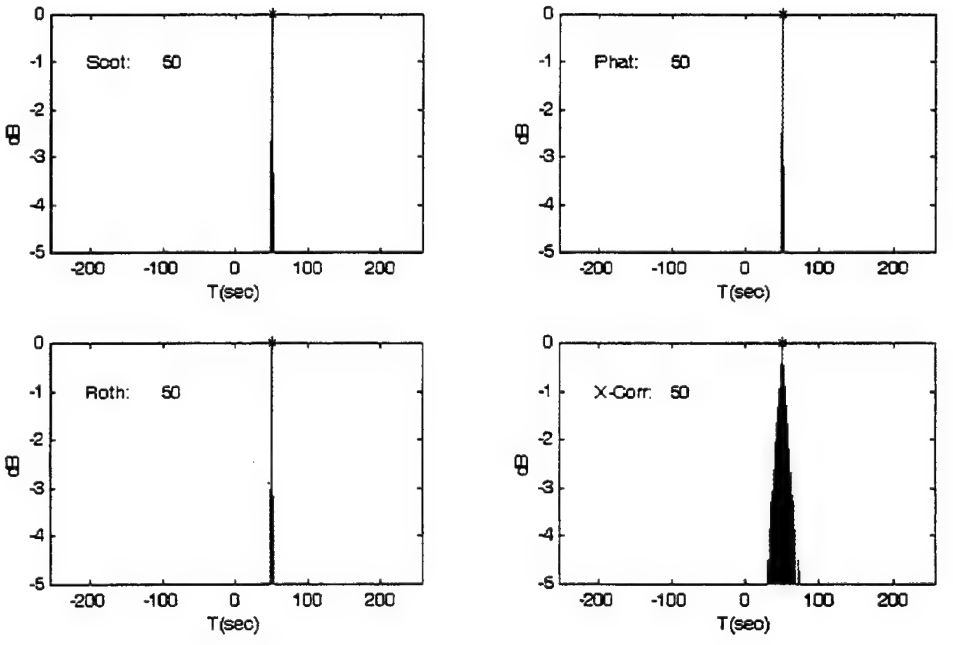

(b)

Figure 70. Damped Sinusoidal transient: Actual Tdoa=50s; SNR=15dB; White-Noise (σ_o^2). (a) Subspace methods, Covariance Size=20. (b) Classical methods, number of segments=2.

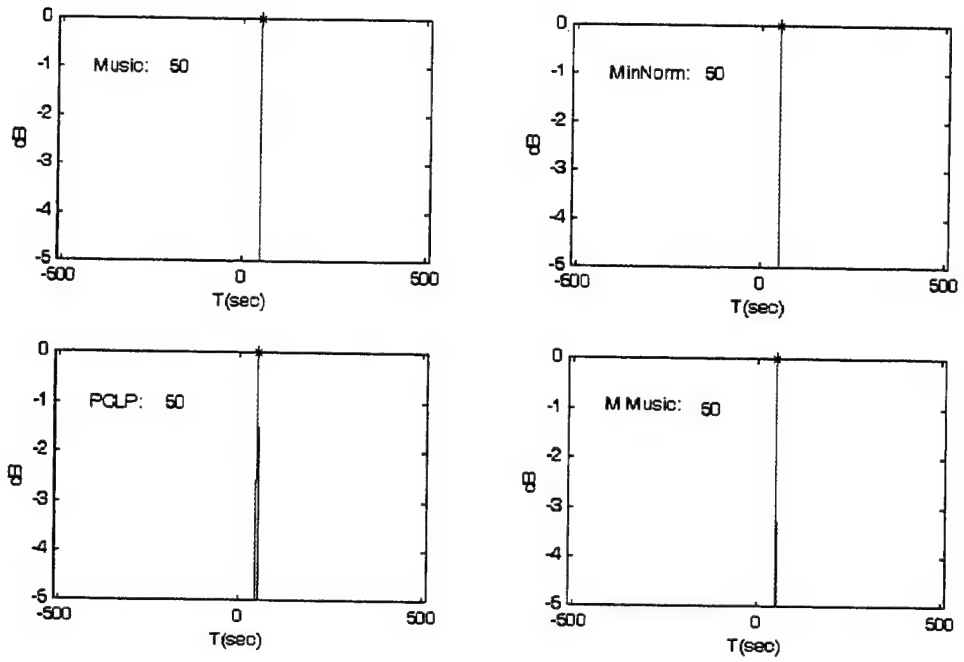

(a)

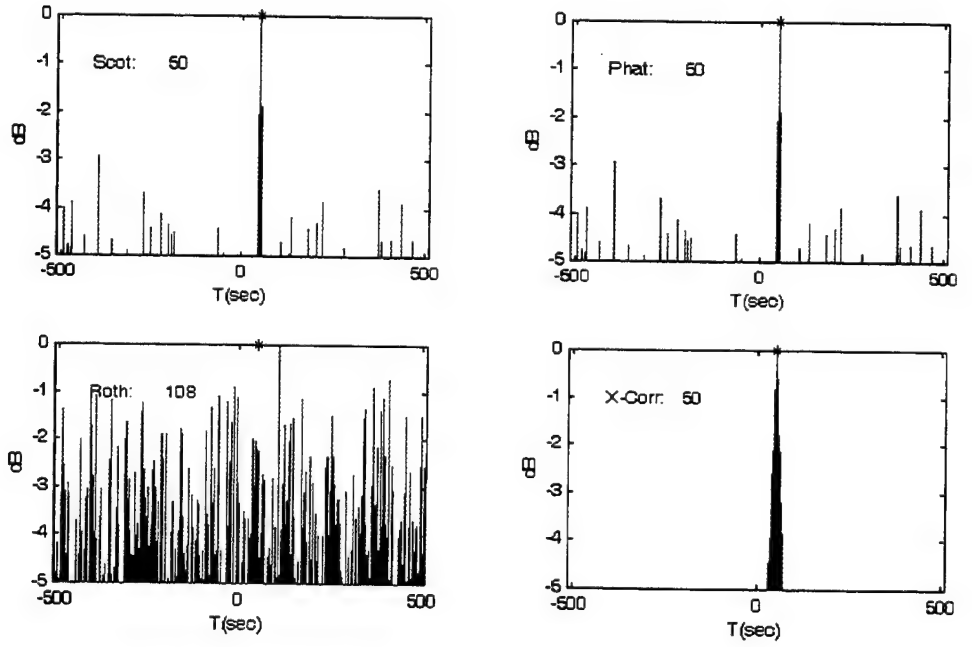

(b)

Figure 71. Damped Sinusoidal transient: Actual Tdoa=50s; SNR=10dB; White-Noise (σ_o^2). (a) Subspace methods, Covariance Size=10. (b) Classical methods, number of segments=1.

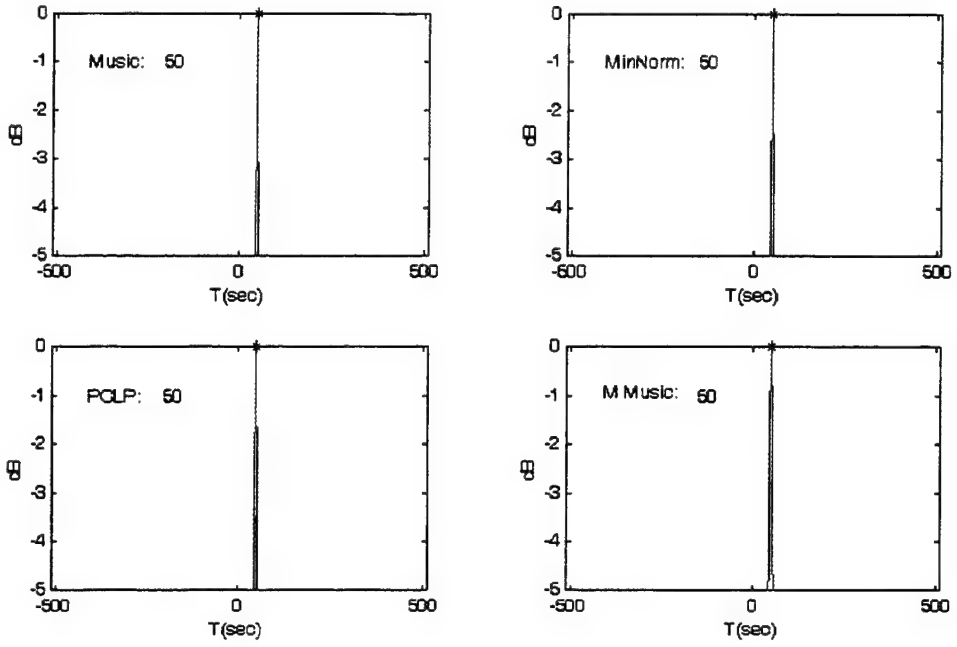

(a)

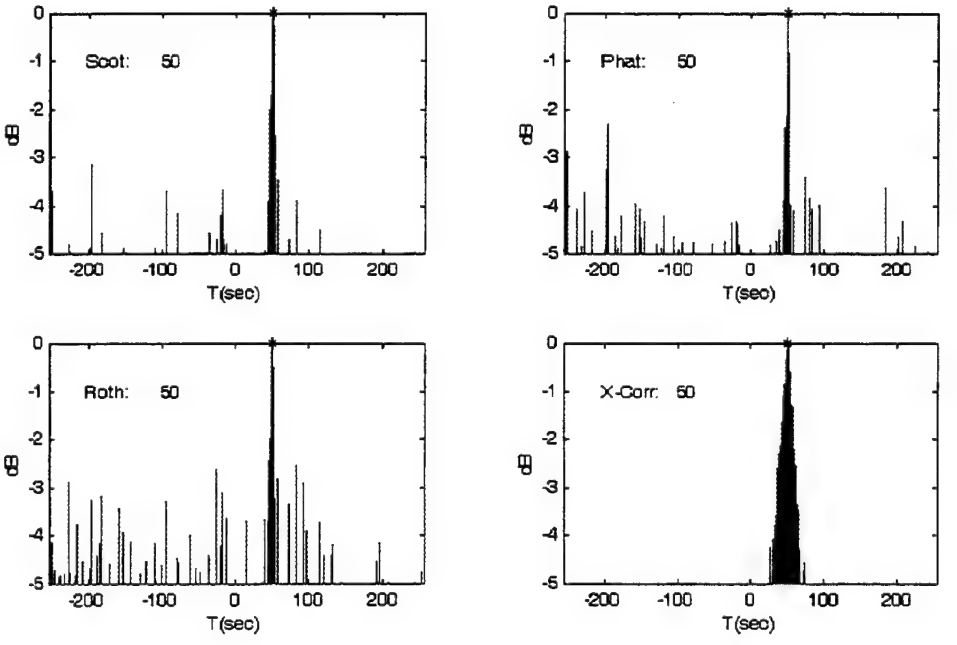

(b)

Figure 72. Damped Sinusoidal transient: Actual Tdoa=50s; SNR=10dB; White-Noise (σ_o^2). (a) Subspace methods, Covariance Size=20. (b) Classical methods, number of segments=2.

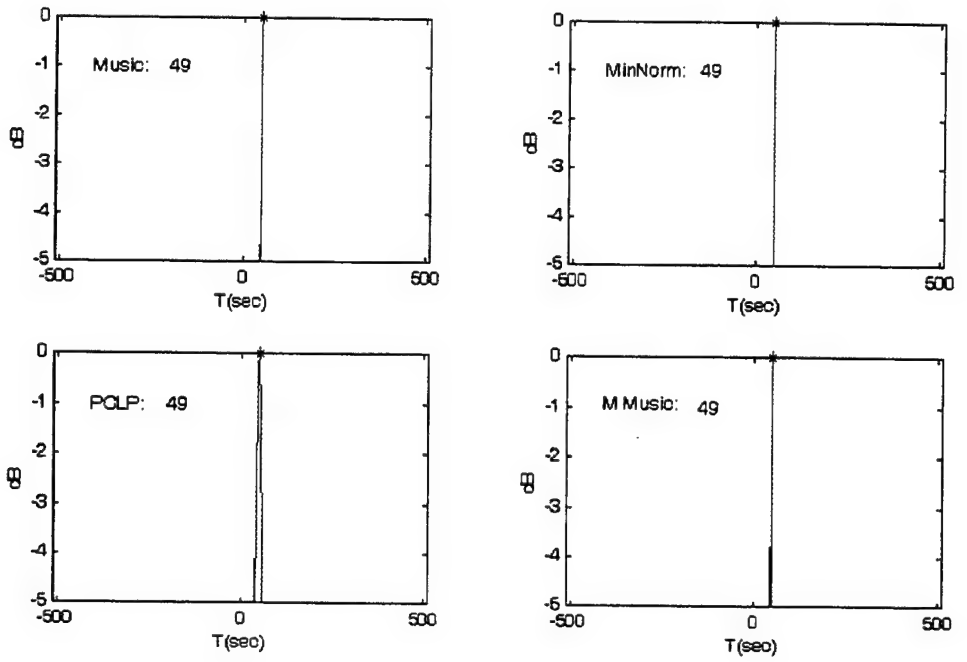

(a)

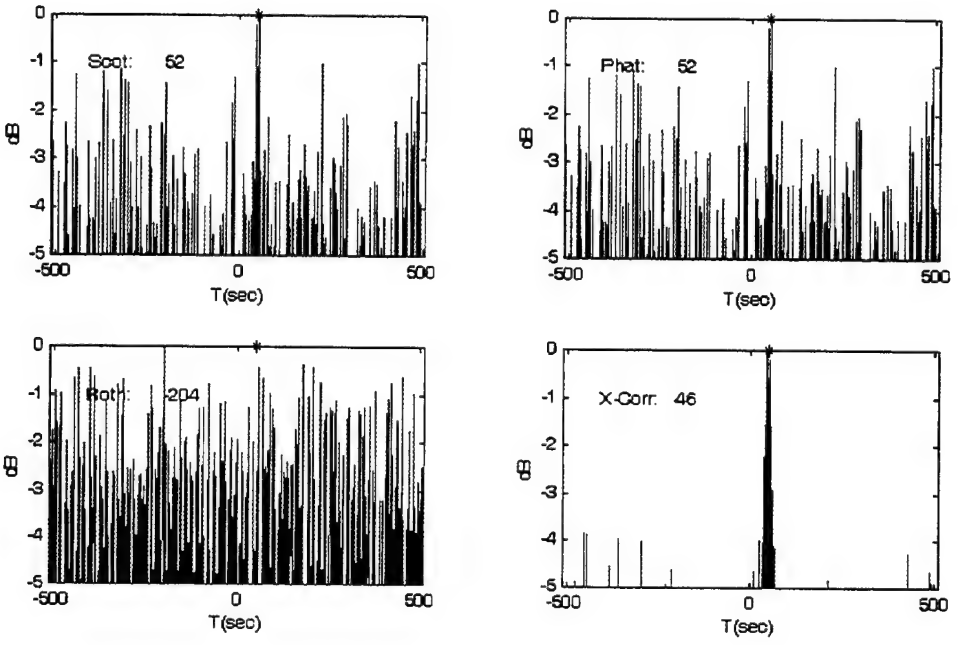

(b)

Figure 73. Damped Sinusoidal transient: Actual Tdoa=50s; SNR=05dB; White-Noise (σ_o^2). (a) Subspace methods, Covariance Size=10. (b) Classical methods, number of segments=1.

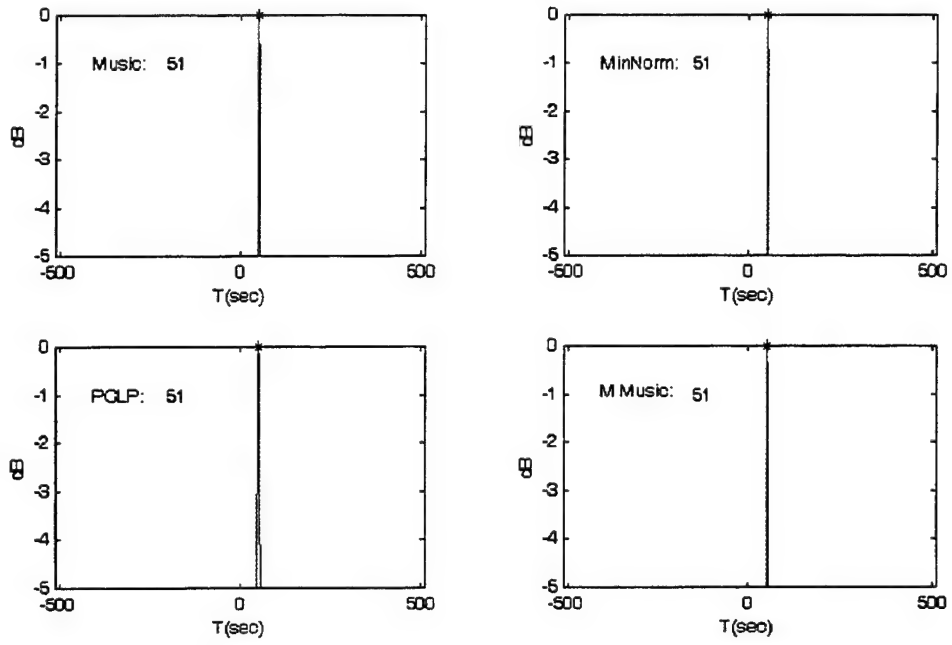

(a)

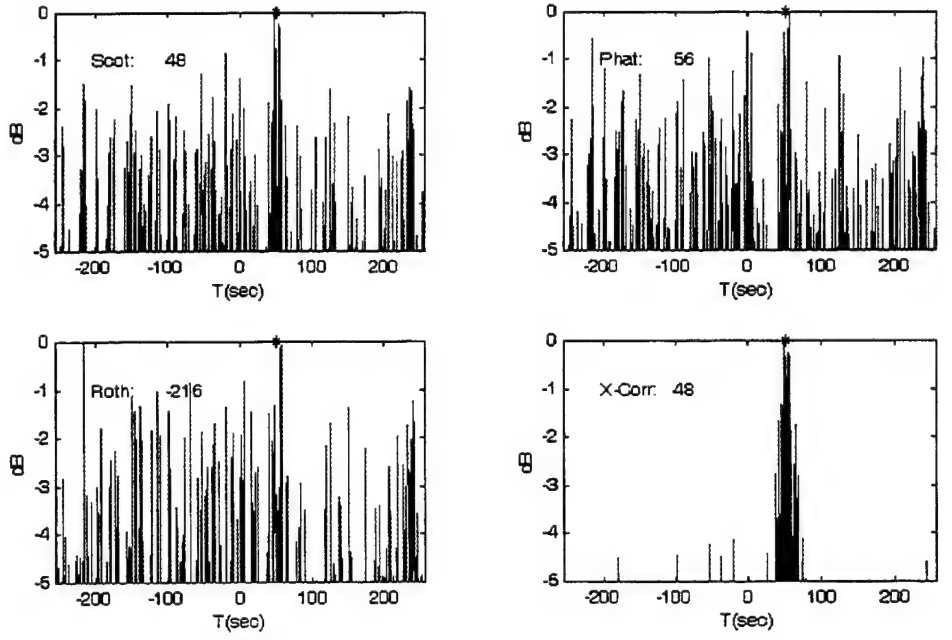

(b)

Figure 74. Damped Sinusoidal transient: Actual Tdoa=50s; SNR=05dB; White-Noise (σ_o^2). (a) Subspace methods, Covariance Size=20. (b) Classical methods, number of segments=2.

Method	Parameters	Exp	Sin	Damped Sin	Chirp	Damped Chirp
MUSIC	Cov-Mat: 10	51	50	49	53	51
	Cov-Mat: 20	49	52	51	48	51
Modified-MUSIC	Cov-Mat: 10	52	50	49	53	51
	Cov-Mat: 20	50	51	51	48	51
MIN-NORM	Cov-Mat: 10	50	50	49	57	50
	Cov-Mat: 20	49	52	51	50	50
PCLP	Cov-Mat: 10	52	50	49	56	50
	Cov-Mat: 20	49	52	51	50	50
ESPRIT	Cov-Mat: 10	50	50	49	53	49
	Cov-Mat: 20	50	52	51	50	51
Root-MUSIC	Cov-Mat: 10	49	50	49	52	50
	Cov-Mat: 20	49	52	51	49	51
SCOT	#-Segs: 1	92	40	52	50	50
	#-Segs: 2	47	42	48	50	49
PHAT	#-Segs: 1	92	40	52	50	50
	#-Segs: 2	47	46	56	50	49
Roth	#-Segs: 1	248	478	-204	50	50
	#-Segs: 2	-204	42	-216	50	49
X-Corr	#-Segs: 1	53	48	46	50	50
	#-Segs: 2	47	46	48	50	50

Table XXIV. Transients: same length; white noise ($\sigma_o^2 = 2$); SNR=05dB; actual TDOA=50s.

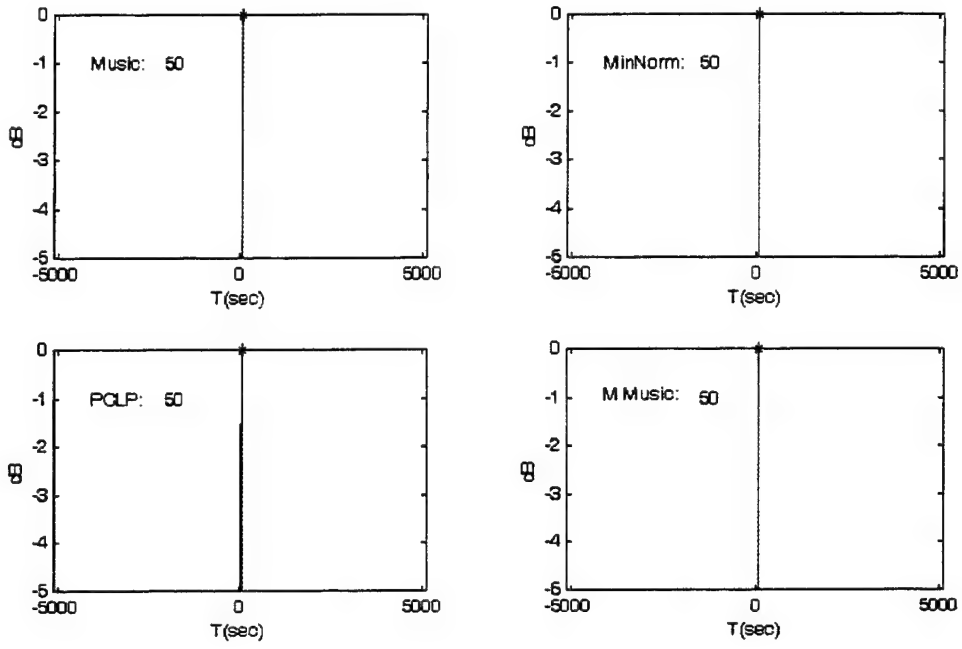

(a)

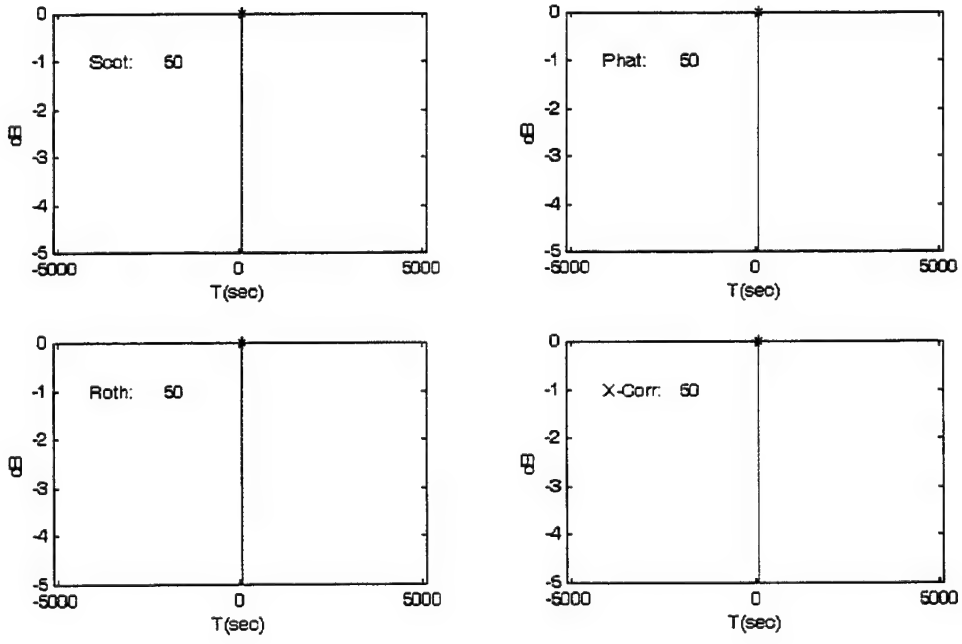

(b)

Figure 75. Chirp transient: Actual Tdoa=50s; SNR=15dB; White-Noise (σ_o^2). (a) Subspace methods, Covariance Size=10. (b) Classical methods, number of segments=1.

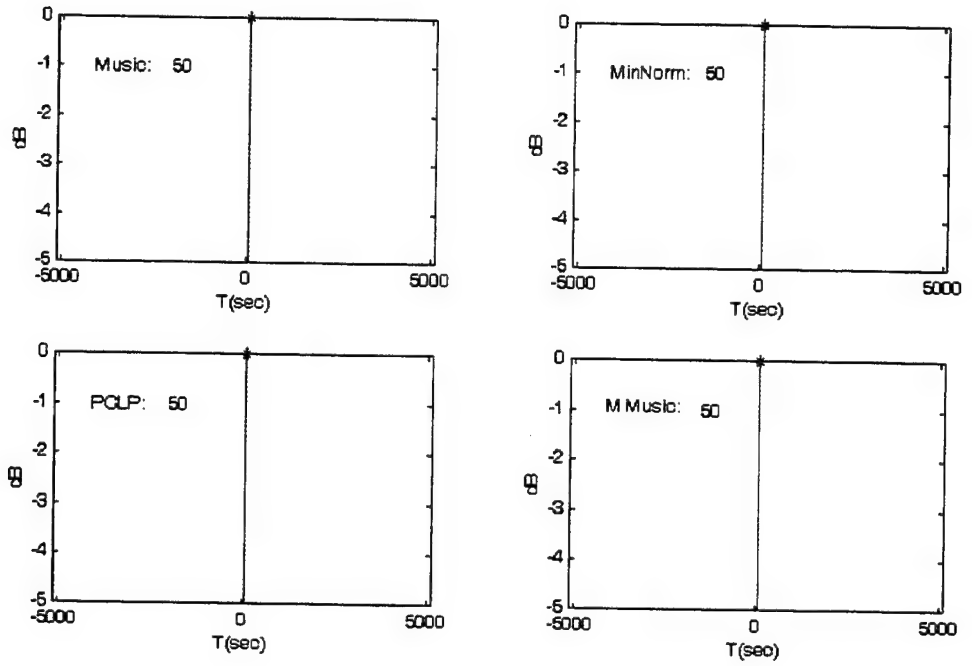

(a)

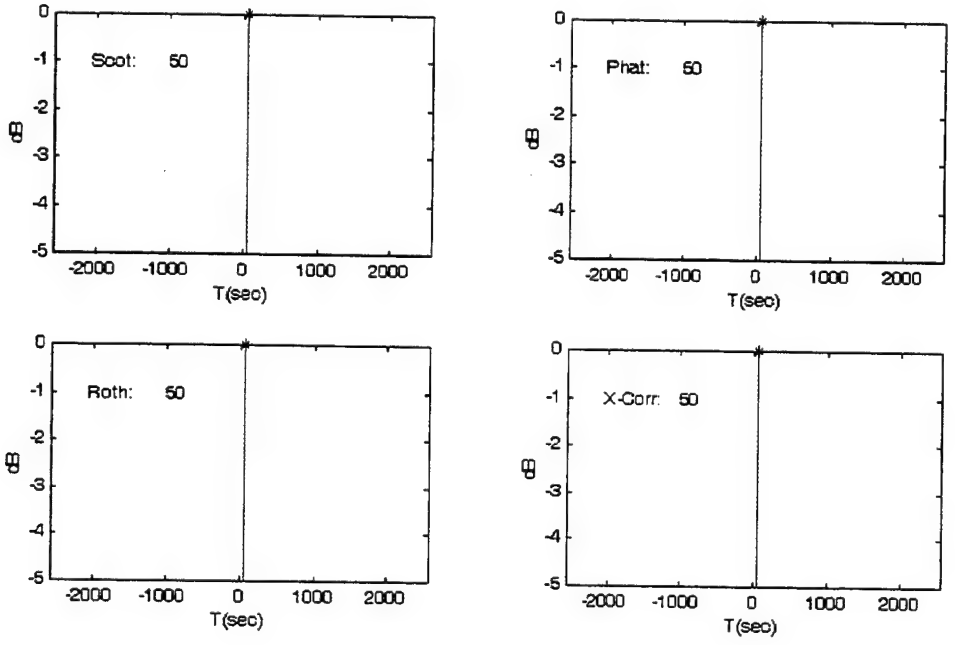

(b)

Figure 76. Chirp transient: Actual Tdoa=50s; SNR=15dB; White-Noise (σ_o^2). (a) Subspace methods, Covariance Size=20. (b) Classical methods, number of segments=2.

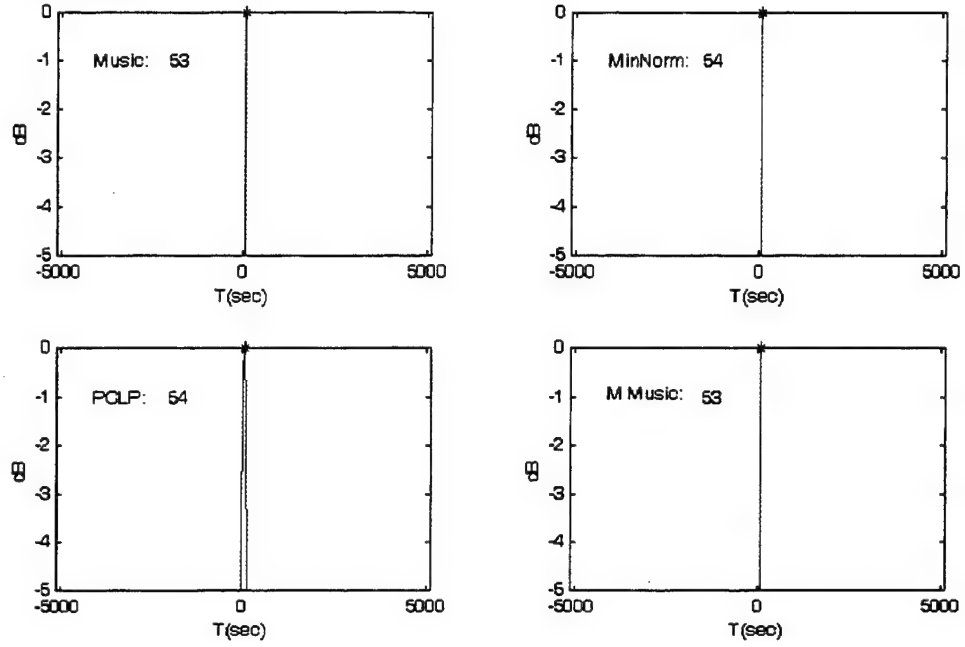

(a)

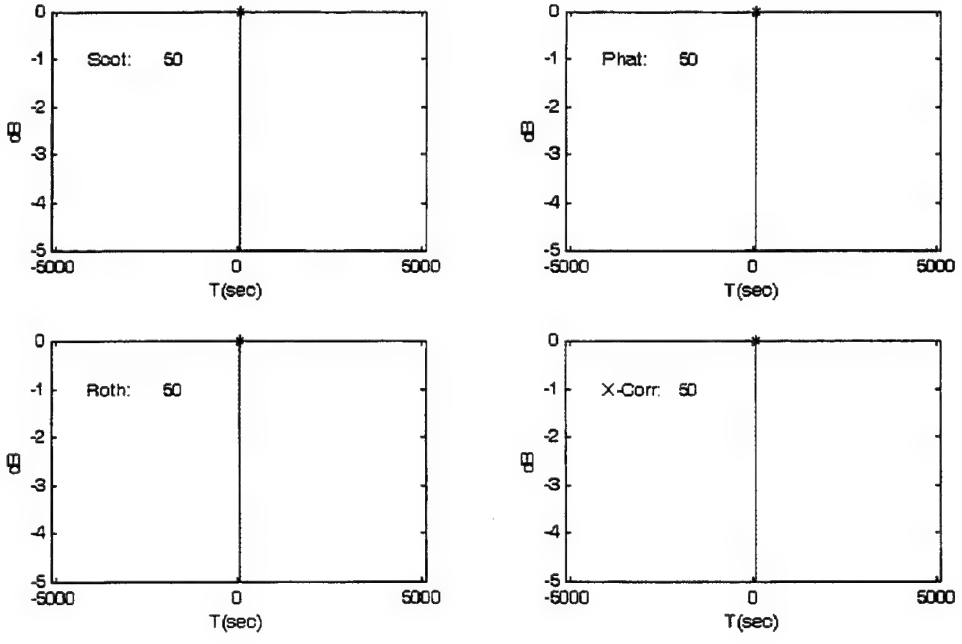

(b)

Figure 77. Chirp transient: Actual Tdoa=50s; SNR=10dB; White-Noise (σ_o^2). (a) Subspace methods, Covariance Size=10. (b) Classical methods, number of segments=1.

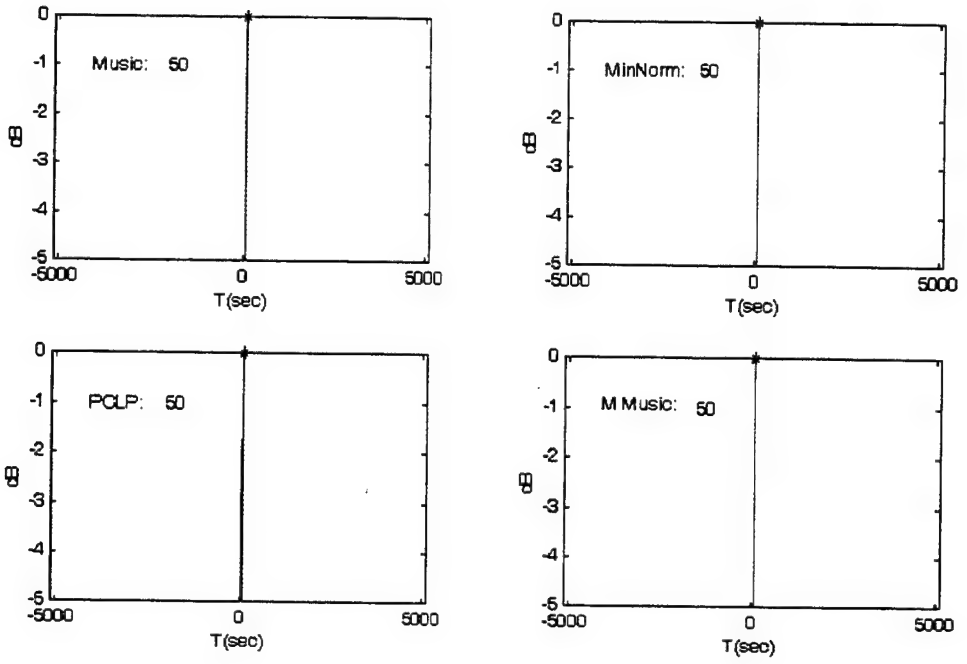

(a)

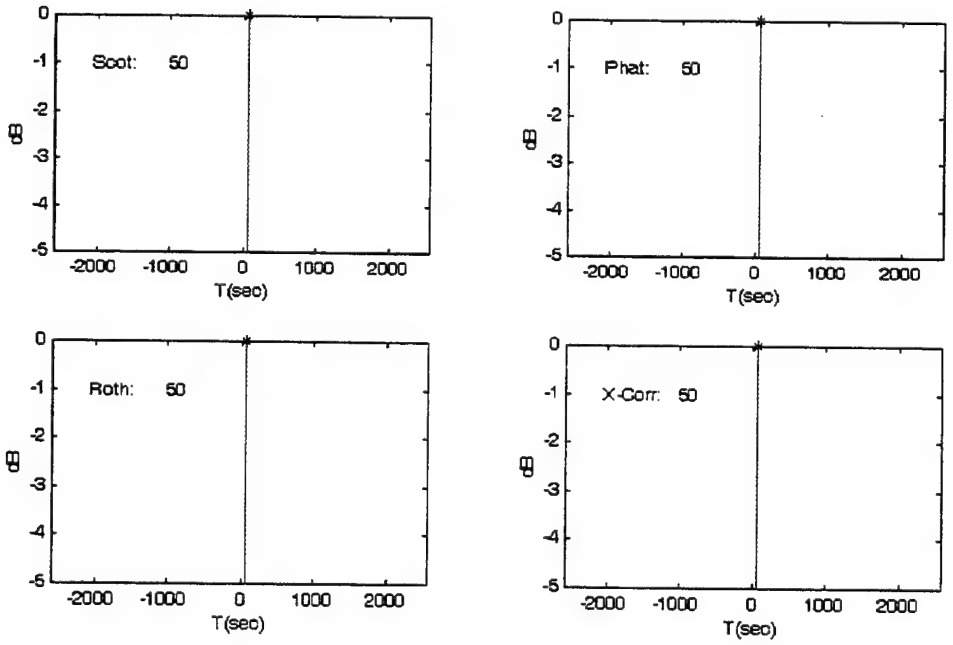

(b)

Figure 78. Chirp transient: Actual Tdoa=50s; SNR=10dB; White-Noise (σ_o^2). (a) Subspace methods, Covariance Size=20. (b) Classical methods, number of segments=2.

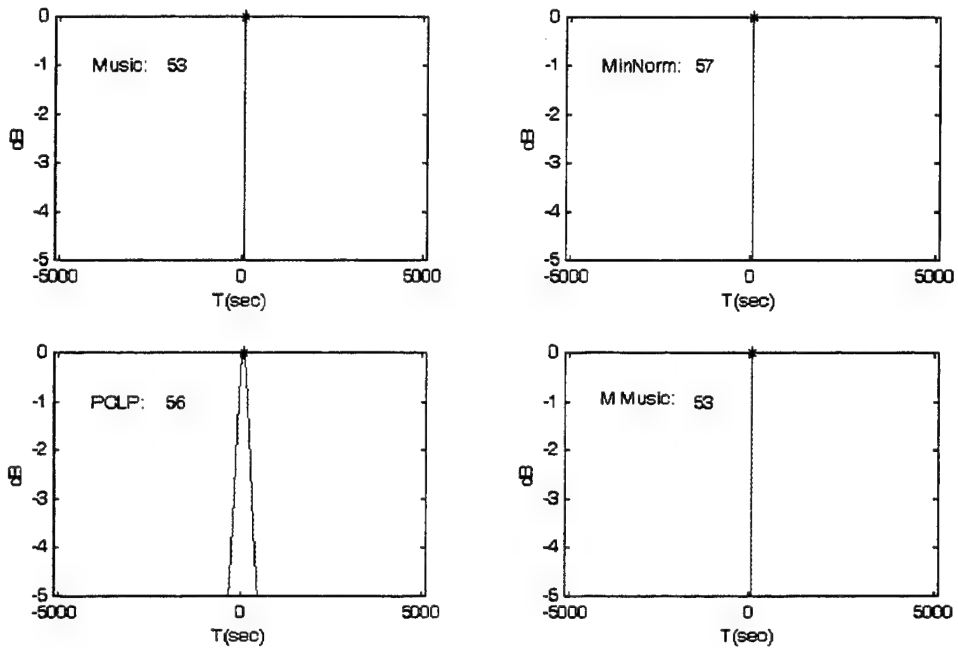

(a)

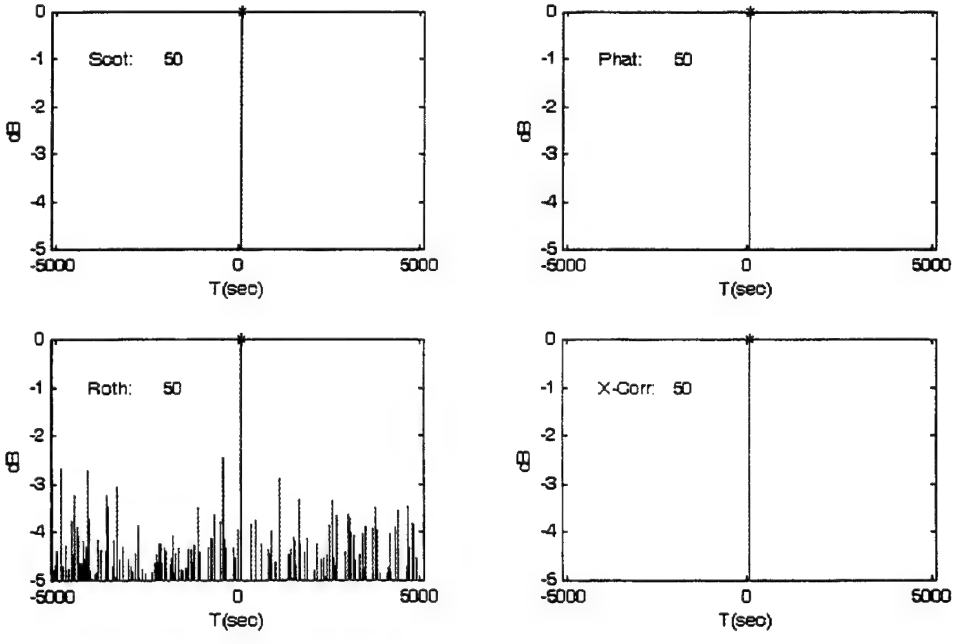

(b)

Figure 79. Chirp transient: Actual Tdoa=50s; SNR=05dB; White-Noise (σ_o^2). (a) Subspace methods, Covariance Size=10. (b) Classical methods, number of segments=1.

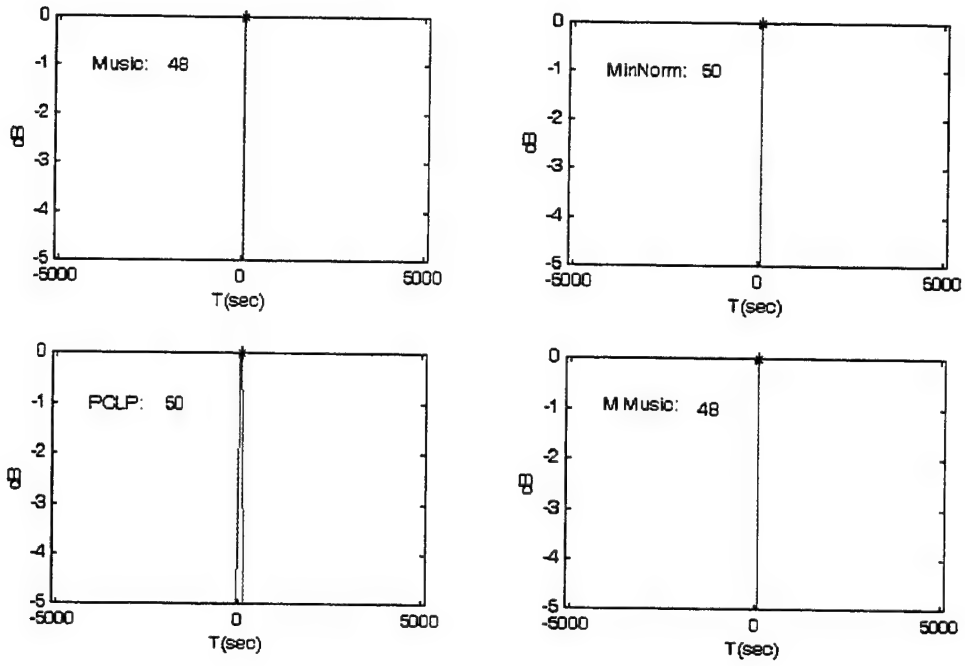

(a)

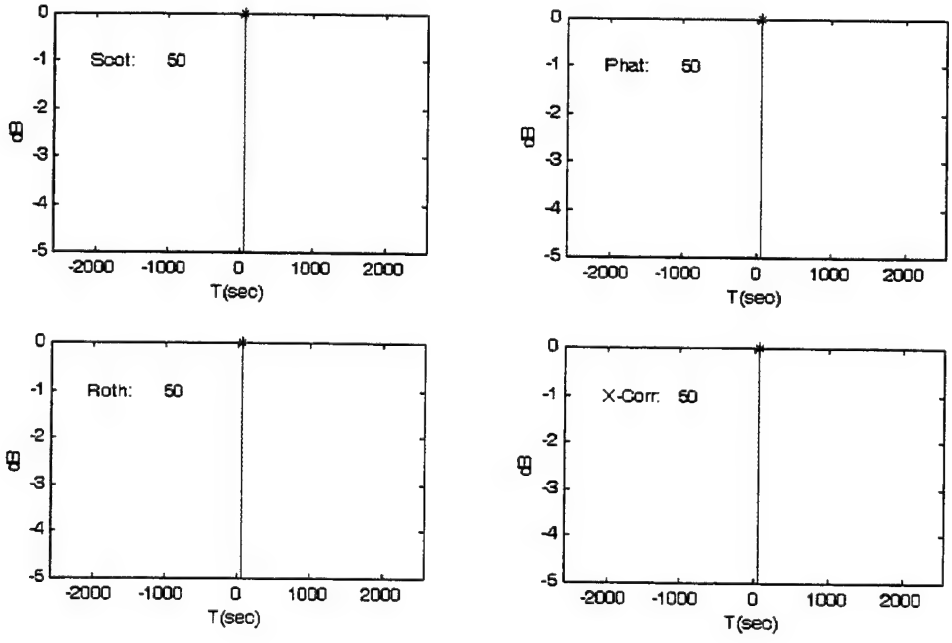

(b)

Figure 80. Chirp transient: Actual Tdoa=50s; SNR=05dB; White-Noise (σ_o^2). (a) Subspace methods, Covariance Size=20. (b) Classical methods, number of segments=2.

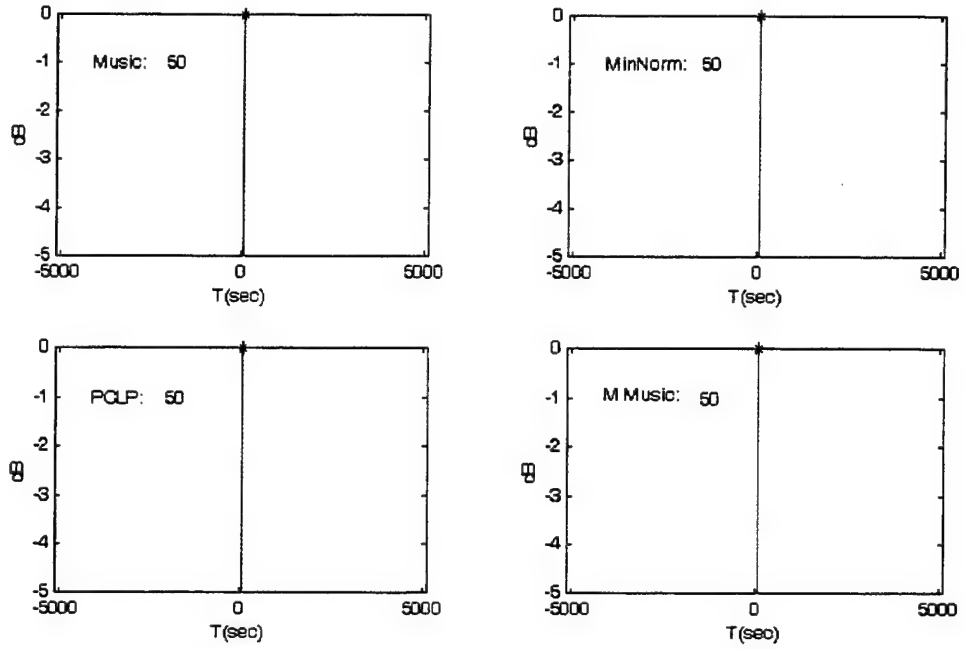

(a)

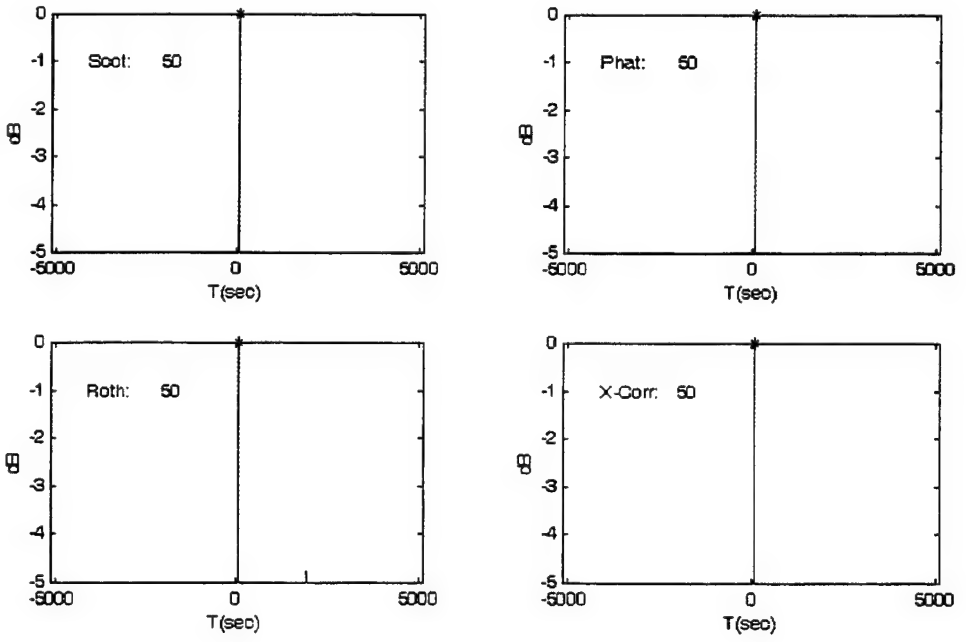

(b)

Figure 81. Damped Chirp transient: Actual Tdoa=50s; SNR=15dB; White-Noise (σ_o^2). (a) Subspace methods, Covariance Size=10. (b) Classical methods, number of segments=1.

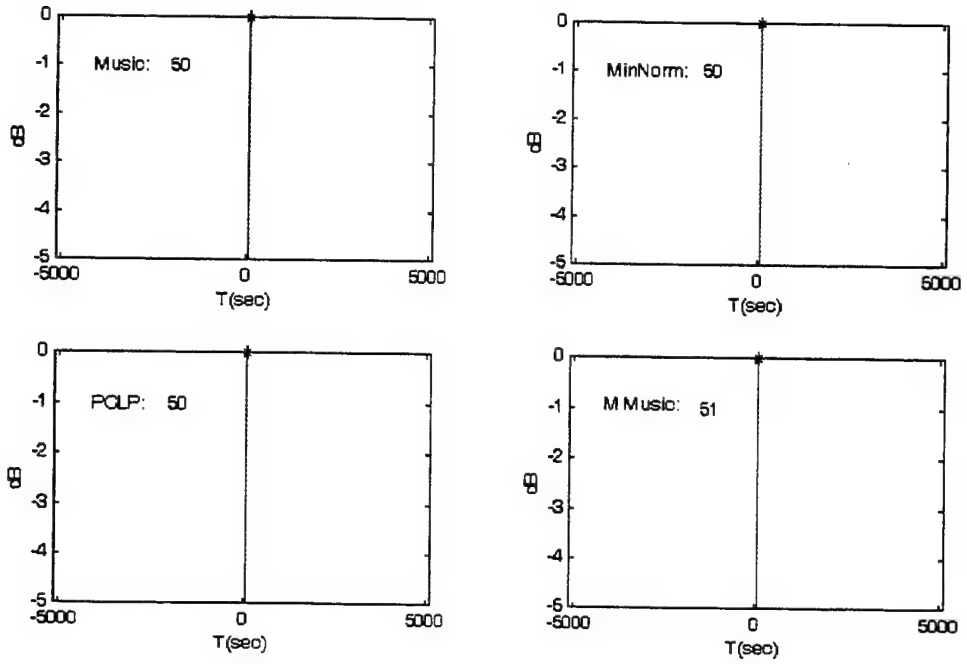

(a)

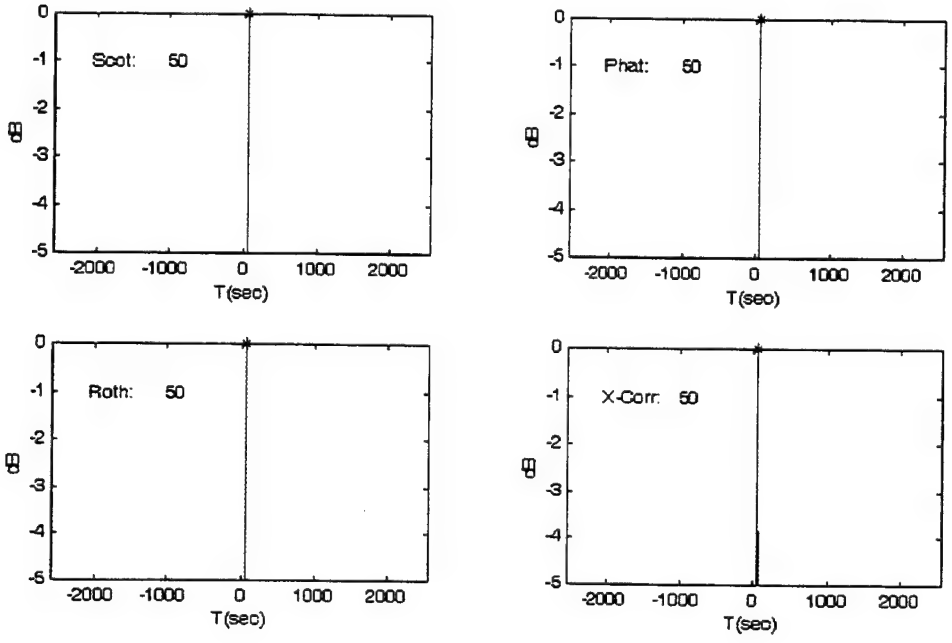

(b)

Figure 82. Damped Chirp transient: Actual Tdoa=50s; SNR=15dB; White-Noise (σ_o^2). (a) Subspace methods, Covariance Size=20. (b) Classical methods, number of segments=2.

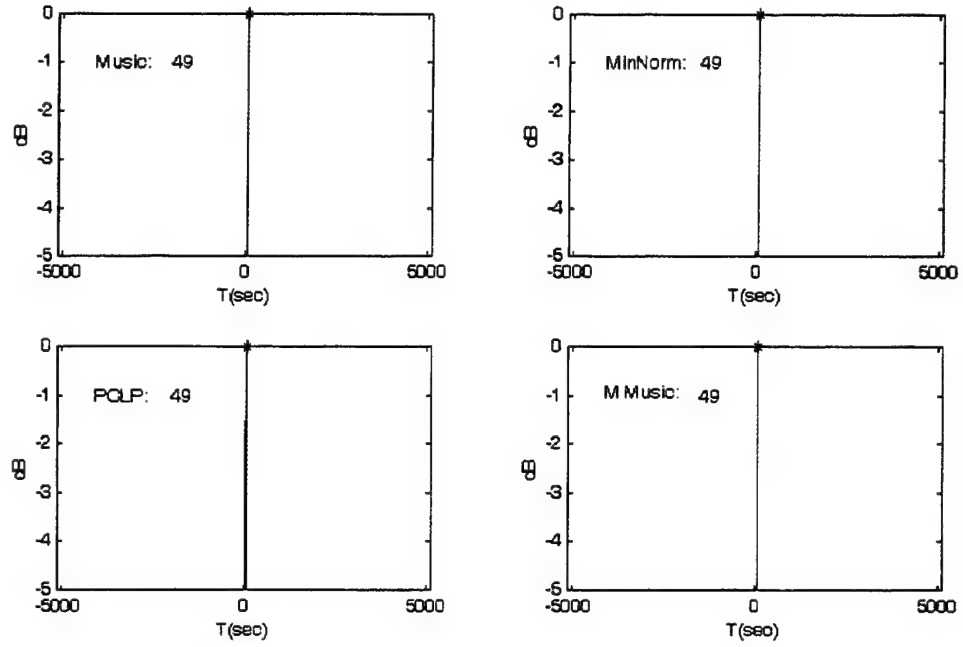

(a)

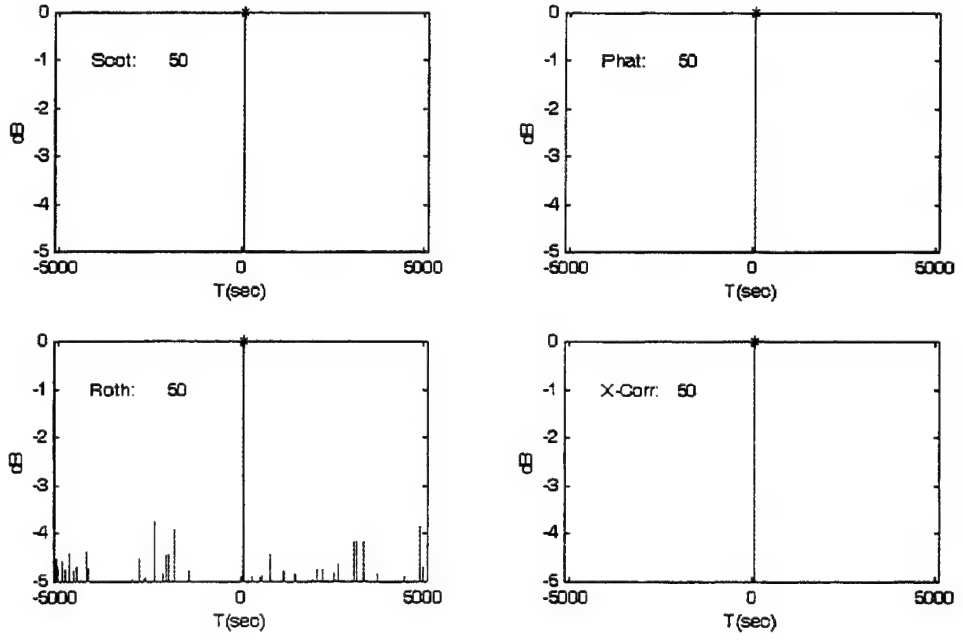

(b)

Figure 83. Damped Chirp transient: Actual Tdoa=50s; SNR=10dB; White-Noise (σ_o^2). (a) Subspace methods, Covariance Size=10. (b) Classical methods, number of segments=1.

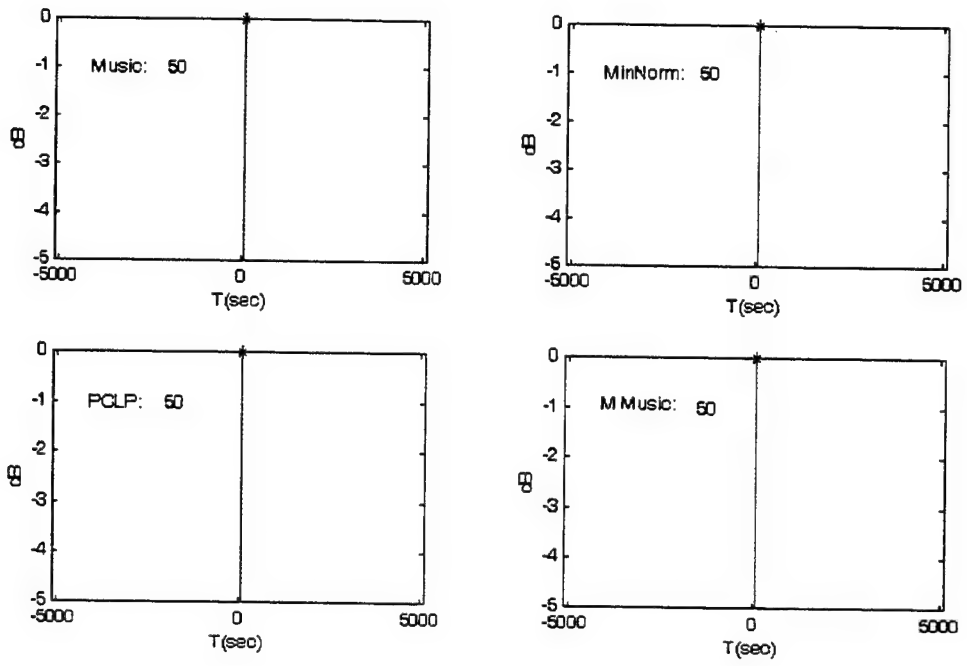

(a)

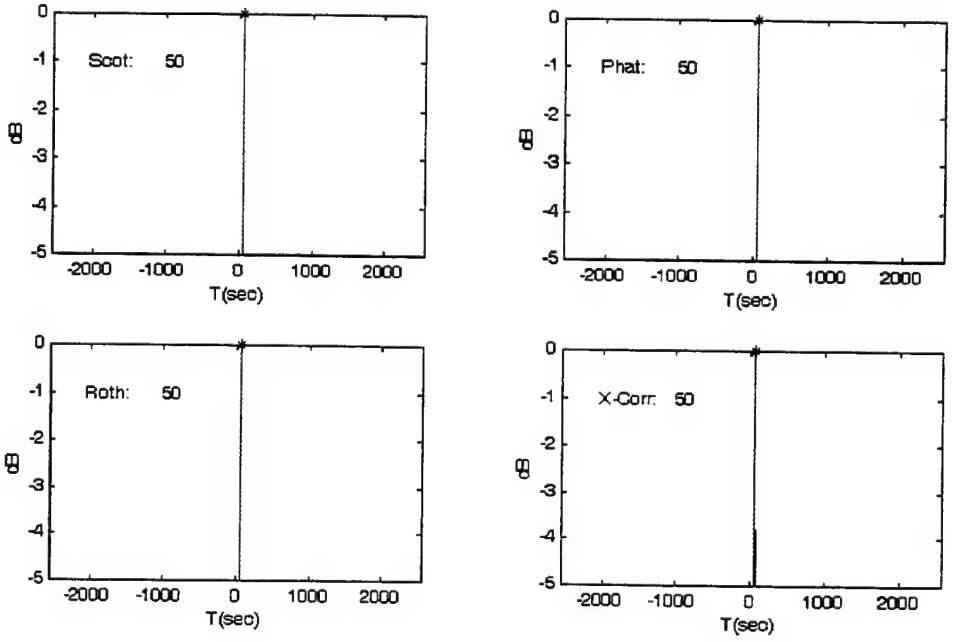

(b)

Figure 84. Damped Chirp transient: Actual Tdoa=50s; SNR=10dB; White-Noise (σ_o^2). (a) Subspace methods, Covariance Size=20. (b) Classical methods, number of segments=2.

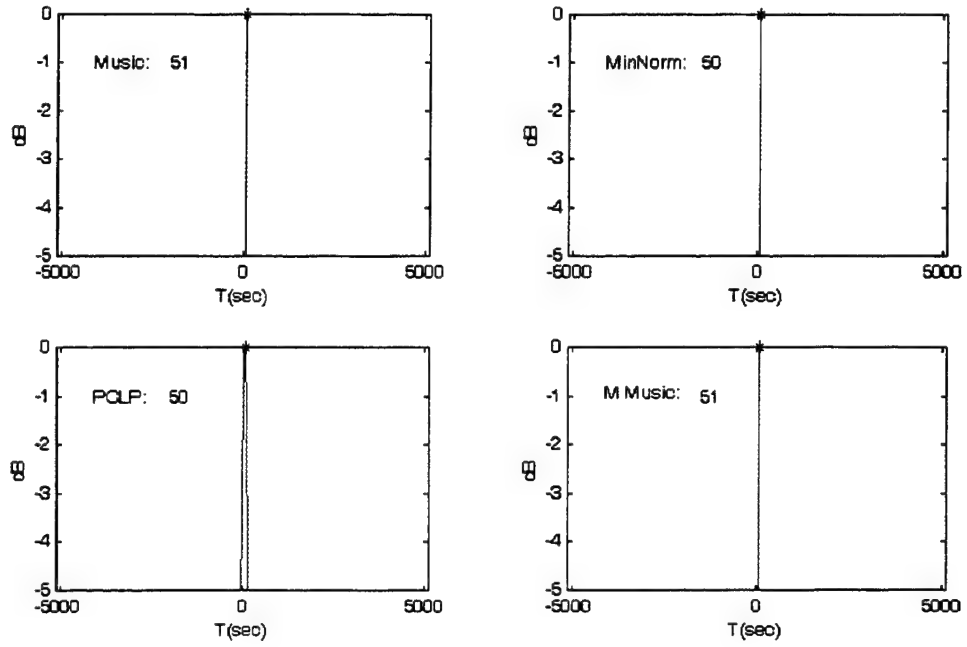

(a)

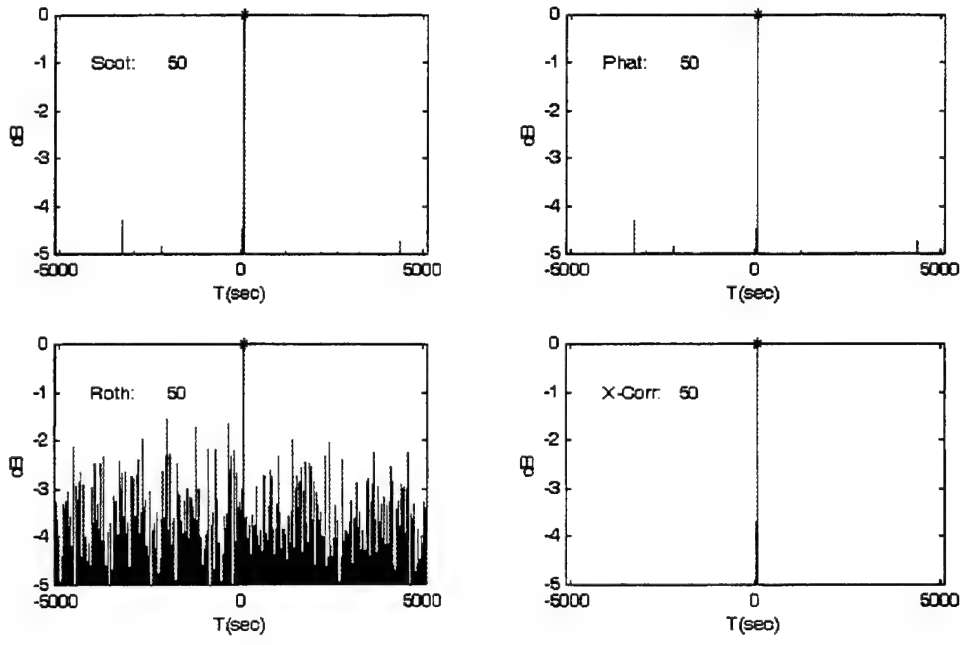

(b)

Figure 85. Damped Chirp transient: Actual Tdoa=50s; SNR=05dB; White-Noise (σ_o^2). (a) Subspace methods, Covariance Size=10. (b) Classical methods, number of segments=1.

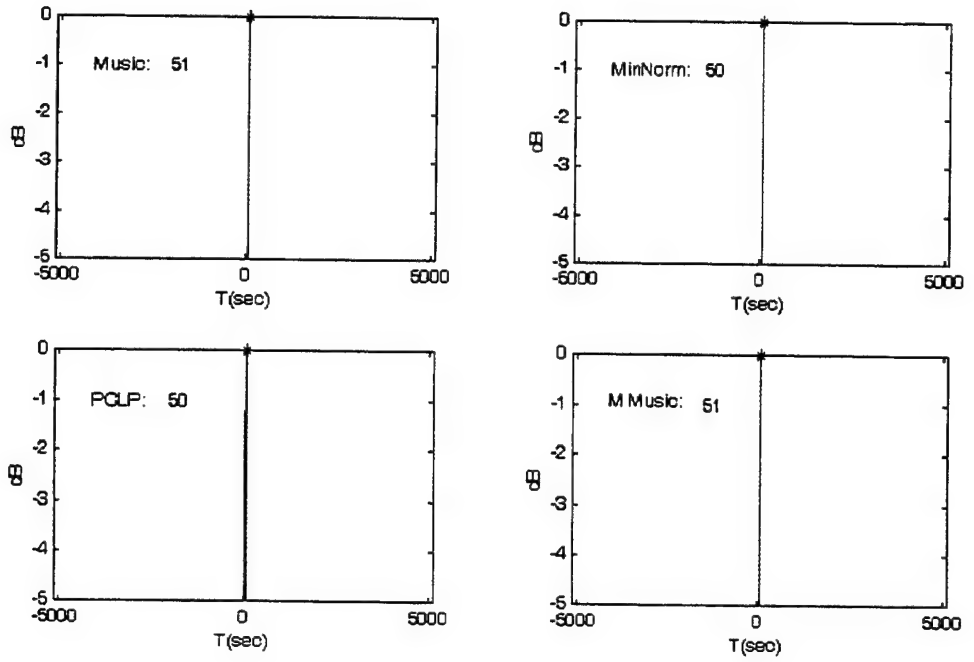

(a)

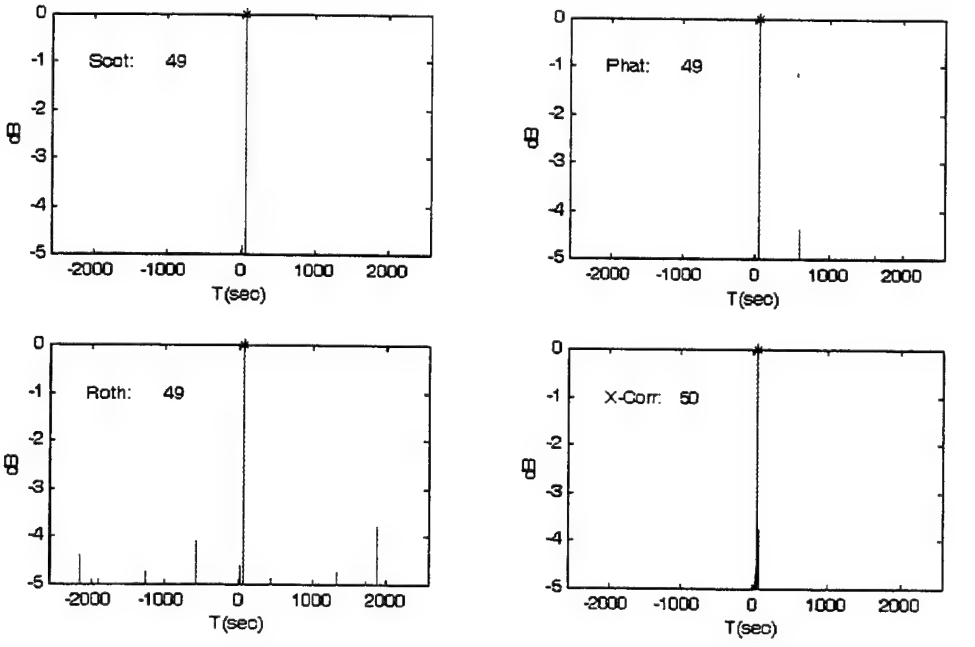

(b)

Figure 86. Damped Chirp transient: Actual Tdoa=50s; SNR=05dB; White-Noise (σ_o^2). (a) Subspace methods, Covariance Size=20. (b) Classical methods, number of segments=2.

LIST OF REFERENCES

[1] G. C. Carter. Time delay estimation for passive sonar signal processing. *IEEE Transactions on Acoustics, Speech, and Signal Processing*, ASSP-29:463–470, June 1981.

[2] G. C. Carter. *Coherence and Time Delay Estimation.* IEEE PRESS, New York, 1996.

[3] G. C. Carter. The smoothed coherence transform SCOT. Technical Report TM TC-159-72, Naval Undersea Warfare Center, Newport Laboratory, Newport, Rhode Island, 1972.

[4] P. R. Roth. Effective measurements using digital signal analysis. *IEEE Spectrum*, 8(4):62–70, April 1971.

[5] C. H. Knapp and G. C. Carter. The generalized correlation method for estimation of time delay. *IEEE Transactions on Acoustics, Speech, and Signal Processing*, 24(4):320–327, August 1976.

[6] Chrysostomos L. Nikias and Athina P. Petropulu. *Higher-Order Spectra Analysis: A Nonlinear Signal Processing Framework.* Prentice Hall, Inc., Englewood Cliffs, New Jersey, 1993.

[7] L. A. Pflug, G. E. Ioup, J. W. Ioup, and R. L. Field. Properties of higher-order correlations and spectra for bandlimited deterministic transients. *J. Acoust. Soc. Am.*, 91(2):975–988, February 1992.

[8] L. A. Pflug, R. L. Field, and G. H. Rayborn. Detection of oscillatory and impulsive transients using higer-order correlations and spectra. *J. Acoust. Soc. Am.*, 91(5):2763–2775, May 1992.

[9] L. A. Pflug, G. E. Ioup, J. W. Ioup, R. L. Field, and J. H. Leclere. Time-delay estimation for deterministic transients using second-and higer-order correlations. *J. Acoust. Soc. Am.*, 94(3):1385–1398, September 1993.

[10] Ralph Schmidt. Multiple emitter location and signal parameter estimation. *IEEE Transactions on Antennas and Propagation*, AP-34:276–290, March 1986.

[11] Richard H. Roy, A. Paulraj, and Thomas Kailath. *ESPRIT* – A subspace rotational approach to estimation of parameters of cisoids in noise. *IEEE Transactions on Acoustics, Speech, and Signal Processing*, ASSP-34(5):1340–1342, October 1986.

[12] J. Capon. High-resolution frequency-wavenumber spectrum analysis. *Proceedings of the IEEE*, 57:119–129, August 1969.

[13] J. Capon. Maximum-likelihood spectral estimation. In Simon Haykin, editor, *Nonlinear Methods of Spectral Analysis*, pages 155–179. Springer-Verlag, New York, second edition, 1983.

[14] K. B. Smith and F. D. Tappert. UMPE: The University of Miami Parabolic Equation Model, Version 1.0. Technical Report 432, Marine Physical Laboratory, 1993.

[15] K. B. Smith. Convergence, stability, and variability of shallow water acoustic predictions using a split-step Fourier parabolic equation model. *Proceedings of the Shallow Water Acoustic Modeling (SWAM '99) Workshop*, 8-10 September 1999. Special Issue of J. Comp. Acoust., 2000 (eds. Kevin B. Smith and Alex Tolstoy, in press).

[16] G. C. Carter, A. H. Nuttall, and P. G. Cable. The smoothed coherence transform. *Proc. IEEE (Lett.)*, 61:1497–1498, October 1973.

[17] C. Eckart. Optimal rectifier systems for the detection of steady signals. Technical Report Rep SIO 12692, SIO Ref 52-11, Univ. California Scripp Inst. Oceanography, Marine Physical Laboratory, 1952.

[18] C. H. Knapp. Optimum linear filtering for multi-element arrays. Technical Report Rep. U417-66-031 SIO 12692, SIO Ref 52-11, Electric Boat Division, Groton, CT, Nov, 1966.

[19] A. H. Nuttall and D. W. Hyde. A unified approach to optimum and suboptimum processing for arrays. Technical Report Rep. 992, Naval Underwater Systems Center, New London Lab., New London, Connecticut, Apr, 1969.

[20] D. W. Hyde and A. H. Nuttall. Linear pre-filtering to enhance correlator performance. Technical Report Tech. Memo 2020-34-69, Naval Underwater Systems Center, New London Lab., New London, Connecticut, Feb. 27, 1969.

[21] A. H. Nuttall. Pre-filtering to enhance clipper correlator performance. Technical Report Tech. Memo TC-11-73, Naval Underwater Systems Center, New London Lab., New London, CT, July 10, 1973.

[22] Charles W. Therrien. *Discrete Random Signals and Statistical Signal Processing.* Prentice Hall, Inc., Englewood Cliffs, New Jersey, 1992.

[23] Don H. Johnson and Stuart R. DeGraaf. Improving the resolution of bearing in passive sonar arrays by eigenvalue analysis. *IEEE Transactions on Acoustics, Speech, and Signal Processing*, ASSP-30(4):638–647, August 1982.

[24] S. S. Reddi. Multiple source location – a digital approach. *IEEE Transactions on Aerospace and Electronic Systems*, AES-15(1):134–139, January 1979.

[25] Ramdas Kumaresan and Donald W. Tufts. Estimating the angles of arrival of multiple plane waves. *IEEE Transactions on Aerospace and Electronic Systems*, AES-19(1):134–139, January 1983.

[26] Donald W. Tufts and Ramdas Kumaresan. Estimation of frequencies of multiple sinusoids: Making linear prediction behave like maximum likelihood. *Proceedings of the IEEE*, 70:975–989, September 1982.

[27] Donald W. Tufts and Ramdas Kumaresan. Singular value decomposition and improved frequency estimation using linear prediction. *IEEE Transactions on Acoustics, Speech, and Signal Processing*, ASSP-30:671–675, August 1982.

[28] Richard H. Roy and Thomas Kailath. *ESPRIT* – estimation of signal parameters via rotational invariance techniques. *IEEE Transactions on Acoustics, Speech, and Signal Processing*, 37(7):984–995, July 1989.

[29] A. Paulraj, Richard H. Roy, and Thomas Kailath. Estimation of signal paramaters via rotational invariance techniques – *ESPRIT*. In *Proceedings of the* 19^{th} *Asilomar Conference on Circuits, Systems, and Computers*, pages 83–89, November 1985. (Pacific Grove, CA).

[30] C. W. Therrien, S. D. Kouteas, and K. B. Smith. Time delay estimation using a signal subspace model. *Proceedings of 34th Asilomar Conference on Signals, Systems and Computers*, 29-31 October 2000.

[31] J. F. Lynch, G. G. Gawarkiewicz, C. S. Chiu, R. Pickart, J. H. Miller, K. B. Smith, A. R. Robinson, K. H. Brink, R. Beardsley, B. Sperry, and G. Potty. Shelfbreak primer - an integrated acoustic and oceanographic field study in the middle atlantic bight. *Proceedings of International Conference on Shallow Water Acoustics*, Beijing(China):205–212, 21-25 April 1997.

[32] Tielburger, Finette, and Wolf. *J. Acoust. Soc. Am.*, 101:789–808.

[33] J. D. Mauser. *Development of an Acoustic Transient Analysis User Interface for Detection and Target Localization.* Naval Postgraduate School, Monterey, California, Master's Thesis, December 1997.

[34] D. B. Kilfoyle and A. B. Baggeroer. The state of the art in underwater acoustic telemetry. *IEEE Journal of Oceanic Engineering*, 25(1):4–27, 2000.

[35] K. B. Smith. Computing the influence of doppler due to source/receiver motion in parabolic equation models. *J. Comp. Acoust.*, 2001. submitted.

THIS PAGE INTENTIONALLY LEFT BLANK

INITIAL DISTRIBUTION LIST

1. Defense Technical Information Center 2
   8725 John J. Kingman Road., STE 0944
   Ft. Belvoir, VA 22060-6218

2. Dudley Knox Library 2
   Naval Postgraduate School
   411 Dyer Rd.
   Monterey, CA 93943-5101

3. Engineering and Technology Curricular Office, Code 34 1
   Naval Postgraduate School
   Monterey, CA 93943-5107

4. Professor Jeffrey B. Knorr, Code EC/Ko 1
   Chairman, Department of Electrical and Computer Engineering
   Naval Postgraduate School
   Monterey, CA 93943-5121

5. Professor Kevin B. Smith, Code PH/Sk 3
   Chairman, Engineering Acoustics Academic Committee
   Naval Postgraduate School
   Monterey, CA 93943-5117

6. Professor Charles W. Therrien, Code EC/Ti 3
   Department of Electrical and Computer Engineering
   Naval Postgraduate School
   Monterey, CA 93943-5121

7. Professor Roberto Cristi, Code EC/Cx 1
   Department of Electrical and Computer Engineering
   Naval Postgraduate School
   Monterey, CA 93943-5121

8. Embassy of Greece 1
   Naval Attache
   2228 Massachusetts Av., NW
   Washington, DC 20008

9. Stefanos D. Kouteas, Ltjg Hellenic Navy 3
   Melpomenis 26, Cholargos
   Athens, TK 15561
   GREECE-HELLAS